Utilizing Remote Sensing of Thematic Mapper Data to Improve Our Understanding of Estuarine Processes and Their Influence on the Productivity of Estuarine-Dependent Fisheries

Final Report to the
National Aeronautics and Space Administration

Joan A. Browder, L. Nelson May, Alan Rosenthal
Robert H. Baumann, and James G. Gosselink

Center for Wetland Resources • Louisiana State University • Baton Rouge, LA 70803-7503

Utilizing Remote Sensing of Thematic Mapper Data to Improve Our Understanding of Estuarine Processes and Their Influence on the Productivity of Estuarine-Dependent Fisheries

Final Report to the
National Aeronautics and Space Administration
Goddard Space Flight Center
Greenbelt, Maryland 20771

Joan A. Browder
Southeast Fisheries Center
National Marine Fisheries Service
75 Virginia Beach Drive
Miami, Florida 33149

L. Nelson May
Coastal Fisheries Institute
Center for Wetland Resources
Louisiana State University
Baton Rouge, Louisiana 70803

Alan Rosenthal
Southeast Fisheries Center
National Marine Fisheries Service
75 Virginia Beach Drive
Miami Beach, Florida 33149

Robert H. Baumann
Center for Energy Studies
Louisiana State University
Baton Rouge, Louisiana 70803

James G. Gosselink
Coastal Ecology Institute
Center for Wetland Resources
Baton Rouge, Louisiana 70803

December 20, 1988

This report should be cited as

Browder, J. A., L. N. May, Alan Rosenthal, R. H. Baumann, and J. G. Gosselink. 1988. Utilizing Remote Sensing of Thematic Mapper Data to Improve Our Understanding of Estuarine Processes and Their Influence on the Productivity of Estuarine-Dependent Fisheries. Final Report to the National Aeronautics and Space Administration. Center for Wetland Resources, Louisiana State University, Baton Rouge.

Contents

List of Figures

Abstract

The land-water interface of coastal marshes may influence the production of estuarine-dependent fisheries more than the area of these marshes. To test this hypothesis, we created a spatial model to explore the dynamic relationship between marshland-water interface and level of disintegration in the decaying coastal marshes of Louisiana's Barataria, Terrebonne, and Timbalier basins. Calibrating our model with Landsat Thematic Mapper satellite imagery, we found a parabolic relationship between land-water interface and marsh disintegration. Aggregated simulation data suggest that interface in the study area will soon reach its maximum and then decline. We found a statistically significant positive linear relationship between brown shrimp catch and total interface length over the past 28 yr. This relationship suggests that shrimp yields will decline when interface declines, possibly beginning about 1995.

Introduction

The loss of Louisiana's coastal wetlands at the average rate of about 100 km^2/yr (Gagliano et al. 1981) is a problem of national concern because of their importance to wildlife and fisheries. Louisiana's seafood production, the highest in the nation, is based on species dependent on estuaries and their associated wetlands, which provide food and shelter for young organisms (Boesch and Turner 1984).

Both natural processes and human interference with these processes are responsible for the rapid wetland loss in Louisiana (Baumann et al. 1984). The leveeing of the Mississippi River has prevented the deposition of marsh-building sediment that could offset subsidence and sea-level rise (Kesel 1988). Drainage and navigation channels have altered the natural hydrologic processes that build coastal and interior marshes and stimulate marsh vegetation growth (Turner and Cahoon 1987).

Despite the loss of wetlands and the known dependence of fishery species on wetlands, statistics indicate that Louisiana's fishery landings have been increasing. The increase in landings, not fully explained by an increase in effort (Nichols 1984), has created a sense of false security that has delayed action to curb wetland loss.

The production of fishery species may be more dependent on the land-water interface than on wetland acreage. Faller (1979), Dow (1982), and Gosselink (1984) found statistically significant relationships between fishery production and land-water interface in neighboring areas. Zimmerman et al. (1984) noted that brown shrimp densities were highest in areas of high shoreline "reticulation."

Using a stochastic computer model, Browder et al. (1984) provided a theoretical description of how the length of the land-water interface changes during marsh disintegration. They found that interface length increased in early stages of simulated marsh disintegration, reached a maximum when the marsh was roughly 50% water, and decreased thereafter. They further noted that the magnitude of maximum interface was variable and was affected by the spatial pattern of land and water--specifically the degree of clumping of water pixels to form water bodies.

In the study reported here, we refined and expanded the Browder et al. (1984) model and calibrated it with Thematic Mapper (TM) imagery covering 70 marsh sites in coastal Louisiana (Appendix A). Then we used our model to simulate the complete cycle of marsh disintegration

at each site and collected data on interface length. We used independent data to roughly convert interface length versus disintegration level to interface length loss versus time at each site. Then we tested total interface length from the 70 simulations for its ability to explain annual brown shrimp catch in estuaries adjacent to the study area. Finding a statistically significant relationship, we used it to estimate future shrimp production. We compared data from the TM imagery to simulated data from our model in order to evaluate Browder et al.'s general observations concerning the relationship of interface length to land loss and the spatial pattern of land and water.

Methods

The study can be viewed as consisting of four steps: model development, model calibration, model evaluation, and model extension. Model development consisted of refining the Browder et al. (1984) model for use with TM data. The model contains three adjustable parameters that were calibrated to the spatial patterns of land and water in 70 marsh sites in Louisiana, as indicated in TM imagery. The TM scenes were classified into land and water pixels, and several measures, or indices, of spatial pattern were obtained from each scene. We developed an expert system that used these spatial-pattern indices to select the model-parameter values to simulate the history of marsh disintegration at each site. Then we made 70 "best fit" simulations of marsh disintegration--one for each scene--and recorded the history of interface length as a function of disintegration level (DL, water area as percentage total area) throughout each simulation.

We evaluated our simulations by several methods. We used regression analysis to compare the spatial-pattern indices of the 70 simulations to those of the TM scenes. We compared the number of water-body groups in the simulation to those in the TM scene, by lobe and marsh type. We visually compared the TM scenes with our simulated scenes at the same stages of disintegration. Finally, we examined the model-parameter values selected by the expert system, comparing them by marsh type and lobe.

We extended our model results to fishery production. First we determined the relationship between brown shrimp catch and simulated interface length in the study area for the past 28 yr. Finding a statistically significant relationship, we used it to estimate future shrimp catches based on simulated future interface length.

Description of the New Model

Our new model simulates marsh disintegration by successively changing land pixels to water pixels. The relative probability that a land pixel will be converted to water at each iteration is governed by a function weighted by three adjustable parameters: interior disintegration (W), shoreline erosion (G), and border-condition (**BC**). The weighting parameters were based on Sasser et al.'s (1986) observation that two patterns of marsh disintegration occur in Louisiana. In one pattern, small, randomly spaced, gradually expanding water bodies develop in solid marshes. In the other, land disappears along the margins of major water bodies, as if lost to waves or other erosive forces. The model simulates the entire disintegration process, starting with solid land and ending with only open water. Each iteration represents passage of time, although time units are unspecified.

The pixel to be disintegrated at each iteration is selected from a numbered list by a pair of randomly generated numbers (RN). The first makes a tentative selection by matching a number on the list; the second random number determines whether the tentative selection is eligible. The pixel is eligible if its total weight at that iteration ($F_{i,j,k}$) is greater than $RN_k \cdot \max\text{-}F_{i,j}$ for that k (i and j = pixel coordinates and k = iteration). The relative probability that a specific pixel will be selected at iteration k ($RP_{i,j,k}$) is the ratio of the total weight of that pixel to the sum of the total weights of all the land pixels:

$$RP_{i,j,k} = F_{i,j,k} \Big/ \sum_{i=1}^{r} \sum_{j=1}^{c} (F_{i,j,k}), \tag{1}$$

where r = number of rows, c = number of columns,

$$F_{i,j,k} = 1 + W \cdot S_{i,j,k} + \sum_{m=1}^{4} [BC_m \cdot G_m \cdot B_{m,i,j,k}]. \tag{2}$$

W = weighting coefficient for each side of the pixel adjacent to water. $S_{i,j,k}$ = number of pixel sides adjacent to water. G = weighting coefficient for pixels bordering a major water body, by border. B = a Boolean value (1 or 0) indicating whether the pixel is on a major water body, by marsh border. Border condition is the vector **BC**. BC_m indicates which marsh borders (n, s, e, or w) are on major water bodies. (Note that throughout this paper, "side" refers to *pixel*

boundary and "border" refers to *marsh* boundary.) Once a pixel is converted to water, it is removed from the selection list, shortening it by one. Figure 1 gives a snapshot view of the progress of marsh disintegration in one simulation. The marsh is initially solid. By the time it is 25% disintegrated (DL = 25%), we see many small water bodies. Water areas are larger and are beginning to coalesce at 50% disintegration. Most water bodies are connected by the time the marsh is 75% disintegrated.

At each iteration of the model, counters keep track of the percentage of the total area that is water and the length of the land-water interface. Percentage water area is referred to throughout this discussion as the level of disintegration (DL). Land-water interface is measured in pixel-lengths--the length of one side of the square pixel. As measured, interface is homologous to the "join" statistic of Moran (1948) and is related to other spatial autocorrelation statistics indicating degree of clumping of the same pixel types (Upton and Fingleton 1985). By affecting the order of pixel disintegration, our model's weighting coefficients determine the degree of clumping of water pixels in simulated marshes. Figure 2 shows two marshes at similar stages of decay simulated by different interior-marsh-decay weighting coefficients. Note that water bodies are larger when W = 3,184 (bottom) than when W = 248 (top). (The erosion weighting coefficient was zero for both.)

The new model differs from the Browder et al. (1984) model in several important details. In the original model, only pixels *initially* on a major water body had the G-weighting (B = 1). The G-effect was inconsequential in sensitivity tests, particularly as the size of the simulated marsh increased. In the new model, any pixel can eventually be assigned B = 1, if it is connected to a designated water border by a continuous water path. The G-parameter now has a much greater effect. The new model allows flexibility in the initial identification of water borders, and up to four water borders can be set. The pixel-selection procedure of the new model is an improvement that made it practical to simulate marshes having as many pixels as the TM images of our study sites, 192 x 192. Appendix B presents the spatial-pattern statistics of simulations using all combinations of W, G, and BC. The new model and all ancillary programs were written in C and executed on an AT&T PC-7300, a 16-bit, 10-MHz computer with a Unix-V operating system.

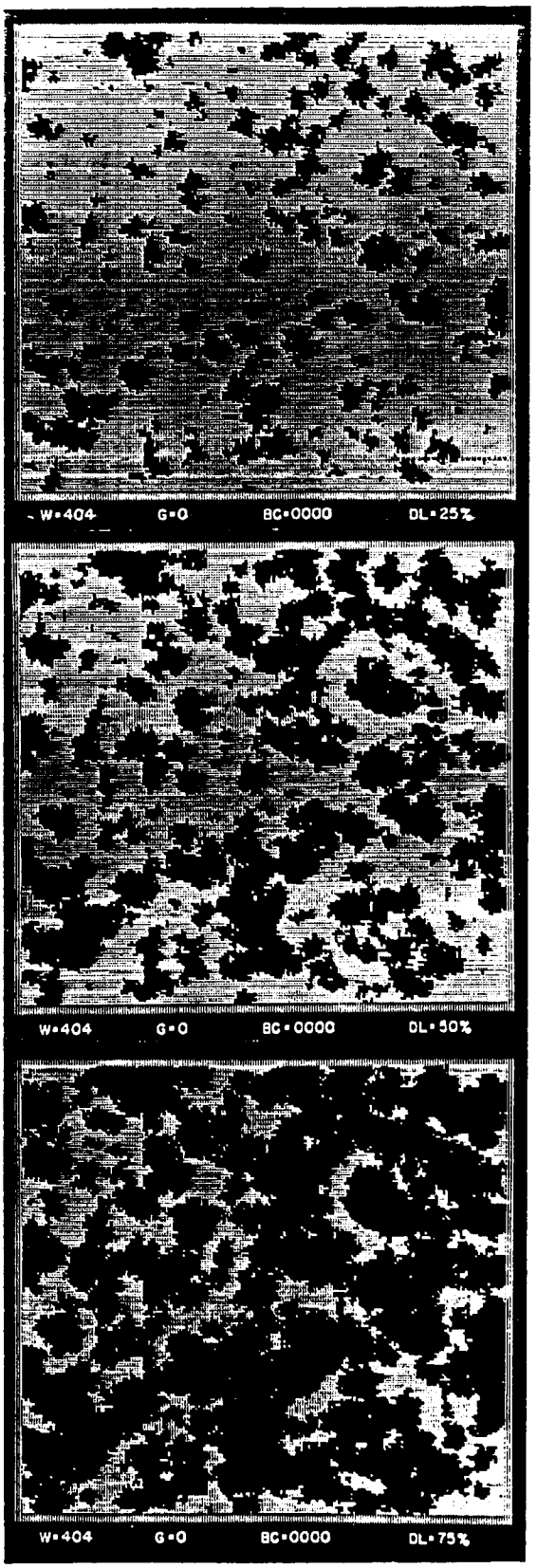

Figure 1. Snapshot view of simulated marsh disintegration at the 25%, 50%, and 75% disintegration levels (percentage open water area).

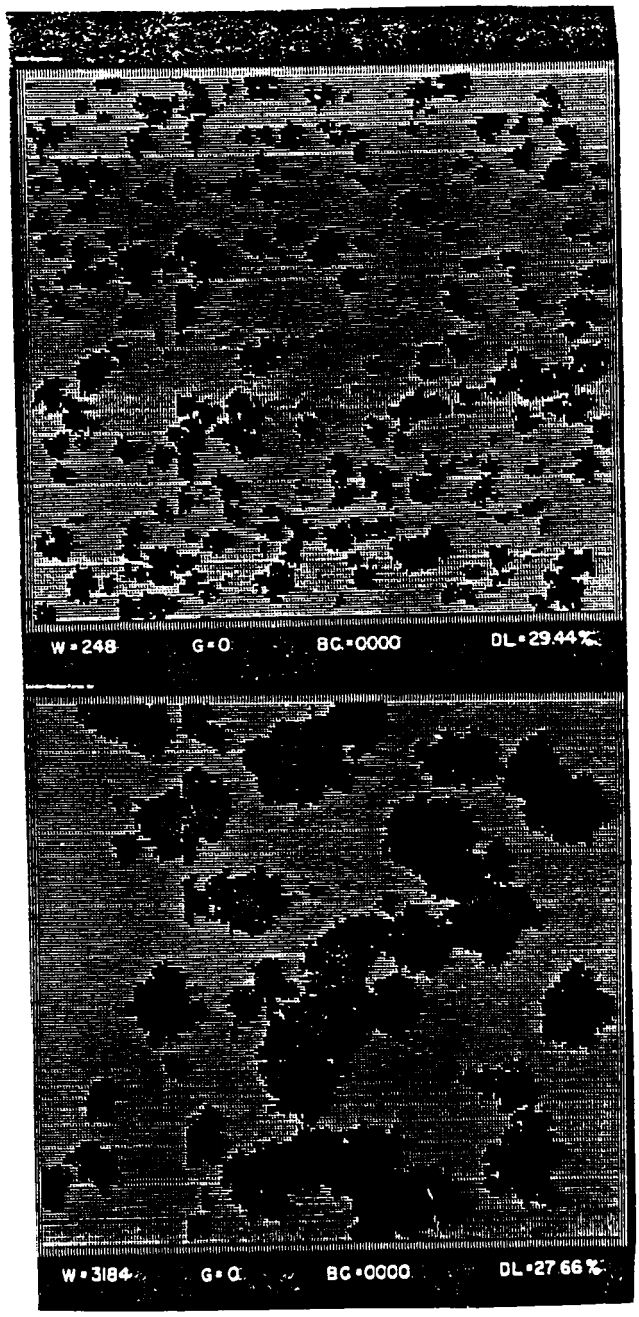

Figure 2. Two simulated marshes at similar levels of disintegration, produced by different values of W, the interior-marsh-decay weighting factor.

Model Calibration

TM image processing. We analyzed the TM scenes on the Fisheries Image Processing System (FIPS) of the National Marine Fisheries Service (NMFS) in Slidell, Louisiana, and a system operated by the Florida Department of Natural Resources in St. Petersburg. Both systems consisted of a minicomputer, color-image display device, and other hardware for processing remotely sensed digital data. The software was a modified version of the Earth Resources Laboratory Applications Software (ELAS) (Graham et al. 1984).

The TM image we used was from a 2 December 1984 Landsat-5 overflight (Scene ID: 50276016022). Covering most of the Mississippi deltaic plain, it was one of the few relatively cloud-free images of our study area (quads 1 and 2 in path 22 and row 40 of the World-Wide Reference System).

ELAS modules PMGC (Georef constants-EROS format) and PMGE (Georef-EROS format) (Graham et al. 1984) were used to digitally rotate the images to fit a Universal Transverse Mercator projection with a north-south orientation. We used these modules to accumulate ground-control points, generate polynomial least-squares mapping equations, and resample the image with bilinear interpolation. Registration accuracies averaged 22-56 m. Resolution was the length of a TM pixel side, 30 m. Land and water pixels were classified by multiplying bands 4 and 5 (0.76-0.90 μm and 1.55-1.75 μm, respectively), rescaling to 0-255, and applying Pun's (1981) global thresholding technique.

Study-site selection. The study sites are located on two abandoned delta lobes of different ages. The early Lafourche lobe was an actively prograding delta within the last 1,800 yr. The late Lafourche lobe was an active distributary of the river within the last 600 yr. Chabreck (1972) distinguished four major types of Louisiana coastal marsh on the basis of vegetation: salt, brackish, intermediate, and fresh. Salt and brackish marshes are the most important marshes to estuarine-dependent fishery species and show a wide range of decay stages. For these reasons, we limited our study to these two more seaward marsh types.

Site locations are within the areas represented by 21 U.S. Geological Survey 7.5-min topographic maps. We used these maps and a coastal habitat map (Chabreck and Linscombe 1978), coupled with our extensive field experience, to distinguish brackish and salt marsh. We defined potential boundaries of study sites by dividing the area of the TM image corresponding

to each topographic map into four contiguous quarters measuring 192 x 192 pixels (5,760 x 5,760 m, roughly 33.18 km^2). The intersection of the quarters corresponded to the center of the map. We selected 70 marsh sites: 38 salt (20 on one lobe, 18 on the other) and 32 brackish (19 and 13 per lobe) (Fig. 3).

Measurement of spatial-pattern indices. We generated 70 binary land-water images from the band-4-x-band-5 images. To measure our spatial-pattern indices, we tabulated the following using ELAS command strings: (1) number of land and water pixels (to determine percentage water area = disintegration level [DL]); (2) number of water pixels by scan line and element column (to determine border condition); (3) number of land-water pixel-side contacts (interface length); (4) number of water pixels, excluding border pixels, with sides adjacent to zero, one, two, three, or four other water pixels (which we will refer to hereafter as the "side-adjacency" statistics); and (5) number of pixels in each water body (water-body size). Diagonal, or corner, contacts by water pixels were considered to connect two parts of the same water body.

We tabulated interface length in a three-step process. First, we generated an intermediate image using the ELAS shoreline-length (SLIN) module (Graham et al. 1984). SLIN uses a 3-x-3-pixel moving-window technique to classify each *land* pixel adjacent to water into 1 of 69 shoreline categories (Dow, 1982; Dow and Pearson, 1982). Second, we used a look-up table to convert the SLIN image to an image file of six classes: land and water pixels and *land* shoreline pixels having one, two, three, or four sides adjacent to water. Our principal spatial-pattern index, interface, was determined by counting the *land*-pixel sides adjacent to water pixels. We determined the number of *water*-pixel sides adjacent to other water pixels with a similar technique to obtain the side-adjacency statistics, which were our other major indices of spatial pattern. Two processing changes were required: *water* pixels adjacent to land were defined as *water* shoreline pixels in SLIN-module processing; and a new look-up table was used to classify *water* pixels with zero, one, two, three, or four sides adjacent to other water pixels. The water-body classifier (WBOD) of ELAS was used to determine water-body size.

The length of an irregular shoreline is a function of measurement unit (Mandelbrot 1967). Our measurements of land-water interface and, possibly, other spatial-pattern indices are valid

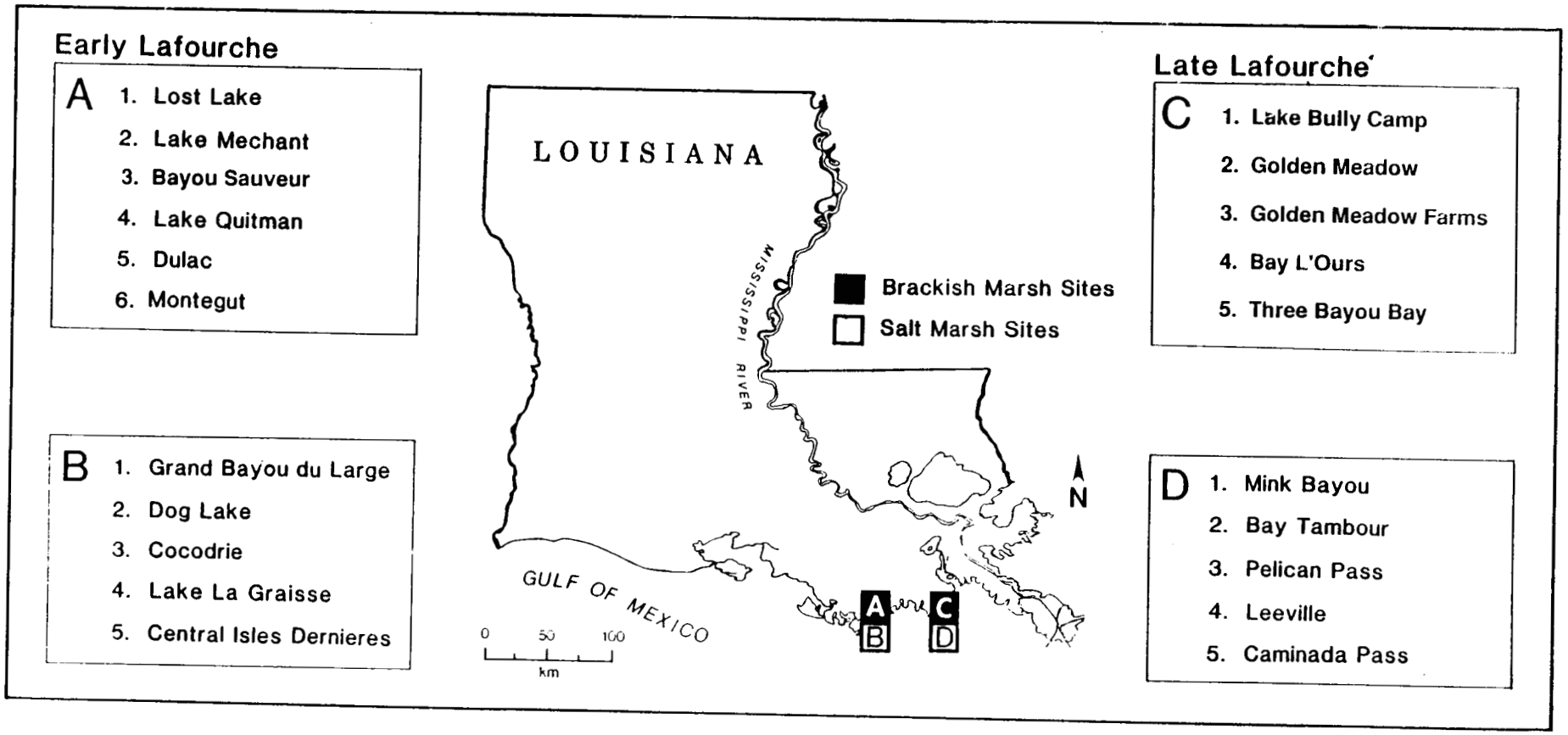

Figure 3. Map of Louisiana showing study area and corresponding U.S. Geological Survey topographic maps covering the area.

only at TM resolution, 30 m. Appendix C presents the spatial-pattern statistics of the TM scenes.

Calibrating the model. An expert system, consisting of a knowledge base and decision process, selected the model parameters W, G, and BC to best approximate the spatial patterns of each study site. Selections were made by matching certain spatial-pattern indices of the imagery to those in a knowledge base built from simulations. Interface length, the five side-adjacency statistics, and a "target" border condition were the indices to be matched. The knowledge base showed how these variables changed in model executions as functions of W, G, and BC. The decision process consisted of rules for selecting the best W-G-BC combination.

The knowledge base was built by running simulations with all possible W and G combinations from the set [0, 4, 20, 60, 180, and 540] for the six types of BC. (Throughout this report, BC is given six possible Boolean values: 0000, 0001, 0011, 0101, 0111, and 1111, which show the specific spatial relationships of the borders, 0 indicating land and 1, water.) For BC = 0000, the set was extended to include W = 1,620 and 9,720. (In addition, power functions extrapolated to larger W's.) Target BC is determined by comparing DL to the percentage water pixels (P_m) in each row or column forming the outer border of the marsh, as follows:

$$\text{Target } BC_m = 1 \text{ if } P_m > DL. \tag{2}$$

The spatial-pattern indices of simulated marshes at the same DL as the study site were used to obtain one or more weighted mean W for every G-BC combination. For each G-BC, there could be one or more W based on each spatial-pattern index. To calculate the mean, W's were weighted by the number of water pixels of the index. For instance, if Adj-4 = 1,940, the weight given to the W obtained by matching this index was 1,940. The weight given to the W obtained by matching interface length was the sum of all water pixels. The weights used to calculate mean W were summed to calculate a "decision number" (DE) for each weighted mean W. DE was used to select the best W-G-BC from the many alternatives calculated for each site.

Another criterion used to select the best W-G-BC was coefficient of variation of the weighted mean W (CV). CV was a useful criterion because low CV indicated a high degree of convergence of W's estimated from all contributing spatial-pattern indices.

BC was the main criterion used to select the best W-G-BC combination. If the target BC was not matched by a solution meeting other criteria, the solution having BC most similar to the

target was selected. In our 70 cases, **BC** usually matched target **BC** or differed by only one border. The decision algorithm selected the W-G-**BC** combination having, first, **BC** most similar to target **BC**; second, high DE (within at least 75% of the highest DE among all alternative W-G-**BC** combinations); and third, lowest CV (see Appendix D, F).

Simulation of study-site spatial patterns. Once selected, model parameters were used to simulate the spatial pattern of each study site and the change in land-water interface with land loss. The land-water maps and spatial-pattern indices of the 70 simulated marshes were captured at the same levels of disintegration as corresponding study sites. In addition, interface length was recorded at each 5% level of disintegration as the simulation proceeded from solid land to open water.

Analysis of brown shrimp catch data. To relate marsh-water interface to annual fishery catch data, we needed to estimate interface length as a function of time. Interface length in our model output was expressed as a function of DL, not time. Therefore, we needed an estimate of the time trend in DL. We used data from Wicker's 1956 and 1978 maps (1980) to estimate this trend. The data were compiled by Liebowitz (Louisiana State University, private communication, 1988), who provided us with water area for each topographic-map area corresponding to our study sites. We estimated average annual change in DL per topographic-map area by expressing water area in 1956 and 1978 as percentage total area and calculating the annual average of the difference. This assumed a linear trend in water area from 1956 to 1978, which we projected into the future. We aggregated the data for each site to obtain, for each lobe, an estimate of interface, by year, from 1956 until the future total loss of marsh and interface. (An in-depth comparison of 1956 and 1978 data from the Wicker maps is presented in Liebowitz and Hill [1988].)

Using regression analysis, we compared 1960-1987 of the simulated interface time-series with unpublished brown shrimp catch data for Barataria, Timbalier, and Terrebonne bays for the same period (G. Davenport, NMFS, Miami, personal communication, 1988) to estimate a relationship between catch and interface. (Barataria Bay is associated with the late Lafourche lobe, and Timbalier and Terrebonne bays are associated with the early Lafourche lobe.) We predicted future shrimp catches from this relationship. Included as independent variables in the

analysis were local rainfall (R. Muller, Louisiana State University, personal communication, 1988) and number of hours from April 9 through 30 in which temperatures were below 20°C (Barrett and Gillespie 1975; B. Barrett, Louisiana Department of Wildlife and Fisheries, personal communication, 1988). Barrett and Gillespie (1975) suggested that salinity and the temperature variable affected brown shrimp catches. We used rainfall as an inverse surrogate for salinity. Lack of reliable effort data precluded inclusion of this variable in our analysis.

Results

Results are organized as (1) interface length versus disintegration level of study sites, (2) evaluation of simulations, (3) simulated site-specific interface length versus DL, (4) aggregated interface length versus year, and (5) possible impacts on fisheries.

Interface Length versus Disintegration Level of Study Sites

A plot of interface length versus DL measured in the classified imagery of the study sites (Fig. 4) suggests that interface increased in the early stages of disintegration, reached a maximum when marshes were 30%-50% disintegrated, and decreased thereafter. Statistically significant ($p < .1$) parabolas were fit to separate data for salt and brackish sites. Most salt marsh sites were more than 50% disintegrated, whereas the DL of brackish sites ranged from low to high. DL and interface length did not differ significantly between early and late lobes, possibly because we excluded open-water areas of both lobes from our analysis.

Evaluation of Simulations

Following are the results of our evaluations of how well the simulations represented the spatial patterns of the study sites. Appendices E and G provide further specific comparisons in tabluar and graphic formats.

Agreement of simulation and study-site interface. Interface length in each simulation was obtained at the same DL as the TM scene it represented. Then the 70 simulation interfaces were regressed on the corresponding TM-scene interfaces. TM-scene interface explained 94% of the variation in simulation interface. The slope of the relationship was 1.06. The greatest

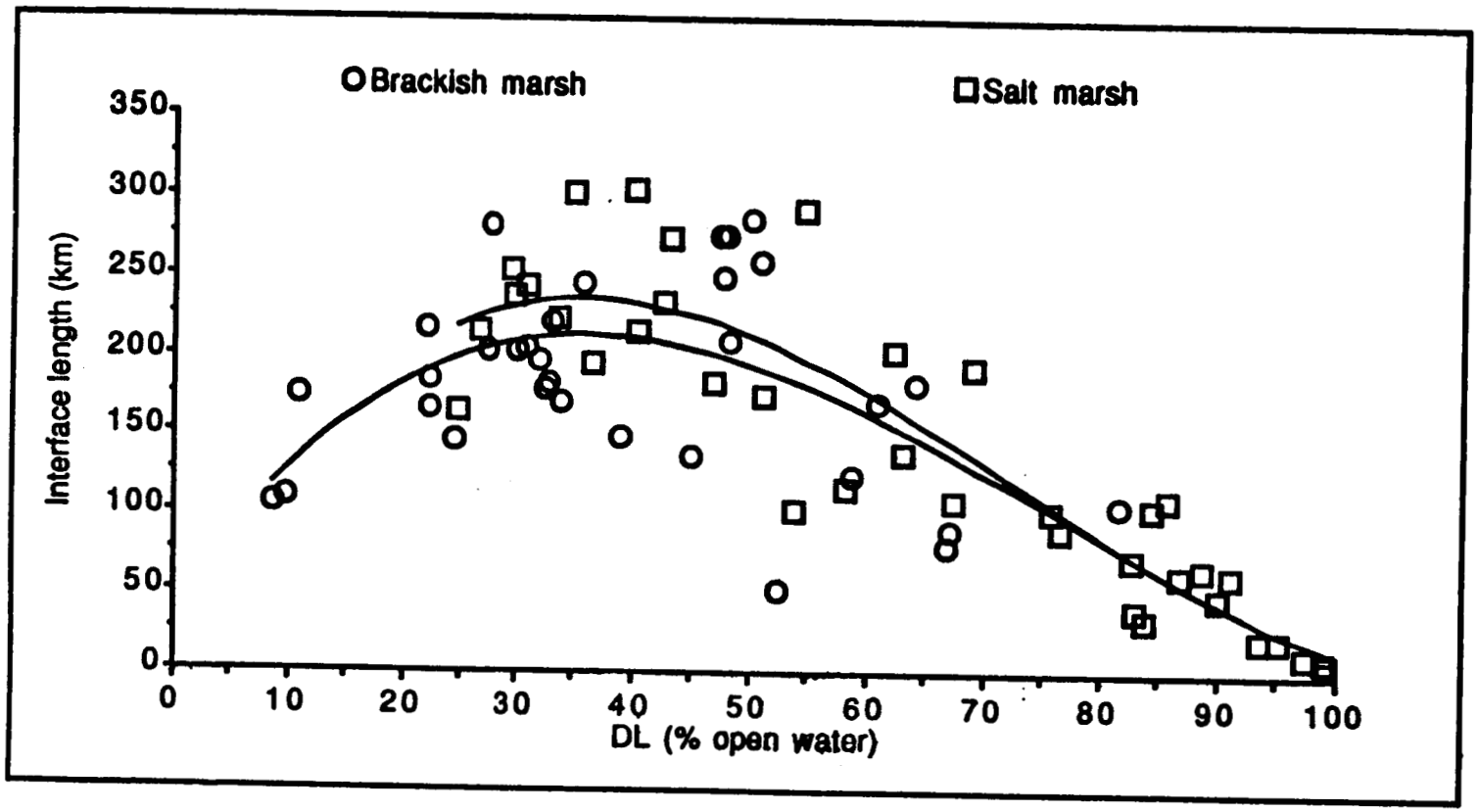

Figure 4. Interface length versus disintegration level (percentage open water area).

departures of simulation from TM-scene interfaces were in the highest values. In most departures, the simulation value was higher than the TM-scene value. Half the simulation interface lengths differed from corresponding TM-scene values by no more than 10%, and 86% differed by no more than 30%. The average absolute difference was 11.7%.

Regression of simulation side-adjacency statistics on their TM-scene corollaries indicated highly significant relationships (F-stat. $p < .001$) for all but Adj-0, with 56%-99% of the variation in the simulation values explained by TM-scene values. R^2's were 0.56 for Adj-1, 0.91 for Adj-2, 0.80 for Adj-3, and 0.99 for Adj-4. Their slope coefficients varied from 0.97 to 1.21. The poor fit of simulation Adj-0 to TM-scene Adj-0 probably was largely due to the usually low value and resultant extremely small influence of this spatial-pattern index in the decision process.

Variation in simulation indices. Three replicate simulations with three sets of model-parameter values revealed the variation in simulation spatial-pattern indices caused by the random aspect of the model. CV averaged across all the spatial-pattern indices ranged from 4.9% to 19.3%. It was highest in the three replicate simulations where G = 540 and lowest in those where G = 0. The CV of Adj-0 was extremely high in the sets of replicate simulations in which G = 180 (CV = 53%) and G = 540)CV = 71%), probably because of the low value of Adj-0 (less than 20 pixels in all cases). Average CV's for the other side-adjacency statistics ranged from 2.17% for Adj-4 to 7.34% for Adj-2. The CV of interface length averaged 6.28%.

Water-body size groups. Water-body size data for sites and simulations were difficult to compare because water bodies were few and their size range enormous. Rather than grouping them by even intervals, we defined breaks between size groups with the following consistently applied algorithm. In a list of water bodies sorted by size, a break was defined if the larger of two adjacent water bodies was more than twice the size of the smaller. Upper and lower boundaries were placed on water-body size groups for each marsh unit. Figure 5 summarizes the differences between number of water-body size groups in each case. The study sites and their simulations had the same number of water-body groups in 23 of 70 cases. In 59 cases, study sites and simulations differed by no more than one group. This was good agreement considering that the status of one pixel in a strategic location could determine whether two

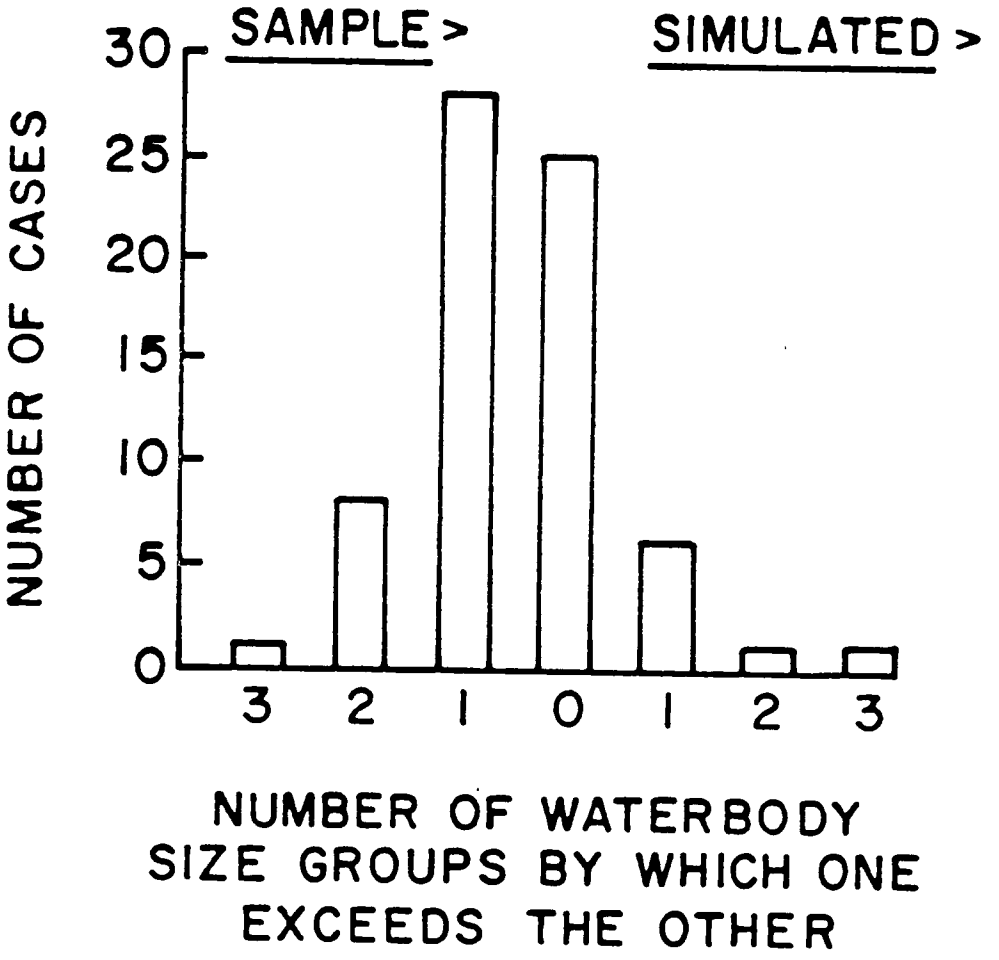

Figure 5. Frequency distribution of cases by difference between number of water-body size groups. Values on the abscissa indicate the number of groups by which the study site exceeds the simulation (values to the left of zero).

clumps of pixels formed one water body or two. Usually, the study site had more groups than the simulated marsh. The average number per study site was 2.7, whereas the average number per simulated marsh was 2.3. Two groups were distinguished for most marshes. Typically, a small percentage of water pixels were distributed among many small water bodies, and the rest were in one large water body. For example, in one study site, 4.3% of the water pixels were in water bodies that included 0.003%-0.752% of the total water pixels, whereas 95.5% were in one water body. Water-body groups in the corresponding simulation were similar. Generally, when more than two water-body groups occurred, the additional ones were at the lower end of the size range.

Visual evaluation. Visual comparisons suggested that the model often succeeded in simulating spatial patterns of the TM scenes, except when high G-values were used to simulate brackish marshes. The simulations did not appear to accurately represent those patterns of land and water heavily influenced by underlying geologic features, such as ridge/swale topography or large lakes, nor man-made features such as canals and diked areas. Despite limitations, the model simulated the general patterns of most marshes well, and matched a few remarkably well. The marsh map in Figure 6 (bottom) was simulated with an interior-marsh-decay coefficient of 311, a shoreline-erosion coefficient of 540, and a BC of 0001. At a DL of 68.89%, it displays a spatial pattern of land and water very similar to that of the classified TM scene at the same decay stage (Fig. 6, top). Interface length in the simulation map differed from that in the TM scene by 10.2%.

Model-parameter values. Some generalizations can be made about the appropriate model-parameter values for simulating marsh disintegration. Lobe age did not appear to influence parameter values, whereas marsh type seemed to be an influencing factor. Based on the knowledge base and our criteria, the expert system gave salt marshes higher shoreline-erosion coefficients, more water borders, and lower interior-decay coefficients than it gave to brackish marshes (Fig. 7). W and G were inversely related in the expert system's selections (Fig. 8A). Our visual comparisons suggested that low-to-medium values of G (0-180) and moderately high values of W (about 200-400) matched the spatial patterns of brackish TM scenes best. Conversely, high G-values (180 and 540) gave the best match to salt marsh scenes. Because salt

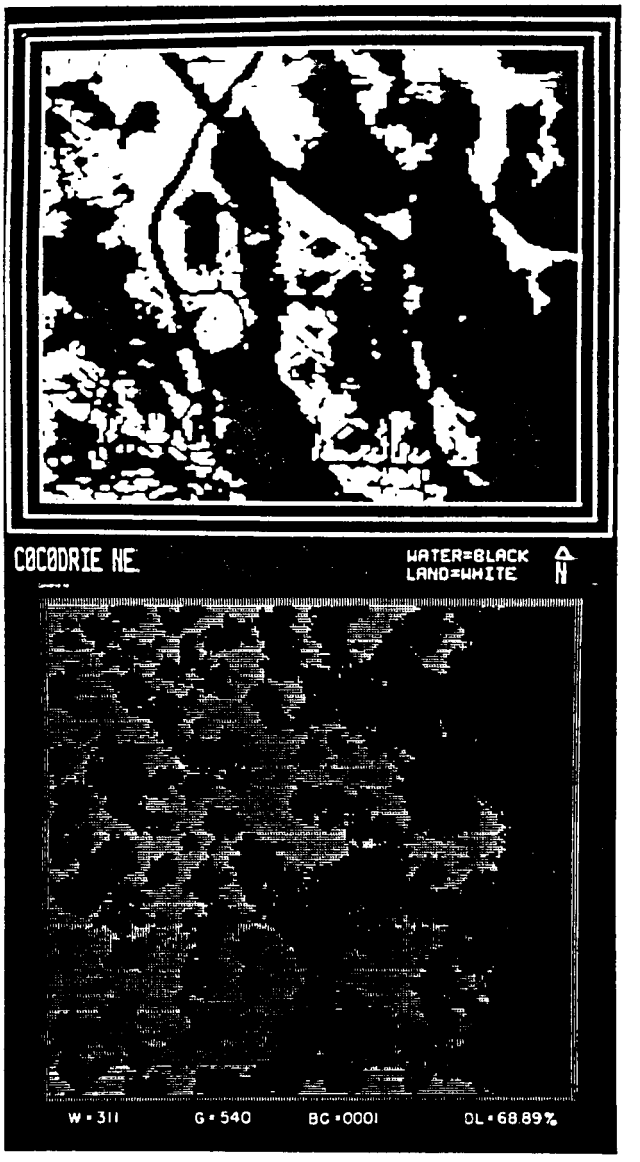

Figure 6. Land-water image of a study site (top) and its simulation (bottom) showing disintegration level (DL) and model coefficients (W, G, and BC) used in the simulation. (In BC, 0 = land and 1 = water.)

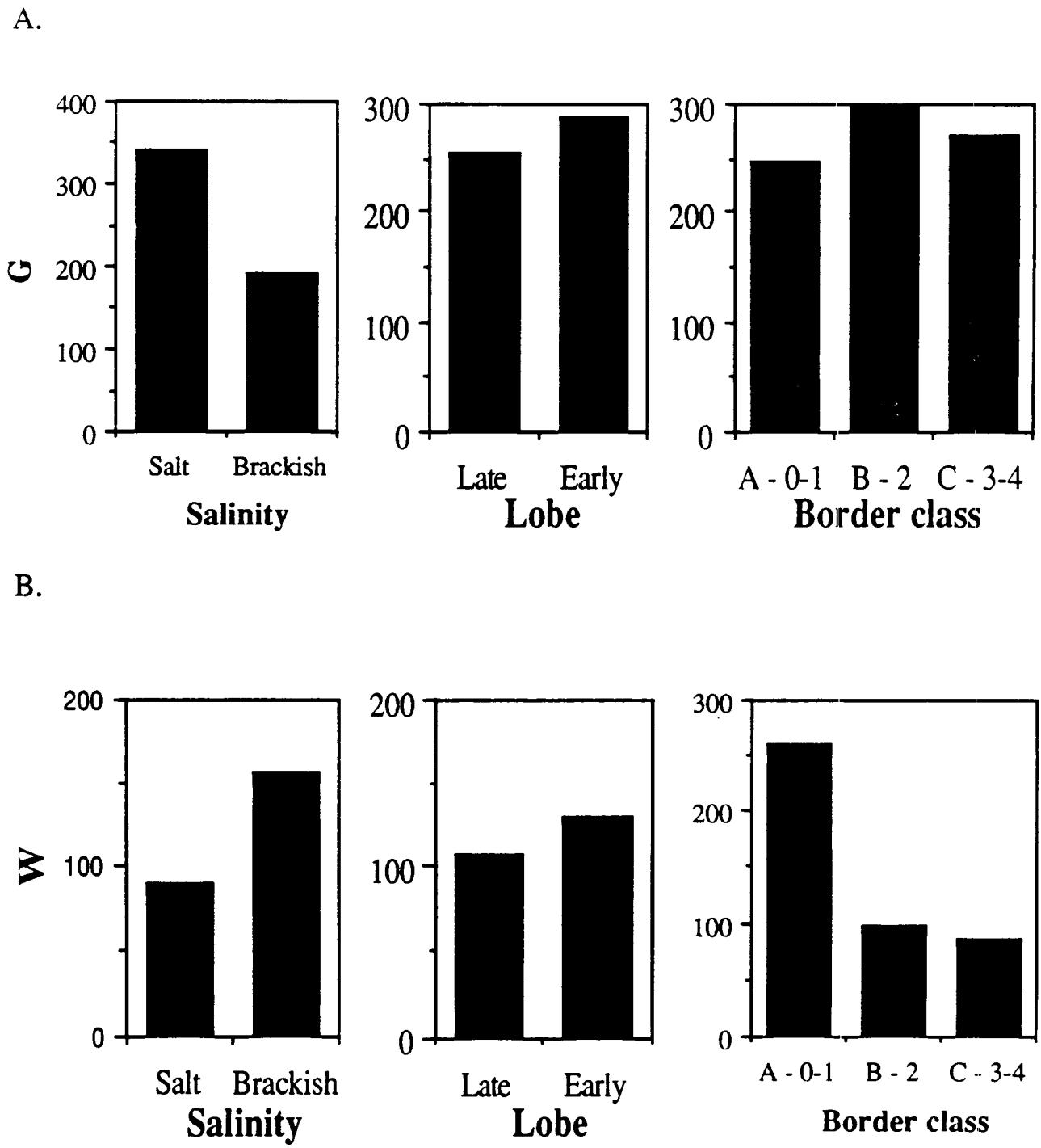

Figure 7. (A) Average G weighting factor (shoreline erosion) and (B) average W weighting factor (interior-marsh-decay) selected by the expert system, by marsh type, lobe (early or late Lafourche), and border condition (BC). (Two extremely high outliers were excluded in cacluclating average W.)

A.

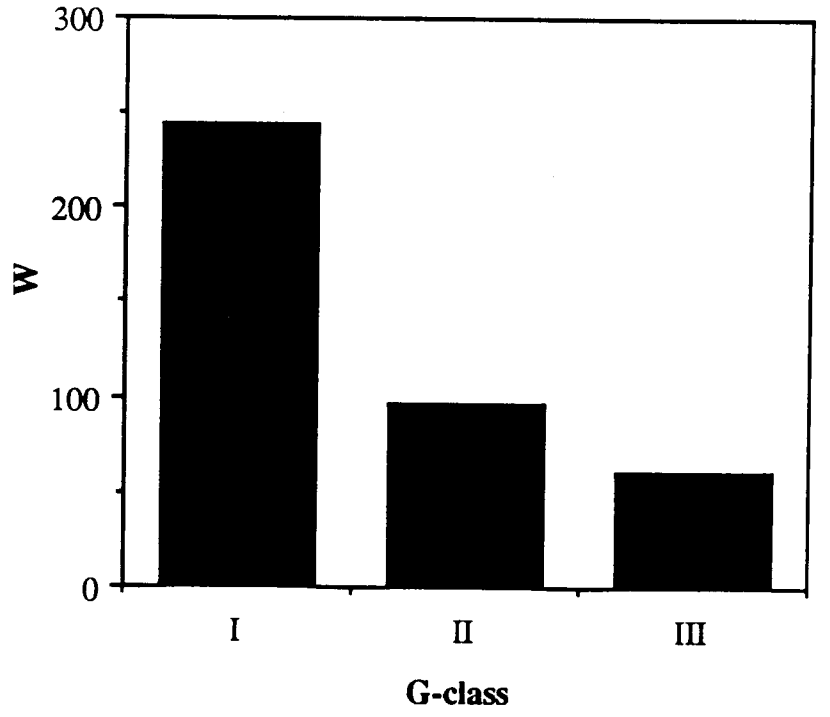

B.

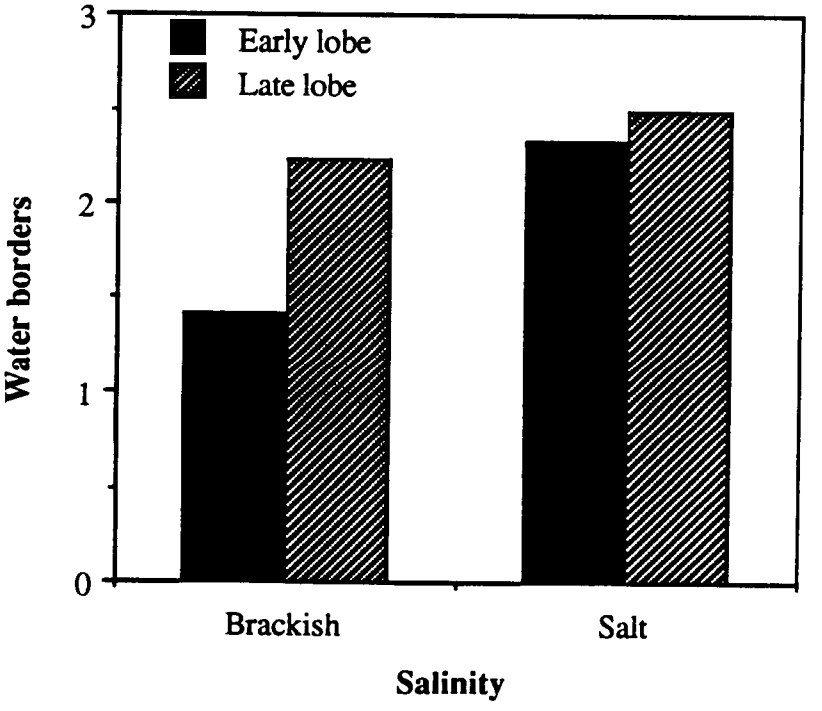

Figure 8. (A) Average W by G-class (Class 1, G = 0, 4, 20, or 60; Class 2, G = 180; Class 3, G = 540).

(B) Average border condition (BC) selected by the expert system, by marsh type and lobe.

marshes have more borders on major water bodies, shoreline erosion is more prevalent in them than is interior decay (Fig. 8B). Interior decay weighting coefficients selected by the expert system were highest for simulated marshes having the fewest water borders (Fig. 7B), which were primarily the brackish marshes (Fig. 8B).

Simulated Site-Specific Interface Length versus DL

We followed interface from 100% land to 100% water in each of the 70 simulations. Many simulations were similar to those of Lost Lake NW, Mink Bayou SW, and Mink Bayou SE (Fig. 9). Interface reached a maximum approaching 10,000 pixel-lengths (300 km) when the marsh was roughly 50% disintegrated. Interface in Pelican Pass SW (Fig. 9) followed a strikingly different path, reaching its unusually low maximum of 2,417 at a DL of only 11%. This is one of two simulations that differed markedly from the rest in reaching maximum interface at a low DL. Both were simulated with G = 540 and BC = 1111. The distribution of maximum interface in the 70 simulations was bimodal, with a lower peak around 2,000-4,000 pixel-lengths and a higher one at 9,000 (Fig. 10A). DL at maximum interface was between 45% and 60% in most simulated marshes (Fig. 10B). Based on the simulations, 37 sites had not yet reached the DL of maximum interface in 1985, whereas two were at maximum-interface DL, and 31 were beyond it (Fig. 10C).

Aggregated Interface Length versus Year

Aggregated 1985 simulation interface was 406,051 pixel-lengths (12,182 km)--82% of the aggregated maximum interface of 496,969 pixel-lengths (14,909 km). According to our estimates from Wicker's (1980) map data, the average annual change in DL in the USGS-topographic-map areas of our study sites varied from 0.125% to 1.145% per year (Appendix H). Using these trends and the year of our TM image to relate DL to time, we transformed our individual-site plots of interface versus DL to the lobe-aggregated plots of interface versus time in Figure 11. Our hindcasts (1956-1985) and predictions (1985+) of interface are plotted as fractions of total maximum interface. The interface curves do not reach 1.0 because all the simulated marshes will not reach their interface maxima concurrently. The 1985 points are near the two maxima on the ascending side. These results suggest that total land-water interface in both deltaic areas has been increasing, but will soon begin decreasing. If the estimated linear

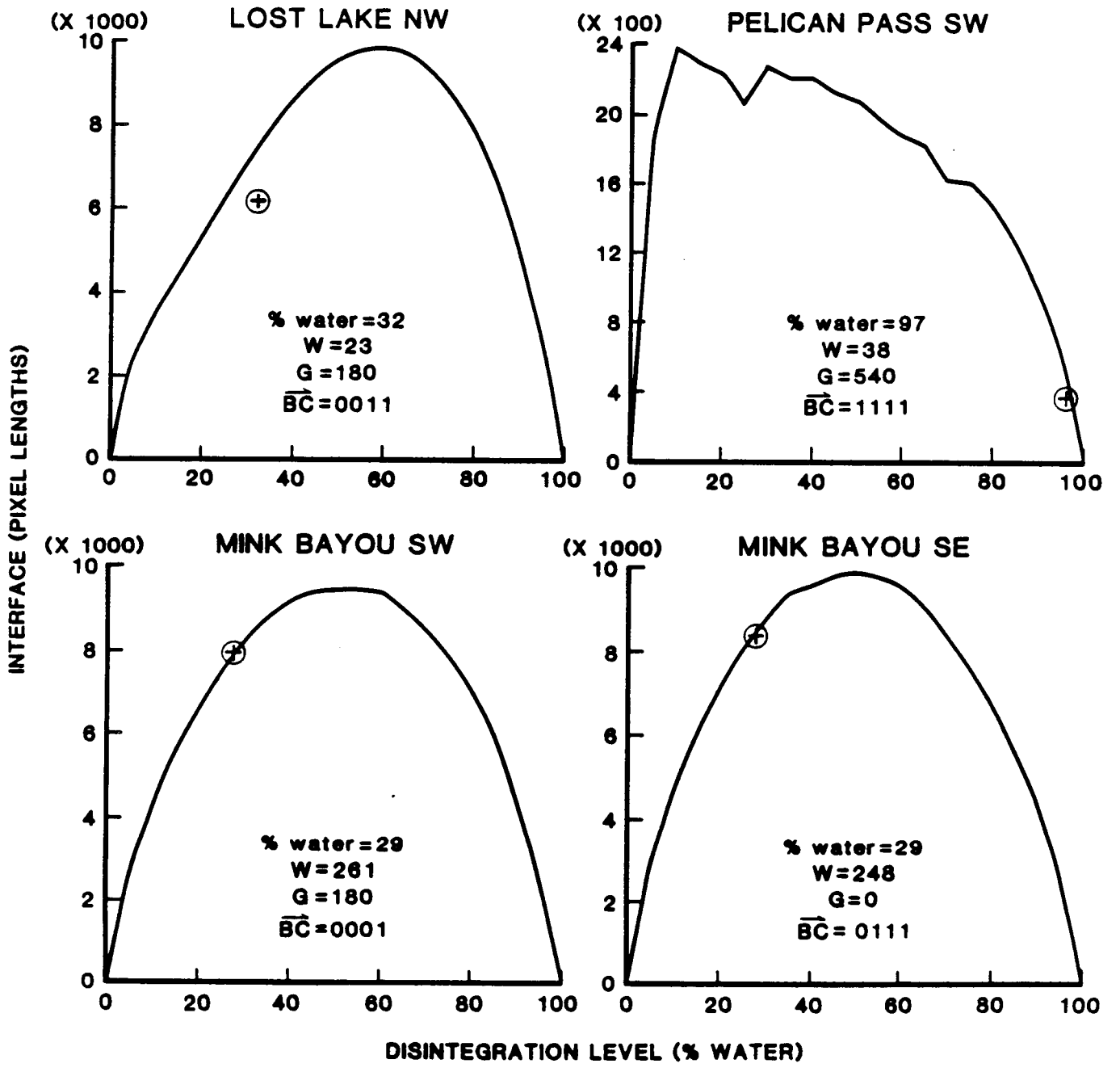

Figure 9. Simulated interface versus disintegration level (DL) for 4 of the 70 cases showing the modeling coefficients (W, G, and BC) used in the simulation.

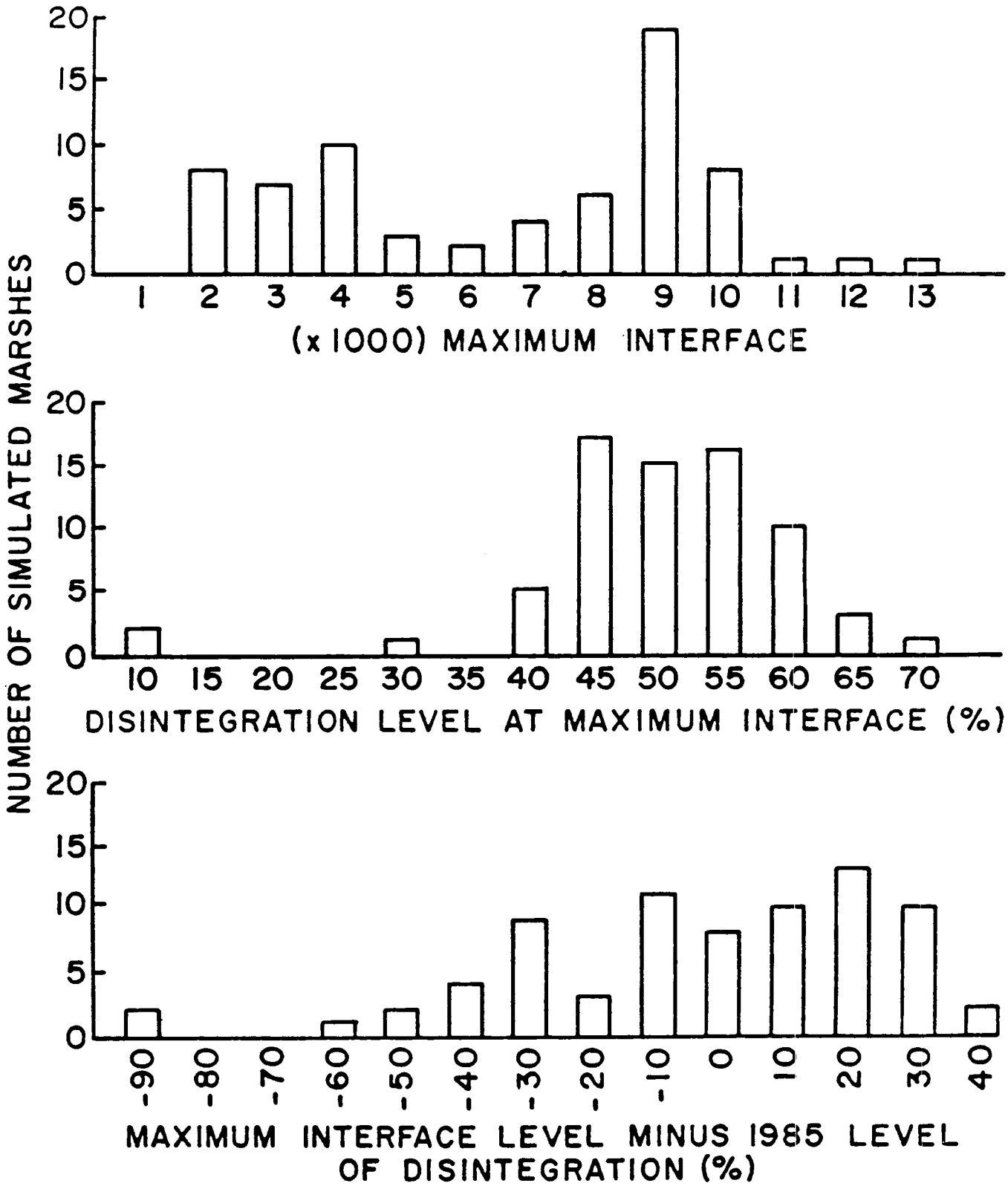

Figure 10. Frequency distributions of cases by simulation maximum interface (A), disintegration level (DL) at maximum interface (B), and maximum-interface DL minus 1985 DL (C). Numbers on the abscissas are the upper values of each interval.

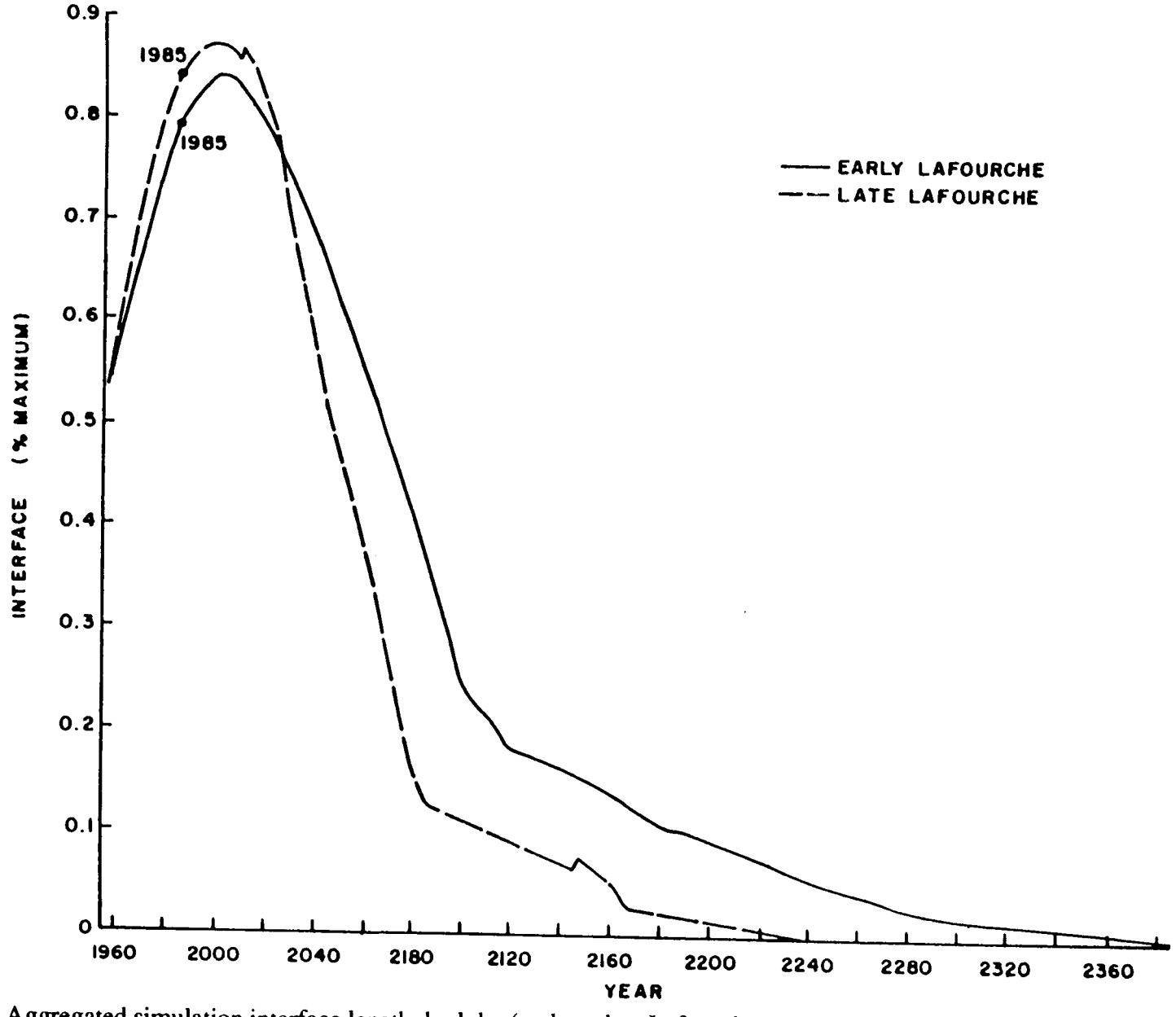

Figure 11. Aggregated simulation interface length, by lobe (early or late Lafourche), expressed as a fraction of aggregated maximum interface, versus year

trends in DL are accurate, the decline will begin about 1995. Sasser et al. (1986) reported an exponential rate of loss in our study area. On the other hand, recent observations by Liebowitz (personal communication) suggest that some large water areas that appeared between 1956 and 1978 may not be growing.

Possible Impacts on Fisheries

We found a statistically significant ($p < .0001$) relationship between brown shrimp catch and interface. The equation is as follows:

$$Y_p = -61.046 + 277.55 \cdot X_1 - 0.39198 \cdot X_2 - 0.12948 \cdot X_3 \quad (3)$$

where Y_p = catch per unit area, X_1 = interface length in pixel sides, X_2 = rainfall in centimeters, and X_3 = hours from April 9 through 30 in which temperatures were below 20°C. The equation explained 49% of the variation in catch for 1960-1987 (Appendix I). Interface length alone explained 32%. The percentage variation in annual catch explained by the equation was high, considering that effort, usually a major factor influencing catch, was not included as an independent variable. Using our interface projections and assuming average conditions of the other independent variables, the equation predicts that brown shrimp catches dependent upon Barataria, Timbalier, and Terrebonne bays may fall to zero within 75 yr (equation confidence limits 52 and 105 yr). Confidence limits do not include the error associated with predicted interface.

Discussion

Our model and expert system appear to have been successful in simulating general features of the spatial patterns of most study sites. The model was not designed to reproduce the exact locations of land and water in each study site but, rather, the general characteristics of the land-water pattern. Since the model is probabilistic, it produced a different pattern in every execution with the same W-G-BC combination. Necessary built-in restrictions such as having only six possible values of G and the same G for all water borders limited our versatility in matching spatial patterns. We could have matched the interface length of the TM scenes more closely had we not also matched the side-adjacency statistics. But selecting W-G-BC on the basis of both interface length and the side-adjacency statistics increased the probability that the

trajectory of interface change with land loss during each simulation of marsh disintegration was realistic for the site.

The statistically significant fit of a parabola to the plot of interface-length versus DL of our 70 TM scenes (Fig. 4) supports Browder et al.'s (1984) first conclusion: In the progress of marsh decay, interface length increases initially, reaches a maximum, and then decreases. The scatter of points about the parabola (Fig. 4) supports their second conclusion: The magnitude of maximum interface (and, consequently, the trajectory of interface change with land loss) differs from marsh to marsh. Our expert system selected model-parameter values to simulate marsh disintegration at each site on the basis of spatial-pattern indices measured in the site's TM scene. The site-specific parameters produced considerably different trajectories of interface change with land loss. Maximum interface varied from about 2,000 pixel-lengths (60 km) to over 13,000 (390 km) (Fig. 10A), and DL at maximum interface varied from about 10% to 70% (Fig. 10B) in the 70 simulations. Simulations with the Browder et al. (1984) model consistently reached maximum interface at a DL of about 50%. Apparently, the greater power of the G-weighting coefficient in our model gave it more flexibility in simulating interface trajectories. Nevertheless, our 70 simulation results were centered around a mean DL at maximum interface of 52.7% (S.D. = 9.95).

In the plot of interface length versus DL with TM-scene data, DL at maximum interface was between 30% and 50%. This might appear to conflict with the site-specific simulation results, summarized in Figure 10B, which suggest that interfaces reach their maxima in most of the sites when they are 45%-60% disintegrated. But, when we plotted the simulated 1985 interface lengths against DL, we found that these data, too, reached maximum interface at 30%-50% DL. Apparently, a plot of interface length versus DL at many sites in different stages of disintegration does not precisely reflect the generalized shape of the curve of interface versus DL at the individual sites.

The resolution of TM imagery seemed adequate for this analysis. Many water features were recognizable that would not have been noticeable in MSS imagery. Our model might be useful for roughly estimating the history of interface length with disintegration in other marshes, even in the absence of the detailed spatial data we acquired for our 70 sites. On the basis of our results, model coefficients could be set as follows: BC = observed water borders, G = our

mean or modal value for salt or brackish marsh (Fig. 7A), and W = our mean or modal value for that border class (Fig. 7B).

Summary

We demonstrated with TM imagery the general relationship of land-water interface length to stage of disintegration. We then simulated the disintegration of 70 specific marshes from hypothetical starting points of solid land, through their present states of disintegration, to total conversion to water. We used unpublished data from digitized maps (Wicker 1980) to quantify site-specific disintegration rates, and we hindcasted and forecasted land-water interface as a function of time. We then aggregated the site-specific data to produce an estimate of interface length, by year, on each lobe. The relationship with time may be tenuous because we assumed a linear trend based on only two points in time. Nevertheless, relating our results to time, even if only roughly, helps the reader comprehend the immediacy of the problem.

We found a statistically significant relationship between a time series of fishery catch data and the length of the land-water interface. Others have found relationships between spatial data on fishery catch and interface. Our analysis may overestimate the importance of interface to brown shrimp production because the conversion of freshwater marsh to brackish marsh (or some other factor not included in our equation) might ameliorate the effect of interface loss in salt and brackish marsh. Nevertheless, the shape of our curve of interface over time, today's location on that curve, and our contribution to the mounting evidence relating fishery catches to interface length should be seriously regarded.

Acknowledgments

We thank the following colleagues for their valuable help during this study: Andrew Kemmerer, Gerald Williamson, Rex Herron, Thomas Leming, Robert Muller, Barney Barrett, Scott Liebowitz, Kenneth Haddad, John Barker, Sharon Rickman, Ferron Risinger, Floyd Stayner, James Scurry, Deborah Fuller, Amy Karns, Mary Hester, Ann Slater, Robin Graham, Robert O'Neill, and three anonymous reviewers. This project was largely funded by a grant from the National Atmospheric and Space Administration under the Thematic Mapper Program. The Beaufort (NC), Mississippi, and Miami (FL) Laboratories of the Southeast Fisheries Center, NMFS, NOAA, also contributed substantially to this project.

References

Barrett, B. B., and M. C. Gillespie. 1975. 1975 Environmental conditions relative to shrimp production in coastal Louisiana. Louisiana Wildlife and Fisheries Tech. Bull. 15.

Baumann, R. H., J. W. Day, Jr., and C. A. Miller. 1984. Mississippi deltaic wetland survival: sedimentation vs coastal submergence. Science 224:1093-1095.

Boesch, D. F., and R. E. Turner. 1984. Dependence of fishery species on salt marshes: the role of food and refuge. Estuaries 7:460-468.

Browder, J. A., H. A. Bartley, and K. S. Davis. 1984. A probabilistic model of the relationship between marshland-water interface and marsh disintegration. Ecological Modeling 29:245-260.

Chabreck, R. H. 1972. Vegetation, water and soil characteristics of the Louisiana coastal region (map). Louisiana State University, Agricultural Experiment Station Bull. 664, Baton Rouge.

Chabreck, R. H., and G. Linscombe. 1978. Vegetative type map of the Louisiana coastal marshes. Louisiana Department of Wildlife and Fisheries, New Orleans.

Dow, D. D. 1982. Software programs to measure interface complexity with remote-sensing data, with an example of a marine ecosystem application. NASA Report No. 219. NASA Earth Resources Laboratory, NSTL, Miss.

Dow, D. D., and R. W. Pearson. 1982. SLIN: a software program to measure interface length, NASA Report No. 208. NASA Earth Resources Laboratory, NSTL, Miss.

Faller, K. H. 1979. Shoreline as a controlling factor in commercial shrimp production. NASA Tech. Memo. 72-732. Earth Resources Laboratory, National Space Technologies Laboratory, NSTL, Miss.

Gagliano, S. M., K. J. Meyer-Arendt, and K. M. Wicker. 1981. Land loss in the Mississippi River deltaic plain, Transactions of the Gulf Coast Association of Geological Societies 31:295-300.

Gosselink, J. G. 1984. The ecology of the delta marshes of coastal Louisiana: a community profile. FWS/OBS-84/09. Office of Biological Services, U.S. Fish and Wildlife Service, Slidell, La.

Graham, M. H., B. G. Junkin, M. T. Kalcic, R. W. Pearson, and B. R. Seyfarth. 1984. ELAS: Earth Resources Laboratory Applications Software. Vol. 2, ELAS User's Guide. NASA Earth Resources Laboratory, NSTL, Miss.

Kesel, R. H. 1988. The decline in the suspended load of the lower Mississippi River and its influence on adjacent wetlands. Environ. Geol. Water Sci. 11:271-281.

Leibowitz, S. G., and J. M. Hill. 1988. Spatial analysis of Louisiana coastal land loss, In R. E. Turner and D. R. Cahoon, eds., Causes of Wetland Loss in the Coastal Central Gulf of Mexico, Vol. 2. OCS Study/MMS 87-0120. Minerals Management Service, New Orleans.

Mandelbrot, B. B. 1967. How long is the coast of Britain? Statistical self similarity and fractional dimension. Science 56:636-638.

Moran, P. A. P. 1948. The interpretation of statistical maps. Journal of the Royal Statistical Society, Series B, 10:243-251.

Nichols, S. 1984. Updated assessments of brown, white, and pink shrimp in the U.S. Gulf of Mexico. Stock Assessment Workshop 1984, Southeast Fisheries Center, National Marine Fisheries Service, NOAA, Miami, Fla.

Pun, Y. T. 1981. Entropic thresholding, a new approach. Computer Graphics and Image Processing 16:210-239.

Sasser, C. E., M. D. Dozier, J. G. Gosselink, and J. M. Hill. 1986. Spatial and temporal changes in Louisiana's Barataria Basin Marshes, 1945-1980. Environmental Management 10:671-680.

Turner, R. E., and D. R. Cahoon. 1987. Causes of wetland loss in the coastal central Gulf of Mexico. 3 vols. OCS Study/MMS 87-0119, 120, 121. Minerals Management Service, New Orleans.

Upton, G., and B. Fingleton. 1985. Spatial Data Analysis by Example. Vol. 1. John Wiley, New York.

Wicker, K.M. 1980. Mississippi deltaic plain region ecological characterization: a habitat mapping study. FWS/OBS-79/07. U.S. Fish and Wildlife Service, Slidell, La., and Minerals Management Service, New Orleans.

Zimmerman, R. J., T. J. Minello, and G. Zamora, Jr. 1984. Selection of vegetated habitat by brown shrimp, *Penaeus aztecus,* in a Galveston Bay salt marsh. U.S. Fisheries Bull. 82:325-336.

Appendix A

Background and Methods

Louisiana's Coastal Wetlands: Geological Background and Previous Remote Sensing Studies

Methods
- Overview
  - Model Specification
  - Model Expansion, Refinement, and Sensitivity Testing
- Study Site Selection
- Image Processing and Analysis
- Measurement of Spatial-Pattern Statistics
- Description of the Expert System

References

Table A1. Look-up table used to classify water and land identified by the ELAS shoreline length module into water pixels and land pixels with zero, one, two, three, or four sides adjacent to water.

Table A2. Calculation of weighted mean W, DE, and CV from a G-BC look-up table in which G = 0, BC = 0000, and DL = 10.90%.

Figure A1. The maximum extent of the influence of deltaic lobes of the Mississippi River on the present geomorphology of Louisiana's coastal wetlands.

Louisiana's Coastal Wetlands

Geological Background and Previous Remote-Sensing Studies

The continuing disintegration of the coastal marshes of Louisiana is one of the major environmental problems of the nation. The average rate of loss for the last 20 yr has been approximately 104 km^2/yr (Gagliano et al. 1981). At this rate, Louisiana's coastal marshes will be gone in 145 yr. Prevailing evidence suggests that the marsh disintegration results from local imbalances between building processes, such as sedimentation and the growth and accumulation of dead vegetative matter, and destructive processes, such as sea level rise, crustal subsidence, erosion, and compaction (Gosselink 1984). Local elevation gradients within the marsh are so low that small changes in water level or land elevation can cause large changes in land and water area (Sasser 1977; Baumann 1980). Water management structures, navigation cuts and channels, and other alterations by man appear to accelerate the disintegration rate (Johnson and Gosselink 1982; Dozier 1983; Gosselink 1984; Turner et al. 1984).

The problem of marsh loss in Louisiana is relevant to fishery management because Louisiana leads the nation in landings of fishery products, and most of the landed species are dependent upon estuaries and their associated tidal marshes. Coastal marshes contribute to estuarine food chains through the export of organic detritus, and the shallow, protected water of marshes serves as fish and shellfish nursery grounds, promoting survival and growth of the young.

Remote-sensing studies by Faller (1979), Dow (1982), and Gosselink (1984) suggest that the abundance of fishery species is more strongly correlated with the length of the interface between land and water in the marsh (shoreline) than with actual area of marshland. Observations from a field study by Zimmerman et al. (1984) support this conclusion. Simulations from a theoretical computer model by Browder et al. (1984) suggested that land-water interface initially increases with marsh disintegration but reaches a maximum when the marsh is 50% water and decreases thereafter. The degree of change in interface with each incremental loss of marsh land and the maximum length of interface attained are a function of the order in which segments of land are converted to water and the resultant pattern of

distribution of land and water. The more clustered the segments of land converted to water, the lower the rate of change and less the maximum interface.

In evaluating the potential effect of marshland loss on fisheries, the first two critical factors to consider are (1) whether land-water interface in actual disintegrating marshes is currently increasing or decreasing, and (2) the magnitude of the change.

This study used Landsat Thematic Mapper (TM) data covering specific sample marshes in coastal Louisiana to (1) test conclusions from the Browder et al. (1984) model with regard to the stage in disintegration at which maximum interface occurs; (2) further explore the relationship between maximum interface and the pattern of destruction of land and water suggested by the model; and (3) determine the direction and degree of change in land-water interface in relation to land loss in actual marshes.

Louisiana's coastal marshes were ideally suited for this examination for several reasons. First, the large, contiguous expanses of marsh enabled us to sample large areas containing only wetlands. Second, this region has been the subject of many scientific investigations concerning ecological principles, geologic processes, and experimental use of remote-sensing techniques. Third, geologic changes are occurring very rapidly here, and fourth, Louisiana's coastal marshes are the most extensive in the United States and support a high proportion of the total U.S. production of estuarine-dependent fish and shellfish.

The coastal wetlands of Louisiana were formed as deltas of the Mississippi River and its tributaries. The large, heterogeneous expanse of deltaic wetlands along the Louisiana coast is very young geologically. This area was formed within the last 3,000-5,000 yr as a series of overlapping deltaic lobes of differing ages (Fig. A1). Instability is a characteristic of youthful geologic environments. Subsidence, a complex set of processes, has pronounced effects on wetlands near sea level. Isostatic adjustments in the form of crustal downwarping from sedimentary loading; tectonic processes that occur contemporaneously, such as folding, fracturing, flowing, and growth faulting; consolidation of underlying sediments due to the weight of natural features (e.g., natural levees); and differential compaction related to textural variability are among those natural processes involved in submerging this coastline. Human activities in the form of fluid withdrawals (hydrocarbons and water), marsh dewatering through reclamation processes, and sediment consolidation resulting from building structures on wetlands all exacerbate coastal submergence. The above subsidence factors, combined with eustatic sea

level rise, have given coastal Louisiana the fastest-submerging coastline in the United States (Hicks 1981).

Submergence results in the "drowning" of marshes and their conversion to bay and lake environments. Sedimentation can balance the effects of submergence and, via the Mississippi River and its tributaries, has resulted in development of the Mississippi delta lobe. The geologic record indicates that, on the average, a major delta lobe complex will build and enlarge over approximately 1,000 yr. This period is followed by one of abandonment characterized by wetland loss, which also lasts approximately 1,000 yr. As one delta complex is being abandoned, another one is simultaneously building. Throughout at least the Holocene, the Mississippi deltaic plain has always concurrently had areas of development and abandonment. Presently, however, the leveeing of the Mississippi River and maintenance of its present course, combined with reductions in sediment loads (Tuttle and Combe 1981) and debouchment of sediment at the edge of the continental shelf, have resulted in widespread wetland loss. The construction of ship channels, pipeline canals, and access canals for hydrocarbon exploration and production has both contributed to and accelerated these losses. Acceleration occurs through the effect of these structures on salinity distributions and sediment deposition. For instance, canals promote saltwater intrusion, which results in the death of brackish-water marsh vegetation and thus retards the accumulation of organic soils. Spoil banks associated with canals prevent deposition of sediment on the marsh surface and reduce exchanges of water and materials between the marsh and open water. The natural geological process of wetland deterioration, which would otherwise take place over several centuries, appears now to have been compressed into several decades.

Chabreck (1972) distinguished four major types of Louisiana coastal marshes on the basis of vegetation: fresh, intermediate, brackish, and saline. Several investigators have found significant differences between these marsh types in various soil, water quality, and other parameters, thereby supporting Chabreck's classification. Gosselink et al. (1979) found considerable differences in the length of land-water interface per unit area among the four marsh types in the neighboring Chenier Plain (marginal Mississippi deltaic plain) of southeast Texas and southwest Louisiana.

Sasser et al. (1986) used photo interpretation of aerial photographs in combination with a computer-based geographic information system (GIS) to detect changes in the percentage water

within wetlands on the late Lafourche delta lobe. They found a pattern of general degradation in wetland area: marshes were degrading into various densities of shallow water bodies. Of the marsh and natural levee area, 91% was solid or less than 10% water in 1945. By 1956, only 77% of the marsh was less than 10% water; by 1969, only 46% was; and by 1980, only 28%. They noted two patterns of disintegration. In one, small, randomly spaced water bodies developed within solid marshes and gradually grew into larger water bodies. In the other, land was lost along the margins of major water masses, as if by mechanical wave attack or erosion. The first pattern seemed to be the more important.

Rosen (1980), in his study of Chesapeake Bay, concluded that shorelines with low tidal ranges have higher rates of erosion than areas with higher tidal ranges, possibly because higher tidal ranges form beaches of higher elevation. On these beaches, storm surges are less likely to reach the elevation of fastland (bluff or dune) material to augment erosion, and wave energy is distributed over a greater distance in the course of a tidal cycle. The tidal range in Chesapeake Bay varies from 0.36 to 1 m over a distance of 120 km. The tidal range in the north-central Gulf of Mexico is approximately 0.6 m.

Leibowitz and Hill (1988) used digital habitat maps for 1956 and 1978 from the U.S. Fish and Wildlife Service (Wicker 1980) to quantify change in coastal marshes during the 22-yr period and to evaluate various possible causes of the change. Their study covered our two study areas--the late Lafourche lobe and the early Lafourche lobe (referred to as Terrebonne in their study). Water, wetland, and upland could be distinguished in the data, which were classified according to the Cowardin et al. (1979) system. Boundaries between saline and freshwater zones were also defined on the basis of vegetation. Liebowitz and Hill classified each map cell on the basis of a comparison of 1956 and 1978 habitat maps as follows: areas that were fresh in 1956, but saline in 1978; areas that changed from saline to fresh between 1956 and 1978; and areas that remained saline during the 22 yr. They also identified the cells in each habitat category that changed from land to water during the 22 yr. Their results revealed a 37% net area change from salt to fresh on the late Lafourche lobe and a 16% net area change from fresh to salt on the early Lafourche lobe. The highest rate of land loss on the late Lafourche lobe was 27% and occurred in the fresh-to-salt area. The highest rate of land loss on the early Lafourche lobe was 16% and occurred in the fresh-to-fresh area. By statistical comparisons, they ruled out saltwater intrusion as a reason for land loss on the early

Lafourche lobe, but concluded that it could be a cause of land loss on the late Lafourche lobe. The highest rates--47%-55%--occurred in the mud flat and beach/dune/reef habitats. Loss rates in fresh and saline marsh averaged approximately 18%. Loss from shoreline erosion accounted for only 2.1% (early Lafourche) and 3.2% (late Lafourche) of all land loss. Thus, the major form of land loss for all three regions was the conversion of land to inland open water (lakes, ponds, or bays).

Several studies have used TM and Landsat MSS imagery with collateral data, such as fish abundance and vegetative biomass, to examine the role of coastal wetlands in estuarine food chains and the production of estuarine-dependent fish and shellfish. These studies were supported by the development of software routines used to determine shoreline density (Faller 1977) and shoreline length (Faller 1977; Dow and Pearson 1982), to identify water bodies (Butera 1982a), and to measure the distance between land-cover classes (Butera 1982b). Faller (1979) found a strong correlation between shrimp yields and shoreline density in subareas of the Louisiana coastal zone. Dow (1982) expanded Faller's (1979) approach and developed predictive equations that related the abundances of selected species of fish and shellfish to shoreline-length estimates for subareas of Apalachicola Bay, Florida. The findings of both authors suggest that abundances of some fish and shellfish could be influenced by the density and length of the marshland-water interface. Butera and Seyfarth (1981) and Butera et al. (1984) used water-body identification, distance measures, shoreline density, and vegetative biomass estimates to quantify organic carbon export into nearby water bodies.

Methods

Overview

We expanded an existing model (Browder et al. 1984) so that it could simulate marshes of substantial size, used actual marshes to calibrate the weighting factors of the models, and then used the model to simulate the disintegration over time of each sample marsh. Model calibration was accomplished by quantifying the spatial-pattern statistics of the sample marshes and matching them to the spatial-pattern statistics expected from simulated marshes, based on a series of simulations in which W, G, and the number of water borders (BC) were varied.

The process consisted of nine steps: (1) expansion, refinement, and sensitivity testing of the model; (2) selection of sample sites; (3) analysis of imagery; (4) measurement of spatial-pattern statistics; (5) development of a knowledge base and an expert system; (6) calibration of the model to the sample marshes; (7) simulation of the disintegration patterns of the sample marshes; (8) evaluation of simulation results; and (9) interpretation.

Model specification. The model used in this study is the second generation of a stochastic spatial computer model introduced by Browder et al. (1984). In the initialization of the model, marsh dimensions are defined in terms of the numbers of rows and columns of pixels. Each pixel can exist in one of two states, land (emergent vegetation) or water. Initially, all the pixels are land and the marsh is solid. One land pixel is converted to water at each iteration. The actual pixel converted is determined by a random number generator linked to a probability function that incorporates two weighting factors that approximate the natural processes of interior marsh decay (the W factor) and shoreline erosion (the G factor). The W factor determines disintegration probability on the basis of the number of sides that the pixel is bordered by water. The G factor governs the probability that the pixel will disintegrate if it borders the main water body. The probability weight of each pixel is calculated by the equation:

$$F_{i,j,k} = 1 + W\, S_{i,j,k} + G_1\, B_{1i,j} + G_2\, B_{12i,j} + G_3\, B_{3i,j} + G_4\, B_{4i,j} \qquad (1)$$

where W = weight coefficient for each side adjacent to water; S = number of sides adjacent to water; G = weight coefficient for pixels adjacent to a major outside water body; and B = a Boolean value (1 or 0) indicating whether the pixel is adjacent to a major outside water body.

The probability weight of a given pixel changes throughout the simulation, depending on what happens to other pixels, particularly those adjacent to it.

In having the weighted probability function approximate natural processes of interior marsh decay (W) and erosion due to tidal action or wind-induced turbulence along the edge of major water bodies (G), we did not assume that marsh loss is a random process, but merely that it could be simulated by a weighted, randomly driven function.

The model simulates the entire process of disintegration, starting with solid land and ending with solid water. Each iteration represents the passage of time, although the units of time are not specified.

At each iteration of the simulation, a counter keeps track of the percentage area represented as water, referred to throughout this discussion as the "level of disintegration," and the length of the land-water interface. The latter is expressed in terms of pixel-lengths, the length of one side of the square pixel; therefore, measuring interface length consisted of counting the number of "joins" between land pixels and water pixels. Thus, interface, as we measured it, is exactly homologous to the "black-white join" (J), the spatial autocorrelation parameter that Moran (1948) introduced into the literature of quantitative geography. Upton and Fingleton (1985) described the common relationship between the join statistic and other spatial-pattern parameters, such as that of Cliff and Ord (1973), and defined the cross-product statistic, R, which is equal to 2 x J.

Upton and Fingleton (1986) provide an intricate set of equations for calculating R, the expected value of R (E[R]), and the variance of the expected value. E(R) assumes a random distribution of black and white (or land and water) cells. R departs from E(R) to the extent that like cells are clumped ($R < E[R]$) or uniformly distributed ($R > E[R]$). They provide simpler equations for calculating J, E(J), and var E(J) for cases in which the area is regular-sided and square in configuration (their equations for the R statistics are more general). In our simulations, we were able to determine J simply by keeping a running total of the number of land-water joins created at each conversion of a land pixel to a water pixel. A method related to counting was used to determine the number of land-water joins in satellite images classified as land and water. Our observations indicate that, for a square area with regular sides, E(J) is approximately equal to one-half the number of land-water joins of an area of the same

dimensions having a checkerboard pattern of distribution of land and water. This can be calculated as follows:

$$E(J) = 2\ N^2 - 4\ N \qquad (2)$$

where N = the number of rows = the number of columns.

The weighting factors affect the order of disintegration of marsh land pixels and the resultant distribution of land and water in the simulated marsh. The higher the values of the weighting factors, the more clumped the water pixels. By affecting the spatial distribution of water pixels, the weighting factors determine interface length in simulated marshes. Taking advantage of this relationship, the approach we took to simulating the disintegration of actual marshes was to use spatial pattern, as expressed by level of disintegration, interface length, and other spatial pattern statistics of the actual marshes, compared to those from simulated marshes, to select W and G weighting factors for the model. The other spatial-patterns statistics that were used were numbers of water pixels with zero, one, two, three, or four sides adjacent to other water pixels, and numbers of water pixels on each of the marsh's four borders. The distribution of water pixels by size of water clusters at the current (i.e., December 1984) level of disintegration was used to test the fit of the simulated marsh to the actual marsh. Comparison of simulated marshes to actual marshes in general suggests that the function will work well for simulating reticulated marshes, such as those on the Gulf coast, although it might not work well for marshes with a more dendritic pattern of land and water, such as those along the U.S. Atlantic coast.

Model Expansion, Refinement, and Sensitivity Testing

The first phase in the study was improving the model. Our improvements were guided by a series of sensitivity tests: (1) tests of the effects of the W and G weighting factors, varied separately; (2) tests of the effect of marsh geometry (i.e., length, relative to width); and (3) tests of the effect of marsh size, in terms of number of pixels.

In the original version of the model, only the pixels *initially* on the major outside water body had the G weighting (B = 1). The G effect was inconsequential in sensitivity tests with the original model, particularly as the size of the marsh simulated was increased. On the basis of this observation, the model was revised so that any pixel, regardless of original location, could

eventually be assigned B = 1. The G factor in the present version of the model has a much greater effect than that in the earlier version.

Other sensitivity tests indicated that the geometry of the marsh (i.e., ratio of length to width) affected the trajectory of change in interface relative to W and G and greatly complicated the process of examining interface as a function of W and G and the number of water borders to the marsh (i.e., simulation results differed depending upon whether a water border was the long or the short border). We decided to work with square marshes, both simulated and actual, in order to avoid this complication.

To eliminate another complicating variable--scaling--we decided to simulate marshes of the same size (same number of pixels) as our sample sites. We determined that it would be practical to simulate marshes up to 192 x 192 pixels, although not with replication. A site represented by 192 x 192 pixels covers 33.18 km^2 and is approximately one quarter of the area covered by a 7.5-minute U.S. Geological Survey topographic map.

Increasing the size of the simulated marsh necessitated streamlining the algorithm for weighting disintegration probability and converting land pixels to water pixels. In the original algorithm, each pixel, identified by its x,y coordinate, was repeated on the list the same number of times as its probability factor (F in equation 1). Each item on the list had a unique number, and the pixel selected was the one that corresponded to the random number at that iteration, providing that it had not already been converted to water at a previous iteration. All occurrences of pixels that had been newly converted to water were cleared from the list at five periodic intervals throughout the simulation. The process got slower and slower as the need for purging the list approached. This algorithm was too slow and awkward to be scaled up in the same form. In our revision, each pixel appears on the numbered list only once, but its probability factor is listed with it. Two random numbers are associated with each selection. The first random number makes a tentative selection, and the second determines whether the pixel is eligible. Eligibility depends on whether the pixels's probability factor is larger than the random number. The selection process continues, with two new random numbers generated each time, until the selection of an eligible pixel is made. Of course, the first random number--the one that makes the tentative selection--is a uniform random number from 0 to 1 that is multiplied by the largest probability factor on the list. A pointer system keeps track of the

pixels on the list and eliminates from the list the pixel that has been converted to water at each iteration.

The model and all ancillary programs were written in C and were executed on an AT&T PC-7300, a 16-bit computer that has a Unix-V operating system.

Study Site Selection

The study sites are located in salt and brackish marsh areas on two abandoned delta lobes of the Mississippi River, the early lafourche and the late Lafourche. The early Lafourche lobe was an actively prograding lobe within the last 1,800 yr; the late Lafourche lobe was active as a main distributary of the river within the last 600 yr. On each lobe we selected sites that corresponded to the boundaries of five contiguous U.S. Geological Survey 7.5-minute topographic maps. Areas defined by each topographic map were divided into four contiguous quarters, each encompassing an area 192 elements wide and 192 scan lines long on the TM image. The intersection of the four quarters was aligned to correspond to the center point of each topographic map. Each area corresponding to a quarter area of the 10 topographic maps was a potential sample site. After excluding sites with upland vegetation and sites for which no cloud-free TM images were available, we had 72 samples to use in the study: 40 salt marsh sites (20 on each lobe) and 32 brackish marsh sites (19 on the early Lafourche lobe and 13 on the late Lafourche lobe). Salt and brackish marshes were distinguished by means of the U.S. Fish and Wildlife Service habitat maps (Cowardin et al. 1979).

Because of small errors in TM imagery, pixels are neither exactly square nor exactly the same size; therefore, it was necessary to eliminate several pixels on the outer boundaries of imagery corresponding to each topographic map in order to have a 192 x 192 image. Our sample images therefore do not provide complete coverage of the area--small strips at the boundaries of the topographic maps are missing. Selecting square samples (samples having the same number of rows and columns of pixels) greatly simplified the analyses of this study in several ways. First, we had fewer alternatives to consider in sensitivity analysis and constructing look-up tables. Second, we could use simpler and less time-consuming equations for estimating spatial autocorrelation statistics. The quarter was the largest square unit into which a topographic map could be evenly divided that could be simulated with practicality in the same dimensions by our computer model on available dedicated hardware.

Image Processing and Analysis

TM scenes were analyzed on the Fisheries Image Processing System (FIPS) maintained by NMFS in Slidell, Louisiana. FIPS uses a Sperry-Univac V77/600 mini-computer, color image display device, and other hardware to process remotely sensed digital imagery. The software is a modified version of the Earth Resources Laboratory Applications Software (ELAS) (Graham et al. 1984).

The TM image acquired for the project represented one of the few relatively cloud-free images covering southern Louisiana (quads 1 and 2 in path 22 and row 40 of the World-Wide Reference System). The Landsat overflight occurred on 2 December 1984 (Scene ID: 50276-16022) and covers most of the Mississippi deltaic plain.

TM images of the sites were georeferenced to fit a Universal Transverse Mercator projection with a north-south orientation. The ELAS modules PMGC and PMGE (Graham et al. 1984) were used to accumulate ground control points, generate polynomial least-squares mapping equations, and resample the image using the bilinear interpolation technique. The average registration accuracies ranged from 22 to 56 m.

Land and water were distinguished in the TM images by first generating a product image from bands 4 and 5 and then applying the global thresholding technique developed by Pun (1981).

Measurement of Spatial-Pattern Statistics

We generated 72 binary land-water images from the product images of the salt and brackish marsh sites. Sequential ELAS commands set up for batch processing were used to measure the following spatial-pattern parameters in each image: (1) total numbers of land and water pixels; (2) total numbers of water pixels by scan line and by element column; (3) the length of the land-water interface, expressed as the total number of land-water joins; (4) total numbers of water pixels with sides adjacent to zero, one, two, three, and four other water pixels; and (5) water-body size frequencies. In determining the total number of water pixels with sides adjacent to other water pixels, we excluded the pixels at the boundary of the sample to avoid biasing the distribution of pixels toward those having less than four sides adjacent to water.

The total number of land-water joins in each image was tabulated using a three-step process. First, an intermediate image was generated using the ELAS shoreline-length (SLIN) module

(Graham et al. 1984). SLIN uses a 3-x-3 moving window technique to classify each land pixel adjacent to water into one of 69 shoreline categories (Dow 1982; Dow and Pearson 1982). Second, we used a look-up table (Table A1) to convert the SLIN image into an image file comprising six classes: (1) land; (2) water; and (3) shoreline pixels with one, two, three, or four sides adjacent to water. Finally, we determined the total number of land-water joins in each sample site by enumerating the number of land pixels sides bordering water pixel sides.

The total number of water pixel sides adjacent to other water pixels was tabulated using a modification of the technique used to count land-water joins. Two changes in the processing sequence were required: (1) water pixels adjacent to land were defined as shoreline pixels during processing with the SLIN module and (2) an additional processing step with a new look-up table was required to correctly classify water pixels with zero, one, two, three, or four sides adjacent to other water pixels.

As Hutchinson (1957) originally pointed out and first Richardson (1961) and then Mandelbrot (1967) elaborated upon, the length of an irregular shoreline is, to some extent, a function of measurement unit. Our measurements of land-water joins and, possibly, the other spatial-pattern statistics, are valid only at the resolution of the TM imagery, the 30-x-30-m pixel. Future measurements cannot be compared to ours unless the same measurement unit is used.

Description of the Expert System

An expert system was developed to select the model parameters--W, G, and BC--that would best approximate the spatial patterns of each study site. The expert system consisted of a knowledge base and a decision process. The knowledge base indicated how each of the spatial pattern indices--interface length and the four side-adjacency statistics--varied as functions of W, G, and BC (border condition). The decision process consisted of the rules for selecting the best W-G-BC combination.

To build the knowledge base for the expert system, we ran simulations with all possible W and G combinations from the set [0, 4, 20, 60, 180, and 540] for six types of study-site border conditions: 0 = no water border, 1 = 1 water border, 2 = 2 adjacent water borders, 3 = 2 opposite water borders, 4 = 3 water borders, and 5 = 4 water borders. For border condition 0, the set was extended to include W = 1620 and 9720. Each simulation contributed information to 21 tables. Each table contained interface length and side-adjacency information collected at

a 5% increment of DL (level of disintegration, or water area as percentage total area). We compiled 21 tables (one for each increment of DL) for each value of G and for each border condition (a total of 6 x 5 = 30 sets of 21 tables). For border condition 0 (no water border), only one set of 21 tables was compiled, since G must equal zero. For each of the other data sets, there were 21 tables for each G value.

The following statistics from each study site were used in the decision process: DL; interface length; and Adj-0, Adj-1, Adj-2, Adj-3, and Adj-4 (number of water pixels having 0, 1, 2, 3, or 4 sides adjacent to water). Target **BC** was an additional factor in the decision process.

The DL of the study site was used to determine which tables were accessed. The tables of the nearest DL's on either side of the study-site DL were accessed. For instance, if the DL of the image was 32%, then the tables for DL's 30% and 35% were accessed. Interpolation between levels was then used to produce, for every G value and border condition, a table of values of spatial-pattern indices for each of the six values of W for the specific DL of the study site.

Then, for each G value and border condition, the study-site interface and side-adjacency values were compared with values for the spatial-pattern index in the tables prepared for the specific disintegration level. If the study-site value for a spatial-pattern index was within the range of values for that index on a particular table, exact matching or interpolation between values was used to estimate W on the basis of that index, given the G value and border condition of that table. If the value of a given index from the study site was not within the range of values for that index in a table, then W could not be estimated from that particular index and table.

We usually obtained several estimates of W from a given G-**BC** table. A weighted mean W for the specific G-value and border condition was obtained from these. In cases where a parabolic relationship between the parameter and W occurred, more than one estimate of W was sometimes obtained for the same index and table. In such cases, each estimate was used alternatively in calculating a weighted mean until we had calculated all possible weighted means from the indices. For instance, interface might yield W = 2, 4; Adj-0, W = 180, 193; and Adj-3, W = 300. Then 2 x 2 x 1 weighted mean W's were calculated. One would involve 2, 180, and 300; another 2, 193, 300; another 4, 180, 300; and another 4, 193, 300. Weighting was a function of the number of water pixels involved in each parameter estimate of W. The value of

the parameter was the estimate of the number of pixels involved in the estimate of W from that spatial-pattern index. Weighted mean W's were calculated as follows:

$$\text{Weighted Mean W} = \text{Sum } (W_i\ V_i) \,/\, \text{Sum } (V_i) \tag{3}$$

where W_i = the estimate of W from statistic i, and V_i = the number of pixels involved (index value), statistic i. Only the water pixels of the spatial-pattern indices involved in the specific calculation of the weighted mean W were summed. As mentioned above, if the index value from the sample was not within the range of values for that index in a particular table, an estimate of W based on that index could not be obtained.

The coefficient of variation (CV) of each weighted mean W also was calculated, as follows:

$$\text{CV} = (\text{Variance})^{1/2} \,/\, \text{Weighted Mean W} \tag{4}$$

In addition, the sum of the water pixels used in calculating the weighted mean W was retained as a "decision number" (DE) for later use in the selection process. Table A2 lists the weights, the W's, and the calculations of weighted mean W, DE, and CV.

By the above procedure, the expert system estimated many W-G-BC combinations for each study site. Weighted mean W's, CV's, DE's, and their corresponding G's and BC's were stored in solution files specific to each study site. The file was sorted by DE and CV.

The first step in selecting the best model parameters to simulate the spatial patterns of a study site was to define a "target" BC. Target BC was the estimated BC of the study site. To make this estimate, the expert system compared the proportion of water pixels on each border to the proportion of water pixels in the marsh as a whole. Those borders having a higher proportion of water pixels than the entire site were assumed to be influenced by a major water body at the border. The BC estimates were confirmed by visual examination of black-and-white photographs of binary land-water images of the sites. In a few cases, estimates were changed on the basis of the visual examination.

Once a target BC was selected, the solution file specific to the spatial pattern indices of that study site was searched for the "best" weighted mean W, specific to calculated G, for that BC. If a solution having the target BC was found in the group of solutions with the highest

DE, it was selected as the best solution. If more than one solution in the group of solutions with the highest DE had the target **BC**, then the one with the lowest CV was selected. If a solution having the target **BC** could not be found within the group having the highest DE, then the expert system sought a solution with the target **BC** among all solutions having DE within 75% of the highest DN. The solution having the target **BC**, the largest DE, and the lowest coefficient of variation was selected. If a solution having the target **BC** was not found in either of the above groups, then solutions having alternative BC were considered. First, solutions with **BC** having no more than one border different from that of the target **BC** were considered. Then, solutions having no more than two borders different from that of the target **BC** were considered. We usually found a solution having the target **BC** or no more than one border different from that of the target **BC**.

References

Adams, R. D., and R. H. Baumann. 1980. Land-building in coastal Louisiana: emergence of the Atchafalaya Bay delta. Center for Wetland Resources, Louisiana State University, Baton Rouge.

Baumann, R. H. 1980. Mechanisms of maintaining marsh elevaion in a subsiding environment. Master's thesis, Louisiana State University, Baton Rouge.

Browder, J. A., H. A. Bartley, and K. S. Davis. 1984. A probablilistic model of hte relationship between marshland-water interface and marsh disintegration. Ecological Modelling 29:245-260.

Butera, M. K. 1982a. Identification of water bodies using remotely sensed multispectral scanner data, with applications for inventory, hydrologic assessment, and habitat evaluation. NASA Tech. Memo. No. TM-84672, NASA Earth Resources Laboratory, NSTL, Miss.

Butera, M. K. 1982b. A distance measurement derived from Landsat MSS data, with application to marsh productivity, efficient crop transport, and environmental distrubance assessment. NASA Tech. Memo. No. TM-84671, NASA Earth Resources Laboratory, NSTL, Miss.

Butera, M. K., and B. R. Seyfarth. 1981. A determination of marsh detritial export from Landsat-MSS data--a function of transport distance and water-body characterization. Proc. Machine Processing of Remotely Sensed Data Symposium. Purdue University, West Lafayette, Indiana.

Butera, M. K., A. L. Frick, and J. A. Browder. 1984. A preliminary report on the assessment of wetland productive capacity from a remote-sensing-based model--a NASA/NMFS joint research project. IEEE Transactions in International Geoscience and REmote Sensing GE-22:502-511.

Chabreck, R. H. 1972. Vegetation, water and soil characteristics of the Louisiana coastal region. Agricultural Experiment Station Bull. 664. Louisiana State University, Baton Rouge.

Cliff, A. D., and J. K. Ord. 1973. Spatial Autocorrelation. Pion, London, England.

Cowardin, L. M., V. Carter, F. C. Golet, and E. T. LaRoe. 1979. Classification of Wetlands and Deepwater Habitats of the United States. FWS/OBS-79/31, Office of Biological Services, U.S. Fish and Wildlife Service, Washington, D.C.

Dow, D. D. 1982. Software programs to measure interface complexity with remote-sensing data, with an example of a marine ecosystem application. NASA Report No. 219. NASA Earth Resources Laboratory, NSTL, Miss.

Dow, D. D., and R. W. Pearson. 1982. SLIN: a software program to measure interface length. NASA Report No. 208. NASA Earth Resources Laboratory, NSTL, Miss.

Dozier, M. D. 1983. Assessment of change in the marshes of southwestern Barataria Basin, Louisiana, using historical aerial photographs and a spatial information system. Master's thesis, Louisiana State University, Baton Rouge.

Faller, K. H. 1977. A procedure for dteection and measurement of interfaces in remotely-acquired data using a digital computer. NASA Tech. Report No. TR R-472. Lyndon B. Johnson Space Center, Houston, Tex.

Faller, K. H. 1979. Shoreline as a controlling factor in commercial shrimp production. NASA Tech. Memo. 72-732. NASA Earth Resources Laboratory, NSTL, Miss.

Gagliano, S. M., K. J. Meyer-Arendt, and K. M. Wicker. 1981. Land loss in the Mississippi River detlaic plain. Transactions of the Gulf Coat Association of Geological Societies 31:295-300.

Gosselink, J. G. 1984. The ecology of the delta marshes of coastal Louisiana: a community profile. FWS/OBS-84/09. Office of Biological Services, U.S. Fish and Wildlife Service, Washington, D.C.

Gosselink, J. G., C. C. Cordes, and J. W. Parsons. 1979. An ecological characterization study of the Chenier Plain coastal ecosystem of Louisiana and Texas. FWS/OBS-78/9 through 78/11 (3 vols.). Office of Biological Services, U.S. Fish and Wildlife Service.

Graham, M. H., B. G. Junkin, M. T. Kalcic, R. W. Pearson, and B. R. Seyfarth. 1984. ELAS: Earth Resources Laboratory Applications Software. Vol. 2, ELAS User's Guide. NASA Earth Resources Laboratory, NSTL, Miss.

Hicks, S. D. 1981. Long-period sea-level variations in the United States through 1978. Shore and Beach 49:26-29.

Hutchnison, G. E. 1957. A Treatise in Limnology. Vol. 1, part 1. John Wiley, New York.

Johnson, W. B., and J. G. Gosselink. 1982. Wetland loss directly associated with canal dredging in the Louisiana coastal zone. Pp. 60-72 in D. F. Boesch, ed., Proceedings of the Conference on Coatal Erosion and Wetland Modification in Louisiana: Causes,

Consequences, and Options. FWS/OBS-82/59. Office of Biological Services, U.S. Fish and Wildlife Service, Washington, D.C.

Leibowitz, S. G., and J. M. Hill. 1988. Spatial analysis of Louisiana coastal land loss. In R. E. Turner and D. R. Cahoon, eds., Causes of Wetland Loss in the Coastal Central Gulf of Mexico. OCS Study/MMS 87-0119. Minerals Management Service, New Orleans.

Mandelbrot, B. B. 1967. How long is the coast of Britain? Statistical self similarity and fractional dimension. Science 56:636-638.

Moran, P. A. P. 1948. The interpretation of statistical maps. Journal of the Royal Statistical Society, Series B, 10:243-251.

Pun, T. 1981. Entropic thresholding, a new approach. Computer Graphics and Image Processing 16:210-239.

Richardson, L. F. 1961. The problem of contiguity: an appendix of statistics of deadly quarrels. General Systems Yearbook 6:139-187.

Rosen, P. S. 1980. Erosion susceptibilityof the Virginia Chesapeake Bay shoreline. Marine Geology 34:45-59.

Sasser, C. E. 1977. Distribution of vegetation in Louisian coastl marshes as response to tidal flooding. Master's thesis, Louisiana State University, Baton Rouge.

Sasser, C. E., M. D. Dozier, J. G. Gosselink, and J. M. Hill. 1986. Spatial and temporatl changes in Louisiana's Barataria Basin marshes, 1945-1980. Environmental Management 10:671-680.

Turner, R. E., K. L. McKee, W. B. Sikora, J. P. Sikora, I. A. Mendelssohn, E. Swenson, C. Neill, S. G. Leibowitz, and F. Pedrazini. 1984. The impact and mitigation of man-made canals in coastal Louisiana. Nat. Sci. Tech. 6:497-504.

Tuttle, J. R., and A. J. Combe. 1981. Flow regime and sediment load affected by alterations of the Mississippi River. Pp. 334-348 in R. D. Cross and D. L. Williams, eds., Proc. National Symposium on Freshwater Inflow to stuaries. FWS/OBS-81/04. Office of Biological Services, U.S. Fish and Wildlife Service, Slidell, La.

Upton, G., and B. Fingleton. 1985. Spatial Data Analysis by Example. Vol. 1. John Wiley, New York.

Wicker, K. M. 1980. Mississippi deltaic plain region ecological characterization: a habitat mapping study. A User's Guide to the Habitat Maps. FWS/OBS-79/07. Office of Biological Services, U.S. Fish and Wildlife Service, Slidell, La.

Zimmerman, R. J., T. J. Minello, and G. Zamora, Jr. 1984. Selection of vegetated habitat by brown shrimp, *Penaeus aztecus*, in a Galveston Bay salt marsh. U.S. Fisheries Bull. 82:325-336.

Table A1. Look-up table used to classify water and land identified by the ELAS shoreline length (SLIN) module into water pixels and land pixels with zero, one, two, three, and four sides adjacent to water.

SLIN output	Class code	SLIN output	Class code	SLIN output	Class code
0	5	24	2	48	3
1	0	25	1	49	3
2	0	26	1	50	2
3	1	27	2	51	2
4	0	28	2	52	2
5	0	29	2	53	3
6	1	30	2	54	3
7	1	31	2	55	3
8	0	32	2	56	3
9	1	33	2	57	3
10	1	34	2	58	3
11	0	35	1	59	3
12	2	36	2	60	3
13	1	37	2	61	3
14	1	38	2	62	3
15	1	39	2	63	3
16	1	40	2	64	3
17	1	41	2	65	4
18	1	42	2	66	4
19	2	43	2	67	4
20	2	44	2	68	4
21	1	45	2	69	4
22	1	46	3	70	ND
23	2	47	3	71	ND

Key to Class Codes:
0 = land pixel with zero sides adjacent to water.
1 = land pixel with one sides adjacent to water.
2 = land pixel with two sides adjacent to water.
3 = land pixel with three sides adjacent to water.
4 = land pixel with four sides adjacent to water.
5 = water pixel.

Table A2. Calculation of weighted mean W, DE, and CV from a G-BC look-up table in which G = 0, BC = 0000, and DL = 10.90%.

Index Name	Weight	W	W • Weight
Interface	4,011	60	240,660
Adj-0	108	53	5,724
Adj-1	805	256	206,080
Adj-2	1,257	121	152,097
Adj-3	1,109	53	58,777
Adj-4	680	156	106,080
	7,970		769,418

Weighted mean W = 97
Decision Number (DE) = 7,970
CV = 64.91%

(Number of border pixels = 52)
(Σ Adj weights = 3,959)

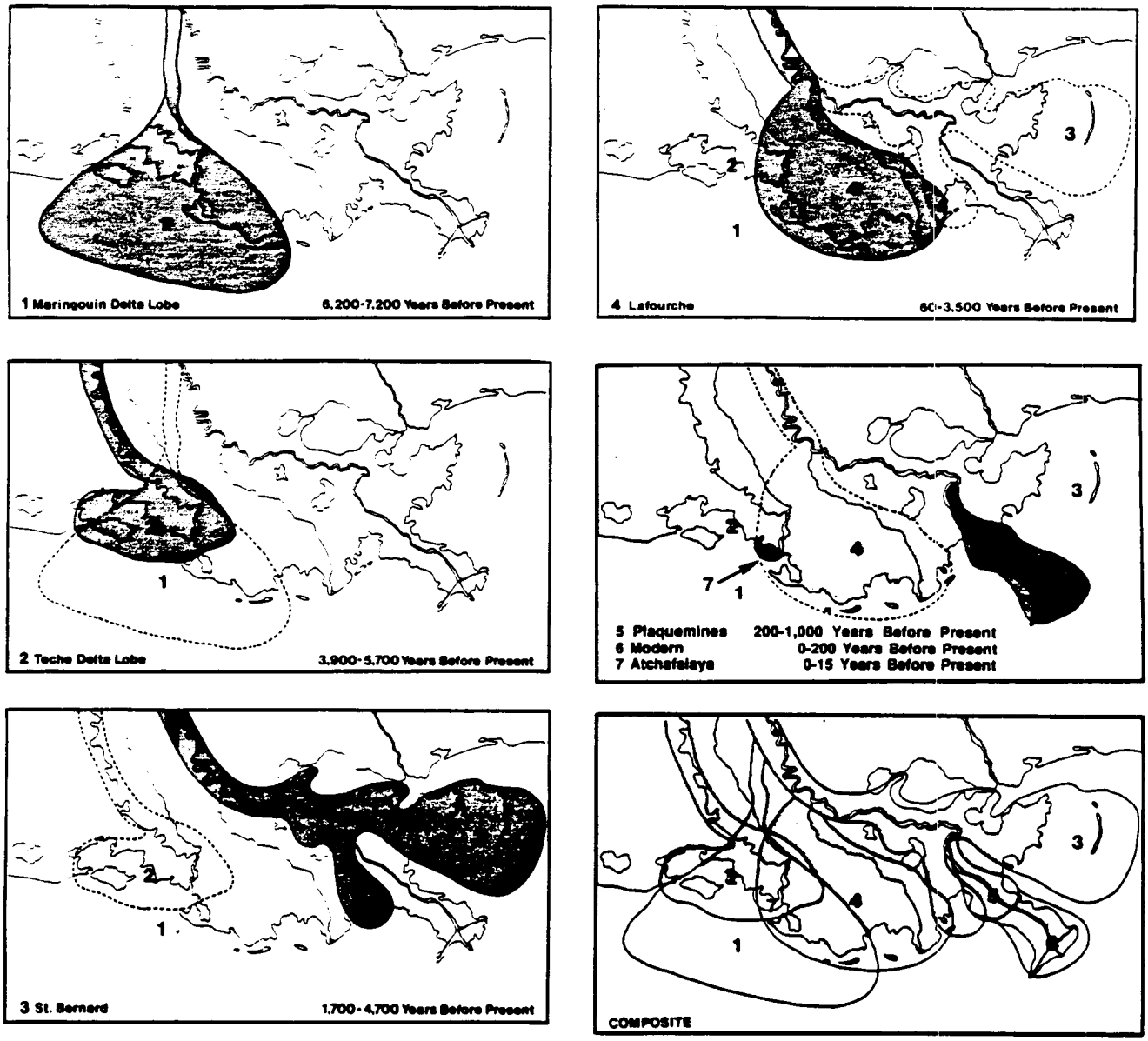

Figure A1. The maximum extent of the influence of deltaic lobes of the Mississippi River on the present geomorphology of Louisiana's coastal wetlands (modified from Adams and Baumann 1980).

Appendix B

Spatial-Pattern Statistics of Simulations Using All Combinations of W, G, and BC

Table B1. Interface length (number of pixels) vs. W, G, and border condition (BC) at 50% disintegration level (DL), from simulations of 192-x-192-pixel marshes.

Table B2. Disintegration level (DL) at maximum interface for simulations of 192-x-192 pixel marshes with varying W, G, and border conditions.

Table B1. Interface length (number of pixels) vs. W, G, and border condition (BC) at 50% disintegration level (DL), from simulations of 192-x-192-pixel marshes.

W	G	Border Condition 0000	0001	0011	0101	0111	1111
0	0	36,695					
4	0	24,946					
20	0	18,243					
60	0	14,357					
180	0	10,921					
540	0	8,113					
0	4		34,573	33,427	33,412	31,888	30,754
4	4		24,801	24,630	24,505	24,243	24,300
20	4		18,516	18,115	18,392	18,264	18,296
60	4		14,434	14,300	14,595	14,385	14,384
180	4		10,726	10,959	10,443	11,053	11,272
540	4		7,672	7,957	8,183	8,156	8,254
0	20		31,208	26,080	28,635	20,395	16,088
4	20		23,401	21,440	22,500	19,311	16,768
20	20		17,924	17,271	17,444	16,867	16,612
60	20		14,273	13,863	14,167	13,766	13,747
180	20		10,937	11,055	10,719	10,999	10,586
540	20		7,940	8,039	7,706	8,058	8,428
0	60		25,752	15,520	20,946	9,667	6,998
4	60		20,540	15,743	18,578	11,001	8,120
20	60		16,791	14,475	16,031	12,348	10,069
60	60		13,777	13,008	13,366	11,792	10,904
180	60		10,771	10,227	10,343	9,927	9,561
540	60		7,789	7,679	7,732	7,895	8,075
0	180		16,113	6,001	9,302	3,836	2,946
4	180		15,994	6,850	10,708	4,251	3,282
20	180		13,866	9,012	11,416	5,402	3,914
60	180		12,481	9,622	11,457	6,687	5,722
180	180		9,919	8,821	9,644	7,551	6,054
540	180		7,789	7,556	7,524	7,404	6,622
0	540		5,961	2,468	3,831	1,939	1,846
4	540		7,093	2,534	4,121	1,979	1,922
20	540		8,826	3,168	5,530	2,205	1,946
60	540		9,322	4,650	7,169	2,737	2,220
180	540		8,513	5,826	7,248	3,693	2,772
540	540		6,877	5,408	6,890	4,572	3,900

0000 = no water borders, 0001 = one water border, 0011 = two adjacent water borders, 0101 = two opposite water borders, 0111 = three water borders, 1111 = four water borders.

Table B2. Disintegration level (DL) at maximum interface for simulations of 192-x-192 pixel marshes with varying W, G, and border conditions.

W	G	Border Condition 0000	0001	0011	0101	0111	1111
0	0	49.56					
4	0	47.24					
20	0	49.99					
60	0	45.10					
180	0	52.40					
540	0	52.55					
0	4		46.51	45.35	44.74	43.98	42.64
4	4		47.42	48.99	48.76	47.17	47.71
20	4		49.90	50.24	--	47.35	50.55
60	4		49.66	49.53	47.99	51.21	48.13
180	4		47.59	50.33	50.53	57.19	55.88
540	4		57.06	44.78	46.68	52.37	54.76
0	20		45.11	49.76	46.42	52.42	48.42
4	20		47.78	49.98	49.18	51.18	50.76
20	20		52.63	50.43	51.19	47.46	48.57
60	20		47.39	52.37	51.41	48.01	48.37
180	20		49.70	49.25	54.64	51.47	51.36
540	20		48.21	45.57	42.41	49.38	49.13
0	60		49.02	57.92	50.40	49.56	40.26
4	60		47.17	54.83	51.14	51.94	51.91
20	60		50.50	47.74	52.20	54.46	49.21
60	60		52.80	50.51	54.88	49.13	53.12
180	60		50.49	50.81	50.47	49.37	44.85
540	60		47.00	49.67	54.79	46.17	50.40
0	180		57.35	59.07	57.26	49.01	36.41
4	180		55.18	57.84	57.12	53.10	33.12
20	180		48.04	55.26	56.49	59.55	53.95
60	180		49.80	49.30	51.49	55.46	56.67
180	180		51.01	47.94	54.02	50.60	51.47
540	180		51.84	52.39	56.04	48.08	44.68
0	540		56.58	49.25	55.69	31.70	11.22
4	540		59.41	55.14	--	39.76	13.02
20	540		59.55	59.64	61.17	44.34	17.11
60	540		50.65	62.83	50.22	68.04	15.17
180	540		52.96	62.62	49.95	61.40	47.89
540	540		54.74	47.00	57.95	56.73	53.37

0000 = no water borders, 0001 = one water border, 0011 = two adjacent water borders, 0101 = two opposite water borders, 0111 = three water borders, 1111 = four water borders.

Appendix C

Spatial-Pattern Statistics of TM Scenes

Table C1. Values of the spatial-pattern indices measured in the TM imagery.

Table C-1. Values of the spatial pattern indices measured in the TM imagery: interface length, the side-adjacency statistics (number of water pixels with 0, 1, 2, 3, and 4 sides adjacent to other water pixels), and number of water pixels on the marsh border.

Quad	Quarter	DL	Interface Length	Adj-0	Adj-1	Adj-2	Adj-3	Adj-4	Border Pixels
Late Lafourche, salt									
Leeville	NW	42.94	9,093	114	439	2,124	2,964	9,856	332
	NE	34.93	10,025	159	713	2,315	2,473	6,860	355
	SE	39.91	10,118	146	519	2,470	2,901	8,369	308
	SW	46.74	6,115	54	253	1,495	2,061	13,064	304
Mink Bayou	NW	26.59	7,166	101	403	1,686	2,067	5,326	219
	NE	24.54	5,519	117	343	1,316	1,289	5,744	236
	SE	29.44	8,420	178	611	1,873	1,977	5,975	237
	SW	29.57	7,937	103	489	1,867	2,192	6,026	225
Caminada Pass	NW	62.09	6,778	80	344	1,669	1,998	18,306	493
	NE	82.87	1,341	3	20	418	411	29,050	646
	SE	99.27	101	0	1	34	25	35,792	741
	SW	58.02	3,884	114	254	952	705	18,845	518
Bay Tambour	NW	51.18	5,818	61	233	1,506	1,788	14,891	388
	NE	76.55	3,047	18	92	773	1,112	25,719	504
	SE	88.72	2,245	24	73	539	826	30,541	704
	SW	84.38	3,515	28	106	833	1,364	28,120	654
Pelican Pass	NW	98.96	341	1	11	67	161	35,491	751
	NE	82.60	2,433	7	93	579	932	28,221	617
	SE	86.68	2,100	13	64	500	839	29,910	629
	SW	97.24	385	0	4	100	160	34,833	751

Table C-1. (cont. 2)

Quad	Quarter	DL	Interface Length	Adj-0	Adj-1	Adj-2	Adj-3	Adj-4	Border Pixels
Early Lafourche, salt									
Grand Bayou du Large	NW	53.83	3,431	48	114	845	1,151	17,371	316
	NE	67.26	3,621	37	158	886	1,145	22,053	514
	SE	40.44	7,174	109	477	1,688	1,839	10,349	444
	SW	83.72	1,111	17	50	254	367	29,643	530
Lake La Graisse	NW	91.13	2,079	17	54	475	853	31,517	679
	NE	99.28	292	0	3	67	143	35,641	744
Central Isles Dernieres	NW	75.77	3,439	31	131	809	1,268	25,018	675
	NE	90.05	1,605	6	33	432	601	31,419	706
	SE	95.18	748	10	18	186	258	33,918	698
	SW	93.53	745	3	12	173	334	33,245	713
Cocodrie	NW	33.43	7,430	106	493	1,692	2,005	7,765	264
	NE	68.89	6,457	40	234	1,454	2,596	20,598	475
	SE	85.79	3,681	32	153	813	1,387	28,656	583
	SW	54.72	9,692	69	410	2,256	3,511	13,522	402
Dog Lake	NW	62.97	4,612	29	159	1,084	1,769	19,788	385
	NE	30.74	8,114	113	449	1,893	2,394	6,218	263
	SE	42.38	7,774	95	403	1,758	2,535	10,514	317
	SW	36.40	6,482	67	331	1,560	1,967	9,106	386

Table C-1. (cont. 3)

Quad	Quarter	DL	Interface Length	Adj-0	Adj-1	Adj-2	Adj-3	Adj-4	Border Pixels
Late Lafourche, brackish									
Lake Bully	NW	33.69	5,689	46	276	1,259	2,079	8,482	276
Camp	NE	47.84	9,158	101	562	2,039	2,845	11,744	344
	SE	22.21	6,157	122	413	1,363	1,578	4,481	230
	SW	50.02	9,502	78	469	2,124	3,373	11,989	406
Golden Meadow	NW	30.91	6,870	81	414	1,530	2,179	6,931	261
Farms	NE	60.69	5,700	80	367	1,181	1,836	18,357	553
	SE	35.56	8,163	86	515	1,813	2,538	7,862	294
	SW	38.95	4,954	47	243	1,085	1,775	11,049	159
Bay L'Ours	SE	81.53	3,572	42	254	820	963	27,359	617
	SW	52.26	1,755	34	106	387	513	17,837	387
Three Bayou	NW	32.93	7,393	108	469	1,670	2,108	7,410	375
Bay	NE	58.71	4,136	60	217	974	1,218	18,775	398
Golden Meadow	SW	27.66	9,367	182	709	2,118	2,184	4,802	202

Table C-1. (cont. 4)

Quad	Quarter	DL	Interface Length	Adj-0	Adj-1	Adj-2	Adj-3	Adj-4	Border Pixels
Early Lafourche, brackish									
Lost Lake	NW	32.65	6,093	62	329	1,352	2,074	8,031	187
	NE	47.32	9,209	107	550	2,069	2,848	11,576	294
	SE	21.81	7,227	126	496	1,644	1,820	3,689	265
	SW	50.78	8,645	75	442	1,912	3,078	12,874	340
Lake Mechant	NW	64.05	6,070	69	325	1,449	1,836	19,400	534
	NE	29.91	6,782	90	379	1,613	1,957	6,710	267
	SE	44.91	4,570	37	168	1,197	1,471	13,303	380
	SW	67.06	3,050	23	122	823	894	22,310	550
Bayou Sauveur	NW	8.72	3,578	82	291	771	791	1,239	42
	NE	10.90	5,847	160	556	1,201	1,030	966	106
	SE	22.23	5,580	79	323	1,309	1,559	4,721	203
	SW	24.31	4,892	36	199	1,245	1,592	5,748	140
Lake Quitman	NE	48.20	6,983	69	348	1,608	2,326	13,105	312
	SE	32.41	5,981	64	302	1,421	1,881	8,035	244
	SW	31.85	6,545	63	365	1,574	1,948	7,490	301
Dulac	NE	9.63	3,708	82	298	791	883	1,468	29
	SE	66.80	2,710	30	115	666	854	22,739	221
Montegut	SE	47.48	8,315	112	479	1,828	2,657	12,077	349
	SW	27.16	6,787	67	423	1,521	2,103	5,661	237

Appendix D

Simulation Results

Table D1. W, G, and BC selected by the expert system to simulate each TM scene.

Table D2. Values of spatial-pattern indices from 70 simulations.

Table D3. Simulation values for interface length and disintegration level compared with TM scene disintegration levels.

Table D4. Coefficients of variation from three sets of three replicate simulations using the same values of W, G, and BC.

Figure D1. "Best-fit" simulations showing interface as a function of disintegration level for 70 marsh sites in coastal Louisiana.

Figure D2. Coefficients of variation of spatial-pattern indices from three sets of three repeated simulations with the same W, G, BC, and DL values.

Table D1. W, G, and border condition (BC) selected by the expert system to simulate each TM scene, with disintegration level (DL), target BC, decision number (DE), and CV. (DE is expressed as percentage total water pixels [TWP].)

Quad	Quarter	DL	W	G	BC	Target BC	DE/TWP	CV
Late Lafourche, salt								
Leeville	NW	42.94	272	60	0011		195.1	42
	NE	34.93	188	0	0111		197.2	43
	SE	39.91	237	4	0011		194.4	42
	SW	46.74	8	180	0011		196.8	128
Mink Bayou	NW	26.59	244	180	0101		197.8	46
	NE	24.54	24	180	0011		197.4	115
	SE	29.44	248	0	0111		197.8	58
	SW	29.57	261	180	0001		193.5	45
Caminada Pass	NW	62.09	58	180	0111		190.6	9
	NE	82.87	13	540	0111	0101	197.8	78
	SE	99.27	1	540	0011		198.0	225
	SW	58.02	28	540	0011		197.6	32
Bay Tambour	NW	51.18	31	180	0111		190.0	41
	NE	76.55	17	540	0011		198.2	84
	SE	88.72	107	540	0111		197.9	53
	SW	84.38	13	180	0111		197.6	74
Pelican Pass	NW	98.96	8	180	0111		197.9	56
	NE	82.60	88	540	0111		198.0	35
	SE	86.68	16	540	0011		197.8	76
	SW	97.24	38	540	1111	0111	197.9	49
Early Lafourche, salt								
Grand Bayou du Large	NW	53.83	30	540	0011		198.4	40
	NE	67.26	29	540	0011		197.9	36
	SE	40.44	14	180	0011		197.0	95
	SW	83.72	0	540	0011	0001	98.1	211
Lake La Graisse	NW	91.13	113	540	0111		198.0	55
	NE	99.28	10	180	0111		197.8	71
Central Isles Dernieres	NW	75.77	26	180	1111		197.1	26
	NE	90.05	43	540	0111		197.8	70
	SE	95.18	16	540	0111	0101	198.0	26
	SW	93.53	33	540	1111	0111	197.9	43
Cocodrie	NW	33.43	115	180	0101		193.9	72
	NE	68.89	311	540	0001		197.2	55
	SE	85.79	69	540	0011		195.6	15
	SW	54.72	233	60	0011		196.0	30
Dog Lake	NW	62.97	44	540	0011	0001	198.3	65
	NE	30.74	213	180	0101		193.7	32
	SE	42.38	120	180	0011		198.0	56
	SW	36.40	123	540	0001	0101	197.1	61

Table D-1. (cont.)

Quad	Quarter	DL	W	G	BC	Target BC	DE/TWP	CV
Late Lafourche, brackish								
Lake Bully	NW	33.69	62	180	0111		197.8	90
Camp	NE	47.84	244	180	0001		198.0	52
	SE	22.21	130	60	0011		192.1	88
	SW	50.02	255	60	1111		197.8	41
Golden Meadow	NW	30.91	129	180	0011		197.7	45
Farms	NE	60.69	160	540	0011		197.5	14
	SE	35.56	308	60	0011		193.8	47
	SW	38.95	3,184	0	0000	0001	198.9	53
Bay L'Ours	SE	81.53	8	180	0111		197.9	58
	SW	52.26	1	540	0011		98.0	807
Three Bayou	NW	32.93	100	60	1111		196.9	80
Bay	NE	58.71	33	540	0011	0001	198.2	43
Golden Meadow	SW	27.66	116	0	0011		198.0	82
Early Lafourche, brackish								
Lost Lake	NW	32.65	23	180	0011		198.4	131
	NE	47.32	245	180	0001		198.3	53
	SE	21.81	111	60	0111		196.7	66
	SW	50.78	290	20	0111		195.8	61
Lake Mechant	NW	64.05	4	180	0011		196.4	132
	NE	29.91	118	60	0011		194.1	86
	SE	44.91	86	540	0011		190.5	35
	SW	67.06	17	540	0011		197.8	81
Bayou Sauveur	NW	8.72	325	0	0000		198.8	78
	NE	10.90	93	0	0000		197.4	61
	SE	22.23	133	180	0011		197.5	45
	SW	24.31	35	540	0001		198.4	141
Lake Quitman	NE	48.20	116	540	0001		196.3	75
	SE	32.41	20	180	0011		197.9	110
	SW	31.85	121	180	0011	0111	197.4	52
Dulac	NE	9.63	701	0	0000		199.2	39
	SE	66.80	10,947	0	0000		---	--
Montegut	SE	47.48	289	180	0101		195.3	59
	SW	27.16	404	0	0000		197.6	70

Key to BC: 0 = land border, 1 = water border. For example, 0101 indicates two opposite water borders.
The maximum possible value of 100 DE/TWP is slightly less than 200.

Table D-2. Values of spatial pattern indices from the 70 simulations: interface length, side-adjacency statistics (number of water pixels with 0, 1, 2, 3, and 4 sides adjacent to other water pixels), and number of water pixels on the marsh border. Disintegration level (DL, water area as percentage total area) is also shown.

Quad	Quarter	DL	Interface Length	Adj-0	Adj-1	Adj-2	Adj-3	Adj-4	Border Pixels
Late Lafourche, salt									
Leeville	NW	42.94	9,133	21	665	1,853	3,295	9,551	443
	NE	34.93	9,935	17	802	2,048	3,279	6,534	195
	SE	39.91	9,811	16	760	1,947	3,440	8,299	251
	SW	46.74	7,780	353	1,174	1,026	721	13,460	497
Mink Bayou	NW	26.59	7,241	658	658	1,455	2,218	5,004	439
	NE	24.54	6,359	237	904	969	730	5,778	426
	SE	29.44	8,681	18	737	1,743	2,845	5,397	110
	SW	29.57	8,163	18	698	1,635	2,678	5,584	289
Caminada Pass	NW	62.09	6,989	33	667	1,396	2,041	18,074	679
	NE	82.87	1,323	76	131	169	280	29,187	705
	SE	99.27	190	12	11	21	53	35,763	733
	SW	58.02	3,946	106	538	653	582	19,006	503
Bay Tambour	NW	51.18	5,884	111	747	1,013	1,153	15,202	640
	NE	76.55	3,057	74	433	478	471	26,191	570
	SE	88.72	2,255	7	164	451	831	30,542	711
	SW	84.38	3,774	70	448	669	796	28,413	708
Pelican Pass	NW	98.96	534	1	34	82	261	35,356	748
	NE	82.60	2,395	11	206	482	763	28,283	703
	SE	86.68	2,357	45	302	418	411	30,161	618
	SW	97.24	442	7	40	80	134	34,822	764

Table D-2. (cont. 2)

Quad	Quarter	DL	Interface Length	Adj-0	Adj-1	Adj-2	Adj-3	Adj-4	Border Pixels
Early Lafourche, salt									
Grand Bayou du Large	NW	53.83	3,797	114	510	618	542	17,550	510
	NE	67.26	4,048	73	534	701	726	22,217	541
	SE	40.44	7,978	298	1,077	1,277	937	10,845	471
	SW	83.72	1,678	266	83	89	158	29,645	619
Lake La Graisse	NW	91.13	2,039	2	148	413	748	31,565	719
	NE	99.28	492	1	22	57	302	35,459	756
Central Isles Dernieres	NW	75.77	3,548	58	382	669	832	25,227	764
	NE	90.05	1,315	19	143	224	360	31,723	727
	SE	95.18	719	11	73	120	210	33,935	739
	SW	93.53	842	17	74	163	226	33,236	764
Cocodrie	NW	33.43	9,375	40	846	1,949	2,741	6,287	461
	NE	68.89	7,116	4	435	1,397	2,931	20,194	436
	SE	85.79	3,240	10	229	659	1,165	28,964	597
	SW	54.72	9,279	7	599	1,822	3,758	13,490	493
Dog Lake	NW	62.97	4,397	57	480	869	954	20,321	532
	NE	30.74	8,129	25	710	1,663	2,542	5,937	453
	SE	42.38	9,434	26	798	1,932	3,026	9,381	459
	SW	36.40	8,615	45	803	1,712	2,545	7,990	321

Table D-2. (cont. 3)

Quad	Quarter	DL	Interface Length	Adj-0	Adj-1	Adj-2	Adj-3	Adj-4	Border Pixels
Late Lafourche, brackish									
Lake Bully Camp	NW	33.69	5,831	71	678	1,126	1,246	8,680	617
	NE	47.84	9,099	9	662	1,800	3,402	11,405	357
	SE	22.21	8,350	44	805	1,732	2,224	2,951	431
	SW	50.02	9,398	13	676	1,845	3,610	11,537	758
Golden Meadow Farms	NW	30.91	8,050	41	761	1,691	2,186	6,281	435
	NE	60.69	6,239	20	512	1,258	2,072	17,993	519
	SE	35.56	8,567	19	683	1,751	2,872	7,320	462
	SW	38.95	4,430	3	319	853	1,731	11,360	92
Bay L'Ours	SE	81.53	3,308	107	443	517	503	27,790	694
	SW	52.26	2,484	386	138	123	269	17,852	495
Three Bayou Bay	SE	32.93	9,304	34	831	1,887	2,887	5,743	758
	SW	58.71	4,108	85	533	749	664	19,110	501
Golden Meadow	SW	27.66	10,187	45	909	2,078	3,029	4,006	129

Table D-2. (cont. 4)

Quad	Quarter	DL	Interface Length	Adj-0	Adj-1	Adj-2	Adj-3	Adj-4	Border Pixels
Early Lafourche, brackish									
Lost Lake	NW	32.65	7,570	199	1,088	1,227	1,008	8,059	453
	NE	47.32	9,387	16	672	1,863	3,512	11,034	347
	SE	21.81	8,247	54	821	1,677	2,152	2,752	584
	SW	50.78	9,253	10	620	1,853	3,545	12,138	555
Lake Mechant	NW	64.05	7,697	412	1,137	976	594	19,940	554
	NE	29.91	9,797	39	857	1,998	3,003	4,663	464
	SE	44.91	4,844	67	526	946	1,089	13,462	465
	SW	67.06	3,223	134	440	474	394	22,755	524
Bayou Sauveur	NW	8.72	3,997	24	430	820	942	959	41
	NE	10.90	6,316	69	776	1,244	1,139	714	76
	SE	22.23	6,737	45	678	1,330	1,833	3,885	422
	SW	24.31	6,319	148	903	1,067	829	5,730	283
Lake Quitman	NE	48.20	9,468	24	773	1,880	3,208	11,475	408
	SE	32.41	7,261	252	989	1,167	897	8,185	456
	SW	31.85	8,002	36	797	1,577	2,283	6,598	449
Dulac	NE	9.63	3,445	10	311	708	1,024	1,460	37
	SE	66.80	2,853	1	182	502	1,265	22,312	363
Montegut	SE	47.48	8,551	19	670	1,674	3,087	11,578	473
	SW	27.16	7,439	14	578	1,577	2,417	5,303	123

Table D3. Simulation values for interface length and disintegration level (DL) compared with TM scene disintegration levels, with deviation and percentage deviation.

Quad	Quarter	Maximum Sim. Interface Length	DL at Sim. Maximum Interface	1985 TM DL	Sign of Diff. (Sim.-TM)
Late Lafourche, salt					
Leeville	NW	9,329	51.8	42.0	+
	NE	10,681	47.6	34.0	+
	SE	10,156	49.3	39.0	+
	SW	8,638	63.8	46.0	+
Mink Bayou	NW	8,905	51.1	26.0	+
	NE	10,200	55.6	24.0	+
	SE	9,923	49.5	29.0	+
	SW	9,543	56.6	29.0	+
Caminada Pass	NW	7,087	60.4	62.0	-
	NE	2,188	33.2	82.0	-
	SE	2,582	42.6	99.0	-
	SW	4,110	67.1	58.0	+
Bay Tambour	NW	6,232	65.7	51.0	+
	NE	3,444	60.2	76.0	-
	SE	3,273	72.6	88.0	-
	SW	5,086	59.6	84.0	-
Pelican Pass	NW	4,608	63.4	98.0	-
	NE	3,113	57.1	82.0	-
	SE	3,265	59.0	86.0	-
	SW	2,417	10.9	97.0	-
Early Lafourche, salt					
Grand Bayou du Large	NW	4,010	60.1	53.0	+
	NE	4,180	61.6	67.0	-
	SE	9,196	59.3	40.0	+
	SW	2,514	54.8	83.0	-
Lake La Graisse	NW	3,430	67.0	91.0	-
	NE	4,738	50.6	99.0	-
Central Isles Dernieres	NW	4,442	53.1	75.0	-
	NE	2,388	54.7	90.0	-
	SE	2,187	60.3	95.0	-
	SW	2,443	13.3	93.0	-
Cocodrie	NW	10,496	50.6	33.0	+
	NE	8,108	46.7	68.0	-
	SE	5,122	59.8	85.0	-
	SW	9,624	47.9	54.0	-
Dog Lake	NW	4,473	59.4	62.0	-
	NE	9,375	53.4	30.0	+
	SE	9,662	45.5	42.0	+
	SW	9,737	51.8	36.0	+

Table D-3. (cont.)

Quad	Quarter	Maximum Interface Length	DL at Maximum Interface	1985 DL	Sign of Diff.
<u>Late Lafourche, brackish</u>					
Lake Bully	NW	7,055	61.7	33.0	+
Camp	NE	9,203	54.4	47.0	+
	SE	10,787	57.4	22.0	+
	SW	9,410	49.6	50.0	-
Golden Meadow	NW	10,033	52.6	30.0	+
Farms	NE	6,393	57.8	60.0	-
	SE	9,142	55.8	35.0	+
	SW	4,459	44.6	38.0	+
Bay L'Ours	SE	4,496	44.6	81.0	-
	SW	2,582	42.6	52.0	-
Three Bayou	SE	9,835	46.6	32.0	+
Bay	SW	4,218	56.8	58.0	-
Golden Meadow	SW	12,284	50.3	27.0	+
<u>Early Lafourche, brackish</u>					
Lost Lake	NW	9,934	57.3	32.0	+
	NE	9,469	51.5	47.0	+
	SE	10,869	52.2	21.0	+
	SW	9,346	45.2	50.0	-
Lake Mechant	NW	7,717	63.2	64.0	-
	NE	11,116	53.2	29.0	+
	SE	5,717	59.0	44.0	+
	SW	3,302	62.3	67.0	-
Bayou Sauveur	NW	9,362	48.1	8.0	+
	NE	13,189	48.7	10.0	+
	SE	8,925	48.7	22.0	+
	SW	10,567	58.0	24.0	+
Lake Quitman	NE	9,602	48.7	48.0	=
	SE	9,235	55.3	32.0	+
	SW	9,378	49.2	31.0	+
Dulac	NE	7,600	49.5	9.0	+
	SE	3,425	41.2	66.0	-
Montegut	SE	8,576	46.7	47.0	=
	SW	8,937	48.8	27.0	+

Table D4. Coefficients of variation (CV) from three sets of three replicate simulations using the same values of W, G, and BC.

Spatial Pattern Index	Set 1	Set 2	Set 3	Mean
Interface	5.02	10.72	3.11	6.24
Adj-0	3.95	71.25	53.29	42.83
Adj-1	8.26	7.75	2.69	6.23
Adj-2	5.57	14.80	1.66	7.34
Adj-3	2.57	10.93	5.37	6.29
Adj-4	4.02	0.54	1.96	2.17
Mean	4.90	19.33	11.35	

Set 1: W = 275, G = 0, BC = 1111, DL = 29.44

Set 2: W = 111, G = 540, BC = 1000, DL = 88.72

Set 3: W = 337, G = 180, BC = 1010, DL = 47.48

Figure D1. "Best-fit" simulations showing interface as a function of disintegration level for 70 marsh sites in coastal Louisiana. The ⊕ symbol indicates the coordinates of the comparable TM scene for each. Quadrangles are presented in the same order as in Table D1.

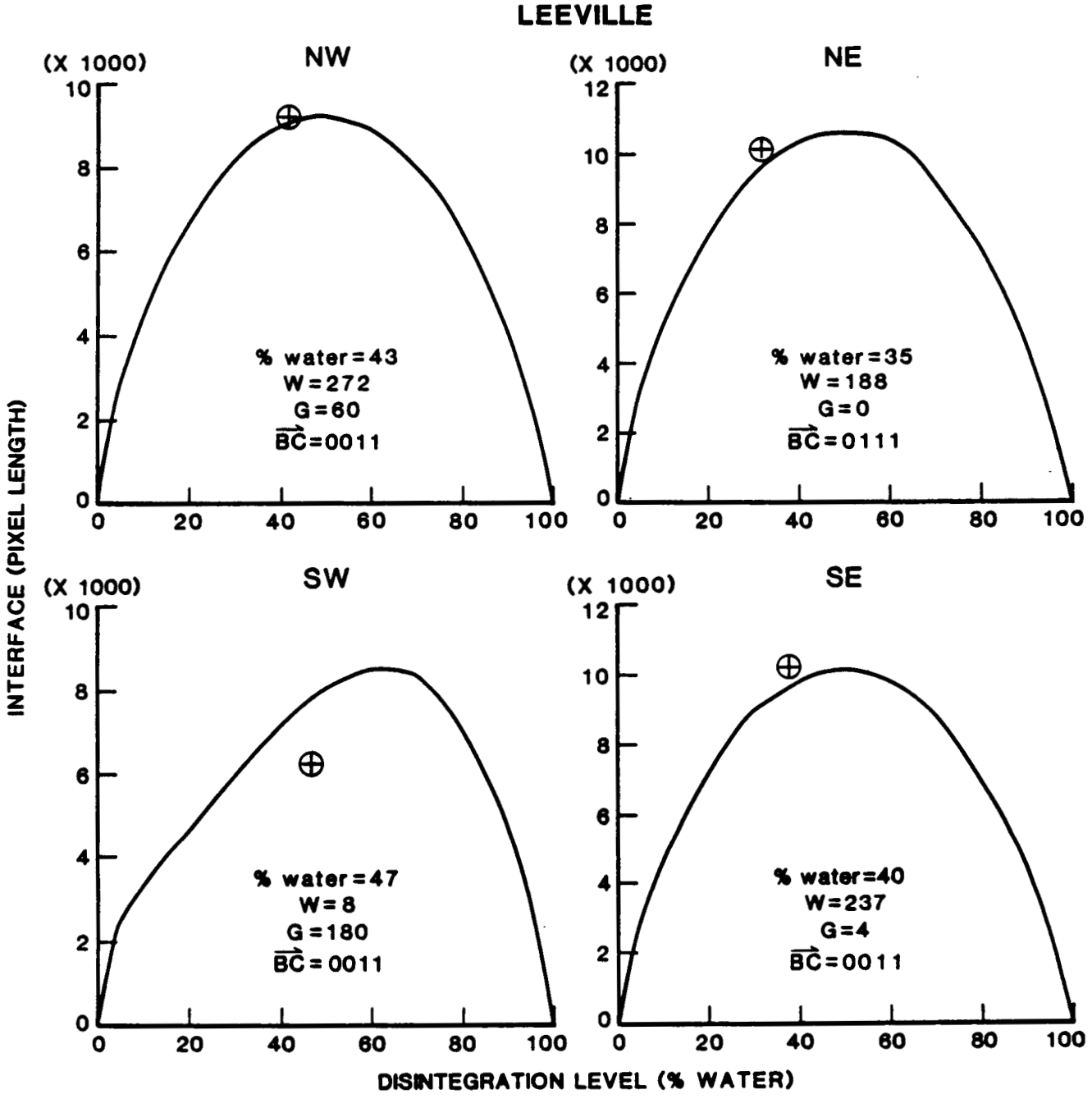

Figure D1-1. Simulated interface versus disintegration level, with TM scene coordinates, for the Leeville quadrangle.

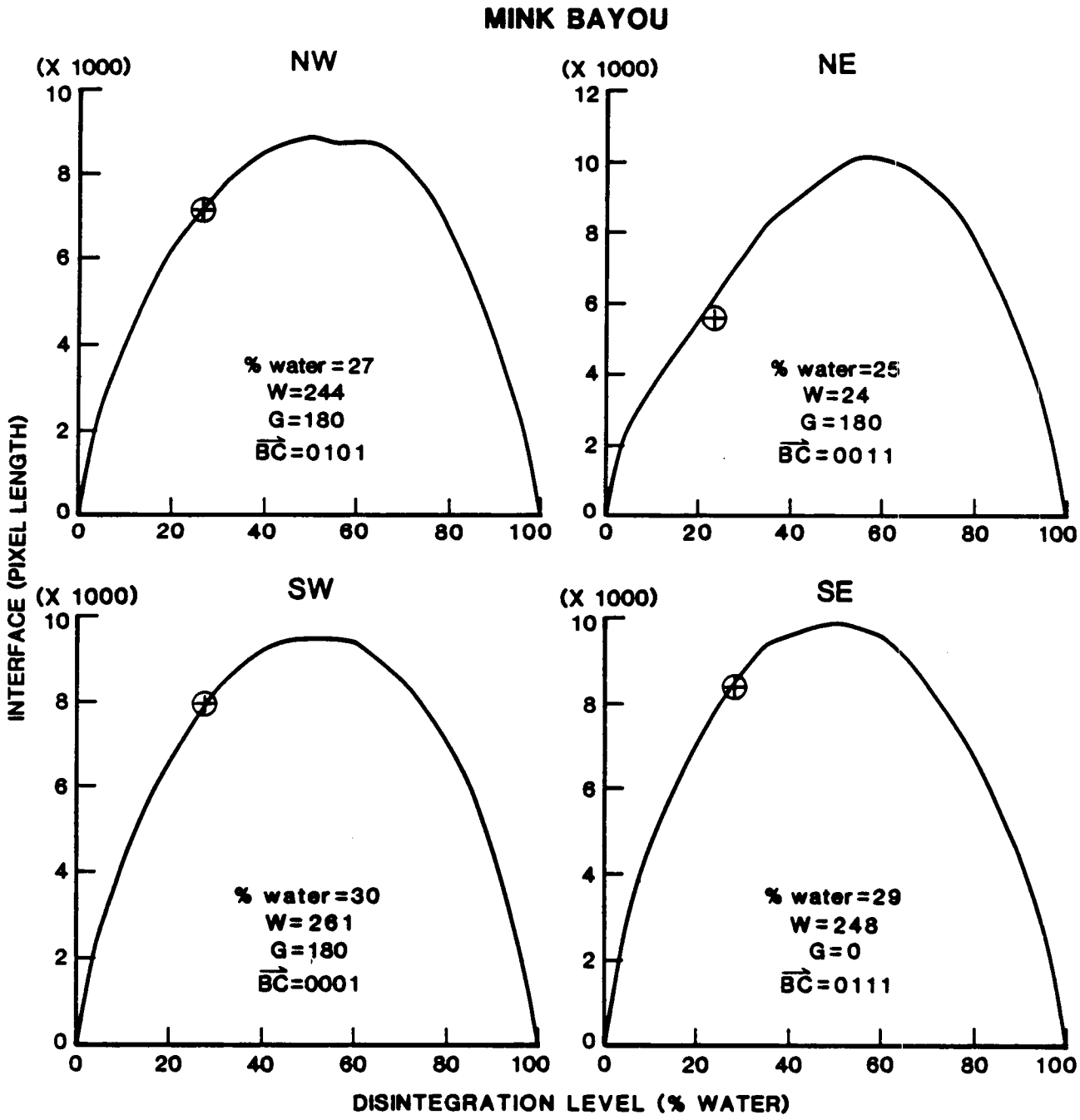

Figure D1-2. Simulated interface versus disintegration level, with TM scene coordinates, for the Mink Bayou quadrangle.

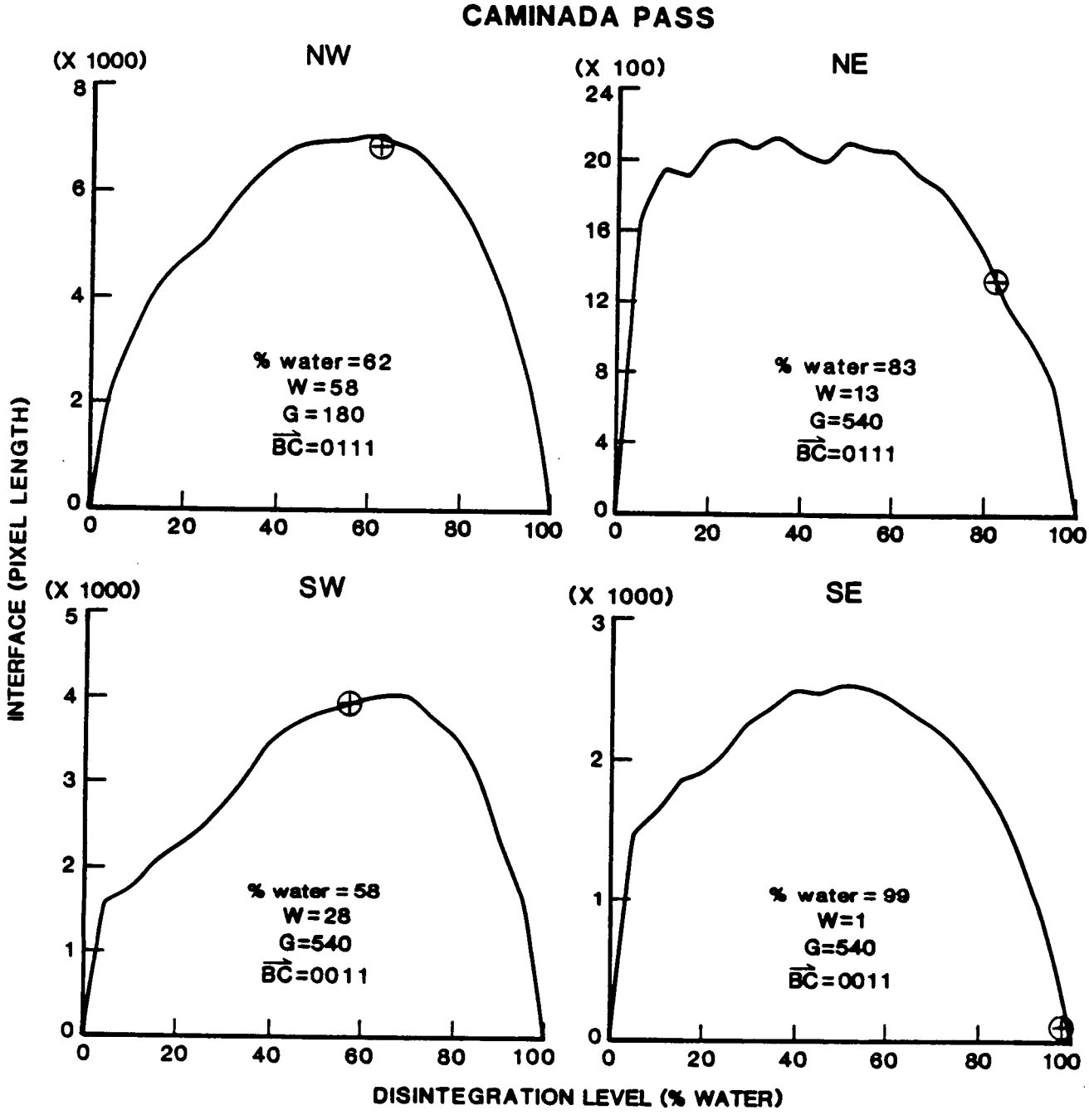

Figure D1-3. Simulated interface versus disintegration level, with TM scene coordinates, for the Caminada Pass quadrangle.

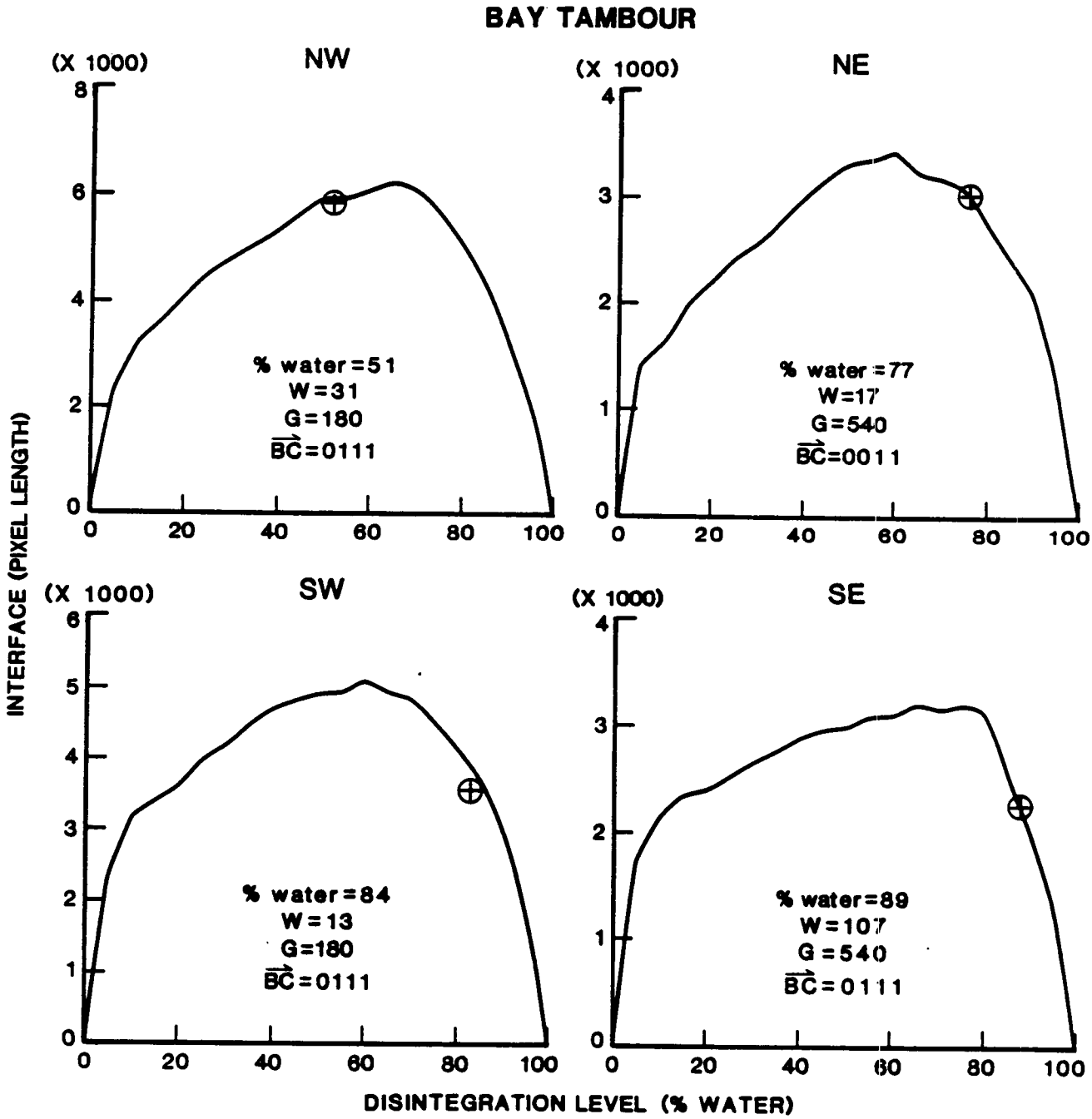

Figure D1-4. Simulated interface versus disintegration level, with TM scene coordinates, for the Bay Tambour quadrangle.

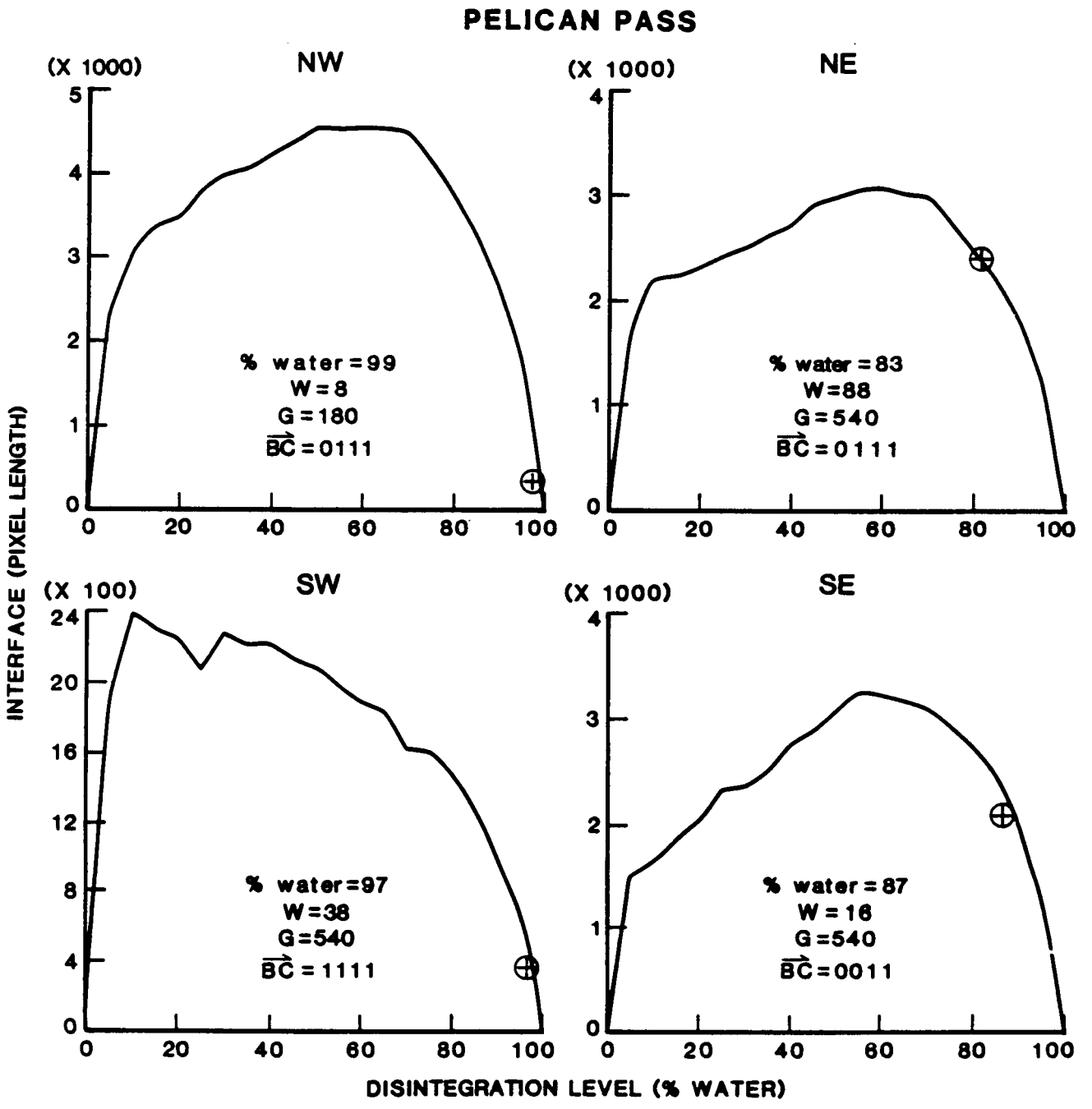

Figure D1-5. Simulated interface versus disintegration level, with TM scene coordinates, for the Pelican Pass quadrangle.

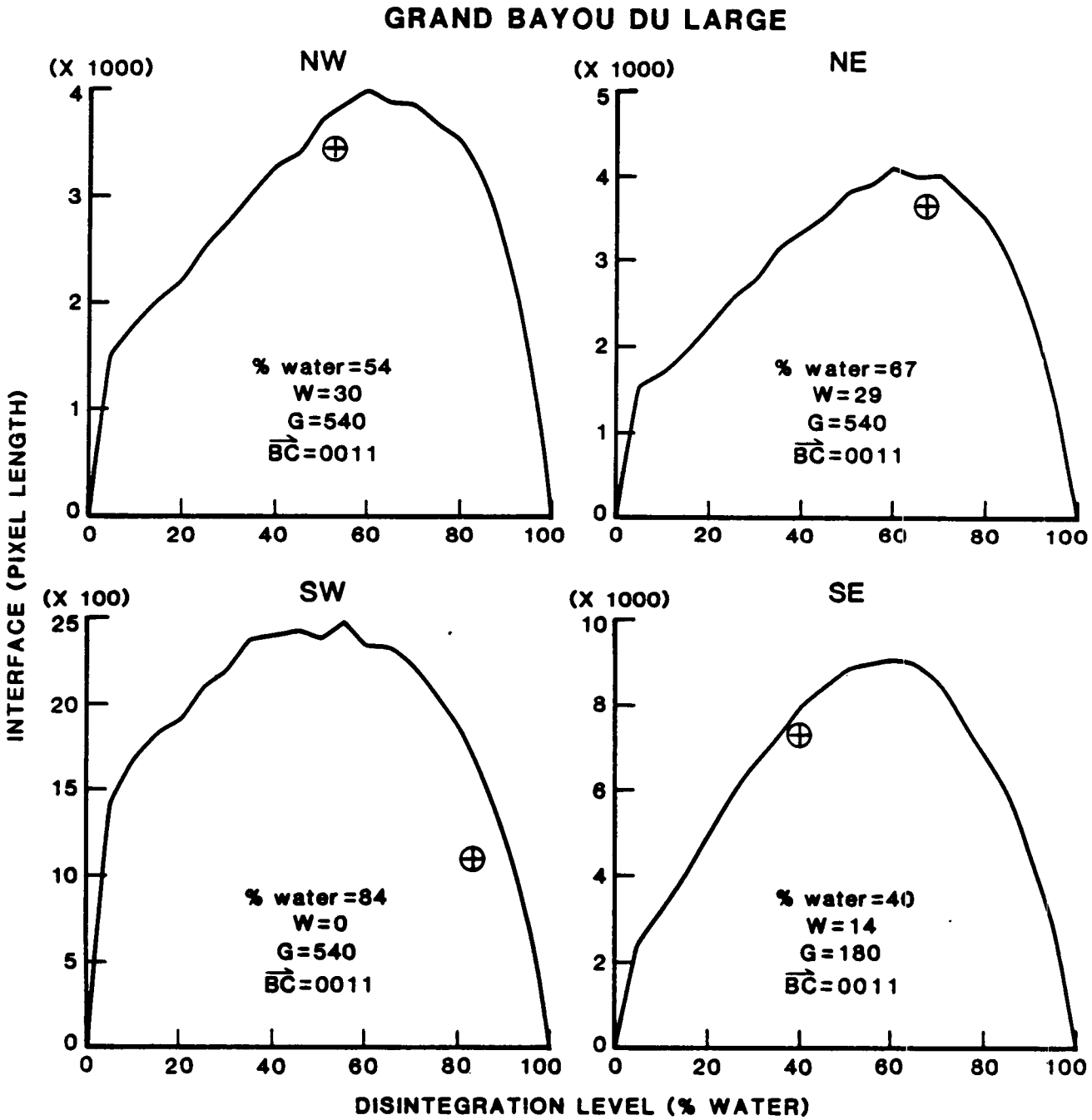

Figure D1-6. Simulated interface versus disintegration level, with TM scene coordinates, for the Grand Bayou du Large quadrangle.

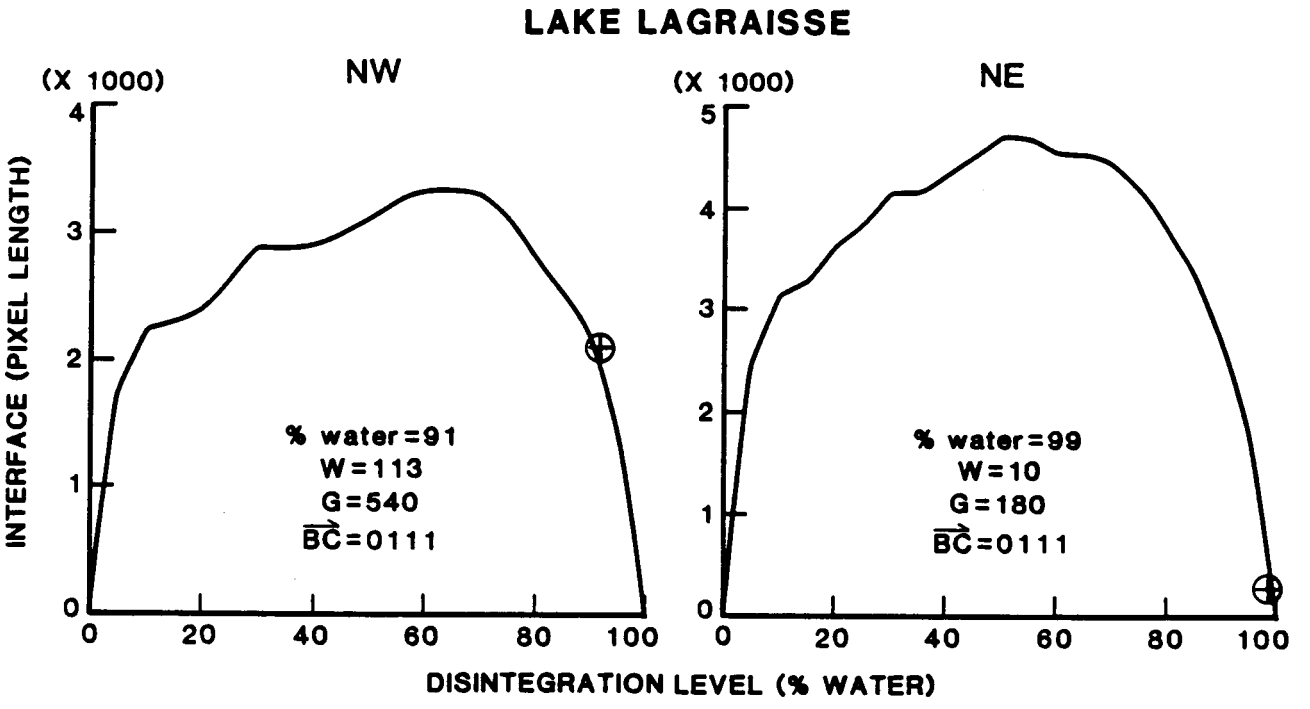

Figure D1-7. Simulated interface versus disintegration level, with TM scene coordinates, for the Lake La Graisse quadrangle.

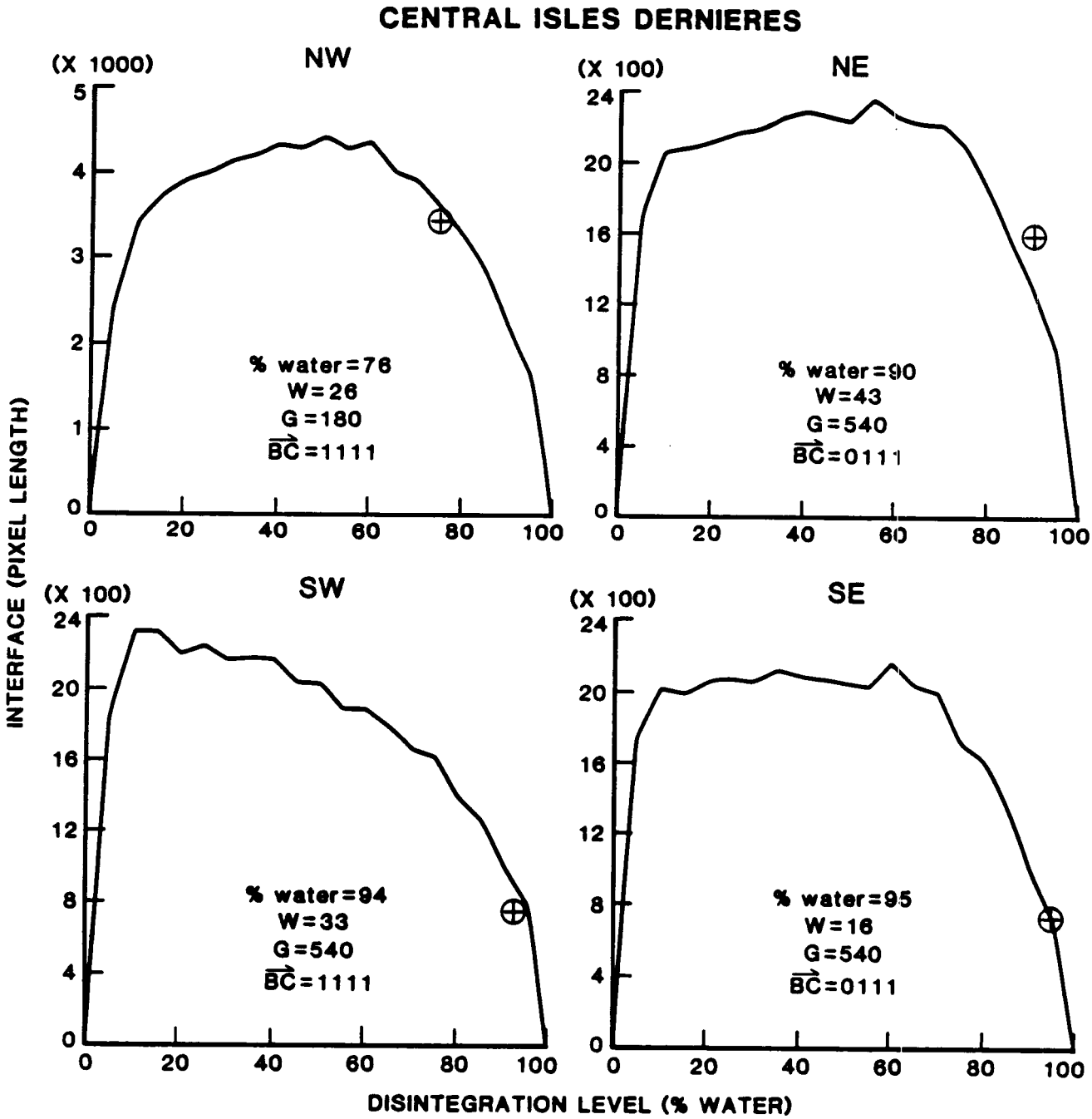

Figure D1-8. Simulated interface versus disintegration level, with TM scene coordinates, for the Central Isles Dernieres quadrangle.

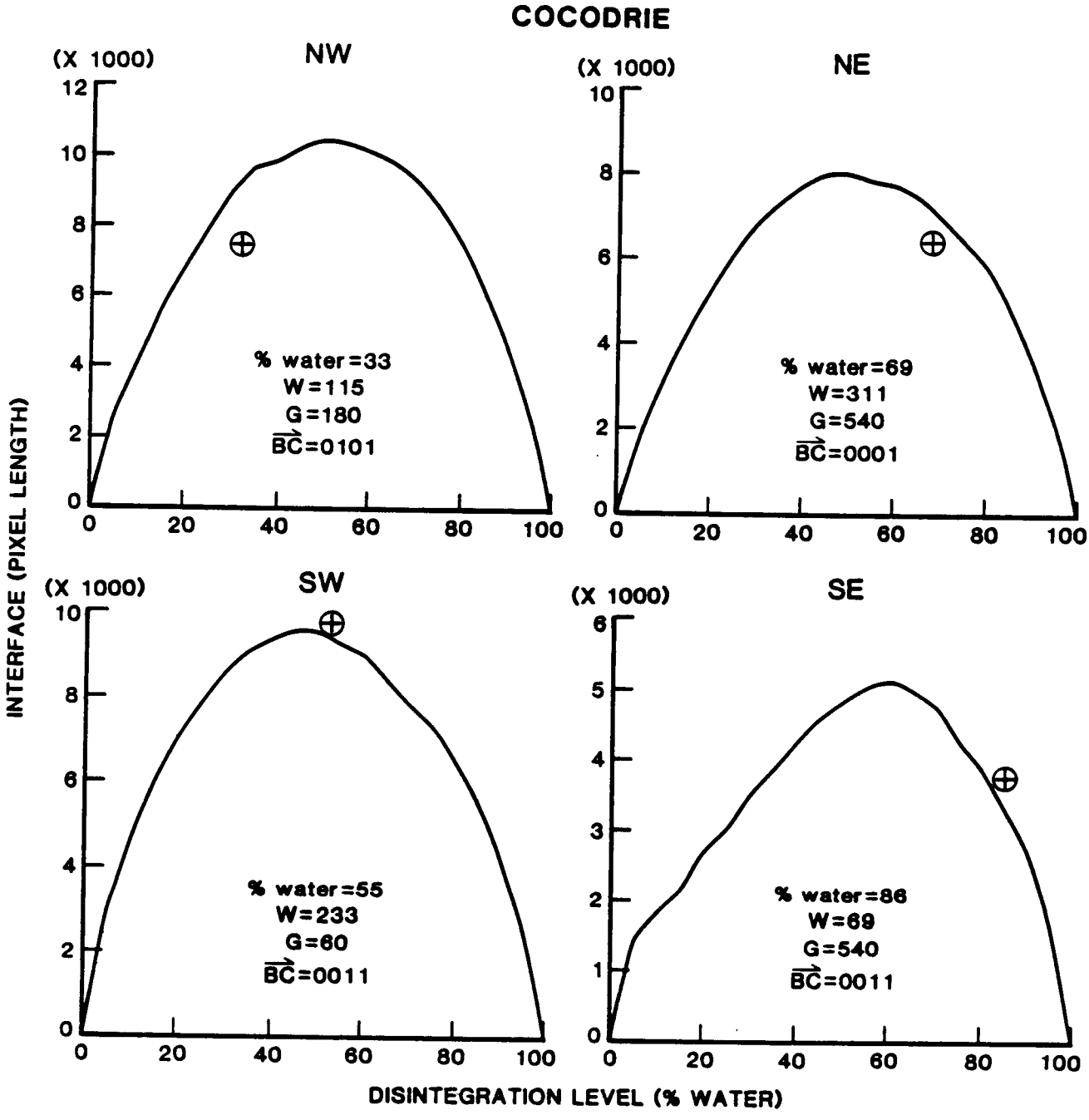

Figure D1-9. Simulated interface versus disintegration level, with TM scene coordinates, for the Cocodrie quadrangle.

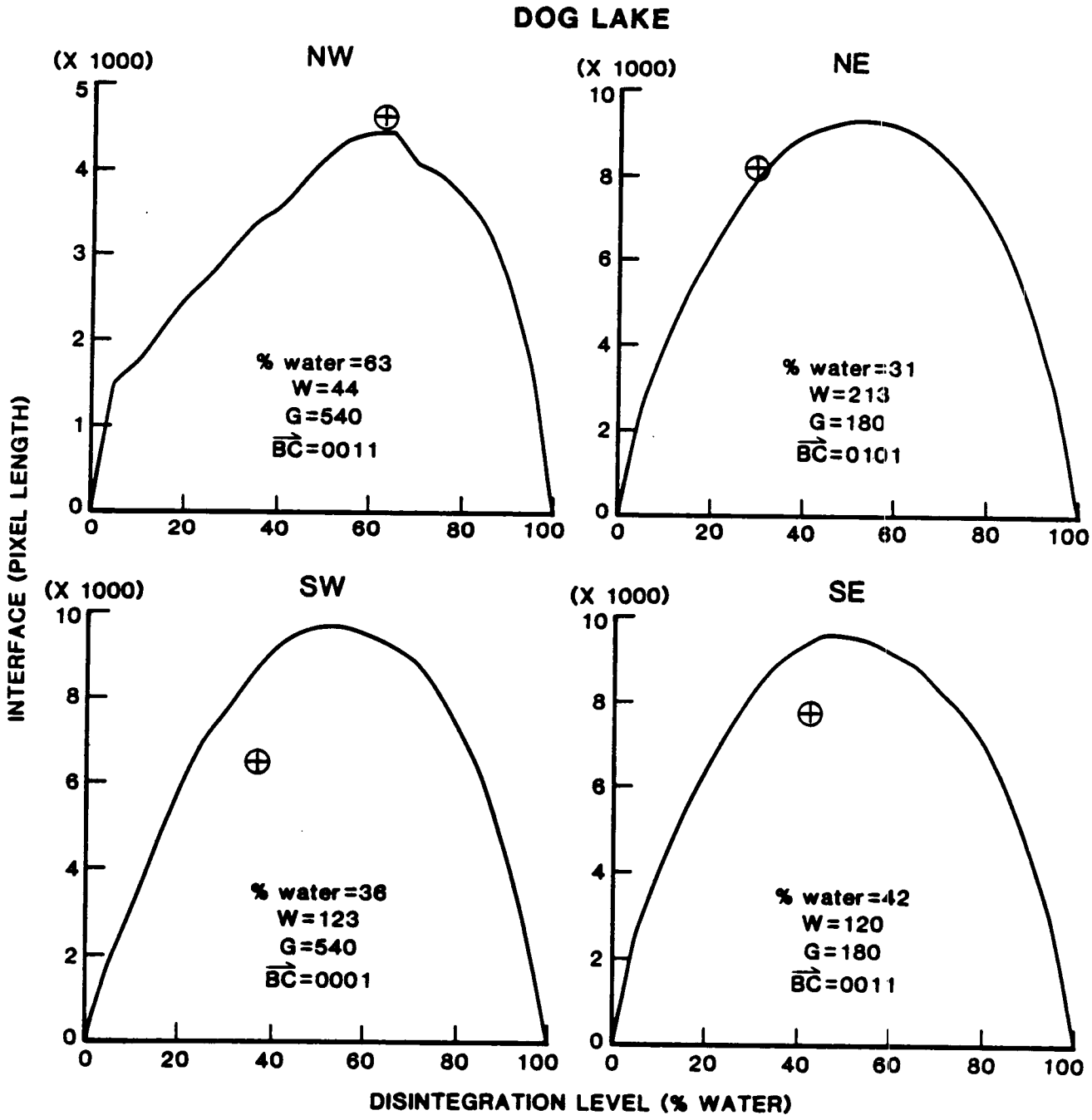

Figure D1-10. Simulated interface versus disintegration level, with TM scene coordinates, for the Dog Lake quadrangle.

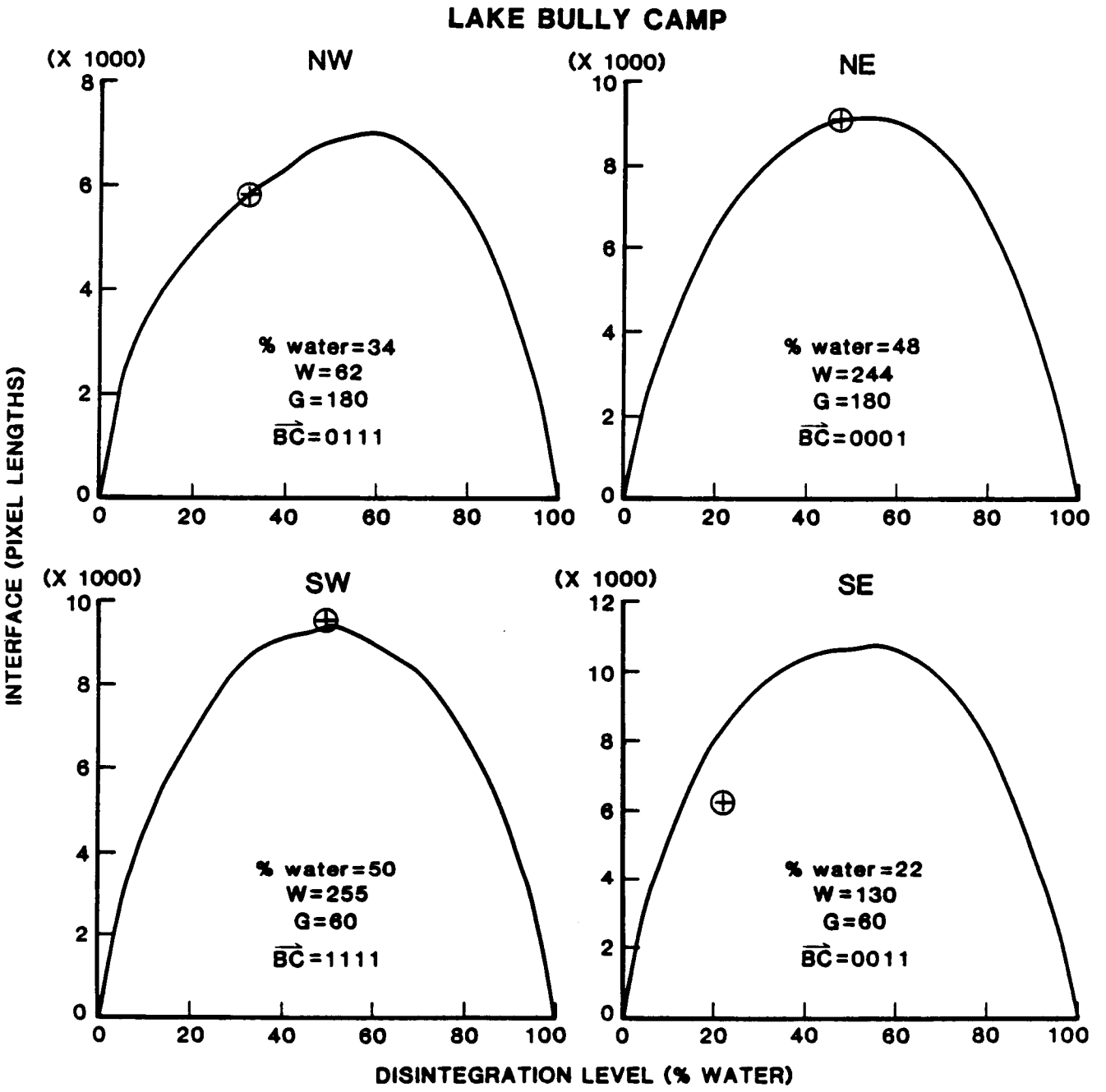

Figure D1-11. Simulated interface versus disintegration level, with TM scene coordinates, for the Lake Bully Camp quadrangle.

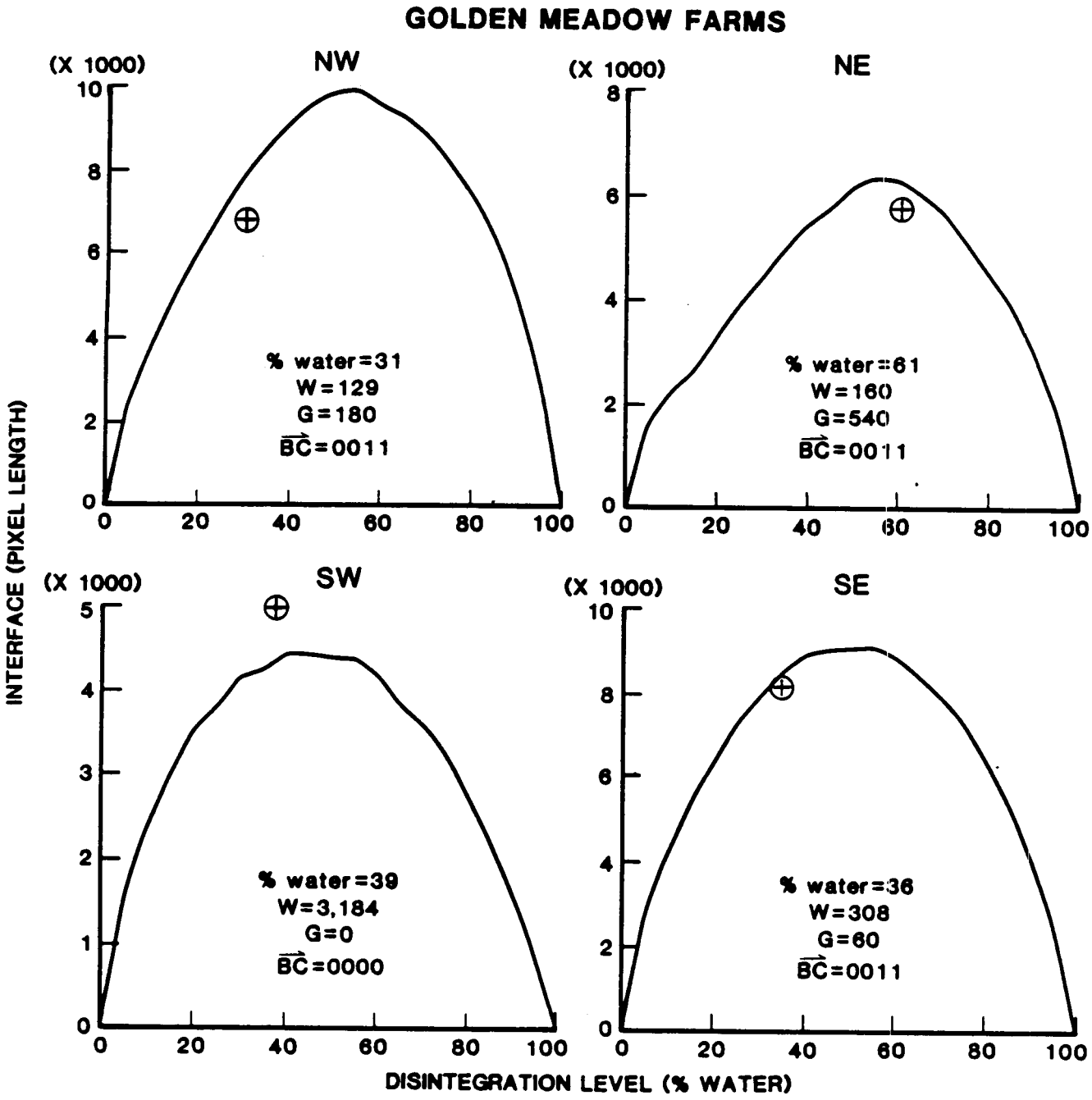

Figure D1-12. Simulated interface versus disintegration level, with TM scene coordinates, for the Golden Meadow Farms quadrangle.

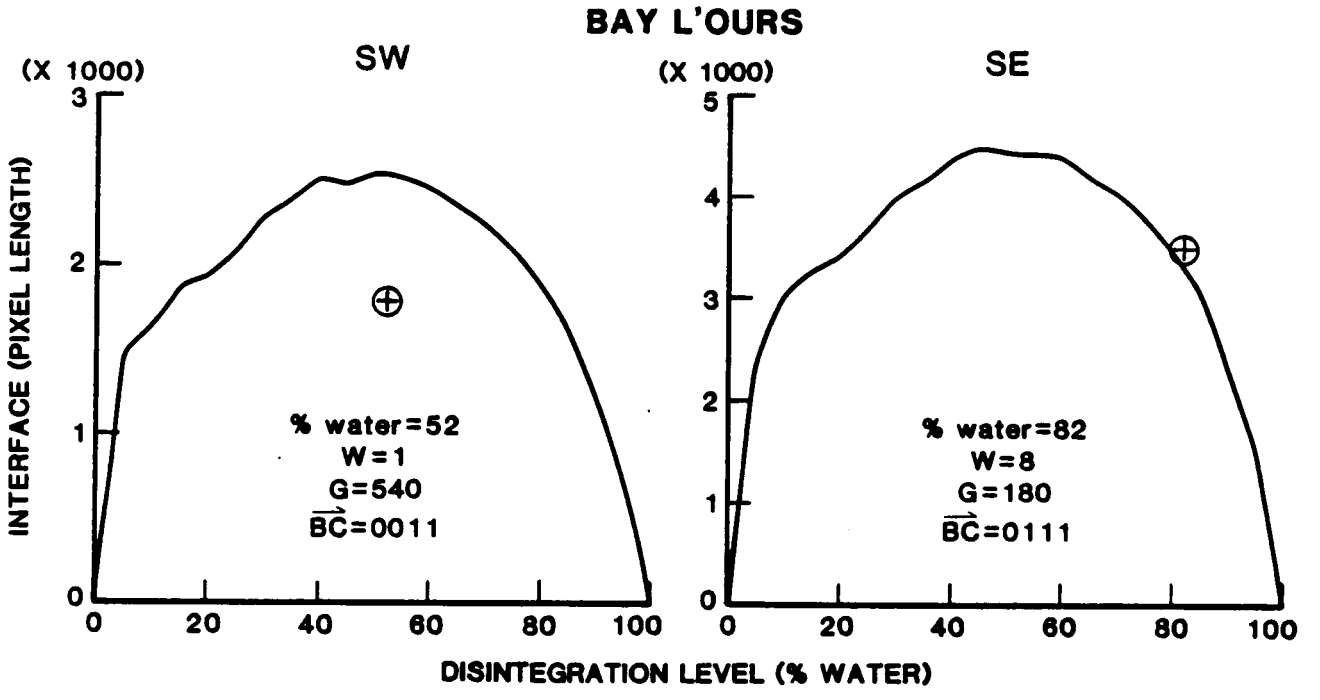

Figure D1-13. Simulated interface versus disintegration level, with TM scene coordinates, for the Bay L'Ours quadrangle.

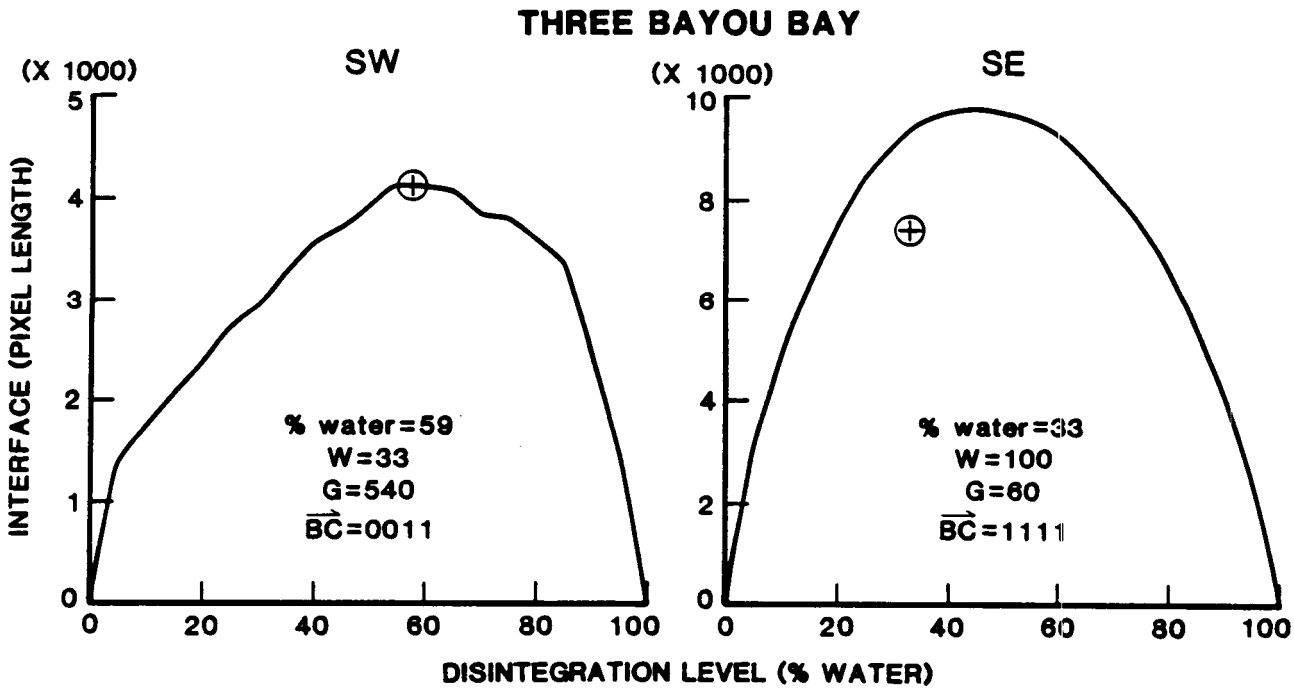

Figure D1-14. Simulated interface versus disintegration level, with TM scene coordinates, for the Three Bayou Bay quadrangle.

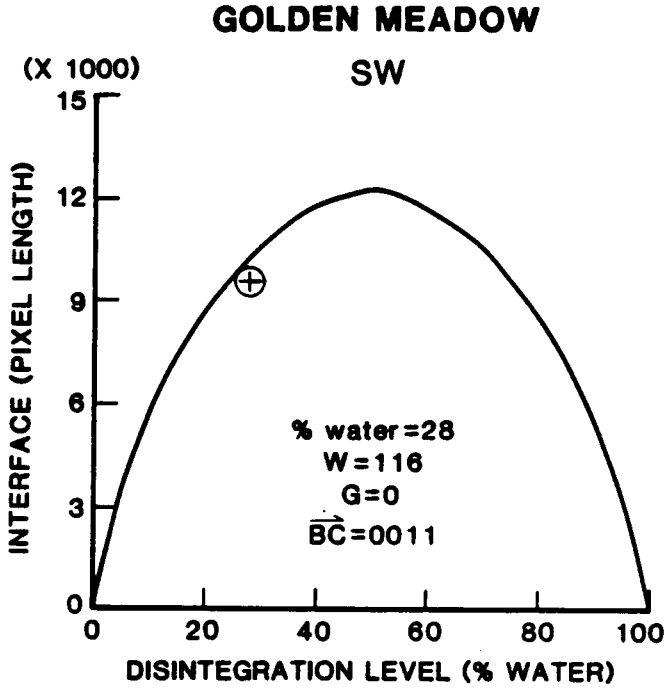

Figure D1-15. Simulated interface versus disintegration level, with TM scene coordinates, for the Golden Meadow quadrangle.

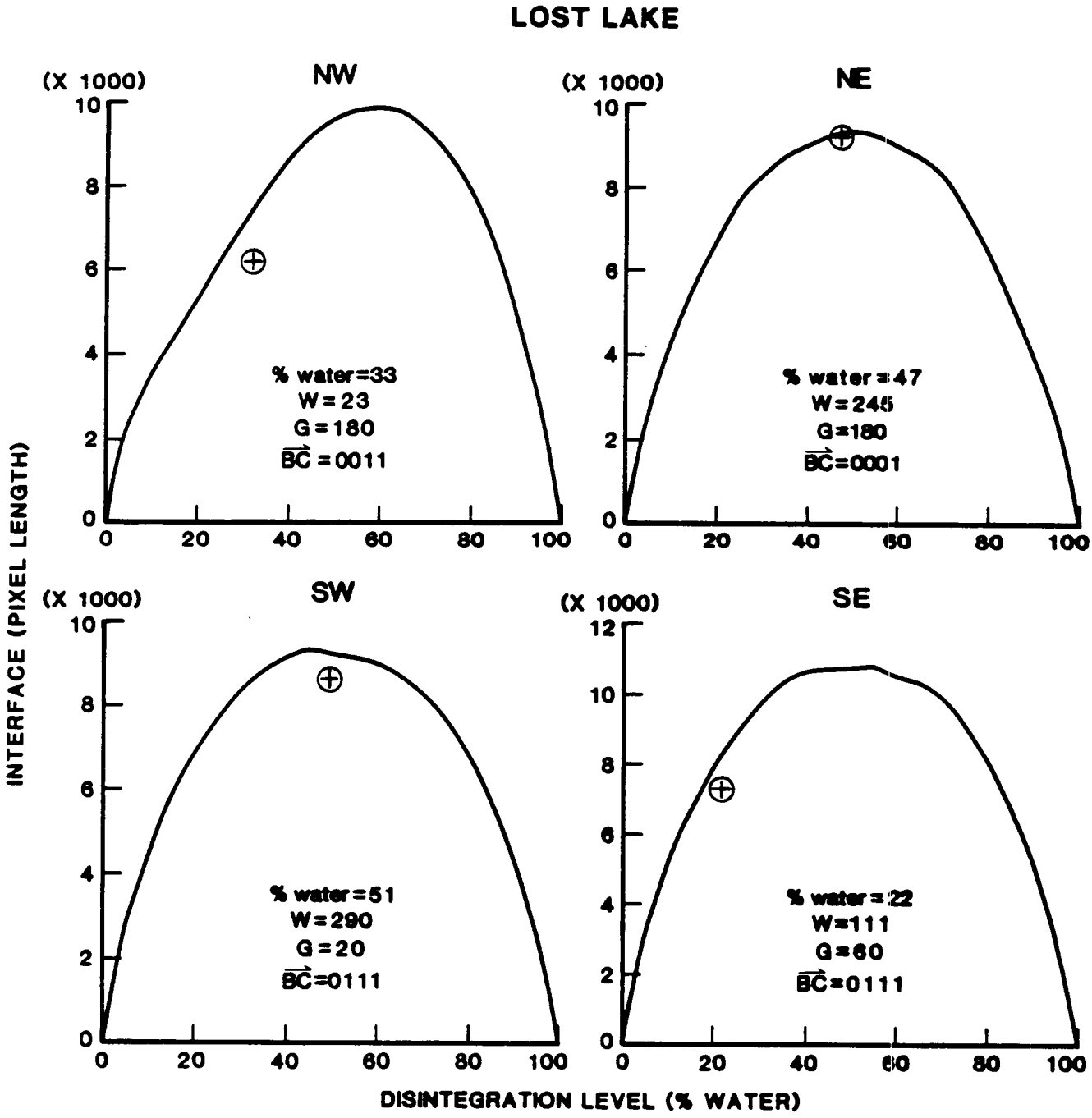

Figure D1-16. Simulated interface versus disintegration level, with TM scene coordinates, for the Lost Lake quadrangle.

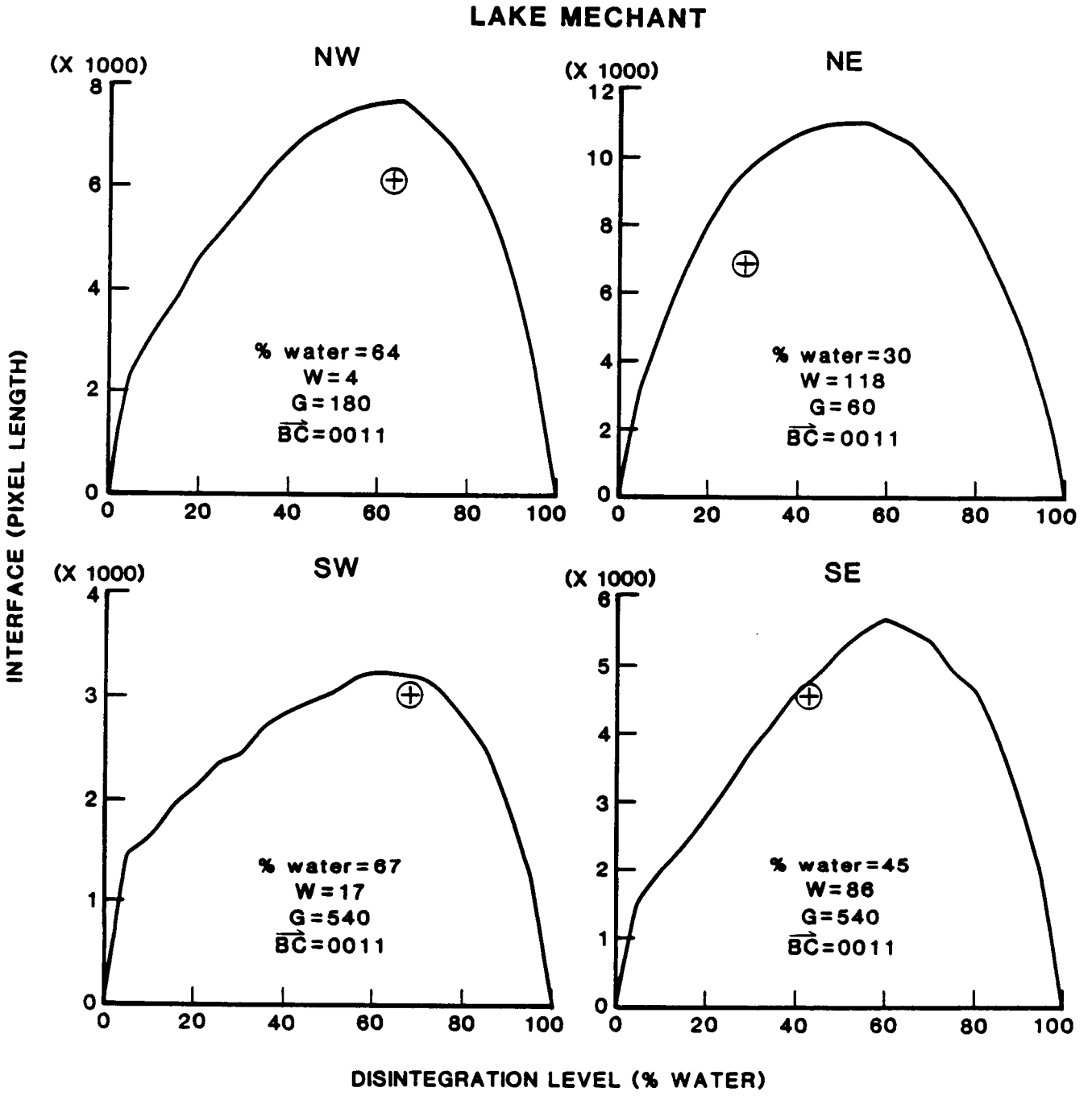

Figure D1-17. Simulated interface versus disintegration level, with TM scene coordinates, for the Lake Mechant quadrangle.

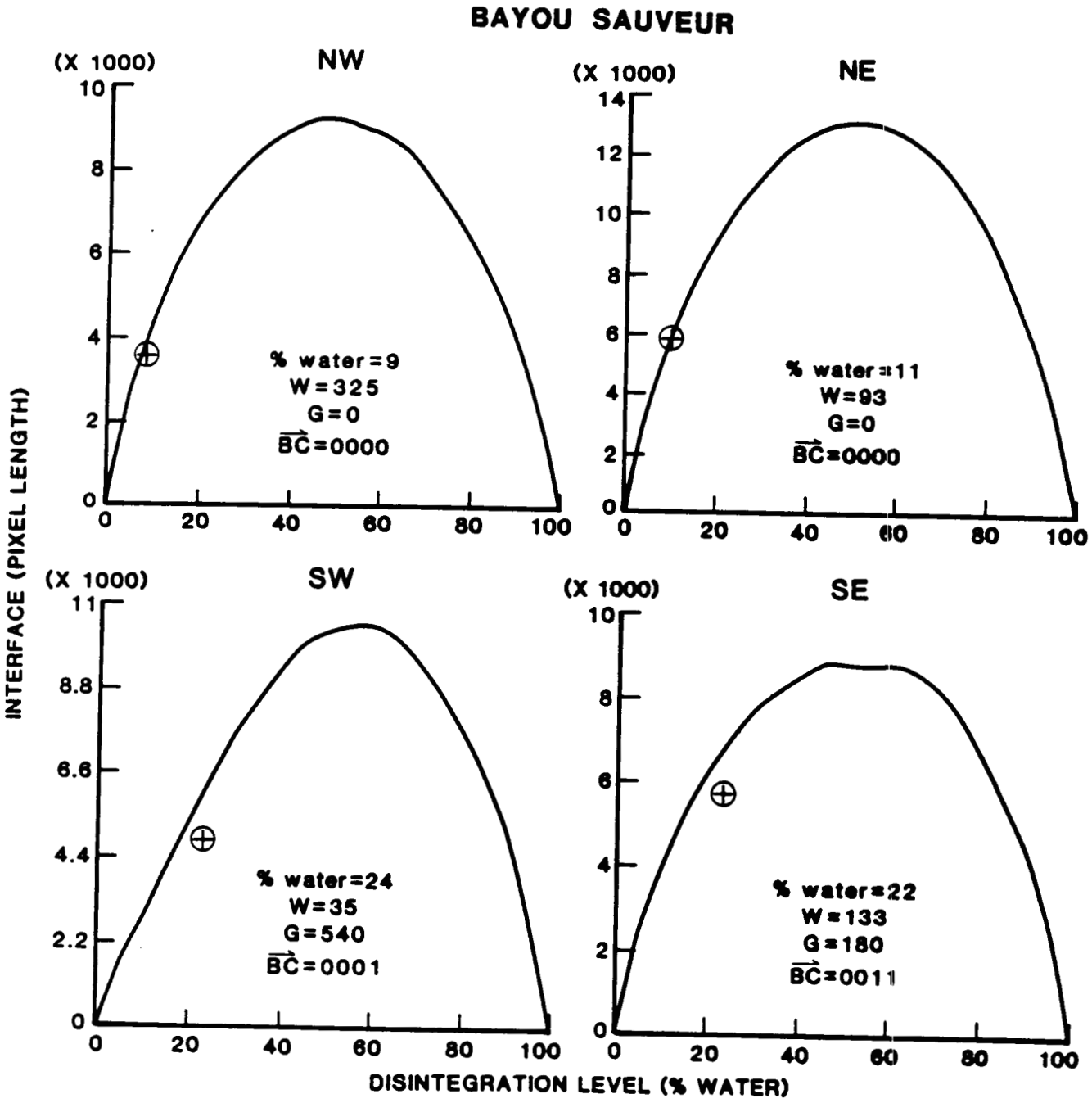

Figure D1-18. Simulated interface versus disintegration level, with TM scene coordinates, for the Bayou Sauveur quadrangle.

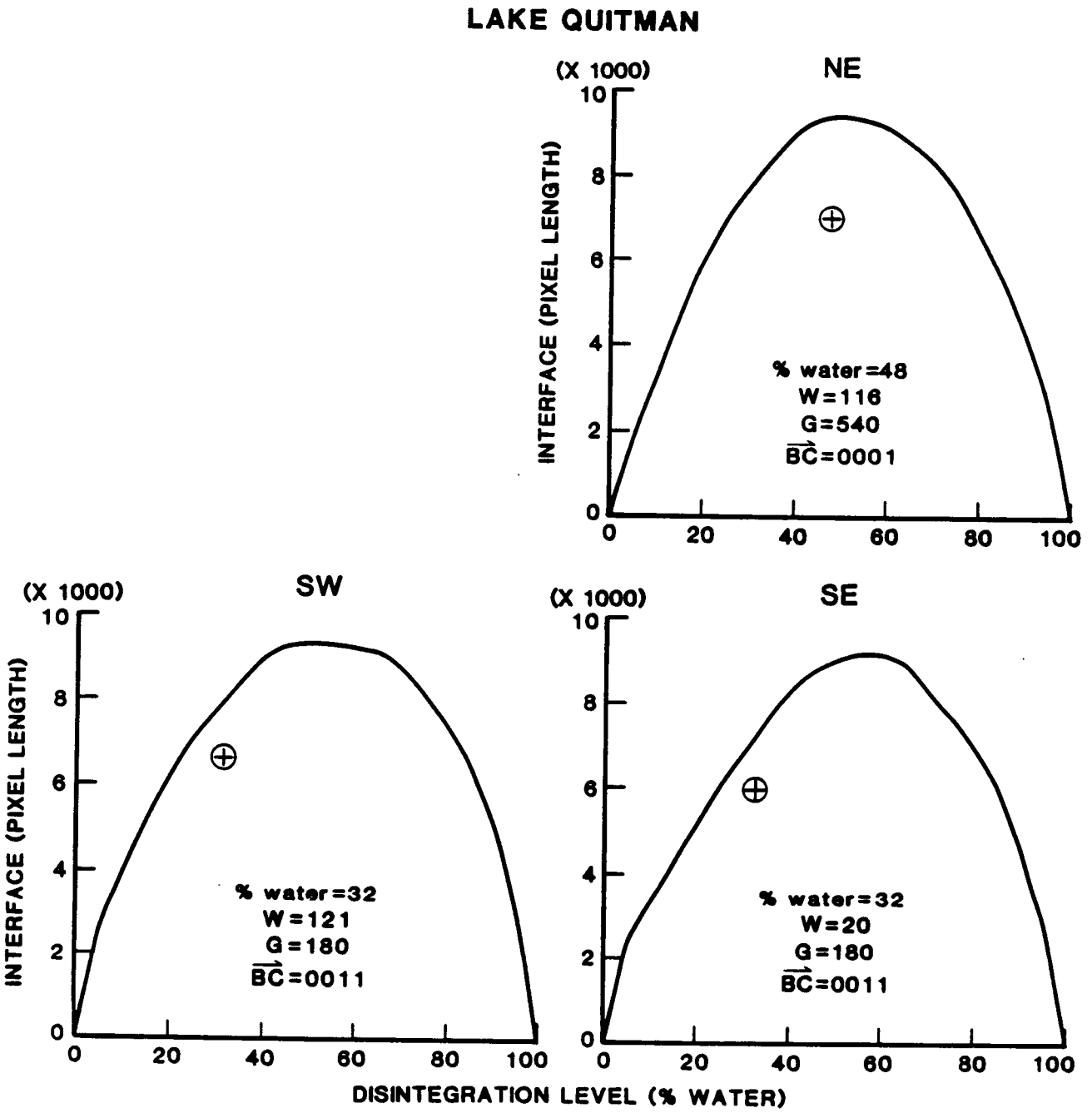

Figure D1-19. Simulated interface versus disintegration level, with TM scene coordinates, for the Lake Quitman quadrangle.

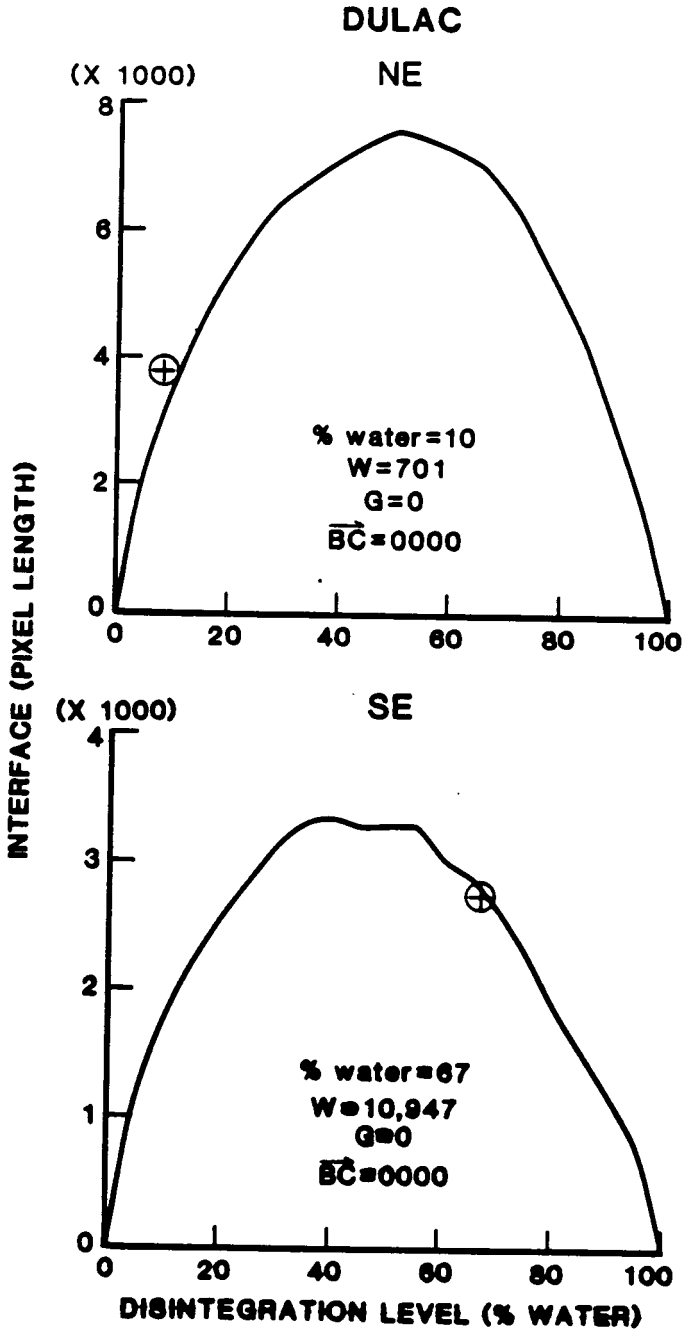

Figure D1-20. Simulated interface versus disintegration level, with TM scene coordinates, for the Dulac quadrangle.

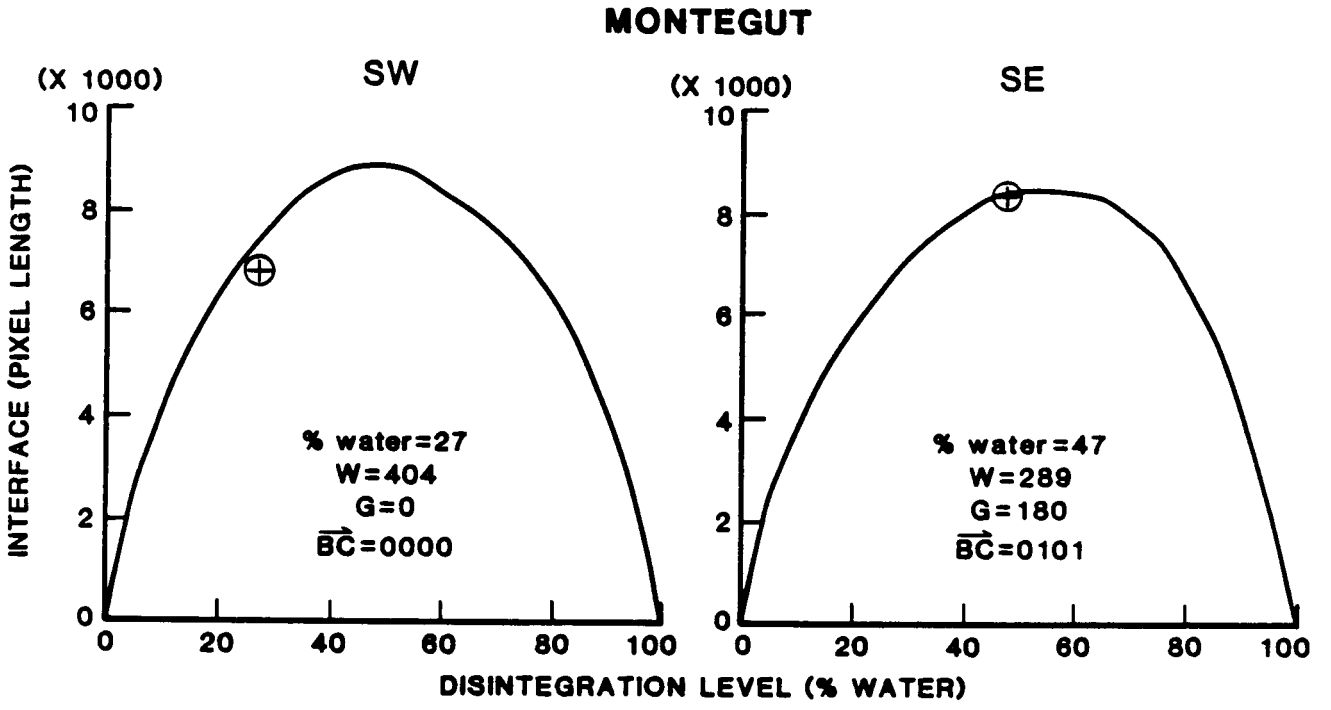

Figure D1-21. Simulated interface versus disintegration level, with TM scene coordinates, for the Montegut quadrangle.

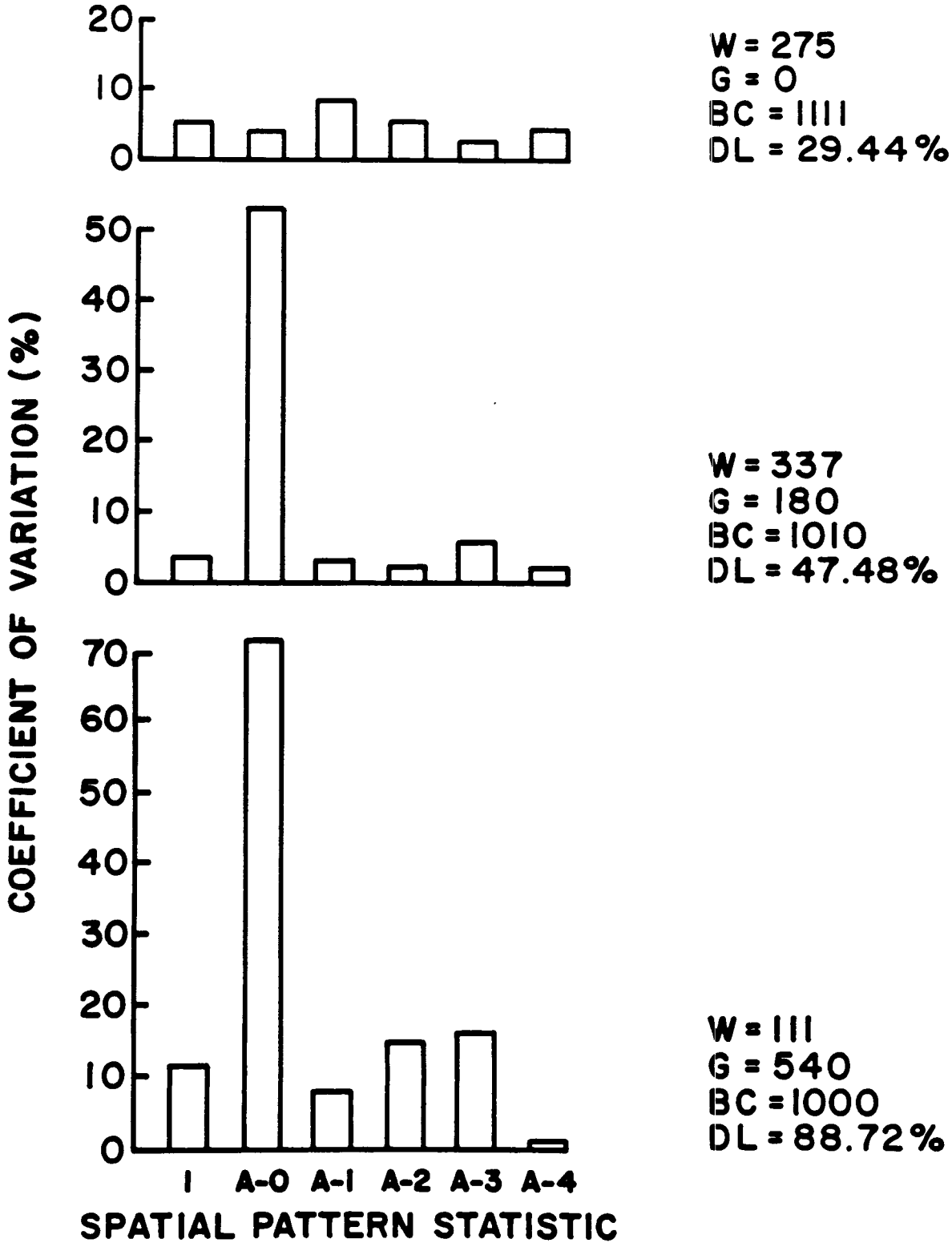

Figure D2. Coefficients of variation of spatial-pattern indices from 3 sets of 3 repeated simulations. The 3 repetitions of each set had the same W, G, BC and DL values. I = total interface; A-0 to A-4 refer to the number of water pixels in each 192 x 192 scene that had 0 to 4 sides adjacent to other water pixels

Appendix E

Comparison of Simulations with TM Scenes

Table E1. TM image and simulation values for interface length, with deviation and percentage deviation.

Quad	Quarter	Interface Length Image	Sim.	Deviation	% Deviation
Late Lafourche, salt					
Leeville	NW	9,093	9,133	40	0.44
	NE	10,025	9,935	-90	-0.90
	SE	10,118	9,811	-307	-3.03
	SW	6,115	7,780	1,665	27.23
Mink Bayou	NW	7,166	7,241	75	1.05
	NE	5,519	6,359	840	15.22
	SE	8,420	8,681	261	3.10
	SW	7,937	8,163	226	2.85
Caminada Pass	NW	6,778	6,989	211	3.11
	NE	1,341	1,323	-18	-1.34
	SE	101	190	89	88.12
	SW	3,884	3,946	62	1.60
Bay Tambour	NW	5,818	5,884	66	1.13
	NE	3,047	3,057	10	0.33
	SE	2,245	2,255	10	0.45
	SW	3,515	3,774	259	7.37
Pelican Pass	NW	341	534	193	56.60
	NE	2,433	2,395	-38	-1.56
	SE	2,100	2,357	257	12.24
	SW	385	442	57	14.81
Early Lafourche, salt					
Grand Bayou du Large	NW	3,431	3,797	366	10.67
	NE	3,621	4,048	427	11.79
	SE	7,174	7,978	804	11.21
	SW	1,111	1,678	567	51.04
Lake La Graisse	NW	2,079	2,039	-40	-1.92
	NE	292	492	200	68.49
Central Isles Dernieres	NW	3,439	3,548	109	3.17
	NE	1,605	1,315	-290	-18.07
	SE	748	719	-29	-3.88
	SW	745	842	97	13.02
Cocodrie	NW	7,430	9,375	1,945	26.18
	NE	6,457	7,116	659	10.21
	SE	3,681	3,240	-441	-11.98
	SW	9,692	9,279	-413	-4.26
Dog Lake	NW	4,612	4,397	-215	-4.66
	NE	8,114	8,129	15	0.19
	SE	7,774	9,434	1,660	21.35
	SW	6,482	8,615	2,133	32.91

Table E1. (cont.)

Quad	Quarter	Interface Length Image	Sim.	Deviation	% Deviation
Late Lafourche, brackish					
Lake Bully	NW	5,689	5,831	142	2.50
Camp	NE	9,158	9,099	-59	-0.64
	SE	6,157	8,350	2,193	35.62
	SW	9,502	9,398	-104	-1.10
Golden Meadow	NW	6,870	8,050	1,180	17.18
Farms	NE	5,700	6,239	539	9.46
	SE	8,163	8,567	404	4.95
	SW	4,954	4,430	-524	-10.58
Bay L'Ours	SE	3,572	3,308	-264	-7.39
	SW	1,755	2,484	729	41.54
Three Bayou	SE	7,393	9,304	1,911	25.85
Bay	SW	4,136	4,108	-28	-0.68
Golden Meadow	SW	9,367	10,187	820	8.75
Early Lafourche, brackish					
Lost Lake	NW	6,093	7,570	1,477	24.24
	NE	9,209	9,387	178	1.93
	SE	7,227	8,247	1,020	14.11
	SW	8,645	9,253	608	7.03
Lake Mechant	NW	6,070	7,697	1,627	26.80
	NE	6,782	9,797	3,015	44.46
	SE	4,570	4,844	274	6.00
	SW	3,050	3,223	173	5.67
Bayou Sauveur	NW	3,578	3,997	419	11.71
	NE	5,847	6,316	469	8.02
	SE	5,580	6,737	1,157	20.74
	SW	4,892	6,319	1,427	29.17
Lake Quitman	NE	6,983	9,468	2,485	35.59
	SE	5,981	7,261	1,280	21.40
	SW	6,545	8,002	1,458	22.26
Dulac	NE	3,708	3,445	-263	-7.09
	SE	2,710	2,853	143	5.28
Montegut	SE	8,315	8,551	236	2.84
	SW	6,787	7,439	652	9.61
Mean		5,283	5,801	518	12.29

Table E2. TM image and simulation values for side-adjacency 0, with deviation and percentage deviation.

		Side-Adjacency 0			
Quad	Quarter	Image	Sim.	Deviation	% Deviation
Late Lafourche, salt					
Leeville	NW	114	21	-93	-81.58
	NE	159	17	-142	-89.31
	SE	146	16	-130	-89.04
	SW	54	353	299	553.70
Mink Bayou	NW	101	658	-74	-73.27
	NE	117	237	120	102.56
	SE	178	18	-160	-89.89
	SW	103	18	-85	-82.52
Caminada Pass	NW	80	33	-47	-58.75
	NE	3	76	73	24.33
	SE	0	12	12	0.00
	SW	114	106	-8	-7.02
Bay Tambour	NW	61	111	50	81.97
	NE	18	74	56	311.11
	SE	24	7	-17	-70.83
	SW	28	70	42	150.00
Pelican Pass	NW	1	1	0	0.00
	NE	7	11	4	57.14
	SE	13	45	32	246.15
	SW	0	7	7	0.00
Early Lafourche, salt					
Grand Bayou du Large	NW	48	114	66	137.50
	NE	37	73	36	97.30
	SE	109	298	189	173.39
	SW	17	266	249	14.65
Lake La Graisse	NW	17	2	-15	-88.24
	NE	0	1	1	0.00
Central Isles Dernieres	NW	31	58	27	87.10
	NE	6	19	13	216.67
	SE	10	11	1	10.00
	SW	3	17	14	466.67
Cocodrie	NW	106	40	-66	-62.26
	NE	40	4	-36	-90.00
	SE	32	10	-22	-68.75
	SW	69	7	-62	-89.86
Dog Lake	NW	29	57	28	96.55
	NE	113	25	-88	-77.88
	SE	95	26	-69	-72.63
	SW	67	45	-22	-32.84

Table E2. (cont.)

Quad	Quarter	Side-Adjacency 0 Image	Sim.	Deviation	% Deviation
<u>Late Lafourche, brackish</u>					
Lake Bully Camp	NW	46	71	25	54.35
	NE	101	9	-92	-91.09
	SE	122	44	-78	-63.93
	SW	78	13	-65	-83.33
Golden Meadow Farms	NW	81	41	-40	-49.38
	NE	80	20	-60	-75.00
	SE	86	19	-67	-77.91
	SW	47	3	-44	-93.62
Bay L'Ours	SE	42	107	65	154.76
	SW	34	386	352	1,035.29
Three Bayou Bay	SE	108	34	-74	-68.52
	SW	60	85	25	41.67
Golden Meadow	SW	182	45	-137	-75.27
<u>Early Lafourche, brackish</u>					
Lost Lake	NW	62	199	137	220.97
	NE	107	16	-91	-85.05
	SE	126	54	-72	-57.14
	SW	75	10	-65	-86.67
Lake Mechant	NW	69	412	343	497.10
	NE	90	39	-51	-56.67
	SE	37	67	30	81.08
	SW	23	134	111	482.61
Bayou Sauveur	NW	82	24	-58	-70.73
	NE	160	69	-91	-56.88
	SE	79	45	-34	-43.04
	SW	36	148	112	311.11
Lake Quitman	NE	69	24	-45	-65.22
	SE	64	252	188	293.75
	SW	63	36	-27	-42.86
Dulac	NE	82	10	-72	-87.81
	SE	30	1	-29	-96.67
Montegut	SE	112	19	-93	-83.04
	SW	67	14	-53	-79.10
Mean		66	68	2	105.15

Table E3. TM image and simulation values for side adjacency 1, with deviation and percentage deviation.

		Side-adjacency 1			
Quad	Quarter	Image	Sim.	Deviation	% Deviation
Late Lafourche, salt					
Leeville	NW	439	665	226	51.48
	NE	713	802	89	12.48
	SE	519	760	241	46.44
	SW	253	1,174	921	364.03
Mink Bayou	NW	403	658	255	63.28
	NE	343	904	561	163.56
	SE	611	737	126	20.62
	SW	489	698	209	42.74
Caminada Pass	NW	344	667	323	93.90
	NE	20	131	111	555.00
	SE	1	11	10	1,000.00
	SW	254	538	284	111.81
Bay Tambour	NW	233	747	514	220.60
	NE	92	433	341	370.65
	SE	73	164	91	124.66
	SW	106	448	342	322.64
Pelican Pass	NW	11	34	23	209.09
	NE	93	206	113	121.51
	SE	64	302	238	371.87
	SW	4	40	36	900.00
Early Lafourche, salt					
Grand Bayou du Large	NW	114	510	396	347.37
	NE	159	534	376	237.97
	SE	477	1,077	600	125.79
	SW	50	83	33	66.00
Lake La Graisse	NW	54	148	94	174.07
	NE	3	22	19	633.33
Central Isles Dernieres	NW	131	382	251	191.60
	NE	33	143	110	333.33
	SE	18	73	55	305.56
	SW	12	74	62	516.67
Cocodrie	NW	493	846	353	71.60
	NE	234	435	201	85.90
	SE	153	229	76	49.67
	SW	410	599	189	46.10
Dog Lake	NW	159	480	321	201.89
	NE	449	710	261	58.13
	SE	403	798	395	98.01
	SW	331	803	472	142.60

Table E3. (cont.)

Quad	Quarter	Side-adjacency 1 Image	Sim.	Deviation	% Deviation
Late Lafourche, brackish					
Lake Bully	NW	276	678	402	145.65
Camp	NE	562	662	100	17.79
	SE	413	805	392	94.92
	SW	469	676	207	44.14
Golden Meadow	NW	414	761	347	83.82
Farms	NE	367	512	145	39.51
	SE	515	683	168	32.62
	SW	243	319	76	31.28
Bay L'Ours	SE	254	443	189	74.41
	SW	106	138	32	30.19
Three Bayou	SE	469	831	362	77.19
Bay	SW	218	533	316	145.62
Golden Meadow	SW	709	909	200	28.21
Early Lafourche, brackish					
Lost Lake	NW	329	1,088	759	230.70
	NE	550	672	122	22.18
	SE	496	821	325	65.52
	SW	442	620	178	40.27
Lake Mechant	NW	325	1,137	812	249.85
	NE	379	857	478	126.12
	SE	168	526	358	213.10
	SW	122	440	318	260.66
Bayou Sauveur	NW	291	430	139	47.77
	NE	556	776	220	39.57
	SE	323	678	355	109.91
	SW	199	903	704	353.77
Lake Quitman	NE	348	773	425	122.13
	SE	302	989	687	227.48
	SW	365	797	432	118.36
Dulac	NE	298	311	13	4.36
	SE	115	182	67	58.26
Montegut	SE	479	670	191	39.88
	SW	423	578	155	36.64
Mean		290	561	271	172.33

Table E4. TM image and simulation values for side-adjacency 2, with deviation and percentage deviation.

		Side-adjacency 2			
Quad	Quarter	Image	Sim.	Deviation	% Deviation
Late Lafourche, salt					
Leeville	NW	2,124	1,853	-271	-12.75
	NE	2,315	2,048	-267	-11.53
	SE	2,470	1,947	-523	-21.17
	SW	1,495	1,026	-469	-31.17
Mink Bayou	NW	1,686	1,455	-231	-13.70
	NE	1,316	969	-347	-26.37
	SE	1,873	1,743	-130	-6.94
	SW	1,867	1,635	-232	-12.43
Caminada Pass	NW	1,669	1,396	-273	-16.36
	NE	418	169	-249	-59.57
	SE	34	21	-13	-38.24
	SW	952	653	-299	-31.41
Bay Tambour	NW	1,506	1,013	-493	-32.74
	NE	773	478	-295	-38.16
	SE	539	451	-88	-16.33
	SW	833	669	-164	-19.69
Pelican Pass	NW	67	82	15	22.39
	NE	579	482	-97	-16.75
	SE	500	418	-82	-16.40
	SW	100	80	-20	-20.00
Early Lafourche, salt					
Grand Bayou du Large	NW	845	618	-227	-26.86
	NE	886	701	-185	-20.88
	SE	1,688	1,277	-411	-24.35
	SW	254	89	-165	-64.96
Lake La Graisse	NW	475	413	-62	-13.05
	NE	67	57	-10	-14.93
Central Isles Dernieres	NW	809	669	-140	-17.31
	NE	432	224	-208	-48.15
	SE	186	120	-66	-35.48
	SW	173	163	-10	5.78
Cocodrie	NW	1,692	1,949	257	15.19
	NE	1,454	1,397	-57	-3.92
	SE	813	659	-154	-18.94
	SW	2,256	1,822	-434	-19.24
Dog Lake	NW	1,084	869	-215	-19.83
	NE	1,893	1,663	-230	-12.15
	SE	1,758	1,932	174	9.90
	SW	1,560	1,712	152	9.74

Table E4. (cont.)

Quad	Quarter	Side-adjacency 2 Image	Sim.	Deviation	% Deviation
Late Lafourche, brackish					
Lake Bully Camp	NW	1,259	1,126	-133	-10.56
	NE	2,039	1,800	-239	-11.72
	SE	1,363	1,732	369	27.07
	SW	2,124	1,845	-279	-13.14
Golden Meadow Farms	NW	1,530	1,691	161	10.52
	NE	1,181	1,258	77	6.52
	SE	1,813	1,751	-62	-3.42
	SW	1,085	853	-232	-21.38
Bay L'Ours	SE	820	517	-303	-36.95
	SW	387	123	-264	-68.22
Three Bayou Bay	SE	1,670	1,887	217	12.99
	SW	974	749	-225	-23.10
Golden Meadow	SW	2,118	2,078	-40	-1.89
Early Lafourche, brackish					
Lost Lake	NW	1,352	1,227	-125	-9.25
	NE	2,069	1,863	-206	-9.96
	SE	1,644	1,677	33	2.01
	SW	1,912	1,853	-59	-3.09
Lake Mechant	NW	1,449	976	-473	-32.64
	NE	1,613	1,998	385	23.87
	SE	1,197	946	-251	-20.97
	SW	823	474	-349	-42.41
Bayou Sauveur	NW	771	820	49	6.36
	NE	1,201	1,244	43	3.58
	SE	1,309	1,330	21	1.60
	SW	1,245	1,067	-178	-14.30
Lake Quitman	NE	1,608	1,880	272	16.92
	SE	1,421	1,167	-254	-17.88
	SW	1,574	1,577	3	0.19
Dulac	NE	791	708	-83	-10.49
	SE	666	502	-164	-24.63
Montegut	SE	1,828	1,674	-154	-8.43
	SW	1,521	1,577	56	3.68
Mean		1,226	1,098	-127	-14.28

Table E5. TM image and simulation values for side-adjacency 3, with deviation and percentage deviation.

		Side-adjacency 3			
Quad	Quarter	Image	Sim.	Deviation	% Deviation
Late Lafourche, salt					
Leeville	NW	2,964	3,295	331	11.17
	NE	2,473	3,279	806	32.59
	SE	2,901	3,440	539	18.58
	SW	2,061	721	-1,340	-65.02
Mink Bayou	NW	2,067	2,218	151	7.31
	NE	1,289	730	-559	-43.37
	SE	1,977	2,845	868	43.91
	SW	2,192	2,678	486	22.17
Caminada Pass	NW	1,998	2,041	43	2.15
	NE	411	280	-131	-31.87
	SE	25	53	28	112.00
	SW	705	582	-123	-17.45
Bay Tambour	NW	1,788	1,153	-635	-35.52
	NE	1,112	471	-641	-57.64
	SE	826	831	5	0.61
	SW	1,364	796	-568	-41.64
Pelican Pass	NW	161	261	100	62.11
	NE	932	763	-169	-18.13
	SE	839	411	-428	-51.01
	SW	160	134	-26	-16.25
Early Lafourche, salt					
Grand Bayou du Large	NW	1,151	542	-609	-52.91
	NE	1,145	726	-419	-36.59
	SE	1,839	937	-902	-49.05
	SW	367	158	-209	-56.95
Lake La Graisse	NW	853	748	-105	-12.31
	NE	143	302	159	111.19
Central Isles Dernieres	NW	1,268	832	-436	-34.39
	NE	601	360	-241	-40.10
	SE	258	210	-48	-18.61
	SW	334	226	-108	-32.34
Cocodrie	NW	2,005	2,741	736	36.17
	NE	2,596	2,931	335	12.90
	SE	1,387	1,165	-222	-16.01
	SW	3,511	3,758	247	7.04
Dog Lake	NW	1,769	954	-815	-46.07
	NE	2,394	2,542	148	6.18
	SE	2,535	3,026	491	19.37
	SW	1,967	2,545	578	29.39

Table E5. (cont.)

Quad	Quarter	Side-adjacency 3 Image	Sim.	Deviation	% Deviation
Late Lafourche, brackish					
Lake Bully Camp	NW	2,079	1,246	-833	-40.07
	NE	2,845	3,402	557	19.58
	SE	1,578	2,224	646	40.94
	SW	3,373	3,610	237	7.03
Golden Meadow Farms	NW	2,179	2,186	7	0.32
	NE	1,836	2,072	236	12.85
	SE	2,538	2,872	334	13.16
	SW	1,775	1,731	-44	-2.48
Bay L'Ours	SE	963	503	-460	-47.77
	SW	513	269	-244	-47.56
Three Bayou Bay	SE	2,108	2,887	779	36.95
	SW	1,218	664	-554	-45.49
Golden Meadow	SW	2,184	3,029	845	38.69
Early Lafourche, brackish					
Lost Lake	NW	2,074	1,008	1,056	-51.40
	NE	2,848	3,512	664	23.32
	SE	1,820	2,152	332	18.24
	SW	3,078	3,545	467	15.17
Lake Mechant	NW	1,836	594	-1,242	-67.65
	NE	1,957	3,003	1,046	53.45
	SE	1,471	1,089	-382	-25.97
	SW	894	394	-550	-55.93
Bayou Sauveur	NW	791	942	151	19.09
	NE	1,030	1,139	109	10.58
	SE	1,559	1,833	274	17.58
	SW	1,592	829	-763	-47.93
Lake Quitman	NE	2,326	3,208	882	37.92
	SE	1,881	897	-984	-52.31
	SW	1,948	2,283	335	17.20
Dulac	NE	883	1,024	141	15.97
	SE	854	1,265	411	48.13
Montegut	SE	2,657	3,087	430	16.18
	SW	2,103	2,417	314	14.93
Mean		1,617	1,609	-8	-3.50

Table E6. TM image and simulation values for side-adjacency 4, with deviation and percentage deviation.

		Side-adjacency 4			
Quad	Quarter	Image	Sim.	Deviation	% Deviation
Late Lafourche, salt					
Leeville	NW	9,856	9,551	-305	-3.10
	NE	6,860	6,534	-326	-4.75
	SE	8,369	8,299	-70	-0.84
	SW	13,064	13,460	396	3.03
Mink Bayou	NW	5,326	5,004	-322	-6.05
	NE	5,744	5,778	34	0.59
	SE	5,975	5,397	-578	-9.67
	SW	6,026	5,584	-442	-7.34
Caminada Pass	NW	18,306	18,074	-232	-1.27
	NE	29,050	29,187	137	0.47
	SE	35,792	35,763	-29	-0.08
	SW	18,845	19,006	161	0.85
Bay Tambour	NW	14,891	15,202	311	2.09
	NE	25,719	26,191	472	1.84
	SE	30,541	30,542	1	0.00
	SW	28,120	28,413	293	1.04
Pelican Pass	NW	35,491	35,356	-135	-0.38
	NE	28,221	28,283	62	0.22
	SE	29,910	30,161	251	0.84
	SW	34,833	34,822	-11	-0.03
Early Lafourche, salt					
Grand Bayou du Large	NW	17,371	17,550	179	1.30
	NE	22,053	22,217	164	0.74
	SE	10,349	10,845	496	4.79
	SW	29,643	29,645	2	0.01
Lake La Graisse	NW	31,517	31,565	48	0.15
	NE	35,641	35,459	-182	-0.51
Central Isles Dernieres	NW	25,018	25,227	209	0.84
	NE	31,419	31,723	304	0.97
	SE	33,918	33,935	17	0.05
	SW	33,245	33,236	-9	-0.03
Cocodrie	NW	7,765	6,287	-1,478	-19.03
	NE	20,598	20,194	-404	-1.96
	SE	28,656	28,964	308	1.08
	SW	13,522	13,490	-32	-0.24
Dog Lake	NW	19,788	20,321	533	2.69
	NE	6,218	5,937	-281	-4.52
	SE	10,514	9,381	-1,133	-10.78
	SW	9,106	7,990	-1,116	-12.26

Table E6. (cont.)

Quad	Quarter	Side-adjacency 4 Image	Sim.	Deviation	% Deviation
Late Lafourche, brackish					
Lake Bully	NW	8,482	8,680	198	2.33
Camp	NE	11,744	11,405	-339	-2.89
	SE	4,481	2,951	-1,530	-34.14
	SW	11,989	11,537	-452	-3.77
Golden Meadow	NW	6,931	6,281	-650	-9.38
Farms	NE	18,357	17,993	-364	-1.98
	SE	7,862	7,320	-542	-6.89
	SW	11,049	11,360	311	2.82
Bay L'Ours	SE	27,359	27,790	431	1.58
	SW	17,837	17,852	15	0.08
Three Bayou	SE	7,410	5,743	-1,667	-22.50
Bay	SW	18,775	19,110	335	1.78
Golden Meadow	SW	4,802	4,006	-796	-16.58
Early Lafourche, brackish					
Lost Lake	NW	8,031	8,059	28	0.35
	NE	11,576	11,034	-542	-4.68
	SE	3,689	2,752	-937	-25.40
	SW	12,874	12,138	-736	-5.72
Lake Mechant	NW	19,400	19,940	540	2.78
	NE	6,710	4,663	-2,047	-30.51
	SE	13,303	13,462	159	1.20
	SW	22,310	22,755	445	2.00
Bayou Sauveur	NW	1,239	959	-280	-22.60
	NE	966	714	-252	-26.09
	SE	4,721	3,885	-836	-17.71
	SW	5,748	5,730	-18	-0.31
Lake Quitman	NE	13,105	11,475	-1,630	-12.44
	SE	8,035	8,185	150	1.87
	SW	7,490	6,598	-892	-11.91
Dulac	NE	1,468	1,460	-8	-0.55
	SE	22,739	22,312	-427	-1.88
Montegut	SE	12,077	11,578	-499	-4.13
	SW	5,661	5,303	-358	-6.32
Mean		35,792	35,763	-227	-4.44

Table E7. TM image and simulation values for border water pixels, with deviation and percentage deviation.

Quad	Quarter	Number of border water pixels			
		Image	Sim.	Deviation	% Deviation
Late Lafourche, salt					
Leeville	NW	332	443	111	33.43
	NE	355	195	-160	-45.07
	SE	308	251	-57	-18.51
	SW	304	497	193	63.49
Mink Bayou	NW	219	439	220	100.46
	NE	236	426	190	80.51
	SE	237	110	-127	-53.59
	SW	225	289	64	28.44
Caminada Pass	NW	493	679	186	37.73
	NE	646	705	59	9.13
	SE	741	733	-8	-1.08
	SW	518	503	-15	-2.90
Bay Tambour	NW	388	640	252	64.95
	NE	504	570	66	13.10
	SE	704	711	7	0.99
	SW	654	708	54	8.26
Pelican Pass	NW	751	748	-3	-0.40
	NE	611	703	86	13.94
	SE	629	618	-11	-1.75
	SW	751	764	13	1.73
Early Lafourche, salt					
Grand Bayou du Large	NW	316	510	194	61.39
	NE	514	541	27	5.25
	SE	444	471	27	6.08
	SW	530	619	89	16.79
Lake La Graisse	NW	679	719	40	5.89
	NE	744	756	12	1.61
Central Isles Dernieres	NW	675	764	89	13.19
	NE	706	727	21	2.98
	SE	698	739	41	5.87
	SW	713	764	51	7.15
Cocodrie	NW	264	461	197	74.62
	NE	475	436	-39	-8.21
	SE	583	597	14	2.40
	SW	402	493	91	22.64
Dog Lake	NW	385	532	147	38.18
	NE	203	453	190	72.24
	SE	317	459	142	44.80
	SW	386	321	-65	-16.84

Table E7. (cont.)

Quad	Quarter	Number of border water pixels Image	Sim.	Deviation	% Deviation
Late Lafourche, brackish					
Lake Bully Camp	NW	276	617	341	123.55
	NE	344	357	13	3.78
	SE	230	431	201	87.39
	SW	406	758	352	86.70
Golden Meadow Farms	NW	261	435	174	66.67
	NE	553	519	-34	-6.15
	SE	294	462	168	57.14
	SW	159	92	-67	-42.14
Bay L'Ours	SE	617	694	77	12.48
	SW	387	495	108	27.91
Three Bayou Bay	SE	375	758	383	102.13
	SW	501	501	0	0.00
Golden Meadow	SW	202	129	-73	-36.14
Early Lafourche, brackish					
Lost Lake	NW	187	453	266	142.25
	NE	294	347	53	18.03
	SE	265	584	319	120.38
	SW	340	555	215	63.24
Lake Mechant	NW	534	554	20	3.75
	NE	267	464	197	73.78
	SE	380	465	85	22.37
	SW	550	524	-26	-4.73
Bayou Sauveur	NW	42	41	-1	-2.38
	NE	106	76	-30	-28.30
	SE	203	422	219	107.88
	SW	140	283	143	102.14
Lake Quitman	NE	312	408	96	30.77
	SE	244	456	212	86.89
	SW	301	449	148	49.17
Dulac	NE	29	37	8	27.59
	SE	221	363	142	64.25
Montegut	SE	349	473	124	35.53
	SW	237	123	-114	-48.10
Mean		404	492	87	29.10

Table E8. Results of simple linear regression of simulation spatial pattern indices on corresponding image spatial pattern indices.

Interface length

Sim = 154.8 + 1.069 • Image R^2 = 94.12
(.4250) (.0001) P of F-stat = .0001

Adj-0

Sim = 73.23 - 0.0739 • Image R2 = .13
(.0005) (.7667) P of F-stat = .7667

Adj-1

Sim = 212.4 + 1.204 • Image R^2 = 56.14
(.0001) (.0001) P of F-stat = .0001

Adj-2

Sim = -88.01 + 0.9680 • Image R^2 = 90.72
(.0929) (.0001) P of F-stat = .0001

Adj-3

Sim = -325.7 + 1.213 • Image R^2 = 79.67
(.0113) (.0001) P of F-stat = .0001

Adj-4

Sim = -640.3 + 1.026 • Image R^2 = 99.77
(.0001) (.0001) P of F-stat = .0001

Note: Values in parentheses are T-stat probability levels.

Figure E1. Comparisons of spatial patterns of marsh disintegration in TM scenes (upper images) with "best-fit" simulations at the same disintegration level (lower images). Quadrangles are presented in the same order as in Table D1.

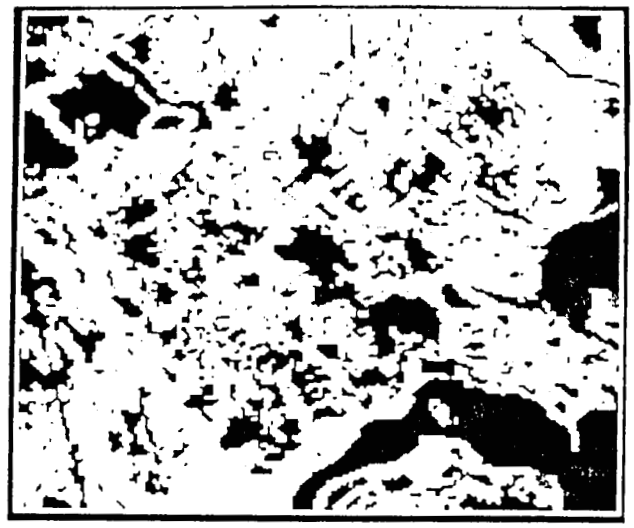

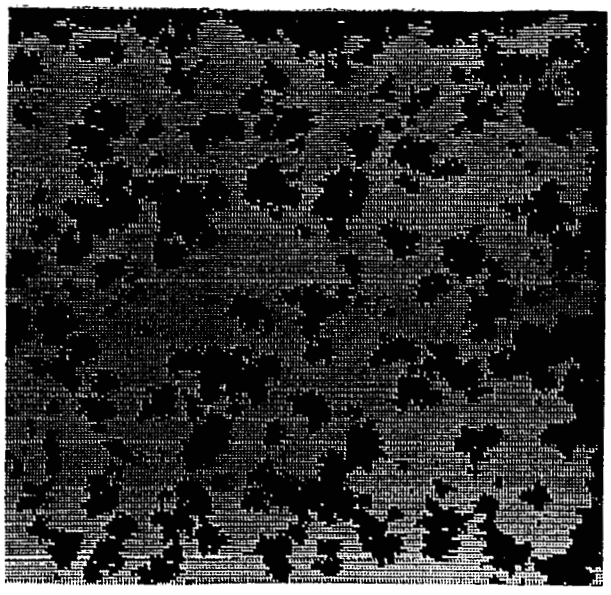

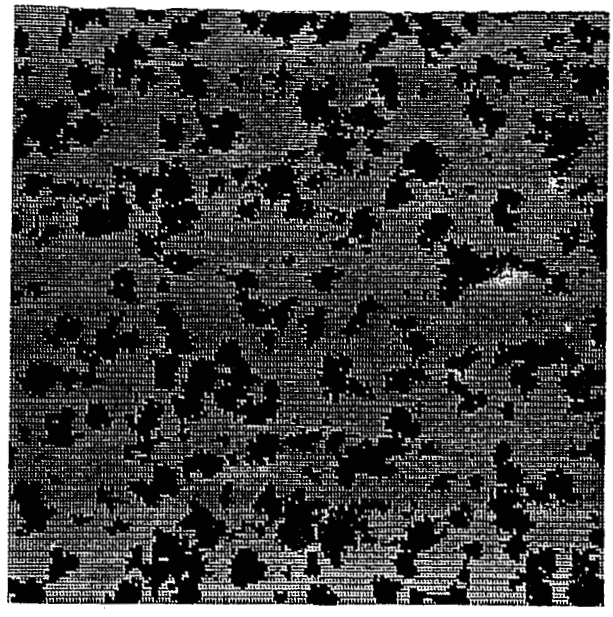

W = 272 G = 60 DL = 42.94 BC = 0011

Figure E1-1. Leeville, NW quadrangle.

W = 188 G = 0 DL = 34.93 BC = 0111

Figure E1-2. Leeville, NE quadrangle.

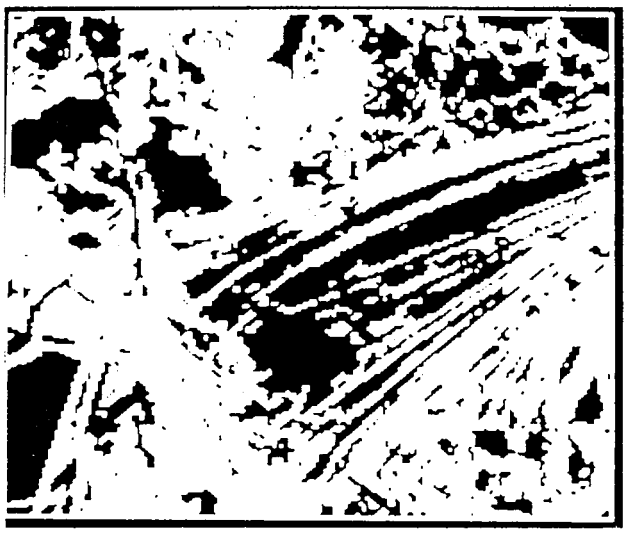

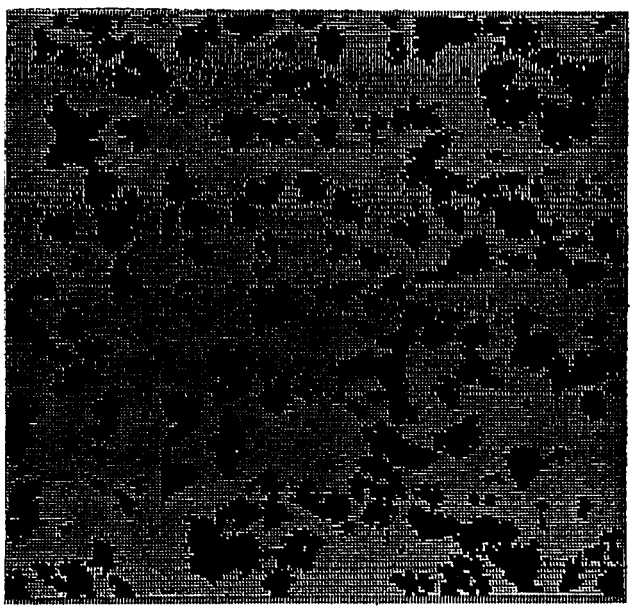

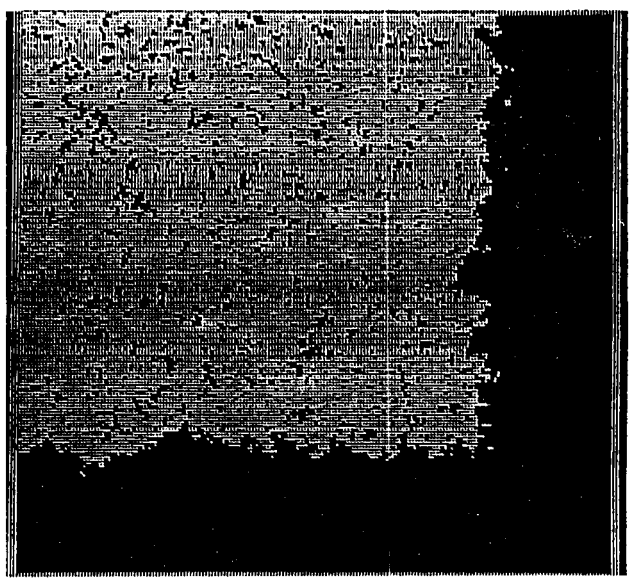

W = 237 G = 4 DL = 39.91 BC = 0011

Figure E1-3. Leeville, SE quadrangle.

W = 8 G = 180 DL = 46.74 BC = 0011

Figure E1-4. Leeville, SW quadrangle.

W = 244 G = 180 DL = 26.59 BC = 0101

Figure E1-5. Mink Bayou, NW quadrangle.

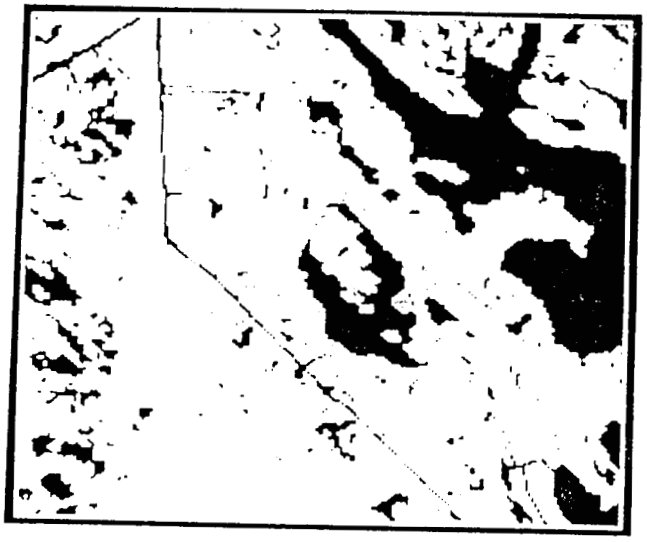

W = 24 G = 180 DL = 24.54 BC = 0011

Figure E1-6. Mink Bayou, NE quadrangle.

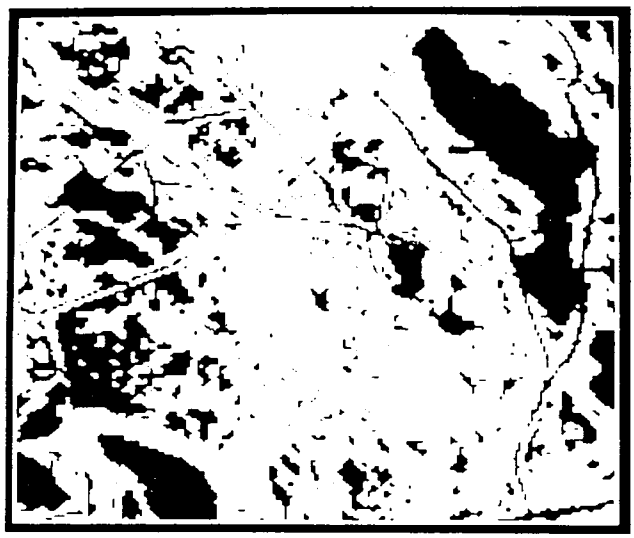

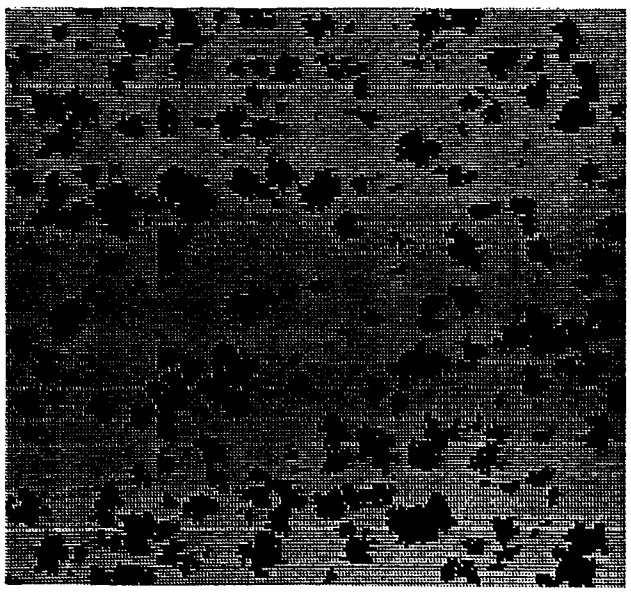

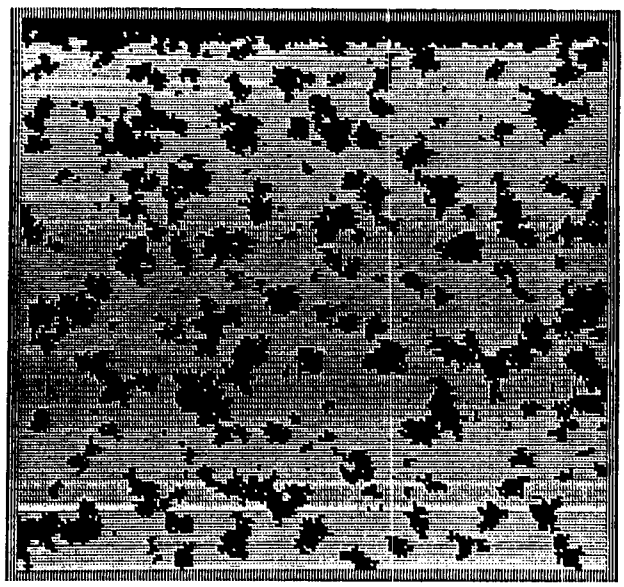

W = 248 G = 0 DL = 29.44 BC = 0111

Figure E1-7. Mink Bayou, SE quadrangle.

W = 261 G = 180 DL = 29.57 BC = 0001

Figure E1-8. Mink Bayou, SW quadrangle.

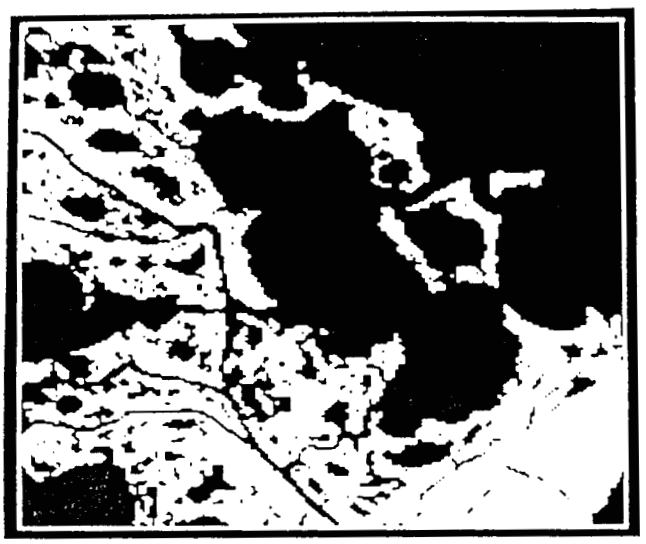

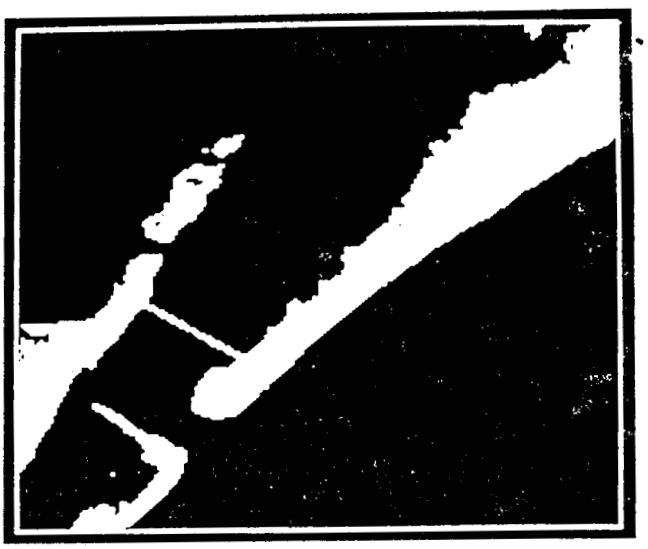

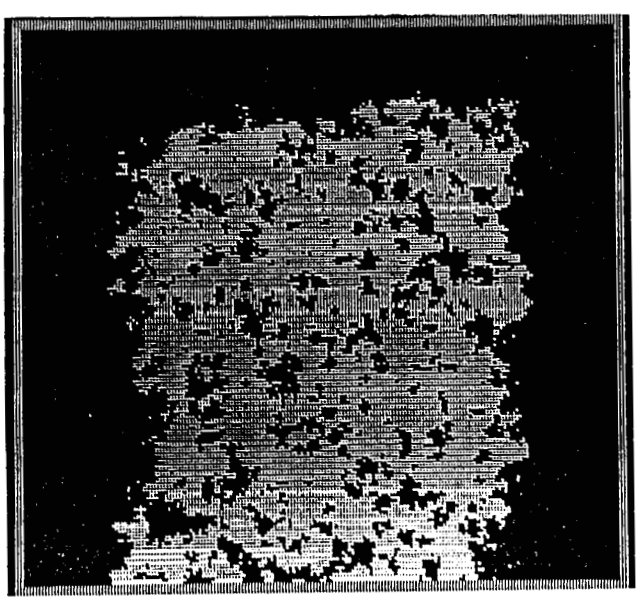

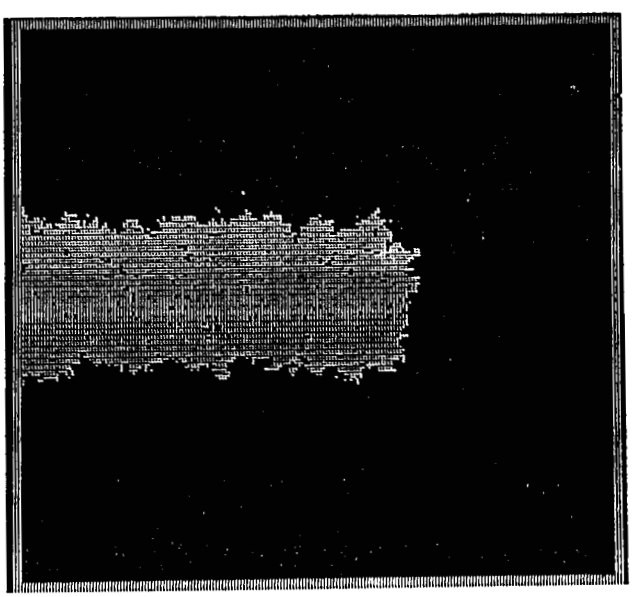

W = 58 G = 180 DL = 62.09 BC = 0111

Figure E1-9. Caminada Pass, NW quadrangle.

W = 13 G = 540 DL = 82.87 BC = 0111

Figure E1-10. Caminada Pass, NE quadrangle.

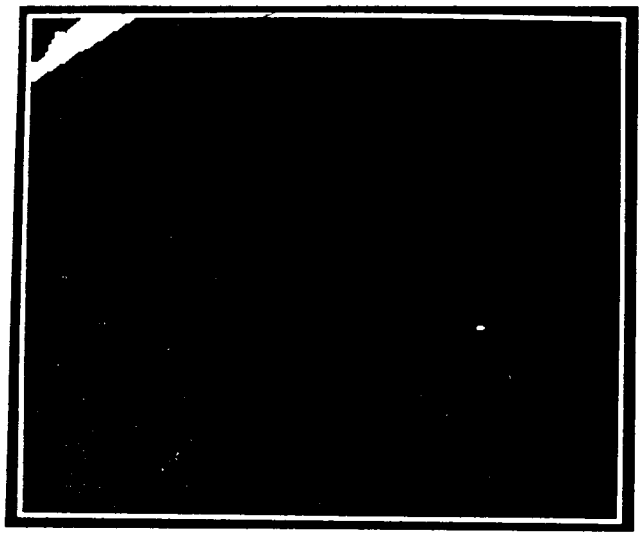

W = 1 G = 540 DL = 99.27 BC = 0011

Figure E1-11. Caminada Pass, SE quadrangle.

W = 28 G = 540 DL = 58.02 BC = 0011

Figure E1-12. Caminada Pass, SW quadrangle.

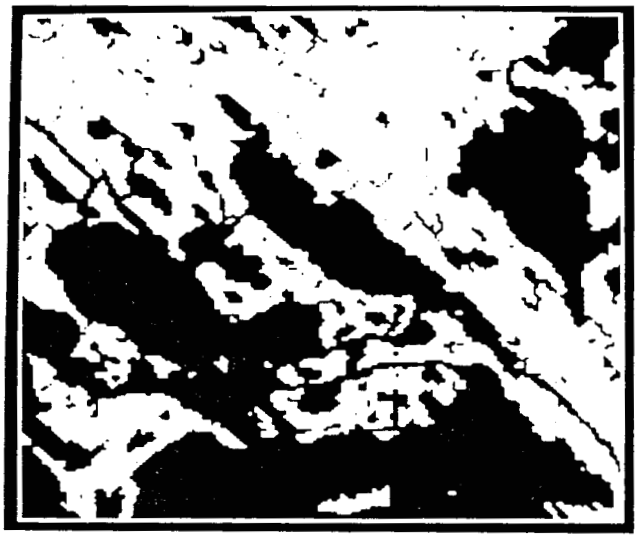

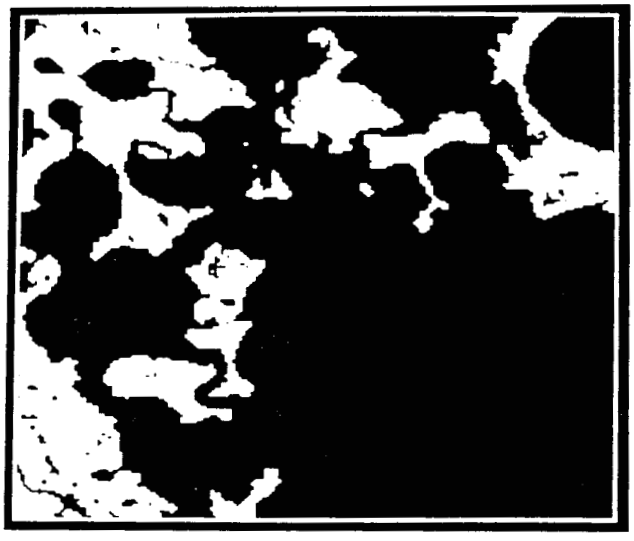

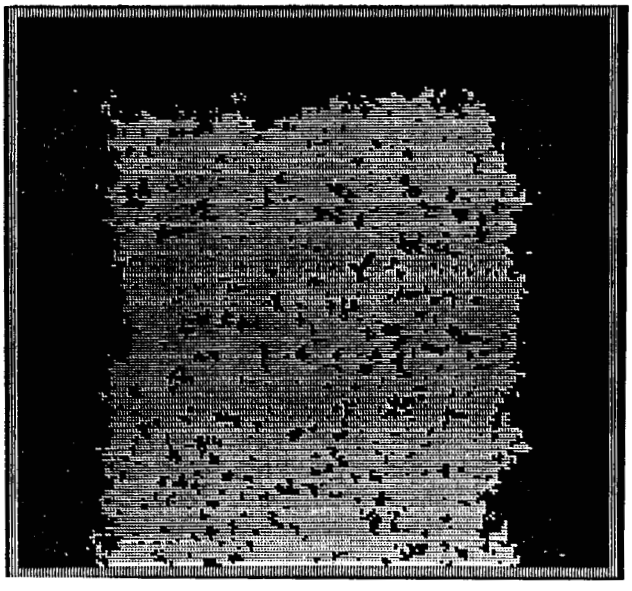

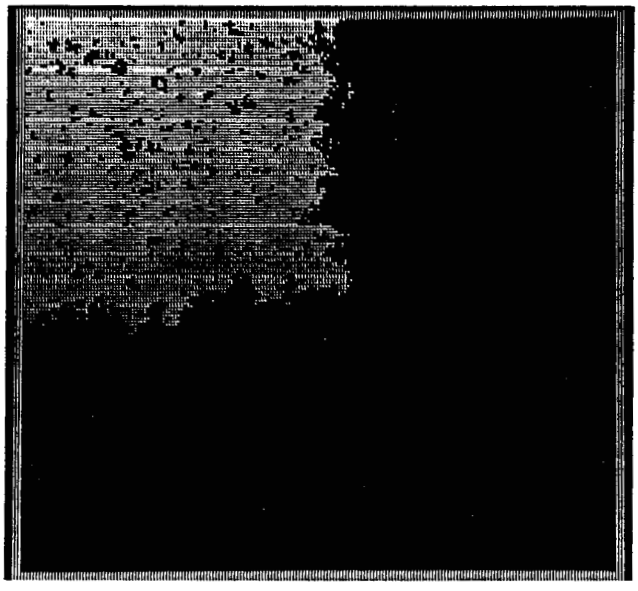

W = 31 G = 180 DL = 51.18 BC = 0111

Figure E1-13. Bay Tambour, NW quadrangle.

W = 17 G = 540 DL = 76.55 BC = 0011

Figure E1-14. Bay Tambour, NE quadrangle.

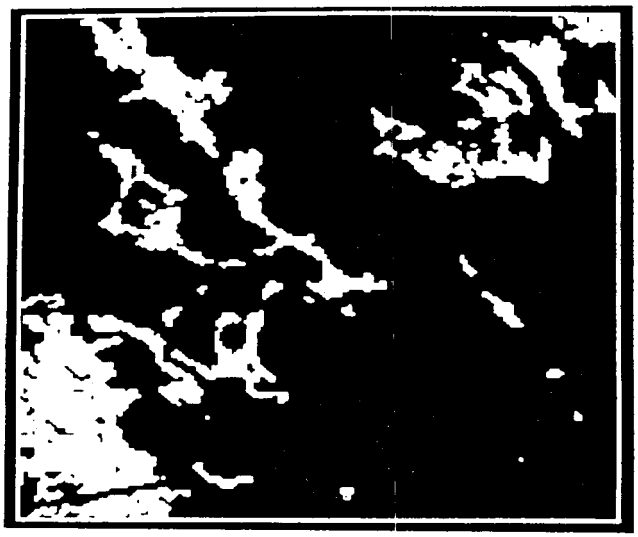

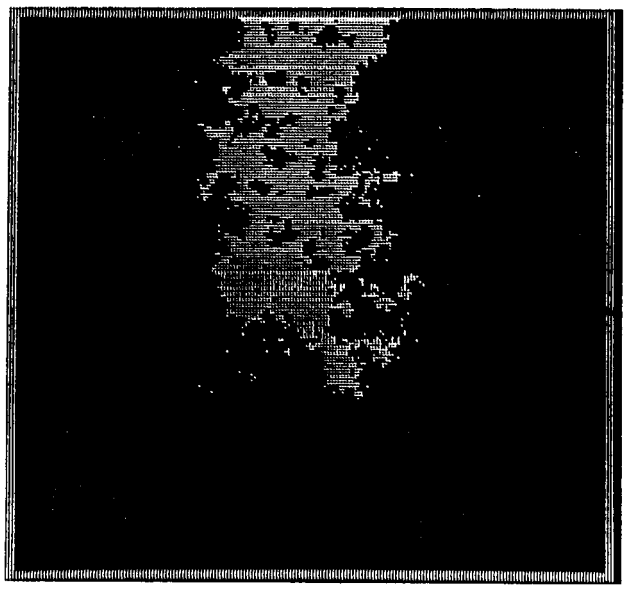

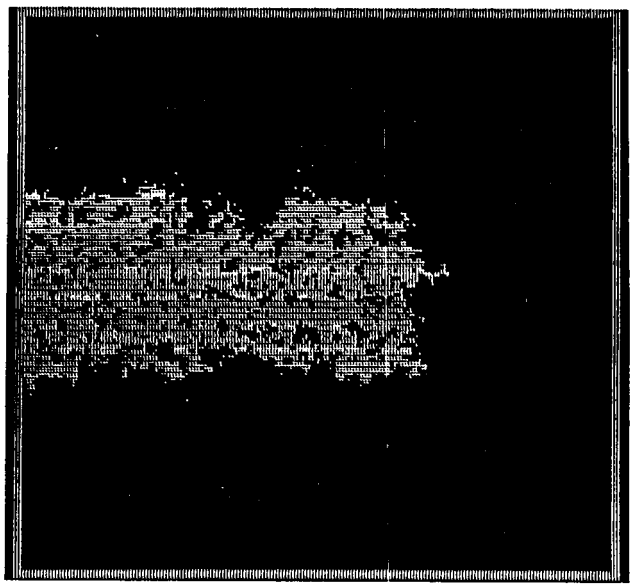

W = 107 G = 540 DL = 88.72 BC = 0111

Figure E1-15. Bay Tambour, SE quadrangle.

W = 13 G = 180 DL = 84.38 BC = 0111

Figure E1-16. Bay Tambour, SW quadrangle.

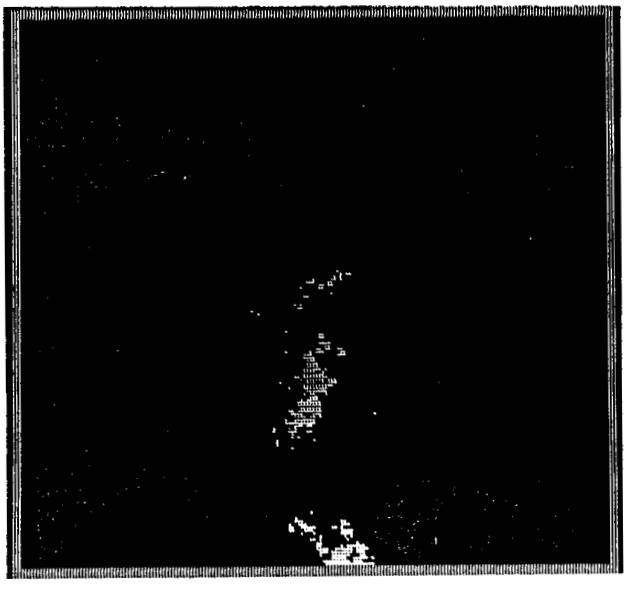

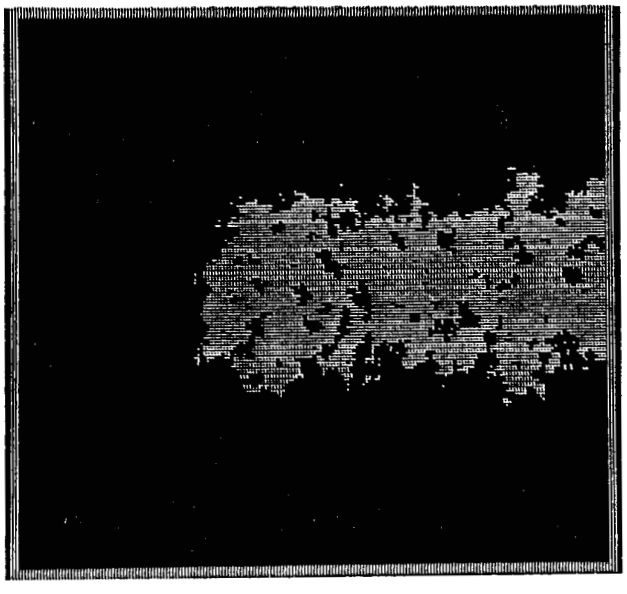

W = 8 G = 180 DL = 98.96 BC = 0111

Figure E1-17. Pelican Pass, NW quadrangle.

W = 88 G = 540 DL = 82.60 BC = 0111

Figure E1-18. Pelican Pass, NE quadrangle.

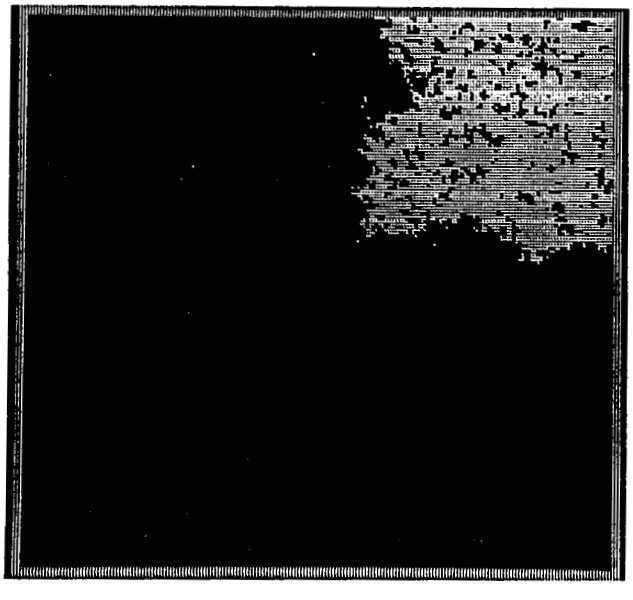

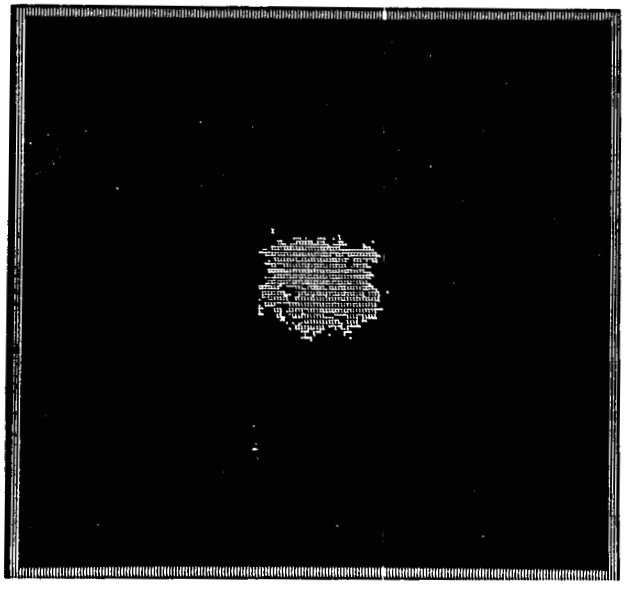

W = 16 G = 540 DL = 86.68 BC = 0011

Figure E1-19. Pelican Pass, SE quadrangle.

W = 38 G = 540 DL = 97.24 BC = 1111

Figure E1-20. Pelican Pass, SW quadrangle.

W = 30 G = 540 DL = 53.83 BC = 0011

Figure E1-21. Grand Bayou Du Large, NW quadrangle.

W = 29 G = 540 DL = 67.26 BC = 0011

Figure E1-22. Grand Bayou Du Large, NE quadrangle.

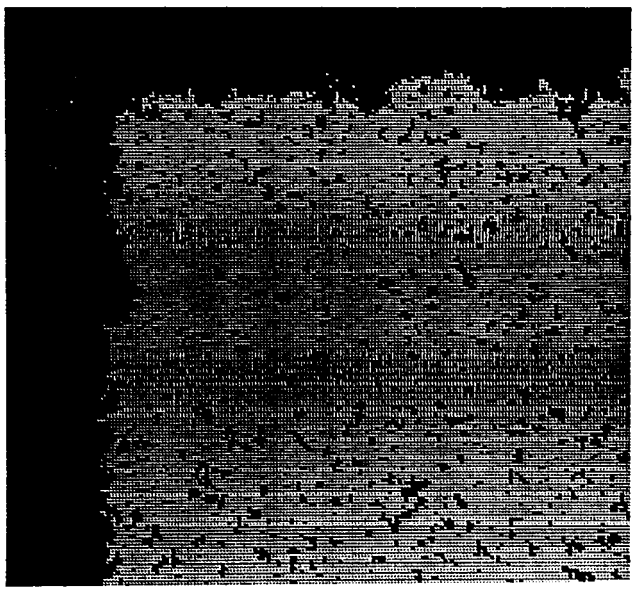

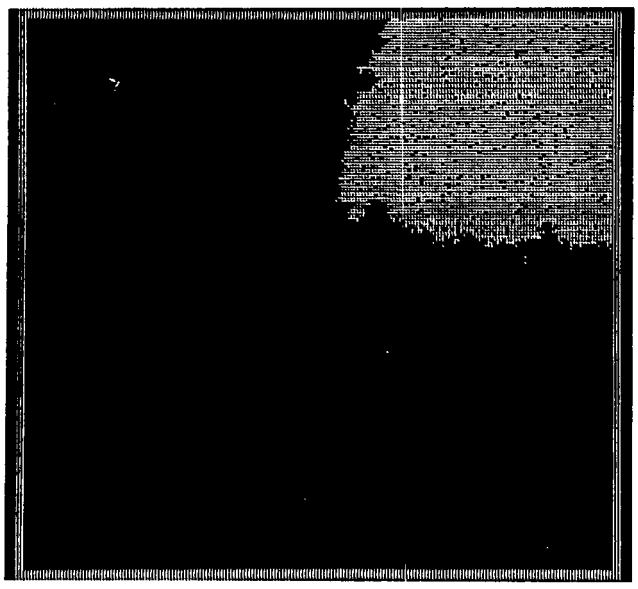

W = 14 G = 180 DL = 40.44 BC = 0011

Figure E1-23. Grand Bayou Du Large, SE quadrangle.

W = 0 G = 540 DL = 83.72 BC = 0011

Figure E1-24. Grand Bayou Du Large, SW quadrangle.

W = 113 G = 540 DL = 91.13 BC = 0111

Figure E1-25. Lake LaGraisse, NW quadrangle.

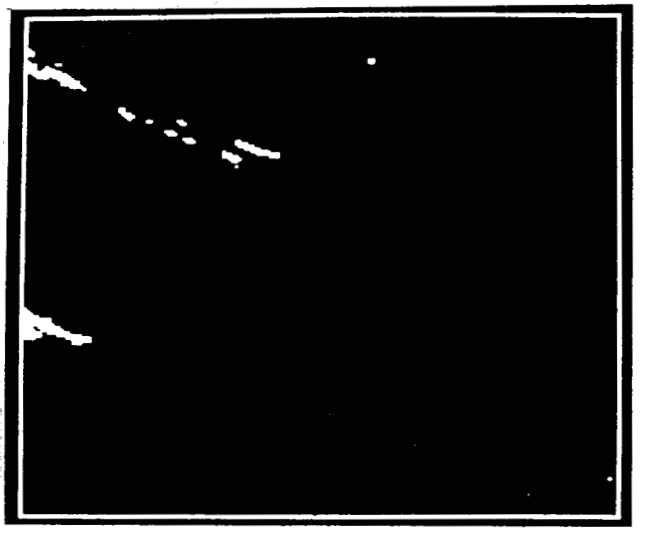

W = 10 G = 180 DL = 99.28 BC = 0111

Figure E1-26. Lake LaGraisse, NE quadrangle.

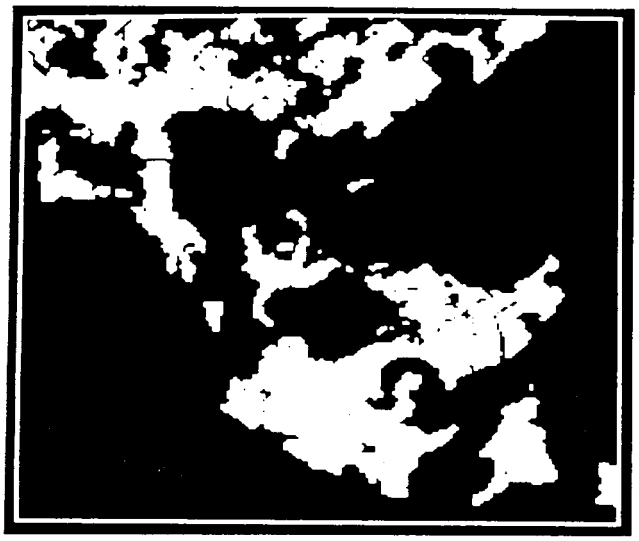

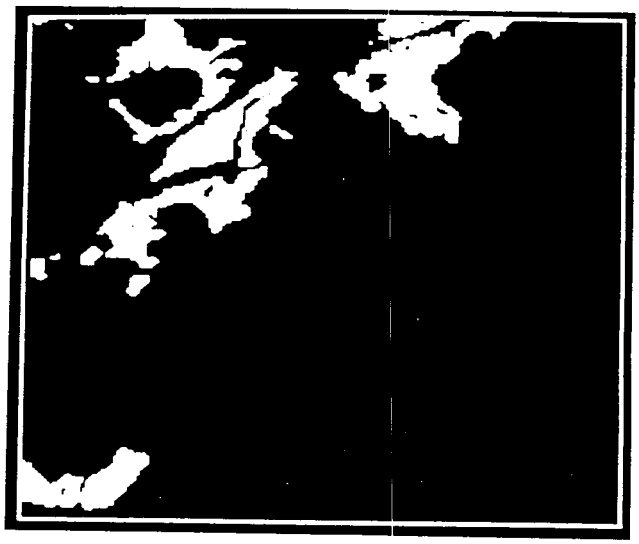

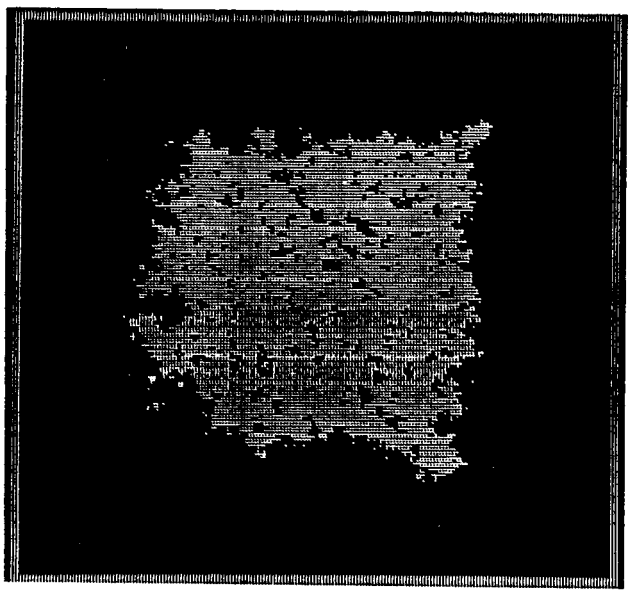

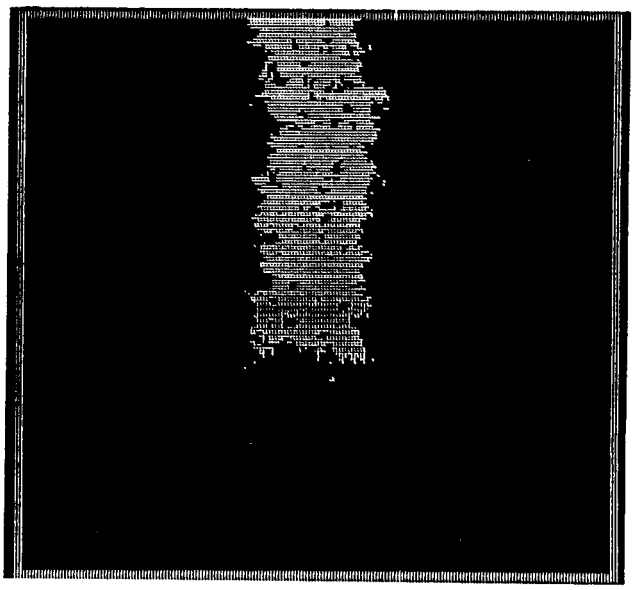

W = 26 G = 180 DL = 75.77 BC = 1111

Figure E1-27. Central Isles Dernieres, NW quadrangle.

W = 43 G = 540 DL = 90.05 BC = 0111

Figure E1-28. Central Isles Dernieres, NE quadrangle.

W = 16 G = 540 DL = 95.18 BC = 0111

Figure E1-29. Central Isles Dernieres, SE quadrangle.

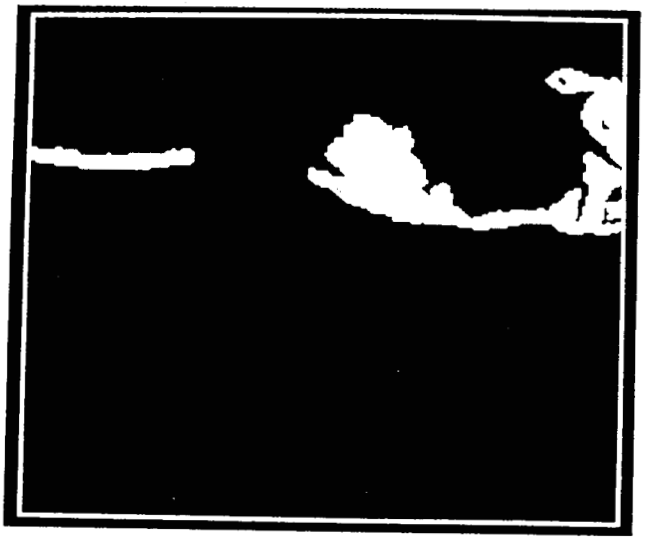

W = 33 G = 540 DL = 93.53 BC = 1111

Figure E1-30. Central Isles Dernieres, SW quadrangle.

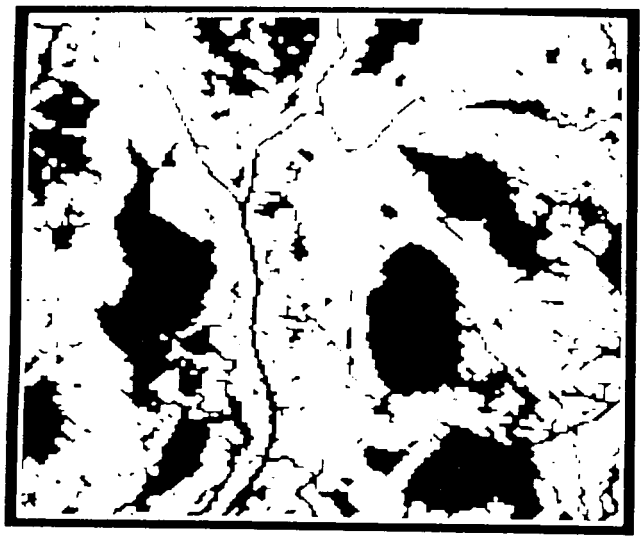

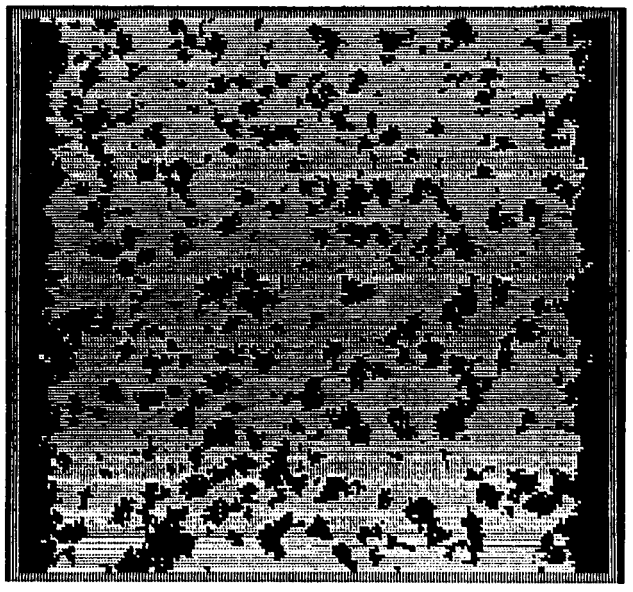

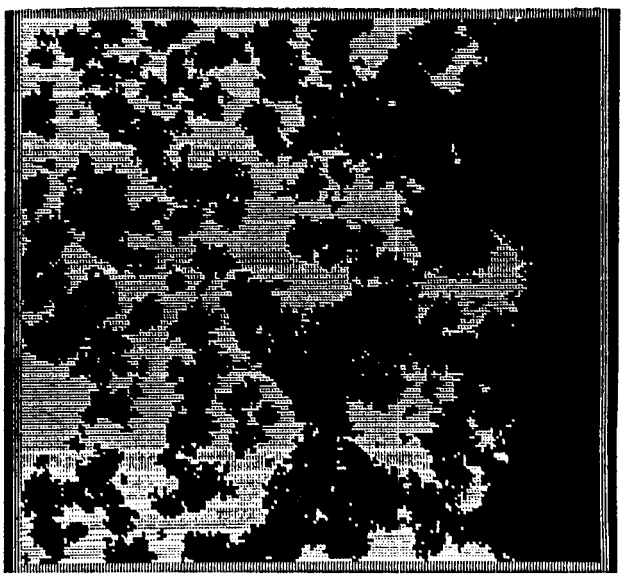

W = 115 G = 180 DL = 33.43 BC = 0101

Figure E1-31. Cocodrie, NW quadrangle.

W = 311 G = 540 DL = 68.89 BC = 0001

Figure E1-32. Cocodrie, NE quadrangle.

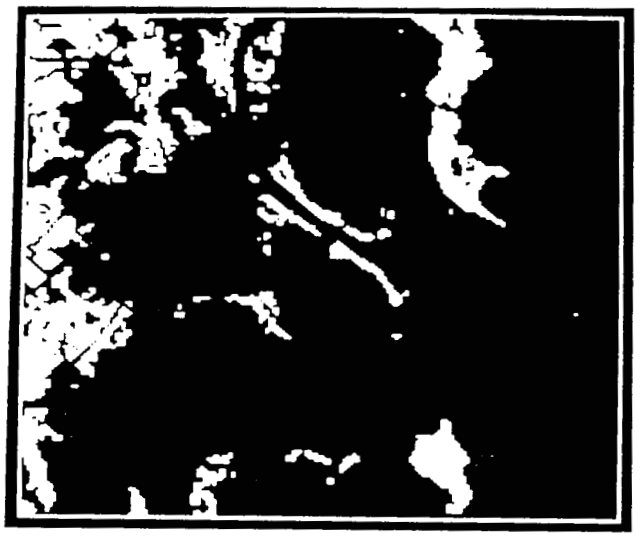

W = 69 G = 540 DL = 85.79 BC = 0011

Figure E1-33. Cocodrie, SE quadrangle.

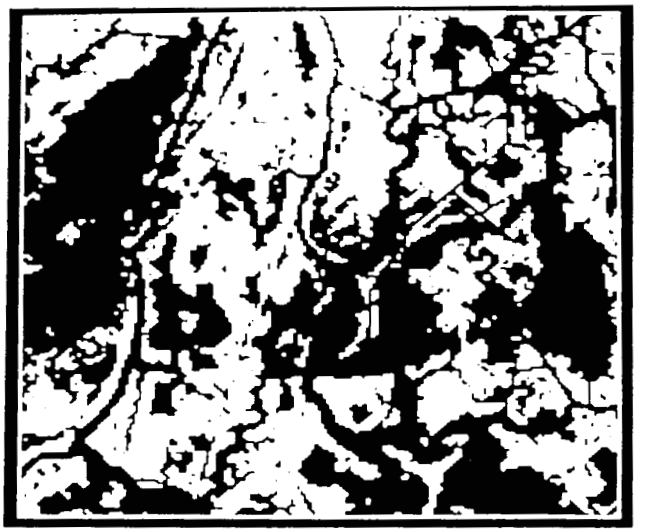

W = 233 G = 60 DL = 54.72 BC = 0011

Figure E1-34. Cocodrie, SW quadrangle.

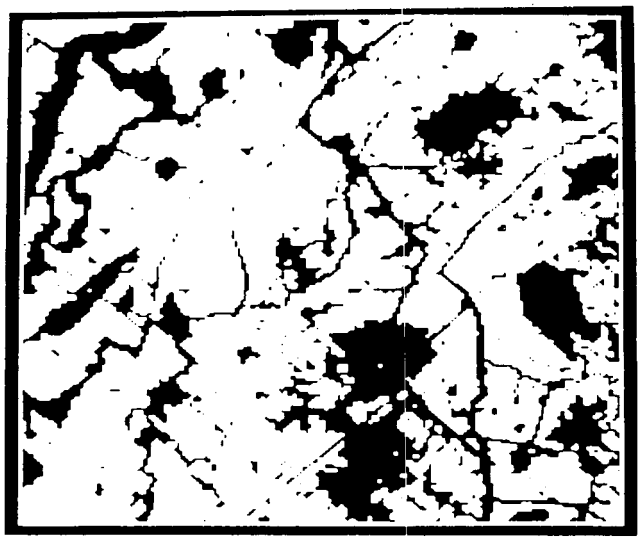

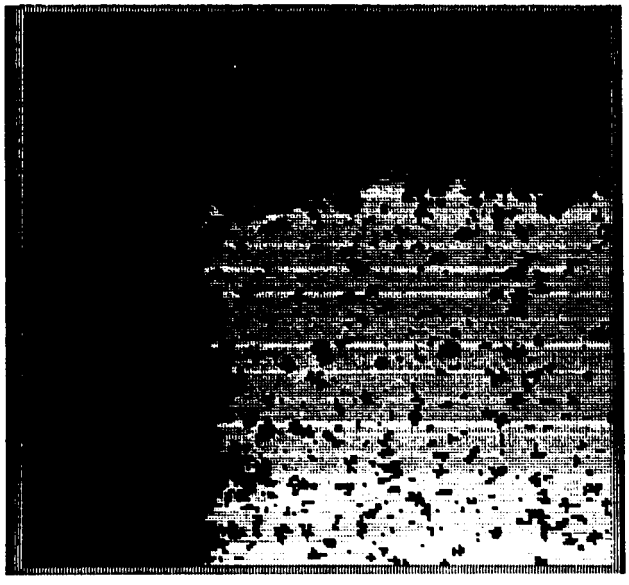

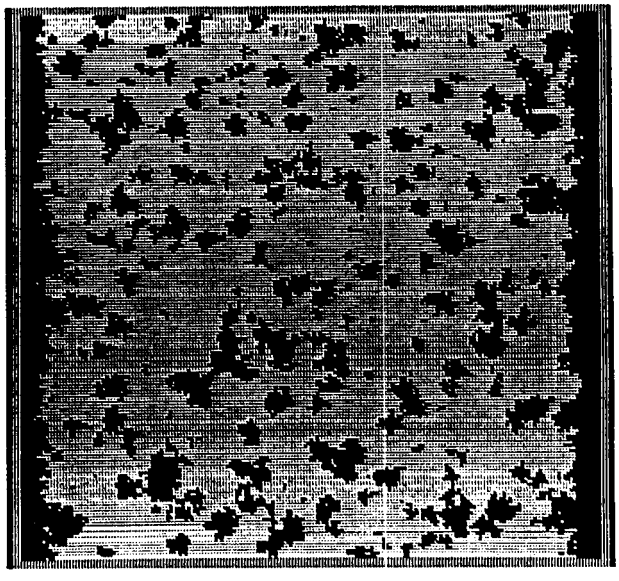

W = 44 G = 540 DL = 62.97 BC = 0011

Figure E1-35. Dog Lake, NW quadrangle.

W = 213 G = 180 DL = 30.74 BC = 0101

Figure E1-36. Dog Lake, NE quadrangle.

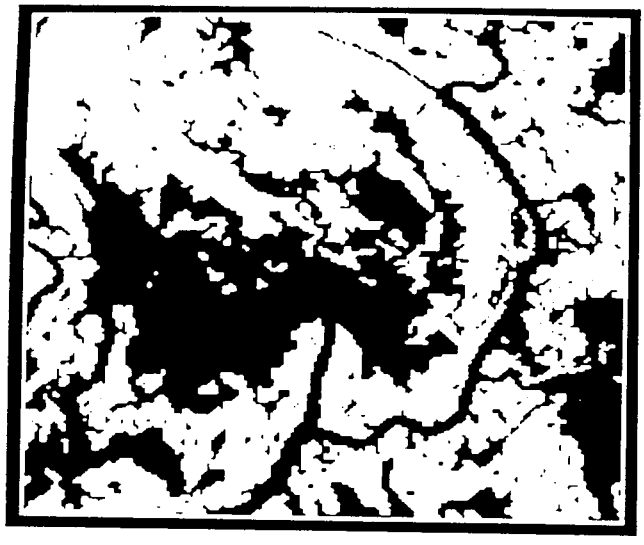

W = 120 G = 180 DL = 42.38 BC = 0011

Figure E1-37. Dog Lake, SE quadrangle.

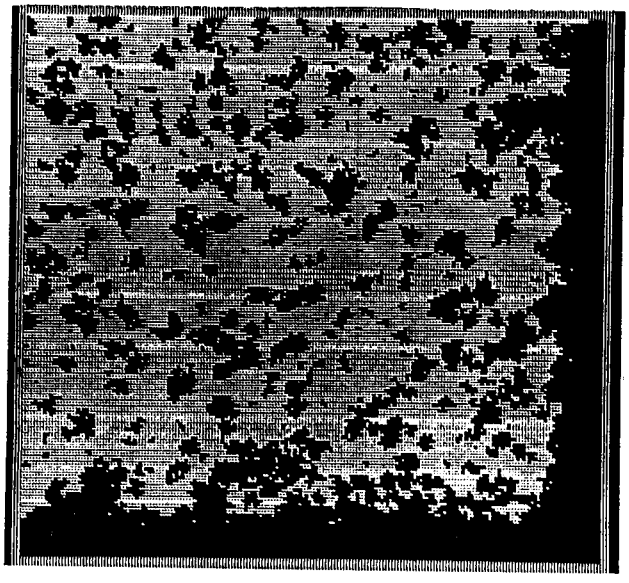

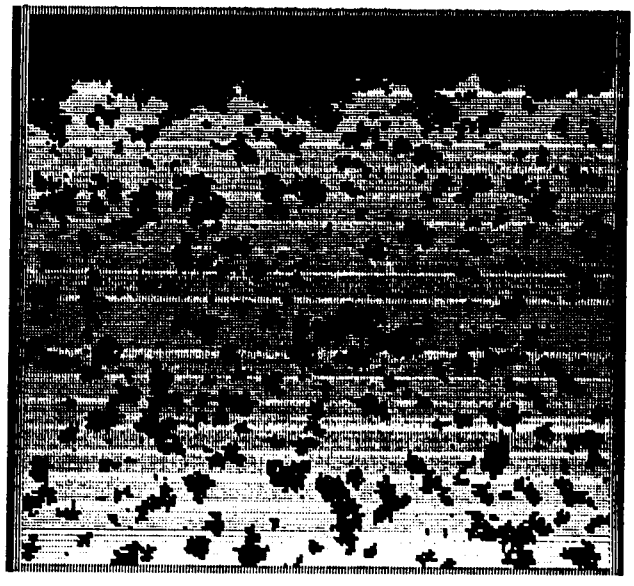

W = 123 G = 540 DL = 36.40 BC = 0001

Figure E1-38. Dog Lake, SW quadrangle.

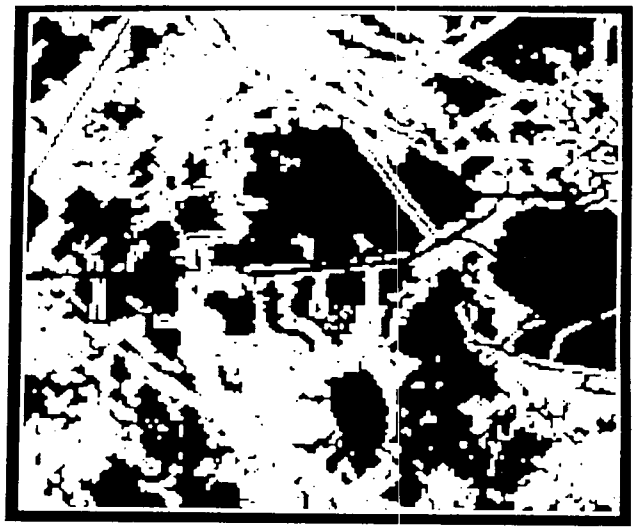

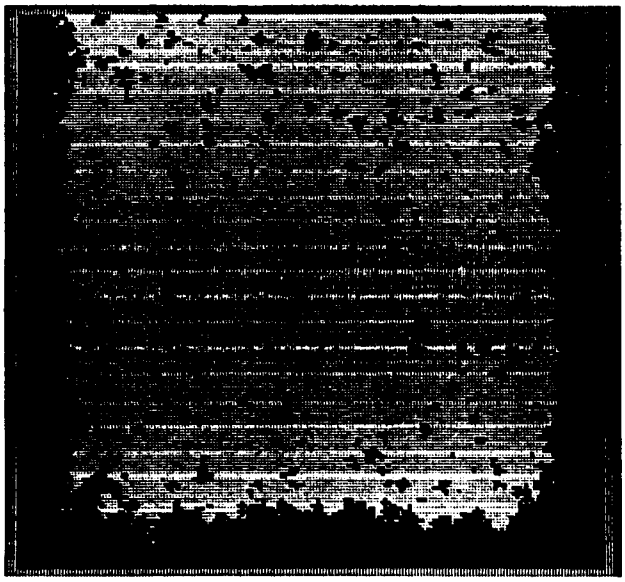

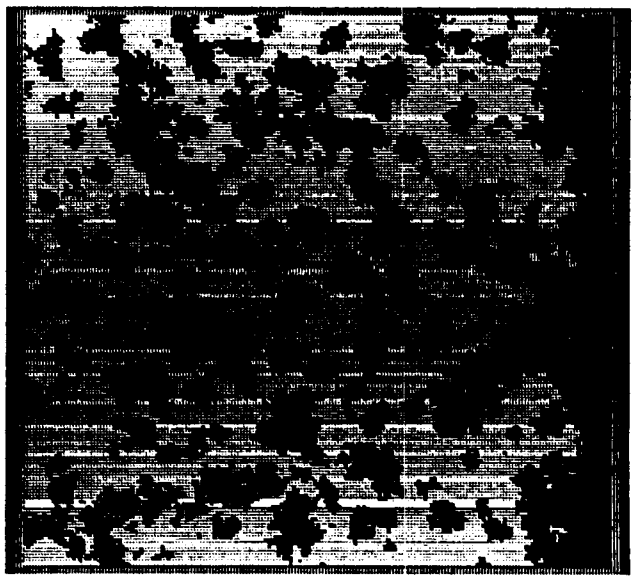

W = 62 G = 180 DL = 33.69 BC = 0111

Figure E1-39. Lake Bully Camp, NW quadrangle.

W = 244 G = 180 DL = 47.84 BC = 0001

Figure E1-40. Lake Bully Camp, NE quadrangle.

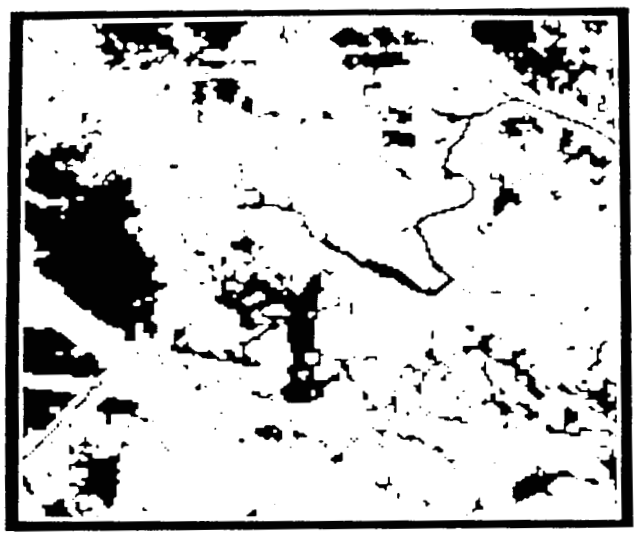

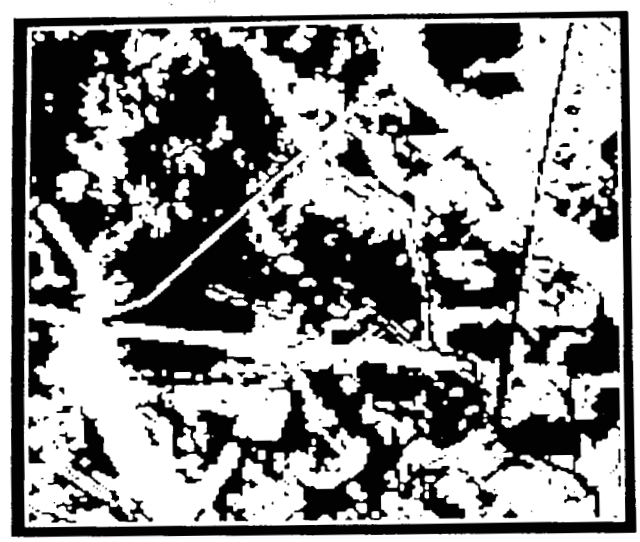

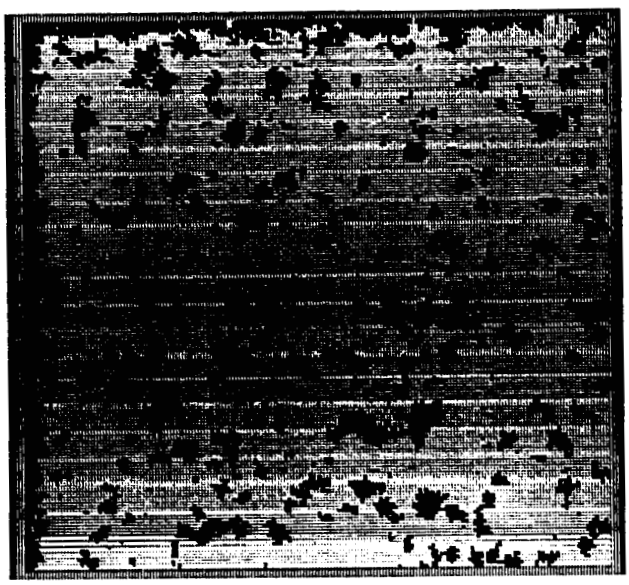

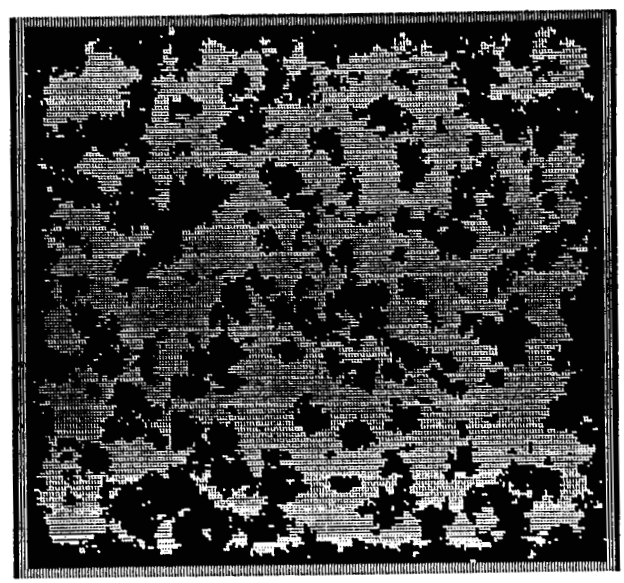

W = 130 G = 60 DL = 22.21 BC = 0011

Figure E1-41. Lake Bully Camp, SE quadrangle.

W = 255 G = 60 DL = 50.02 BC = 1111

Figure E1-42. Lake Bully Camp, SW quadrangle.

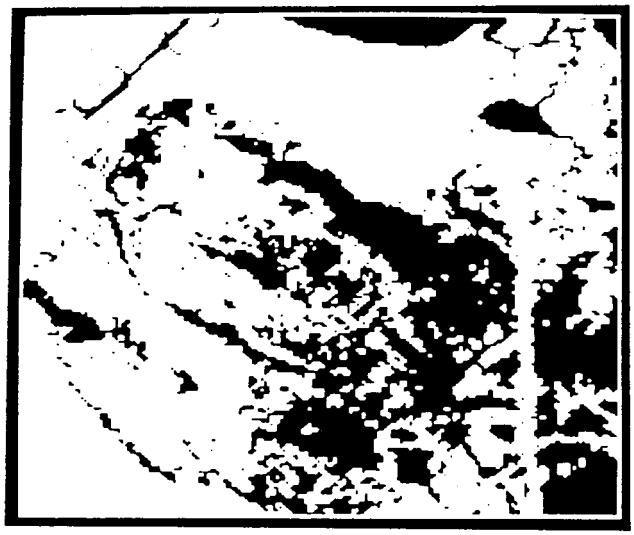

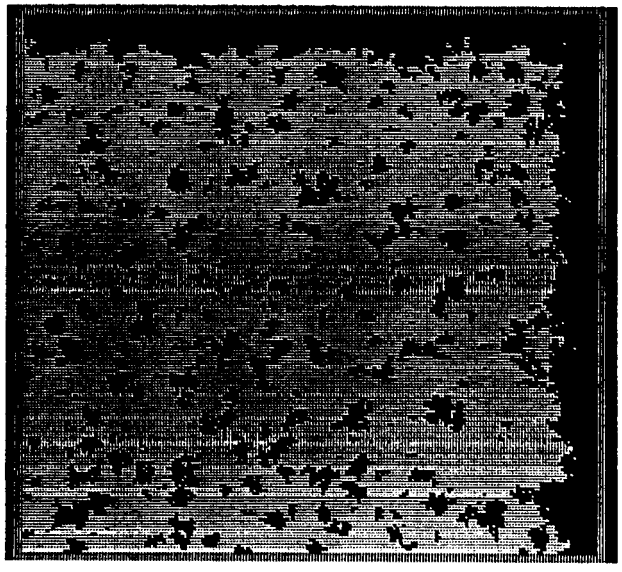

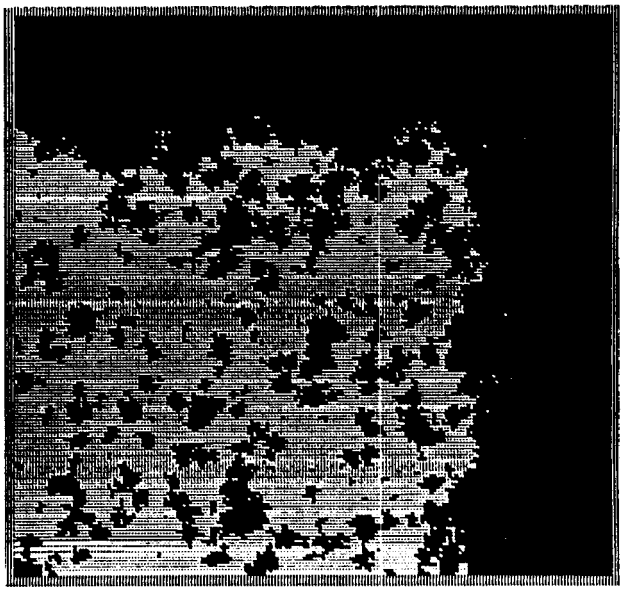

W = 129 G = 180 DL = 30.91 BC = 0011

Figure E1-43. Golden Meadow Farms, NW quadrangle.

W = 160 G = 540 DL = 60.69 BC = 0011

Figure E1-44. Golden Meadow Farms, NE quadrangle.

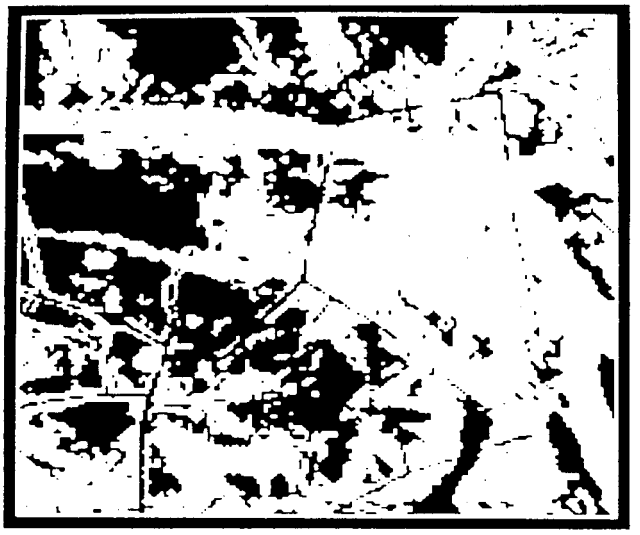

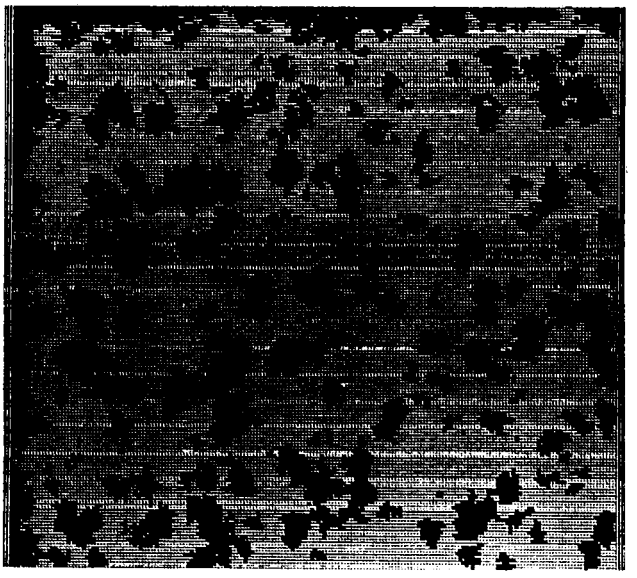

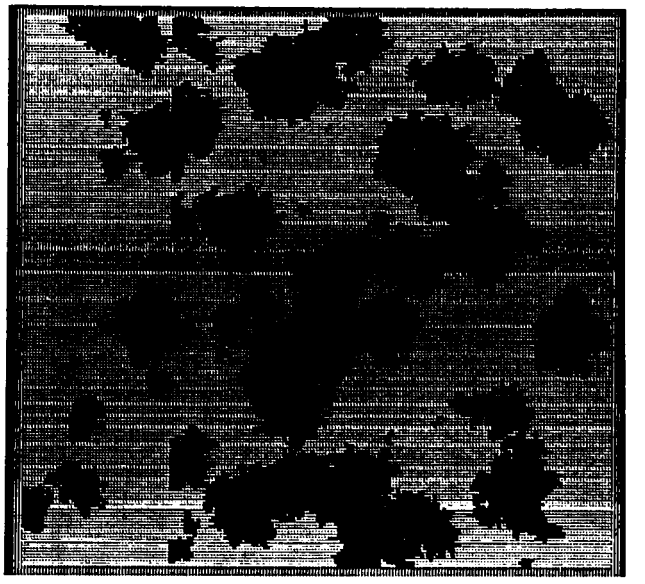

W = 308 G = 60 DL = 35.56 BC = 0011

Figure E1-45. Golden Meadow Farms, SE quadrangle.

W = 3184 G = 0 DL = 38.95 BC = 0000

Figure E1-46. Golden Meadow Farms, SW quadrangle.

W = 8 G = 180 DL = 81.53 BC = 0111

Figure E1-47. Bay L'Ours, SE quadrangle.

W = 1 G = 540 DL = 52.26 BC = 0011

Figure E1-48. Bay L'Ours, SW quadrangle.

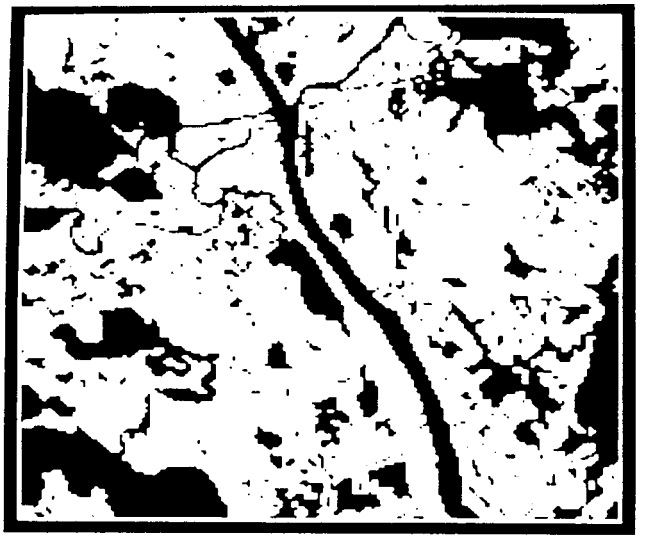

W = 100 G = 60 DL = 32.93 BC = 1111

Figure E1-49. Three Bayou Bay, SE quadrangle.

W = 33 G = 540 DL = 58.71 BC = 0011

Figure E1-50. Three Bayou Bay, SW quadrangle.

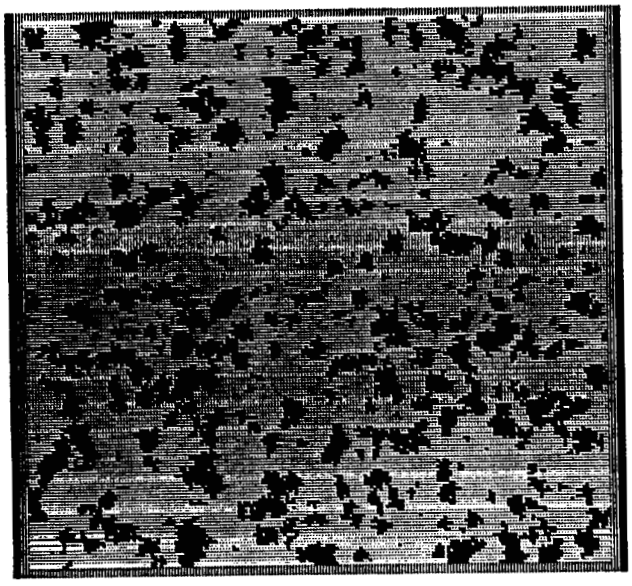

W = 116 G = 0 DL = 27.66 BC = 0011

Figure E1-51. Golden Meadow, SW quadrangle.

W = 23 G = 180 DL = 32.65 BC = 0011

Figure E1-52. Lost Lake, NW quadrangle.

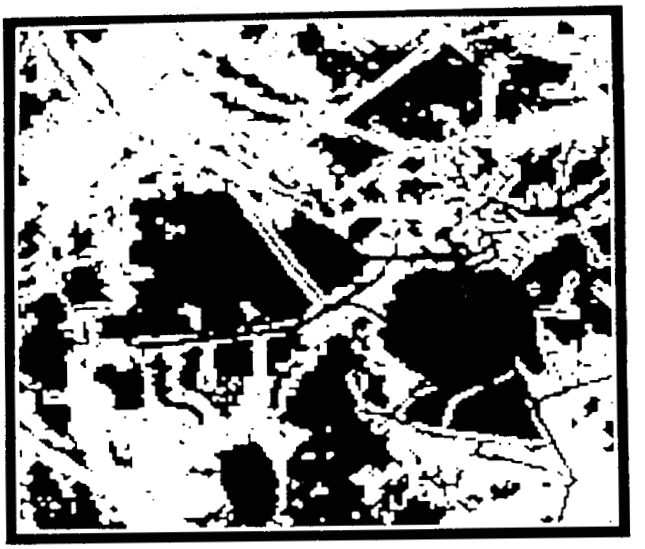

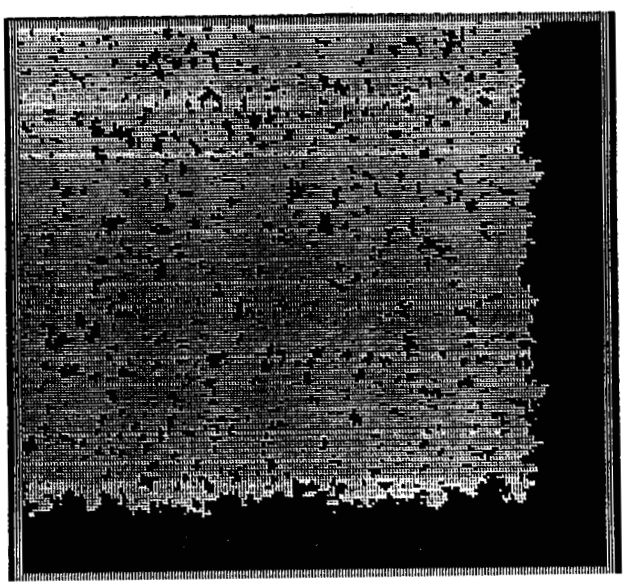

W = 245 G = 180 DL = 47.32 BC = 0001

Figure E1-53. Lost Lake, NE quadrangle.

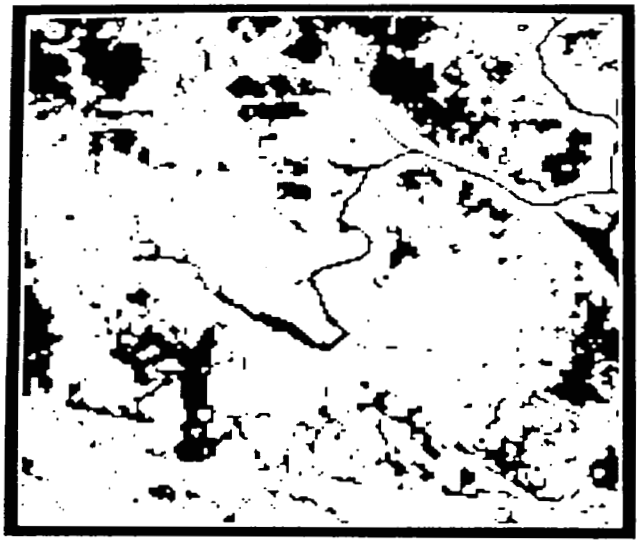

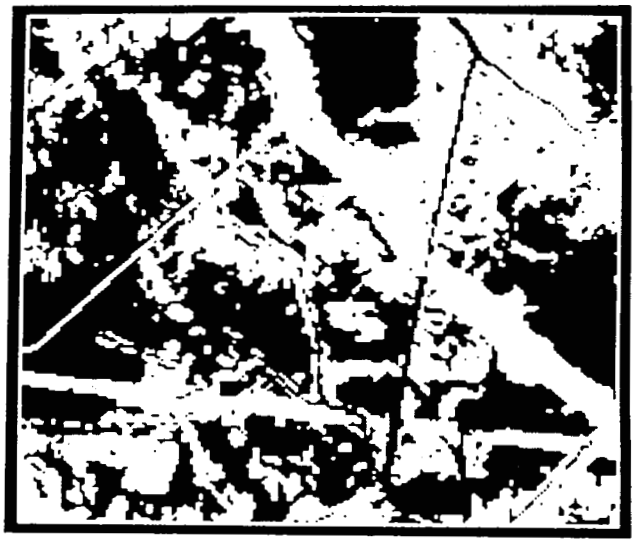

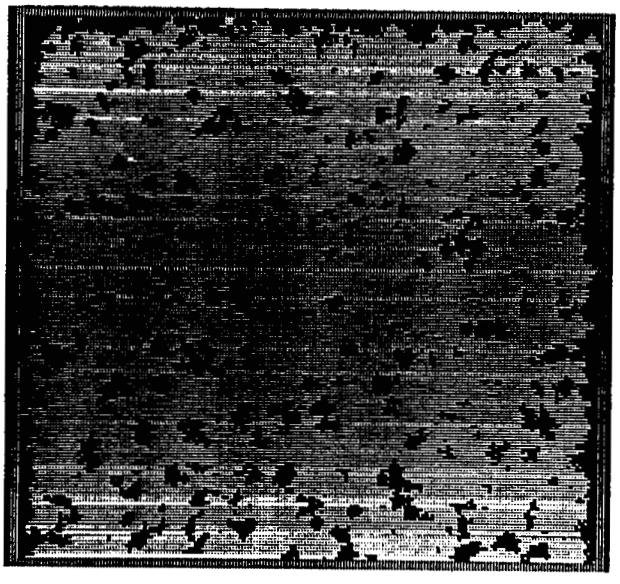

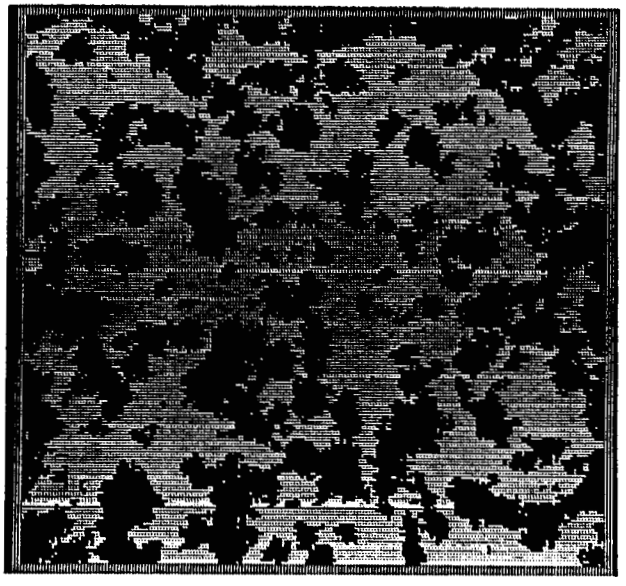

W = 111 G = 60 DL = 21.81 BC = 0111

Figure E1-54. Lost Lake, SE quadrangle.

W = 290 G = 20 DL = 50.78 BC = 0111

Figure E1-55. Lost Lake, SW quadrangle.

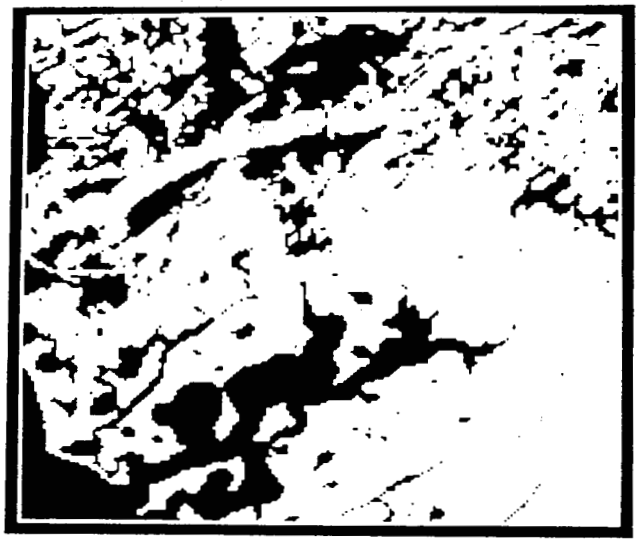

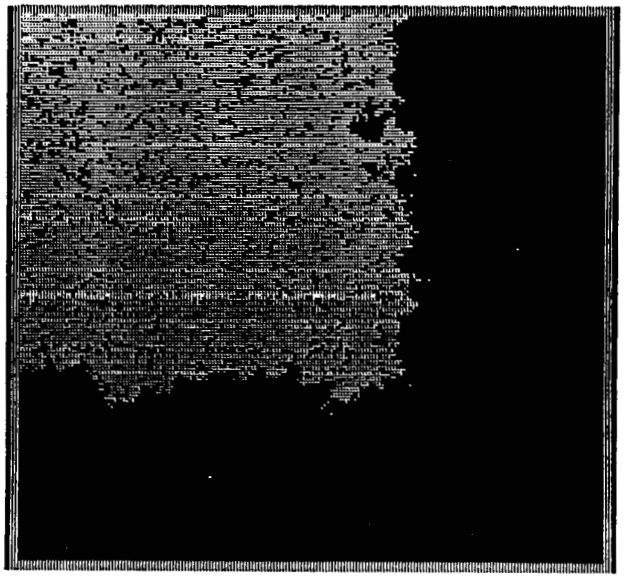

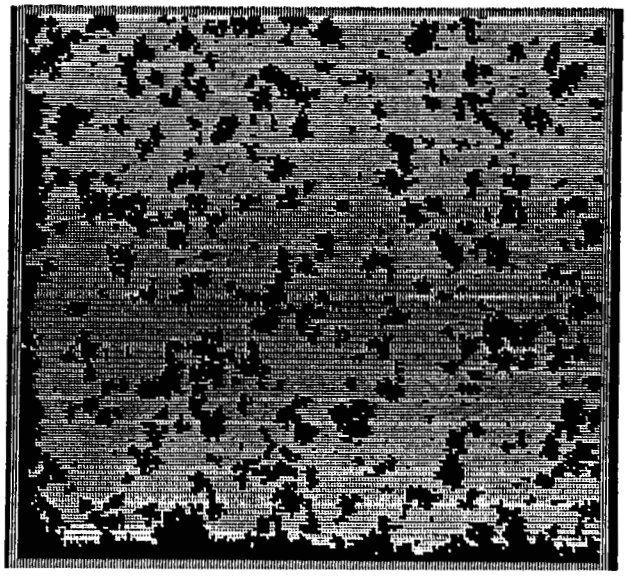

W = 4 G = 180 DL = 64.05 BC = 0011

Figure E1-56. Lake Mechant, NW quadrangle.

W = 118 G = 60 DL = 29.91 BC = 0011

Figure E1-57. Lake Mechant, NE quadrangle.

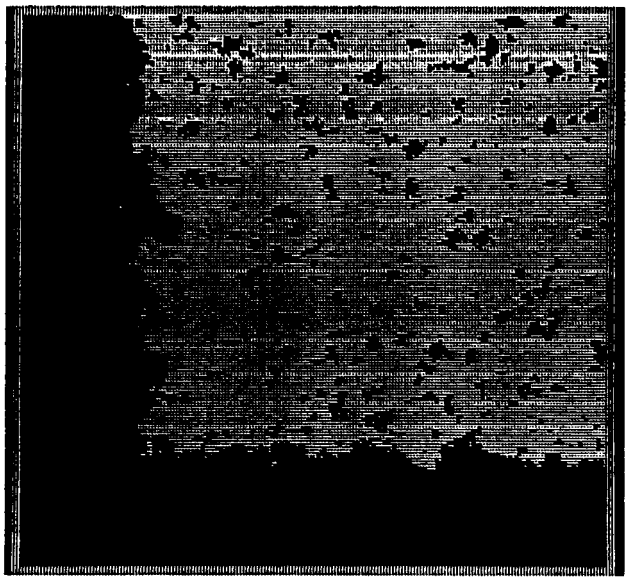

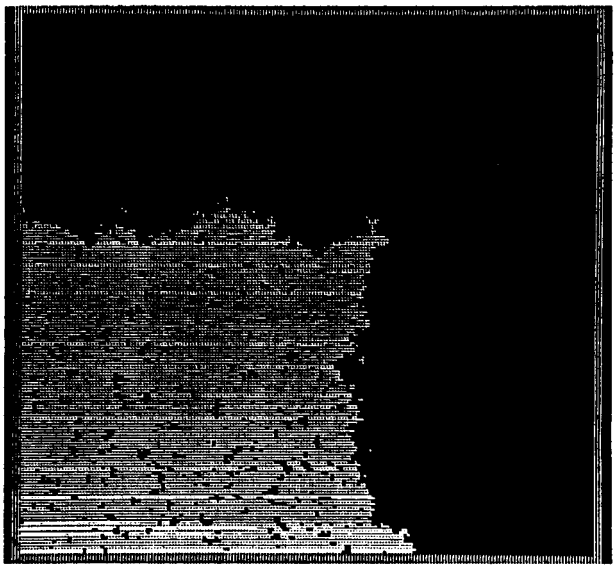

W = 86 G = 540 DL = 44.91 BC = 0011

Figure E1-58. Lake Mechant, SE quadrangle.

W = 17 G = 540 DL = 67.06 BC = 0011

Figure E1-59. Lake Mechant, SW quadrangle.

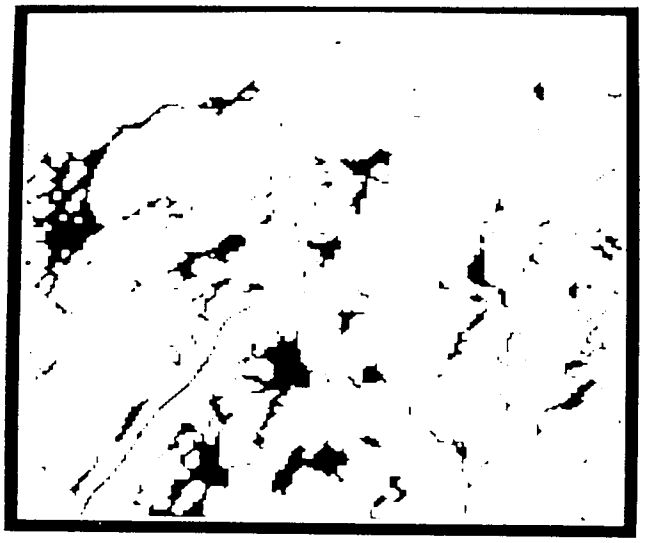

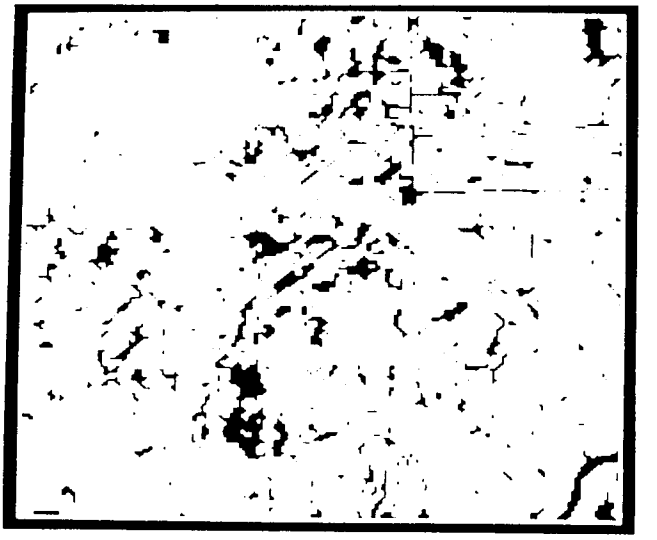

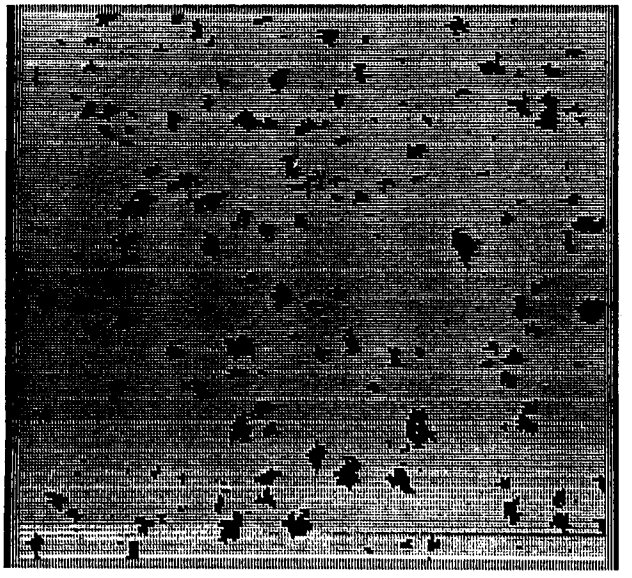

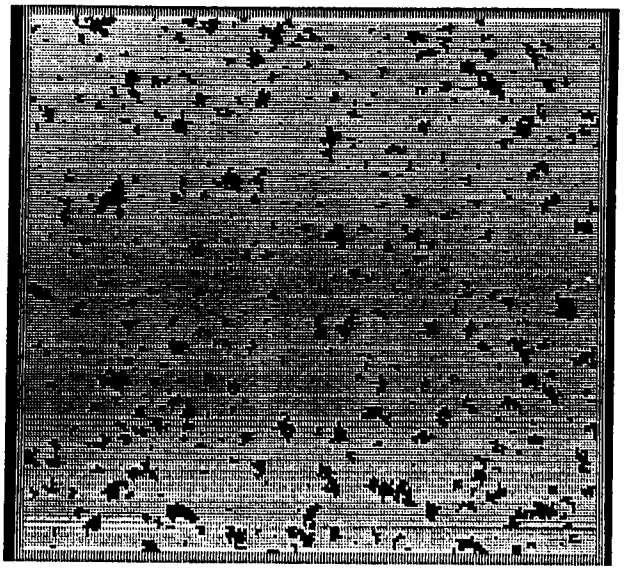

W = 325 G = 0 DL = 8.72 BC = 0000

Figure E1-60. Bayou Sauveur, NW quadrangle.

W = 93 G = 0 DL = 10.90 BC = 0000

Figure E1-61. Bayou Sauveur, NE quadrangle.

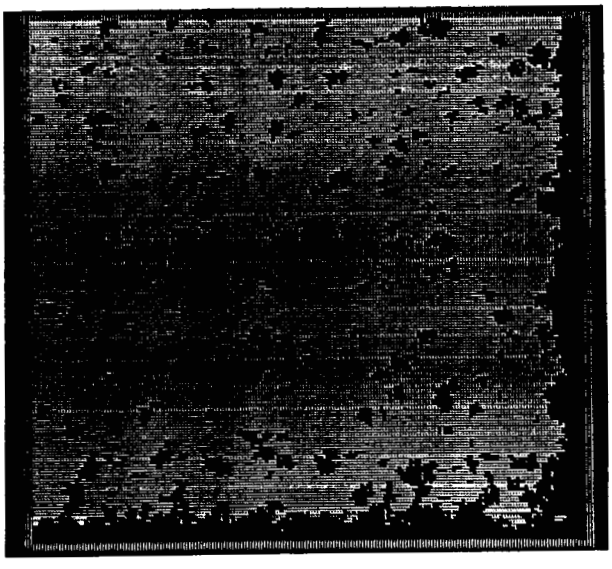

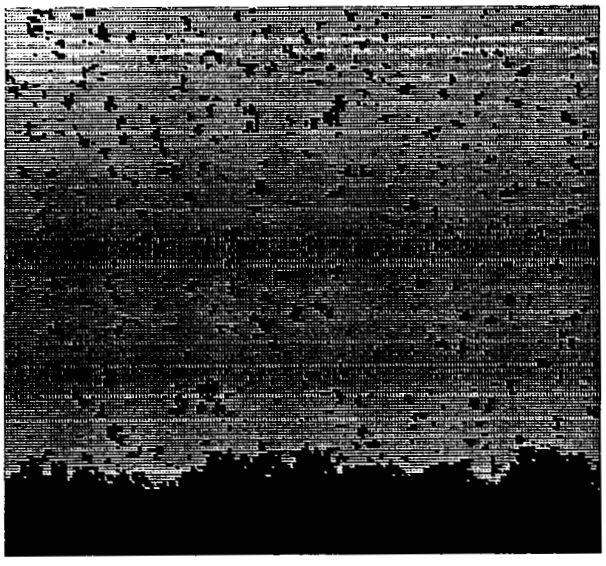

W = 133 G = 180 DL = 22.23 BC = 0011

Figure E1-62. Bayou Sauveur, SE quadrangle.

W = 35 G = 540 DL = 24.31 BC = 0001

Figure E1-63. Bayou Sauveur, SW quadrangle.

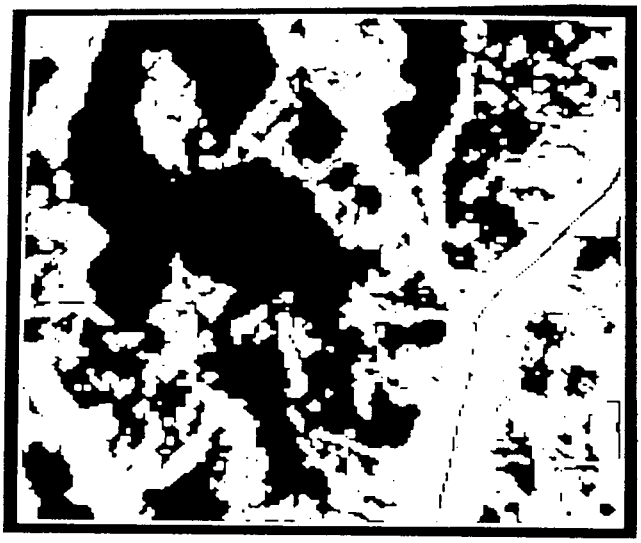

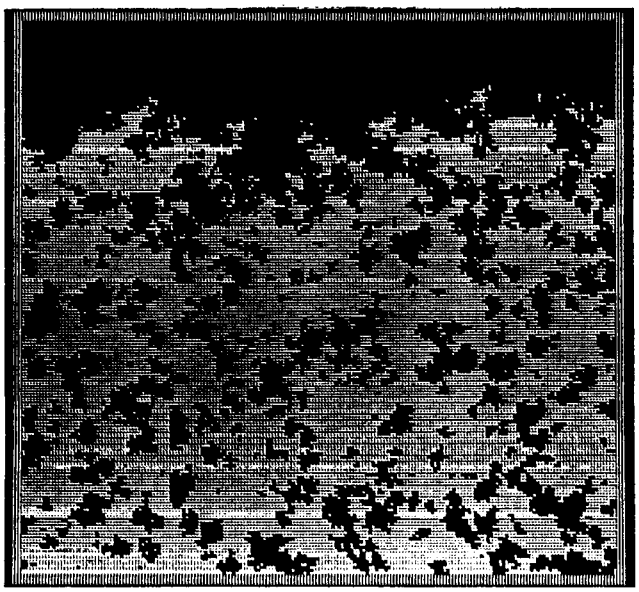

W = 116 G = 540 DL = 48.20 BC = 0001

Figure E1-64. Lake Quitman, NE quadrangle.

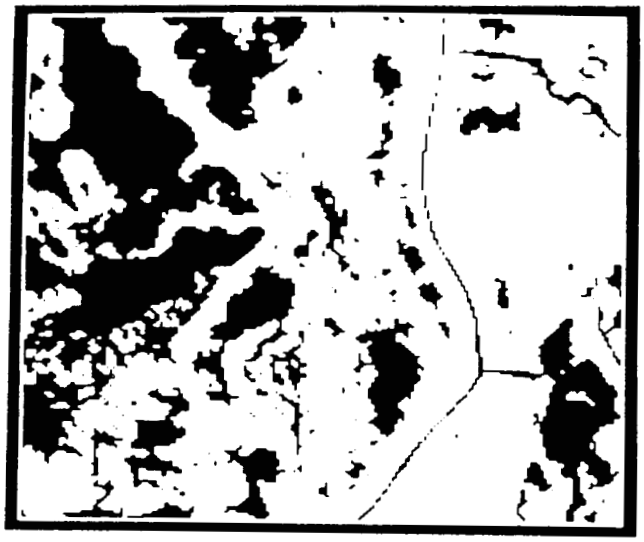

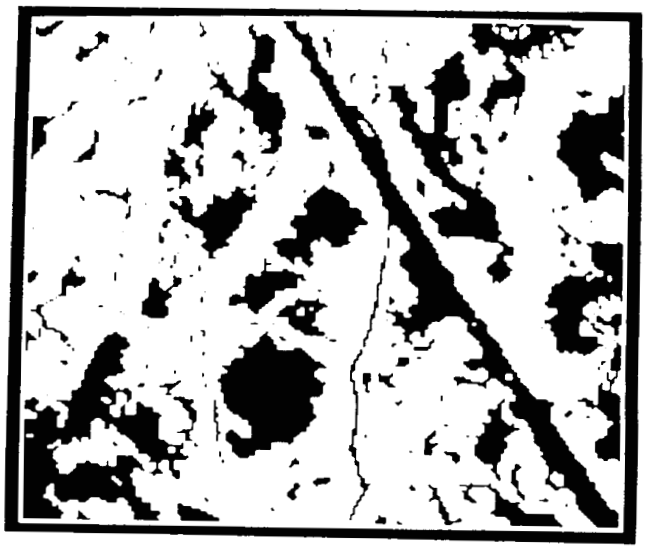

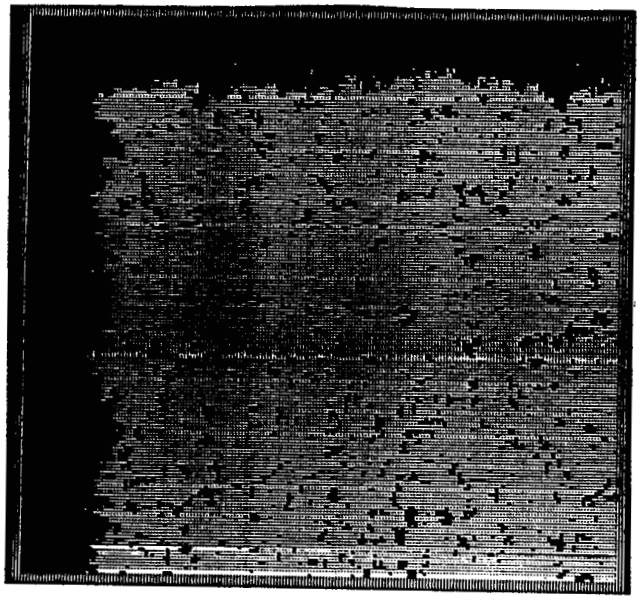

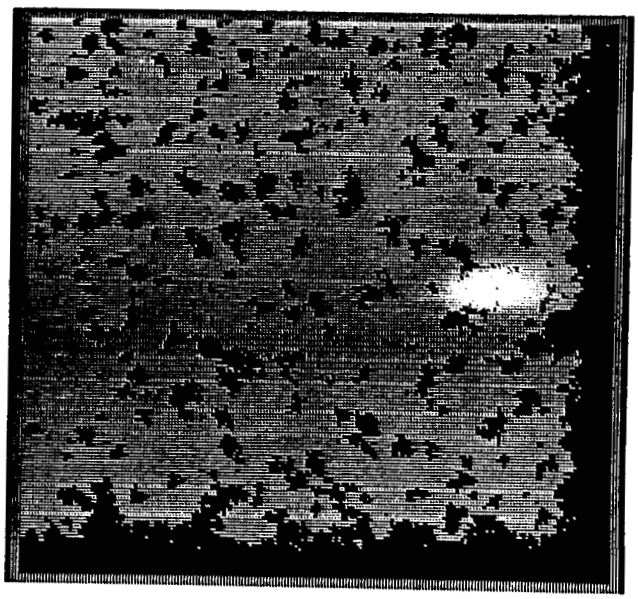

W = 20 G = 180 DL = 32.41 BC = 0011

Figure E1-65. Lake Quitman, SE quadrangle.

W = 121 G = 180 DL = 31.85 BC = 0011

Figure E1-66. Lake Quitman, SW quadrangle.

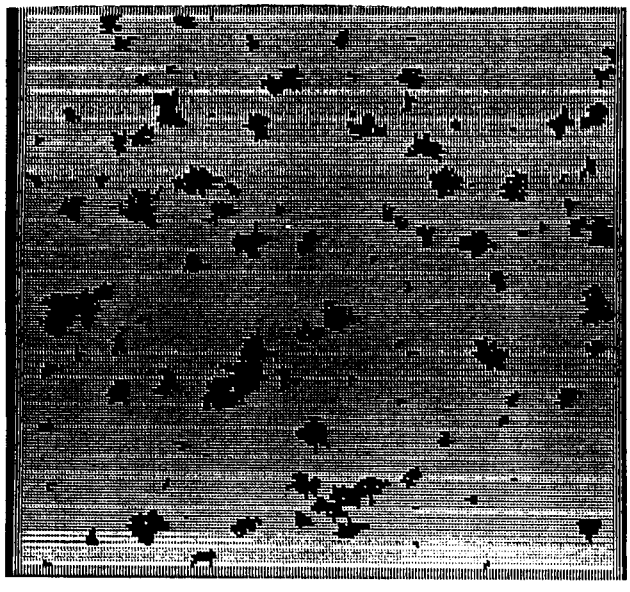

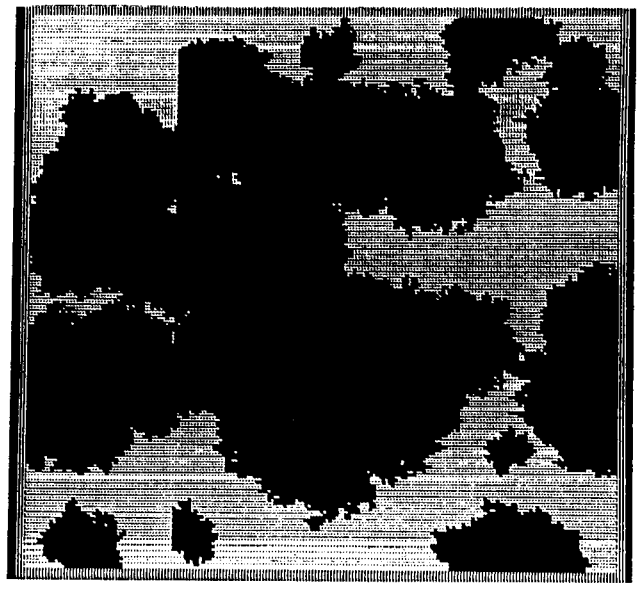

W = 701 G = 0 DL = 9.63 BC = 0000

Figure E1-67. Dulac, NE quadrangle.

W = 10947 G = 0 DL = 66.80 BC = 0000

Figure E1-68. Dulac, SE quadrangle.

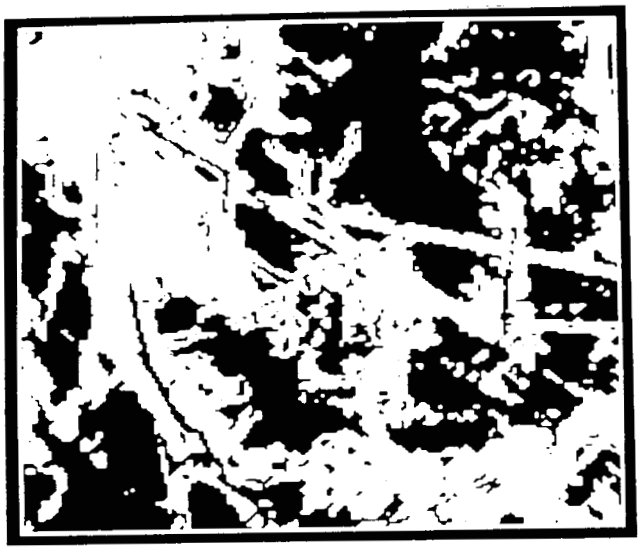

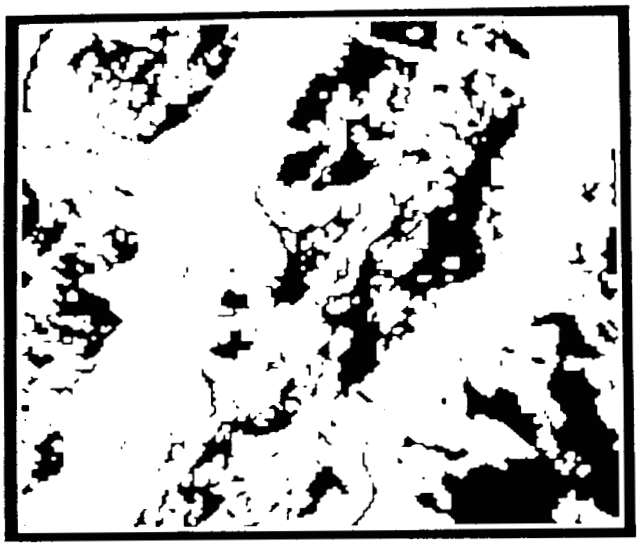

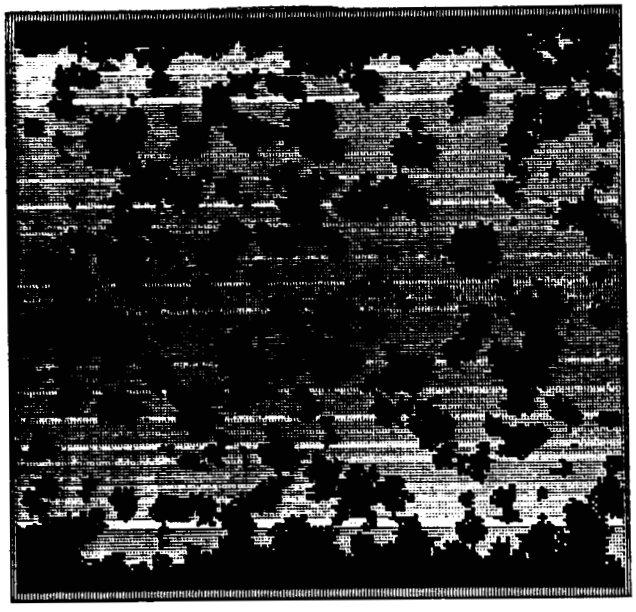

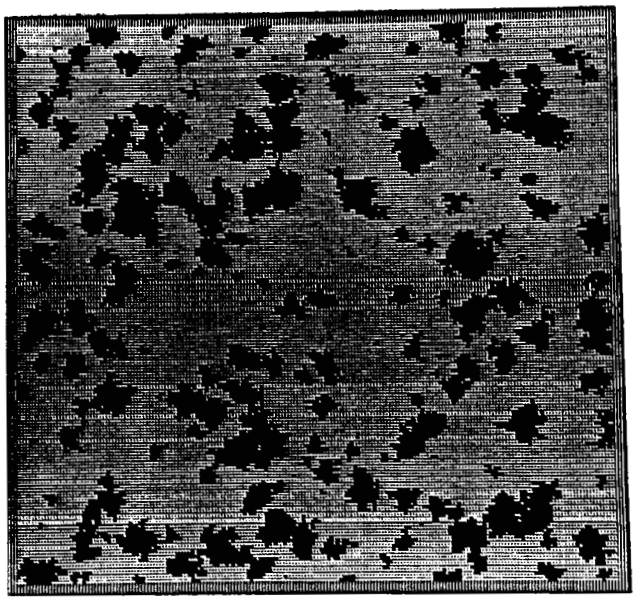

W = 289 G = 180 DL = 47.48 BC = 0101

Figure E1-69. Montegut, SE quadrangle.

W = 404 G = 0 DL = 27.16 BC = 0000

Figure E1-70. Montegut, SW quadrangle.

Figure E2. Comparisons of pond size distributions of TM scenes with the "best-fit" simulations at the same disintegration level. Water-body size is the frequency distribution of water-body classes (in pixel units) expressed as percentage of total number of water pixels. Frequency is the number of pixels in a water-body class, expressed as a percentage of the total number of water pixels. Each mirror image histogram shows one TM scene and its representative simulation. Quadrangles are grouped by age of delta lobe and salinity (as in Table D1).

Late Lafourche, salt

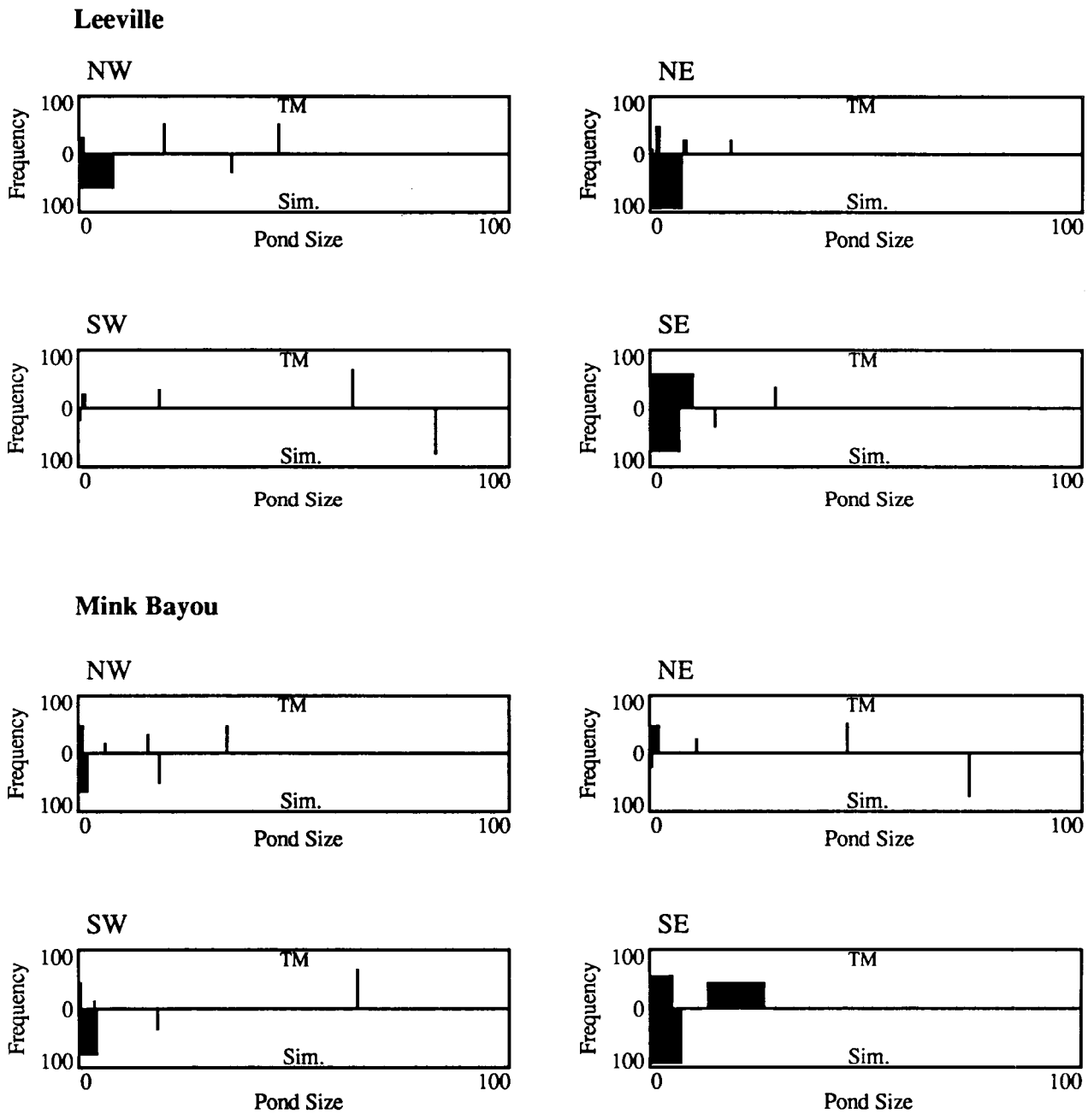

Figure E2-1. Pond size distributions for Leeville and Mink Bayou quadrangles.

Late Lafourche, salt

Caminada Pass

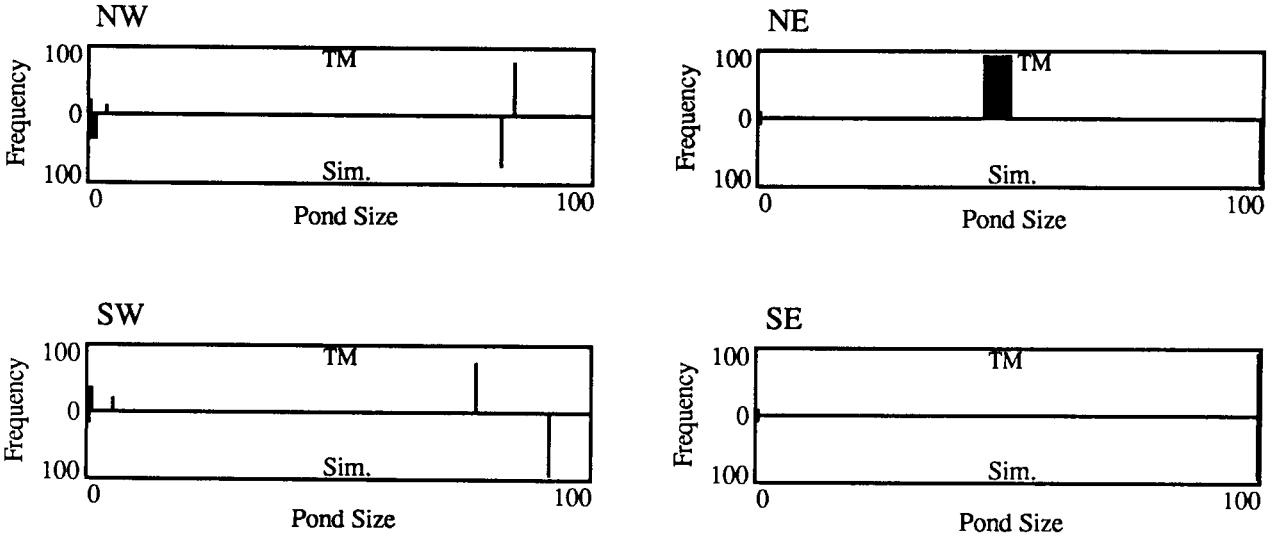

Bay Tambour

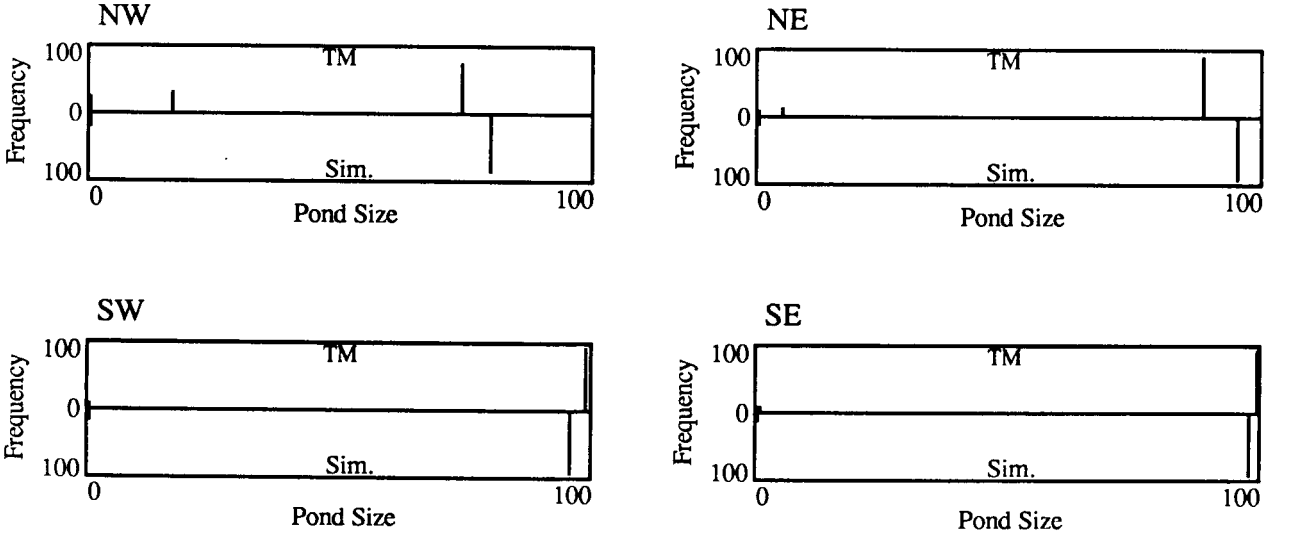

Figure E2-2. Pond size distributions for Caminada Pass and Bay Tambour quadrangles.

Late Lafourche, salt

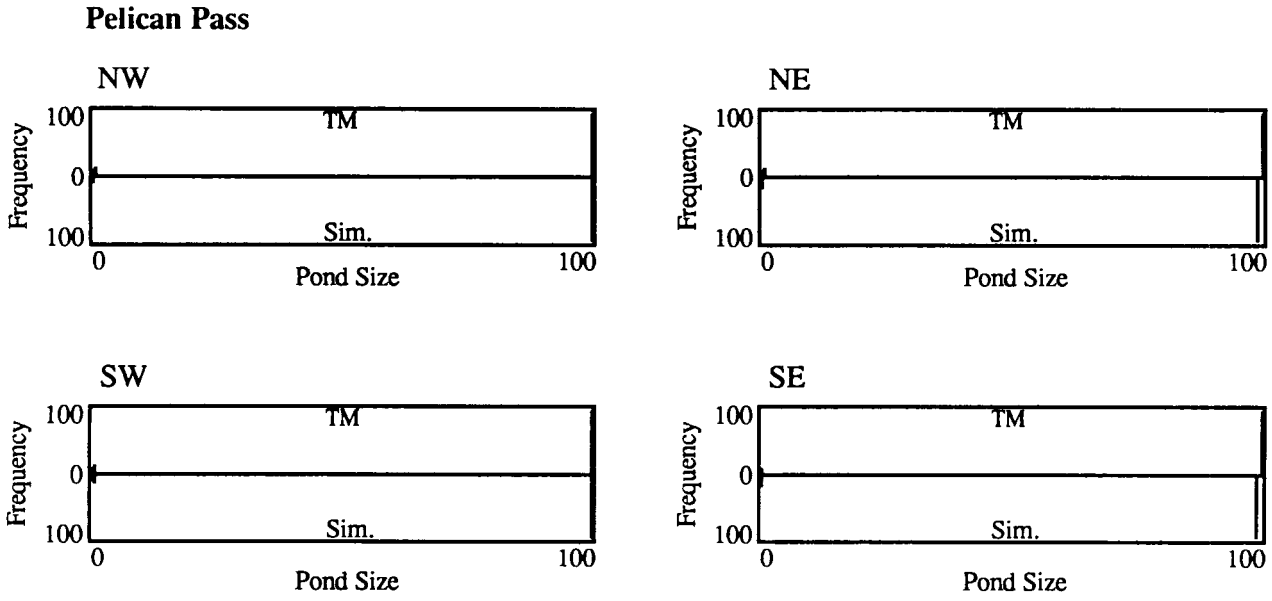

Figure E2-3. Pond size distributions for Pelican Pass quadrangle.

Early Lafourche, salt

Grand Bayou du Large

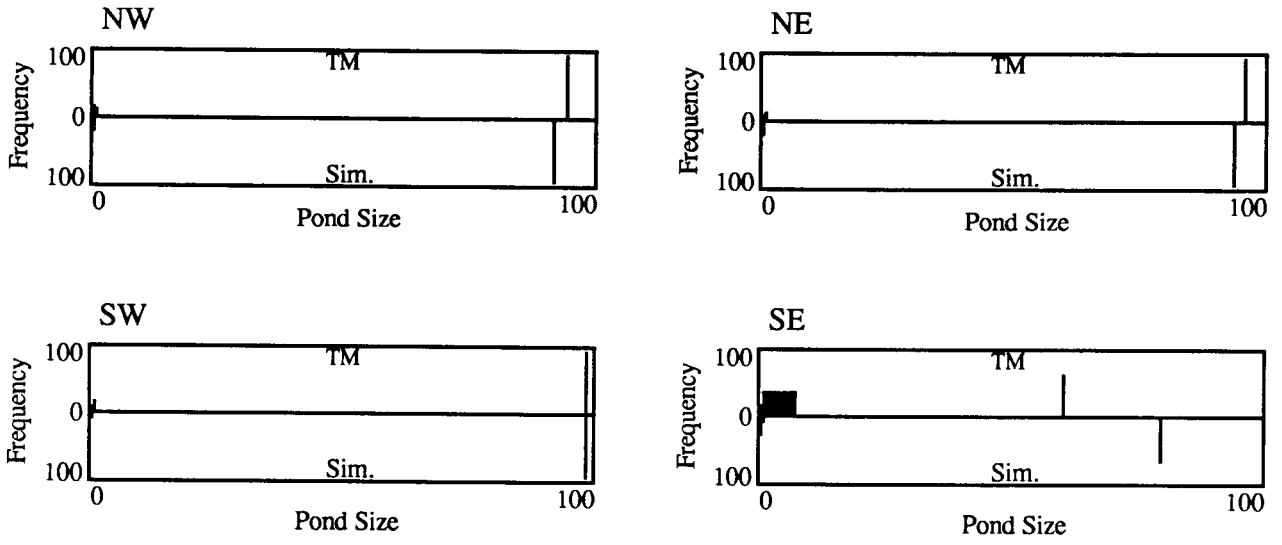

Lake La Graisse

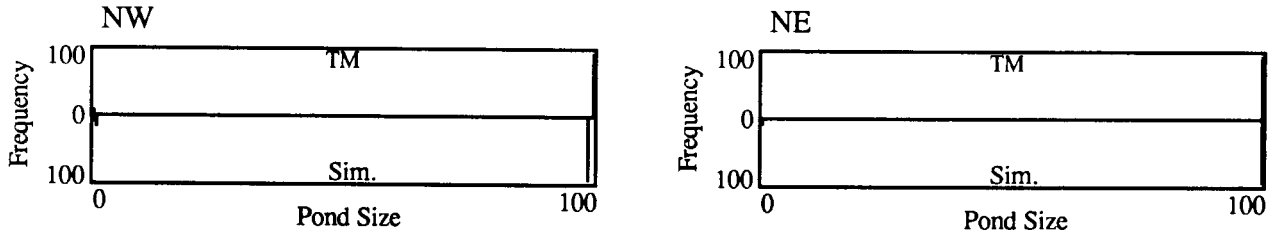

Figure E2-4. Pond size distributions for Grand Bayou du Large and Lake La Graisse quadrangles.

Early Lafourche, salt

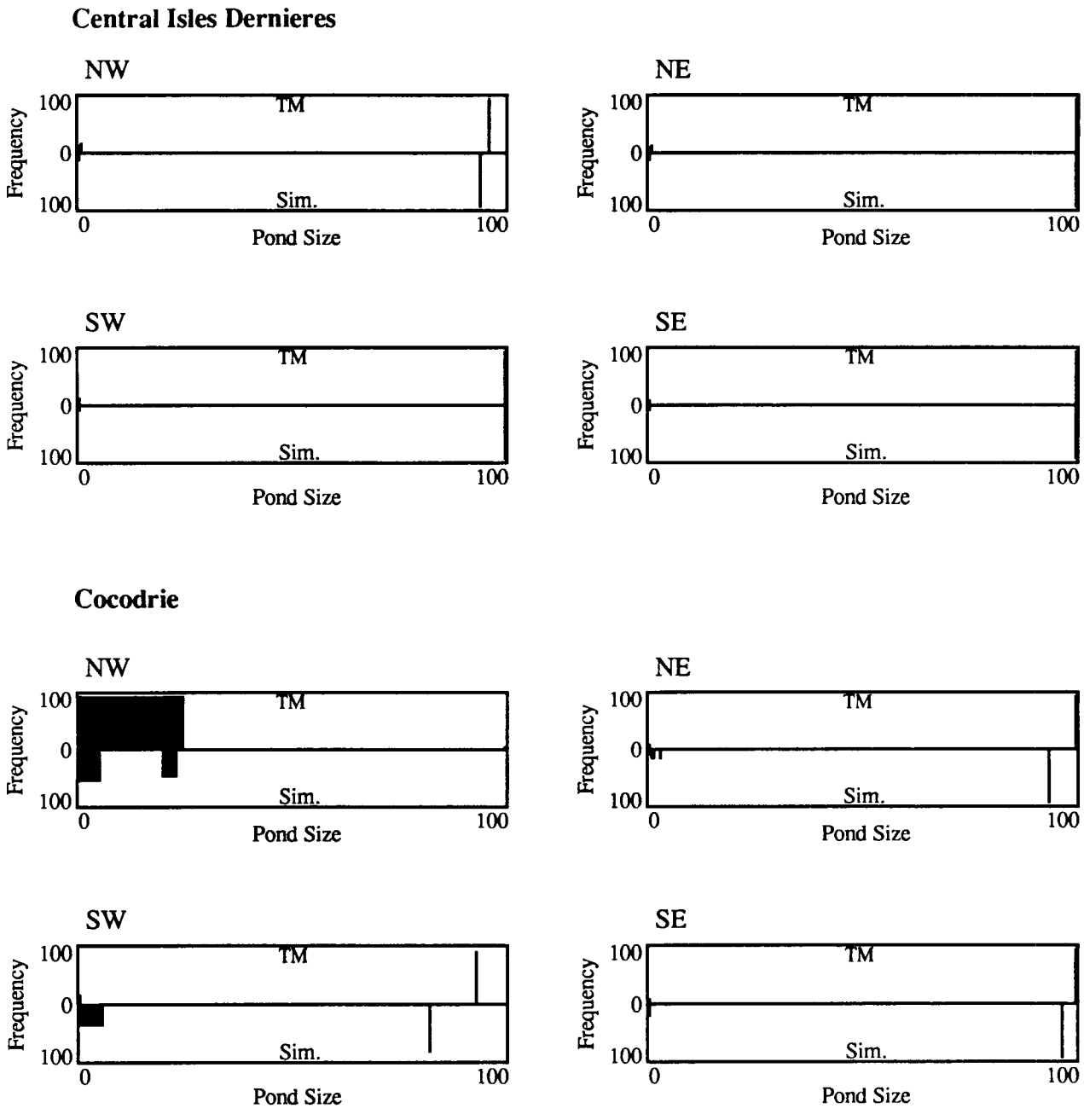

Figure E2-5. Pond size distributions for Central Isles Dernieres and Cocodrie quadrangles.

Early Lafourche, salt

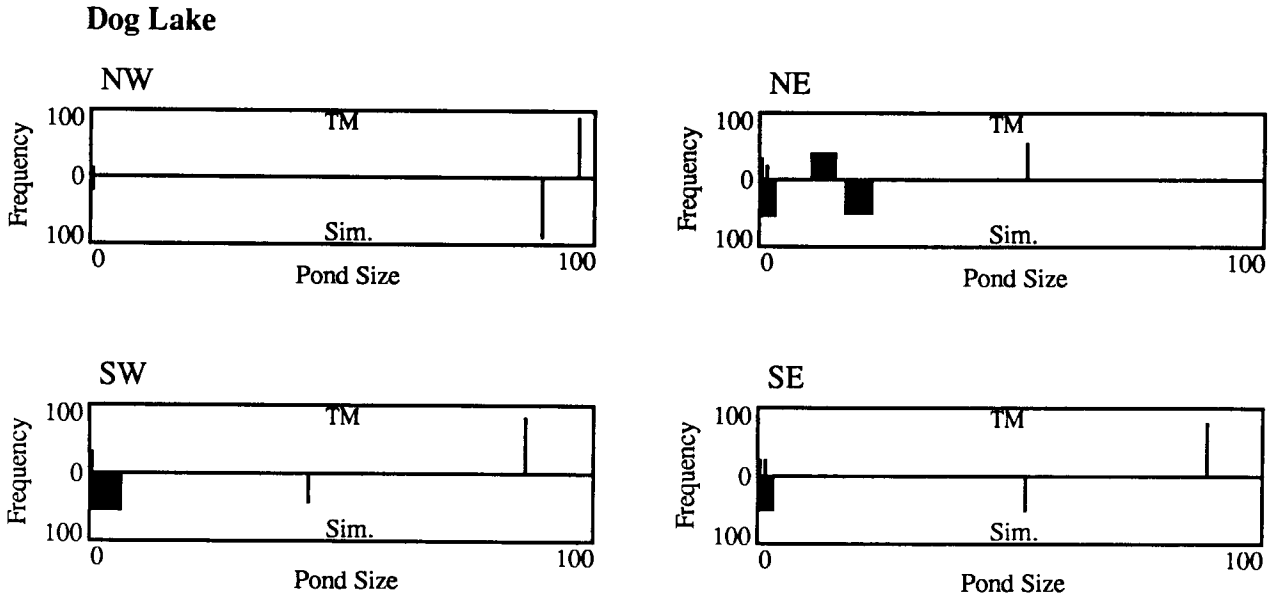

Figure E2-6. Pond size distributions for Dog Lake quadrangle.

Late Lafourche, brackish

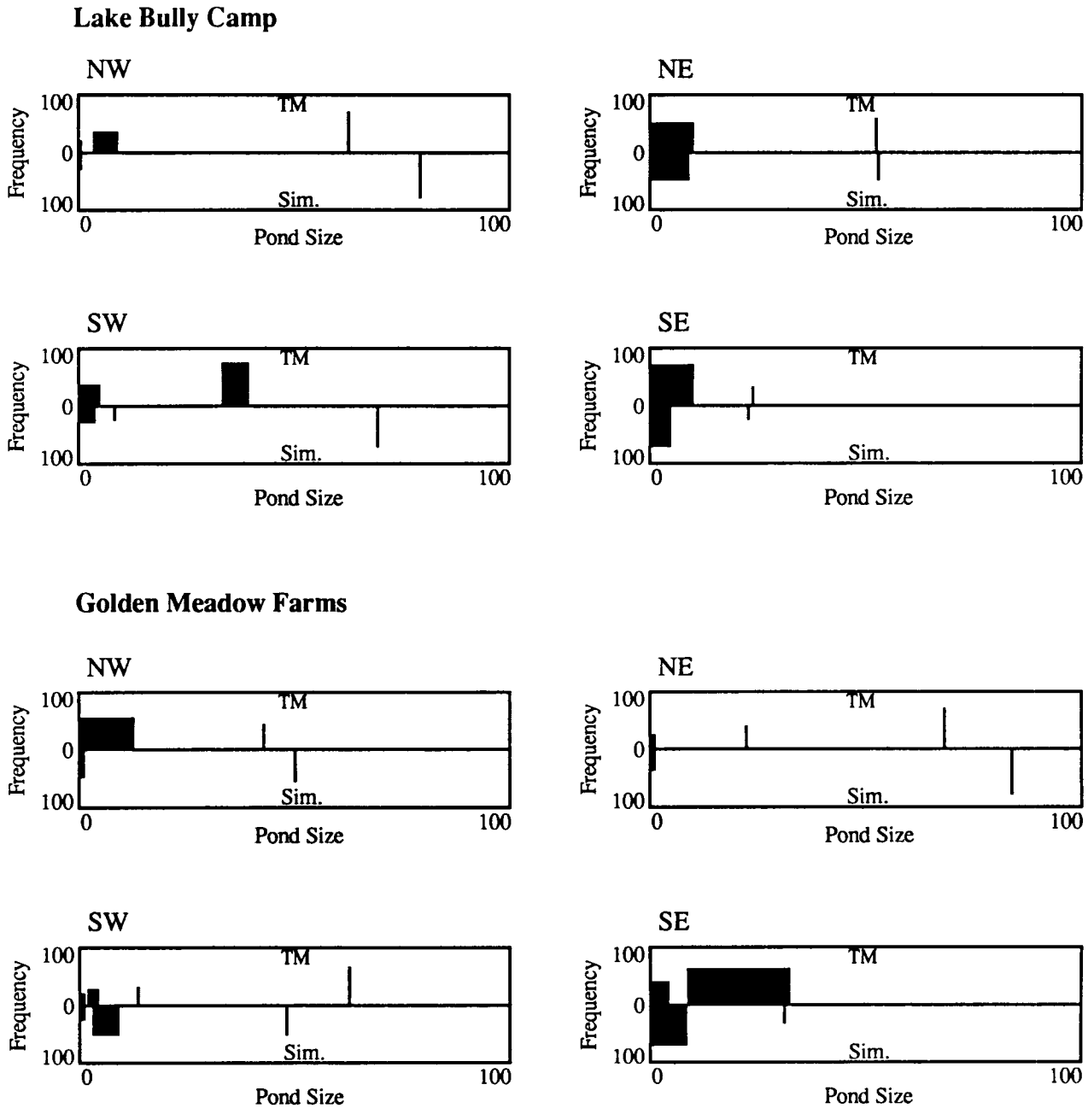

Figure E2-7. Pond size distributions for Lake Bully Camp and Golden Meadow Farms quadrangles.

Late Lafourche, brackish

Bay L'Ours

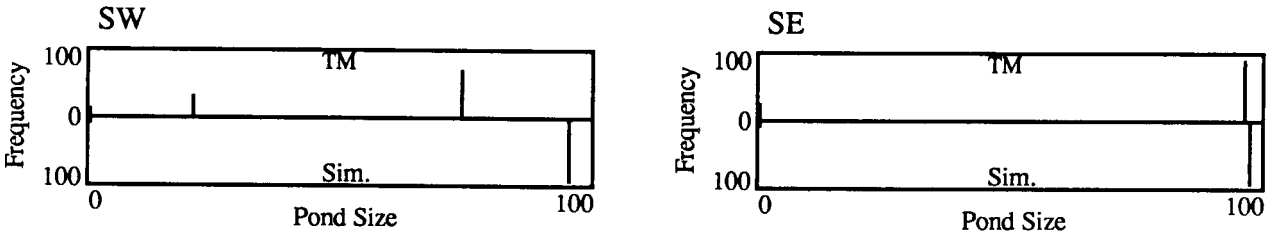

Three Bayou Bay

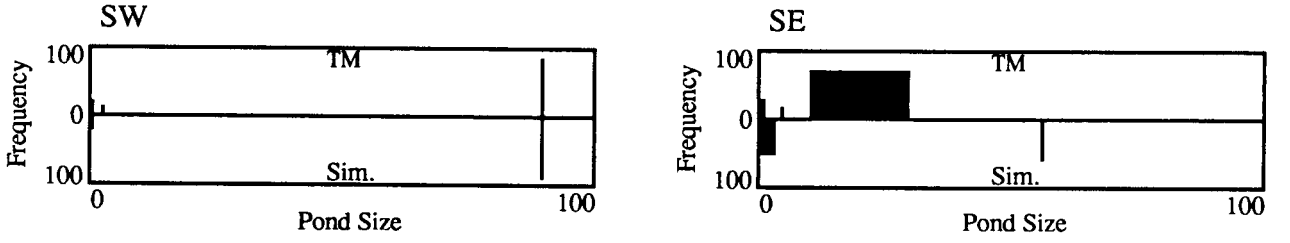

Golden Meadow

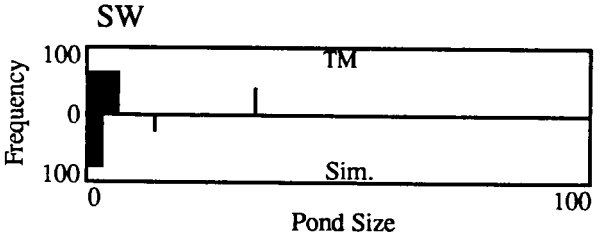

Figure E2-8. Pond size distributions for Bay L'Ours, Three Bayou Bay and Golden Meadow quadrangles.

Early Lafourche, brackish

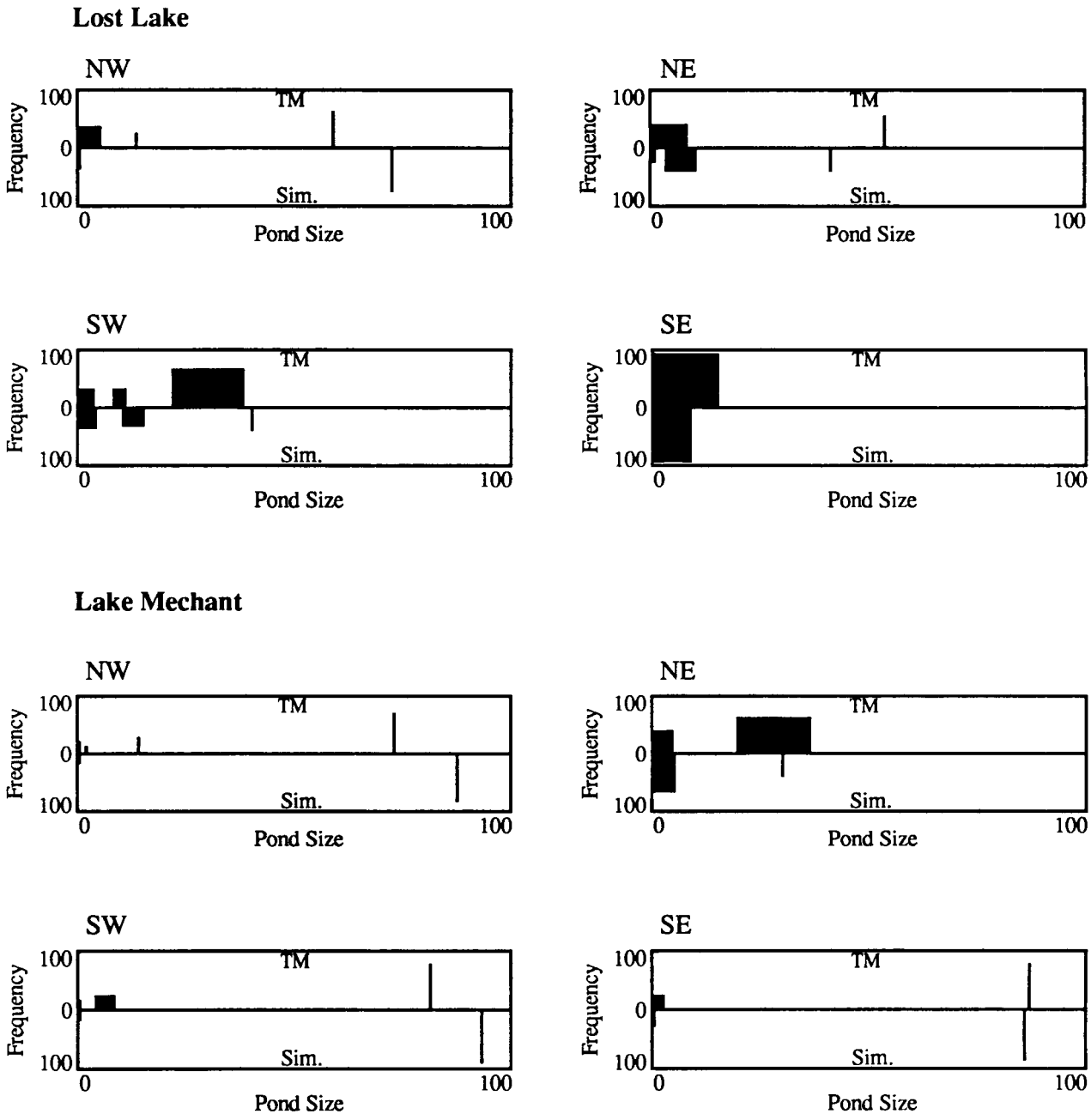

Figure E2-9. Pond size distributions for Lost Lake and Lake Mechant quadrangles.

Early Lafourche, brackish

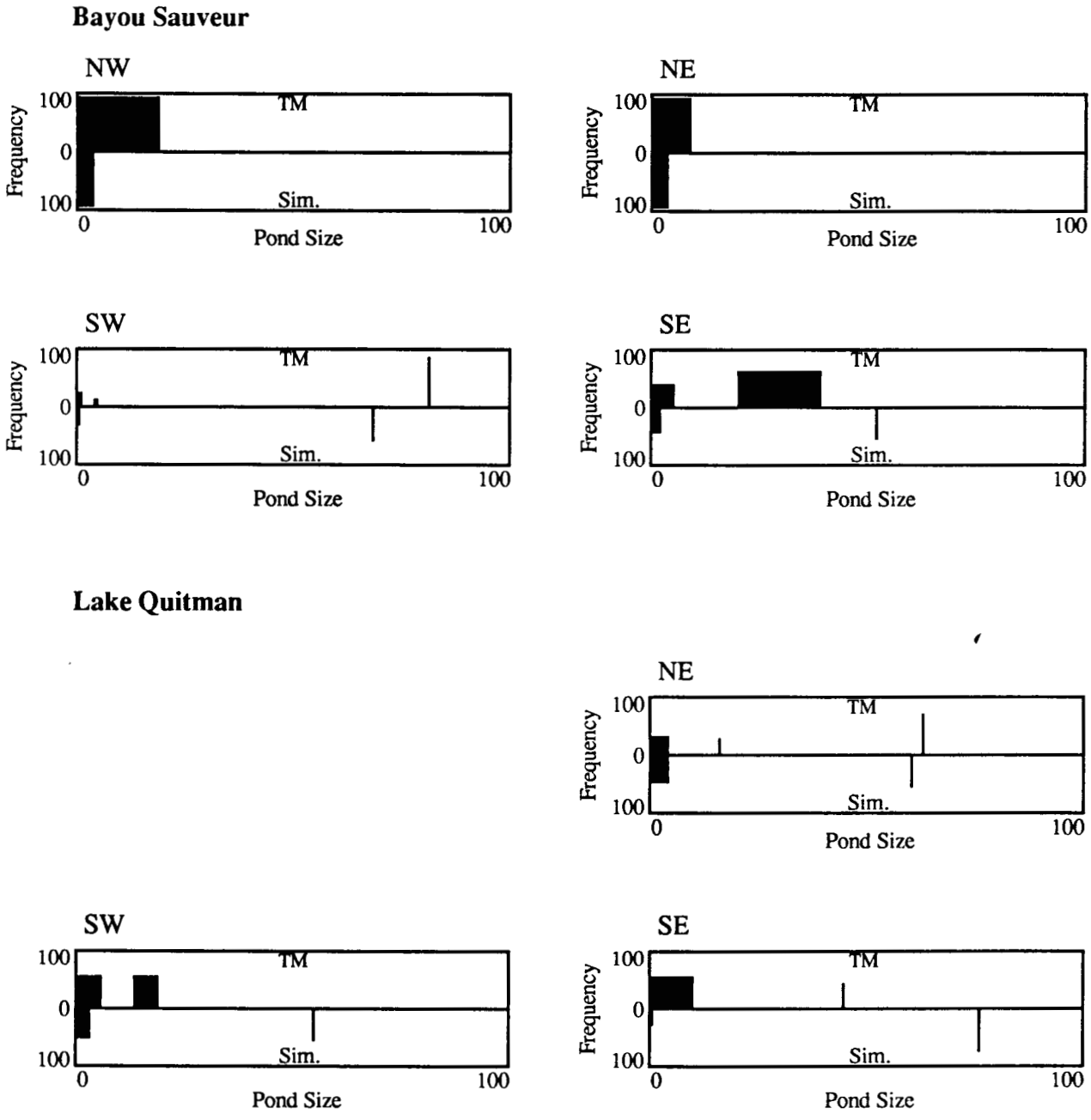

Figure E2-10. Pond size distributions for Bayou Sauveur and Lake Quitman quadrangles.

Early Lafourche, brackish

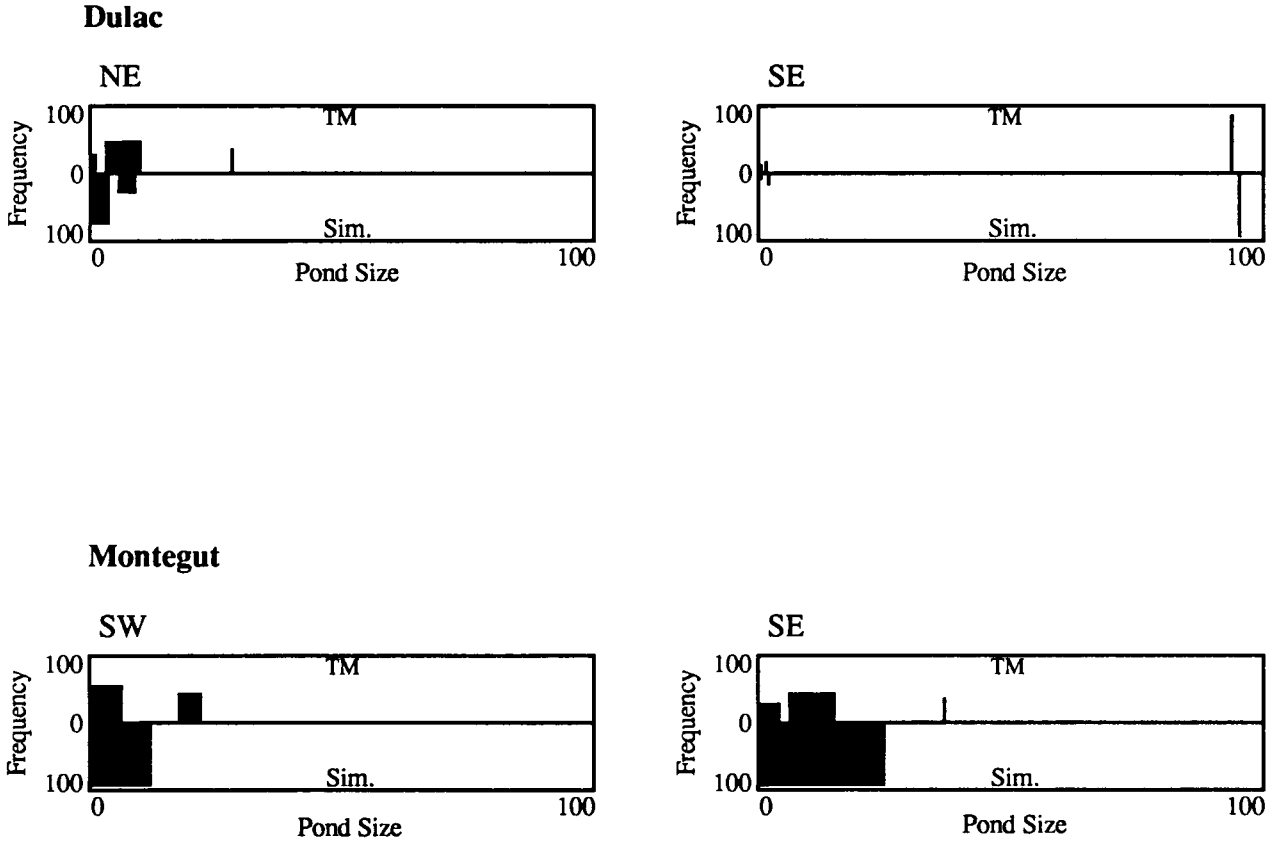

Figure E2-11. Pond size distributions for Dulac and Montegut quadrangles.

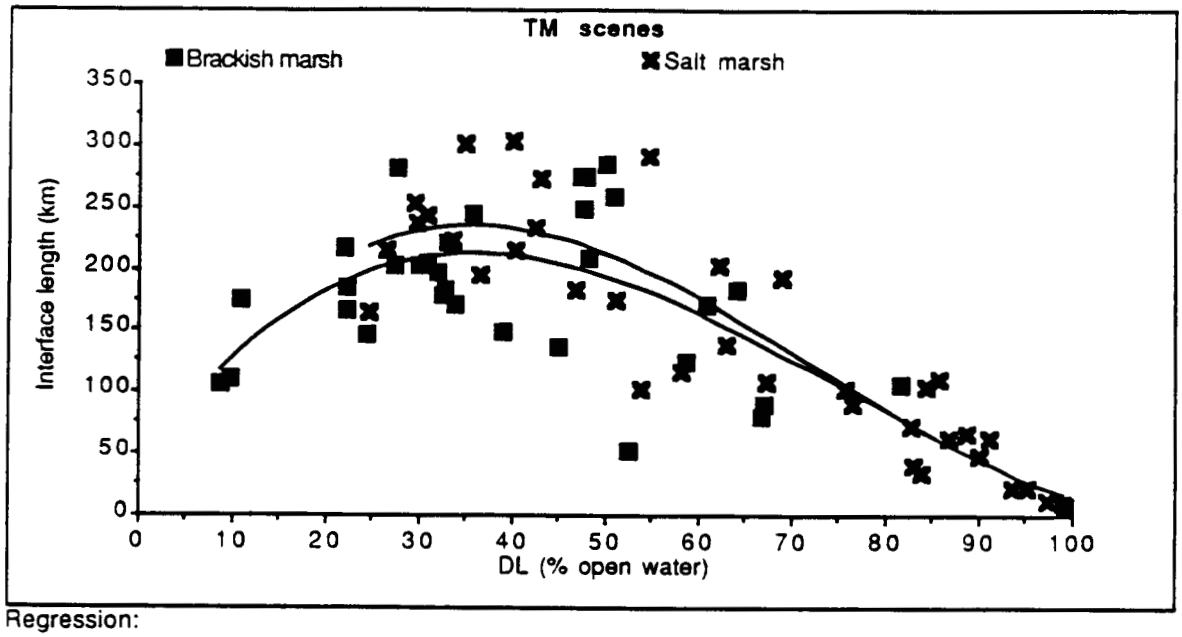

Regression:

TM scenes: Brackish $y = 34.92 + 11.1x - 0.205x^2 + 0.0009x^3$; $R^2 = 0.32$

Salt $y = 23.77 + 13.26x - 0.246x^2 + 0.001x^3$; $R^2 = 0.83$

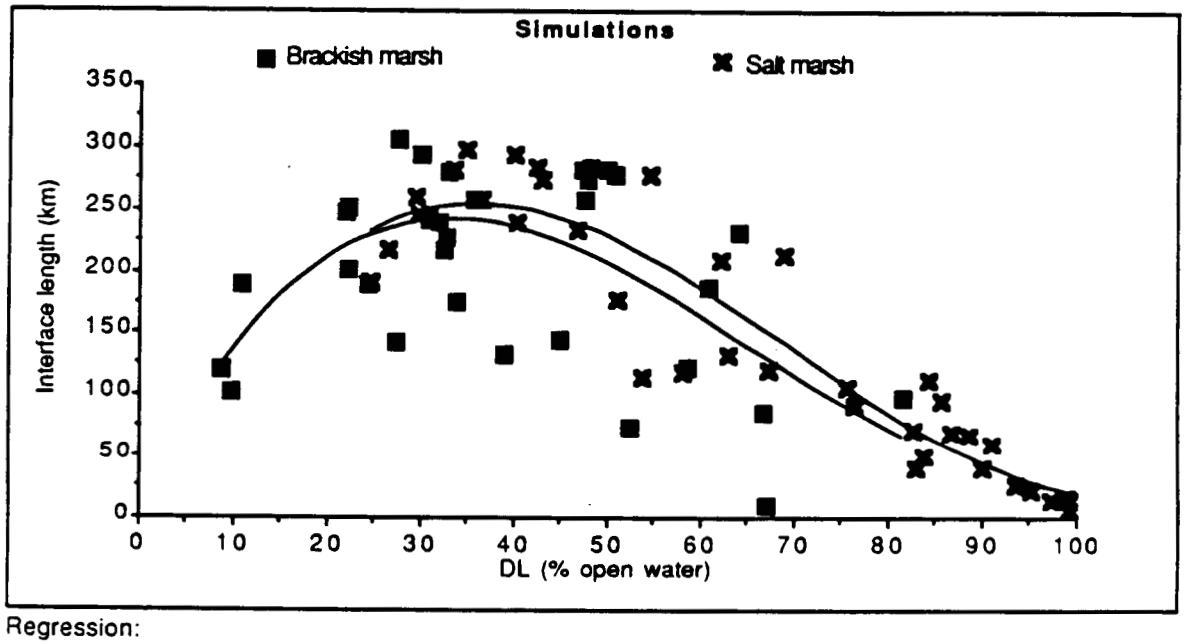

Regression:

Simulations: Brackish $y = 8.29 + 15.8x - 0.319x^2 + 0.0016x^3$; $R^2 = 0.37$

Salt $y = -11.2 + 16.67x - 0.311x^2 + 0.0015x^3$; $R^2 = 0.87$

Figure E3. Comparison of interface as a function of disintegration level for the 70 TM scenes and for simulation at the same disintegration levels.

Figure E4. TM imagery interface and side adjacency statistics (number of pixels) compared with simulations at the same disintegration level. The side adjacency statistic refers to the number of sides of a water pixel that border water and may equal 0-4.

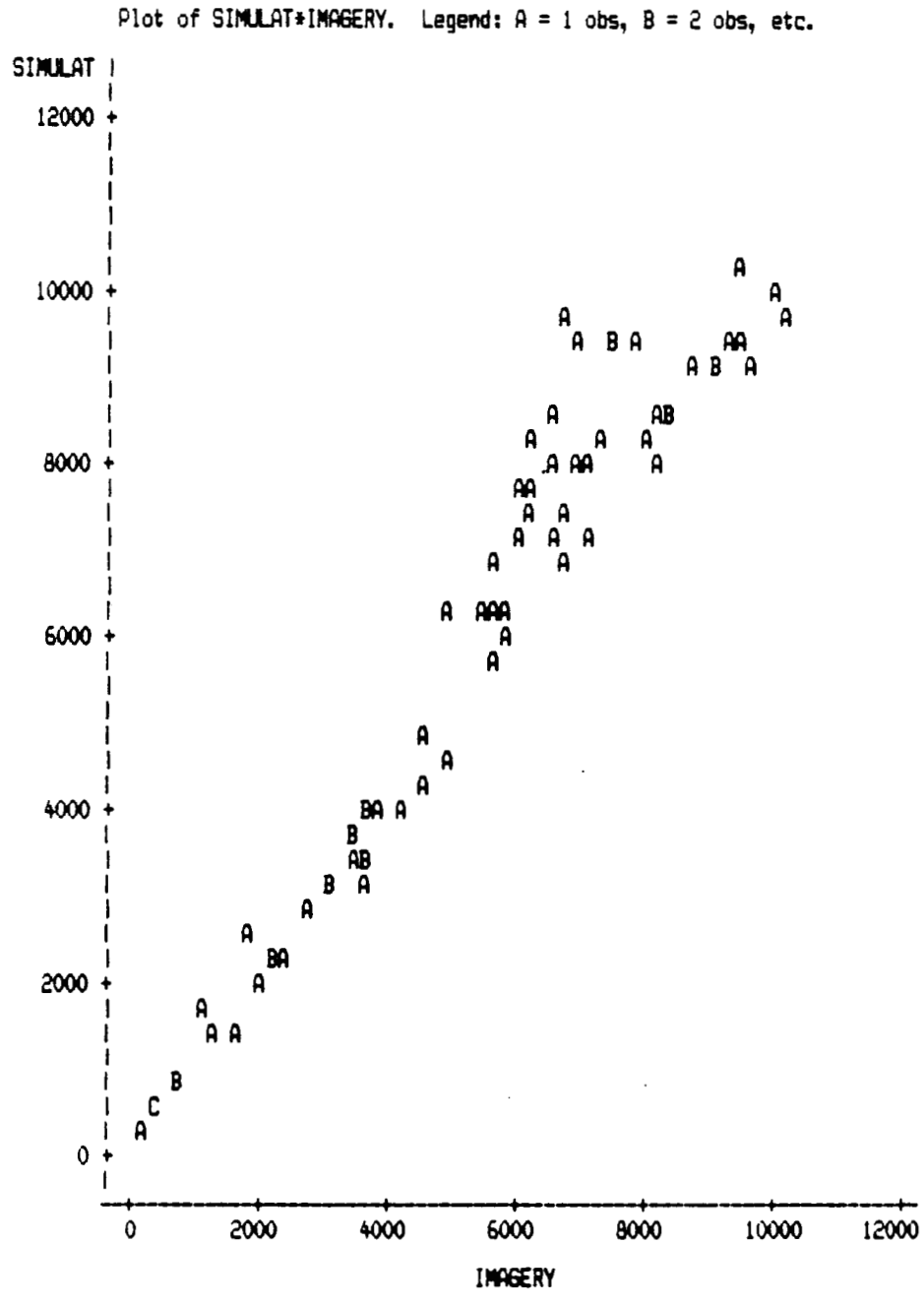

Figure E4-1. Total interface (number of pixels).

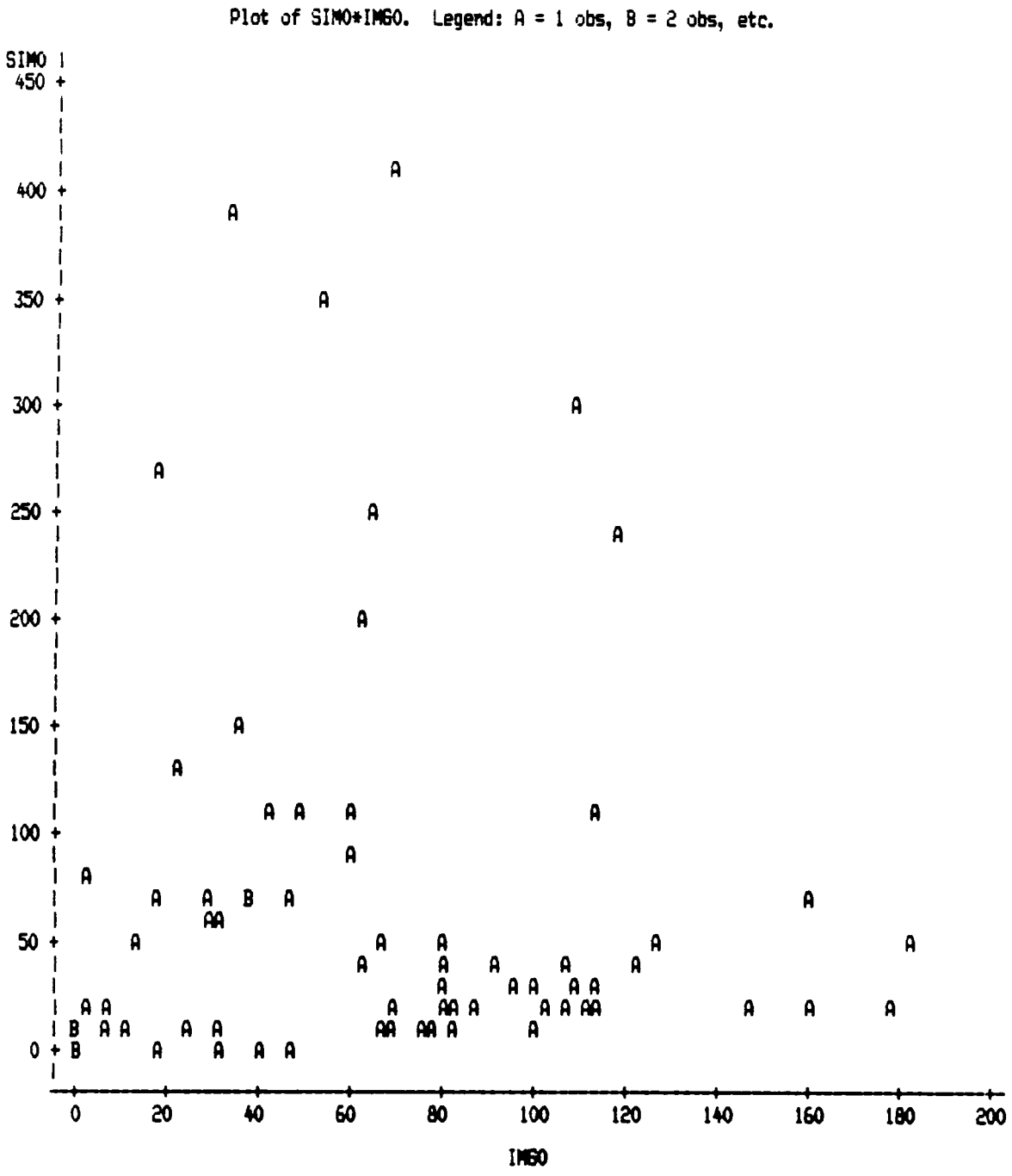

Figure E4-2. TM scenes (SIM0) versus simulations (IMG0) with side adjacency = 0.

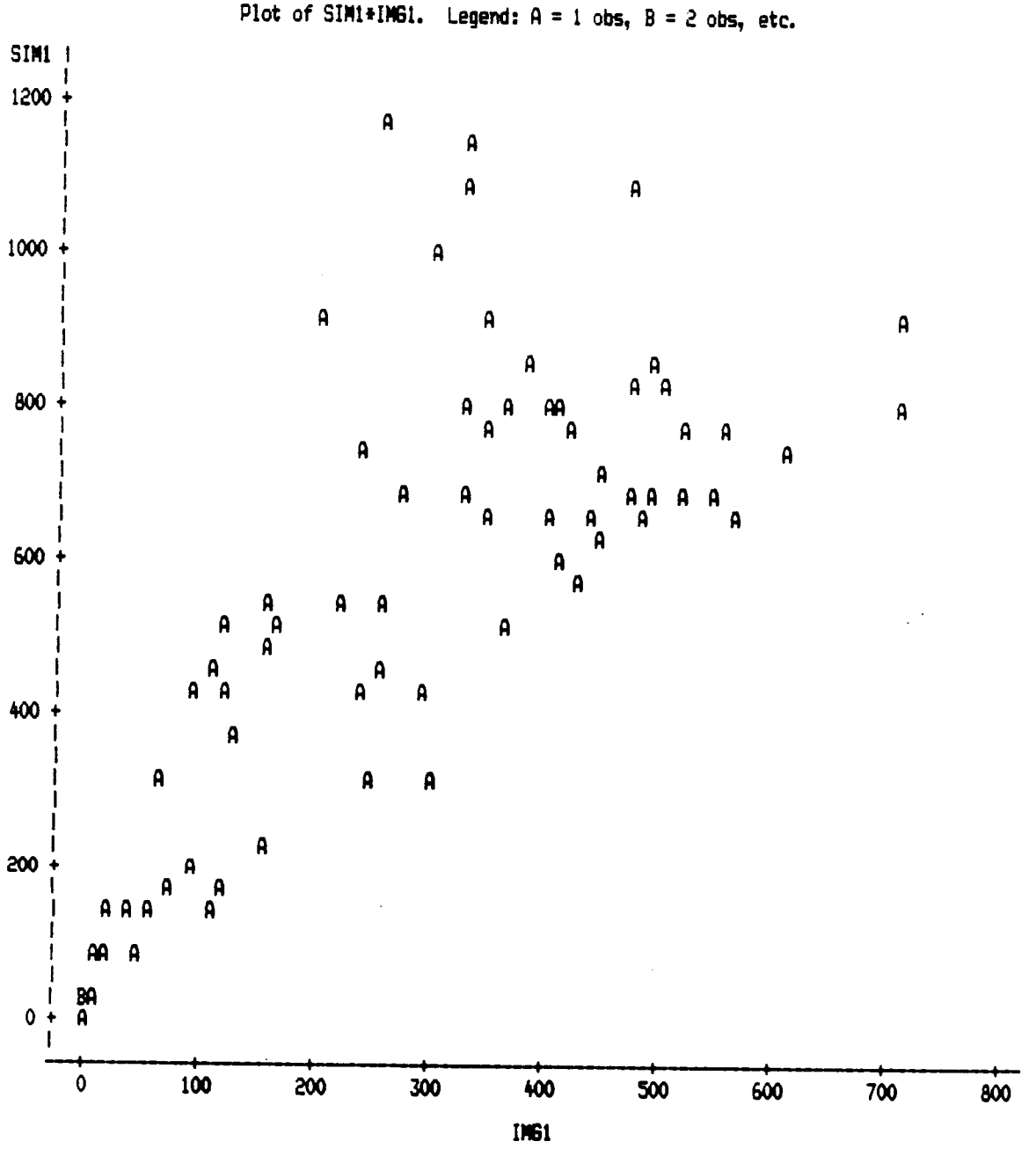

Figure E4-3. TM scenes (SIM1) versus simulations (IMG1) with side adjacency = 1.

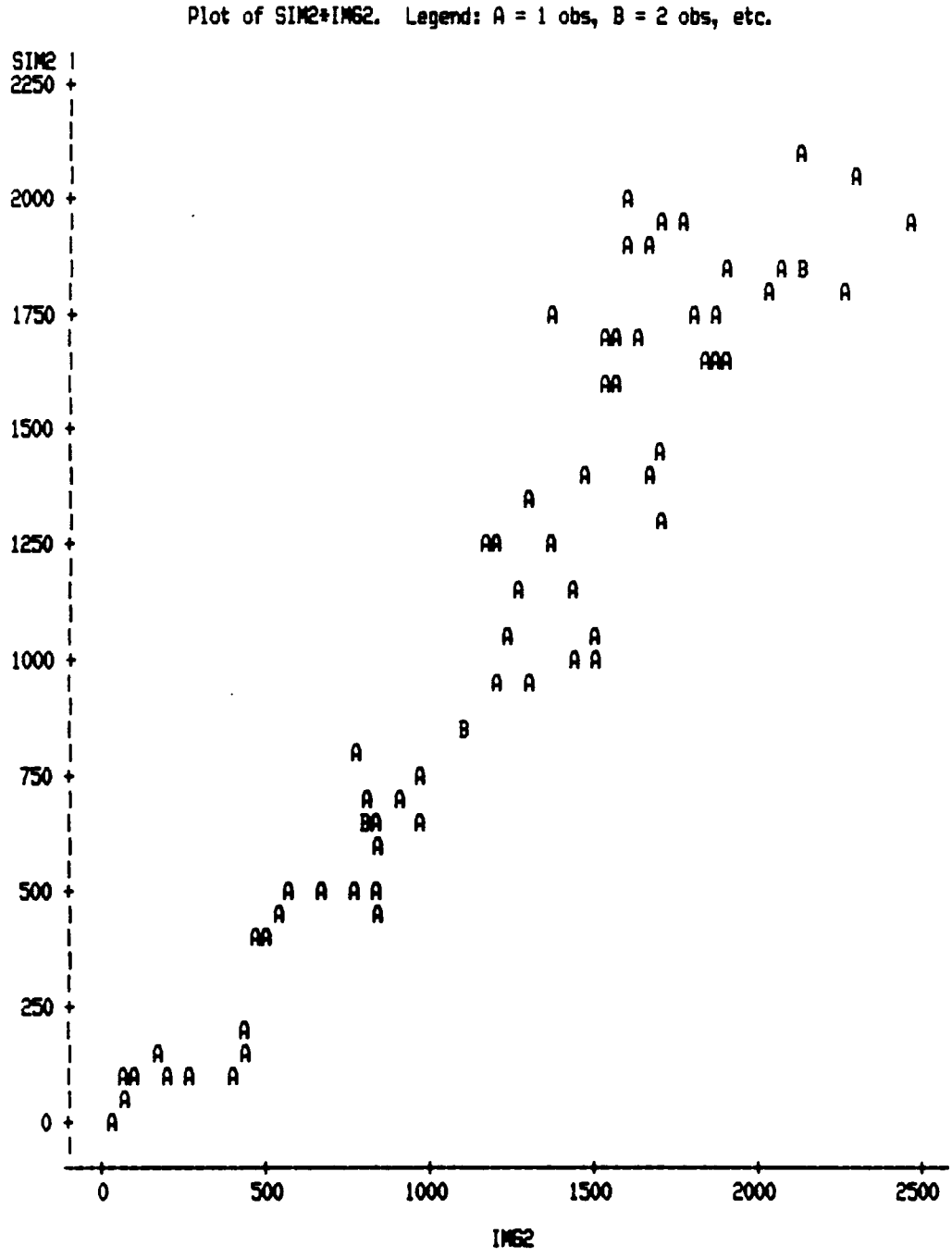

Figure E4-4. TM scenes (SIM2) versus simulations (IMG2) with side adjacency = 2.

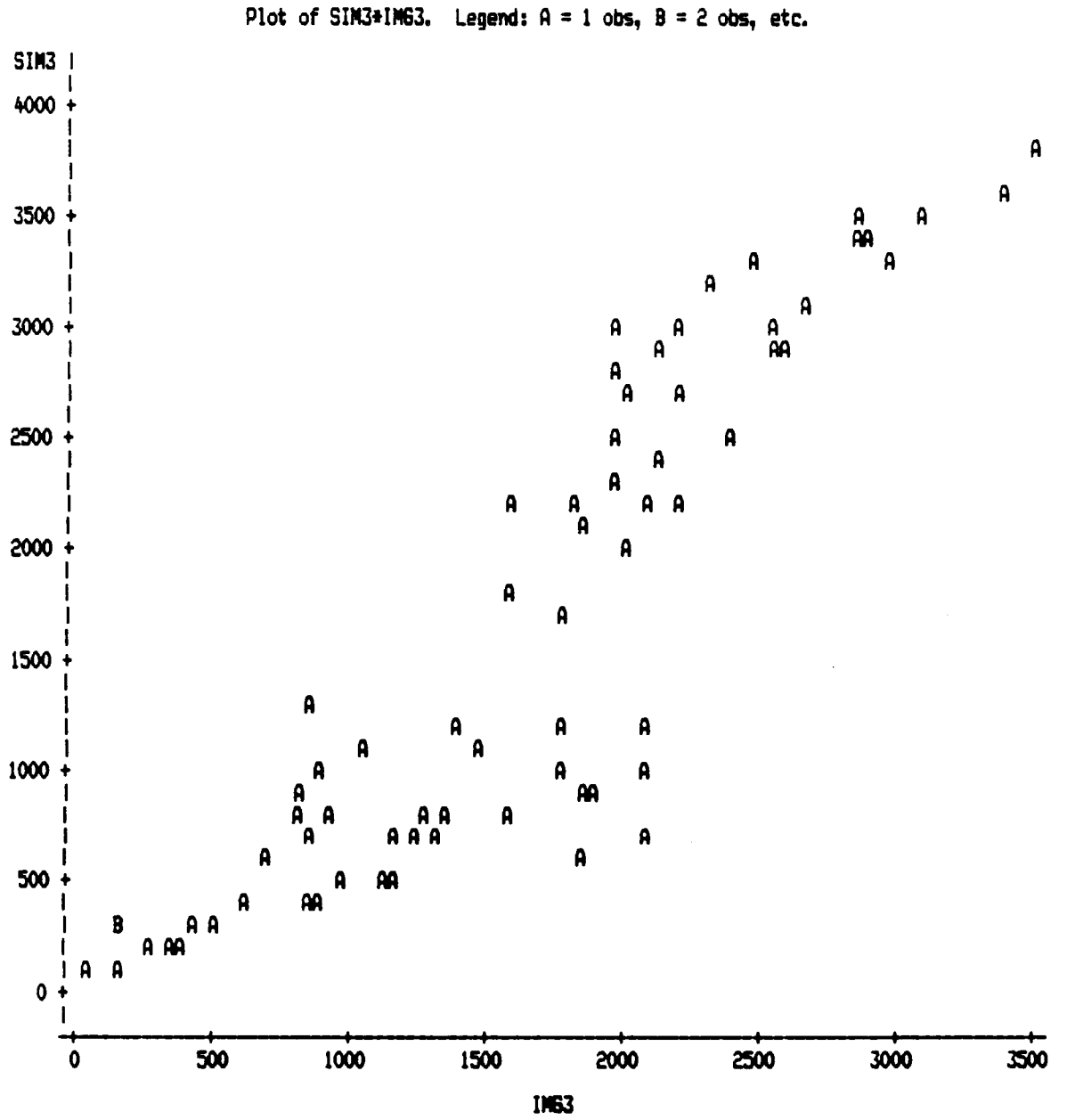

Figure E4-5. TM scenes (SIM3) versus simulations (IMG3) with side adjacency = 3.

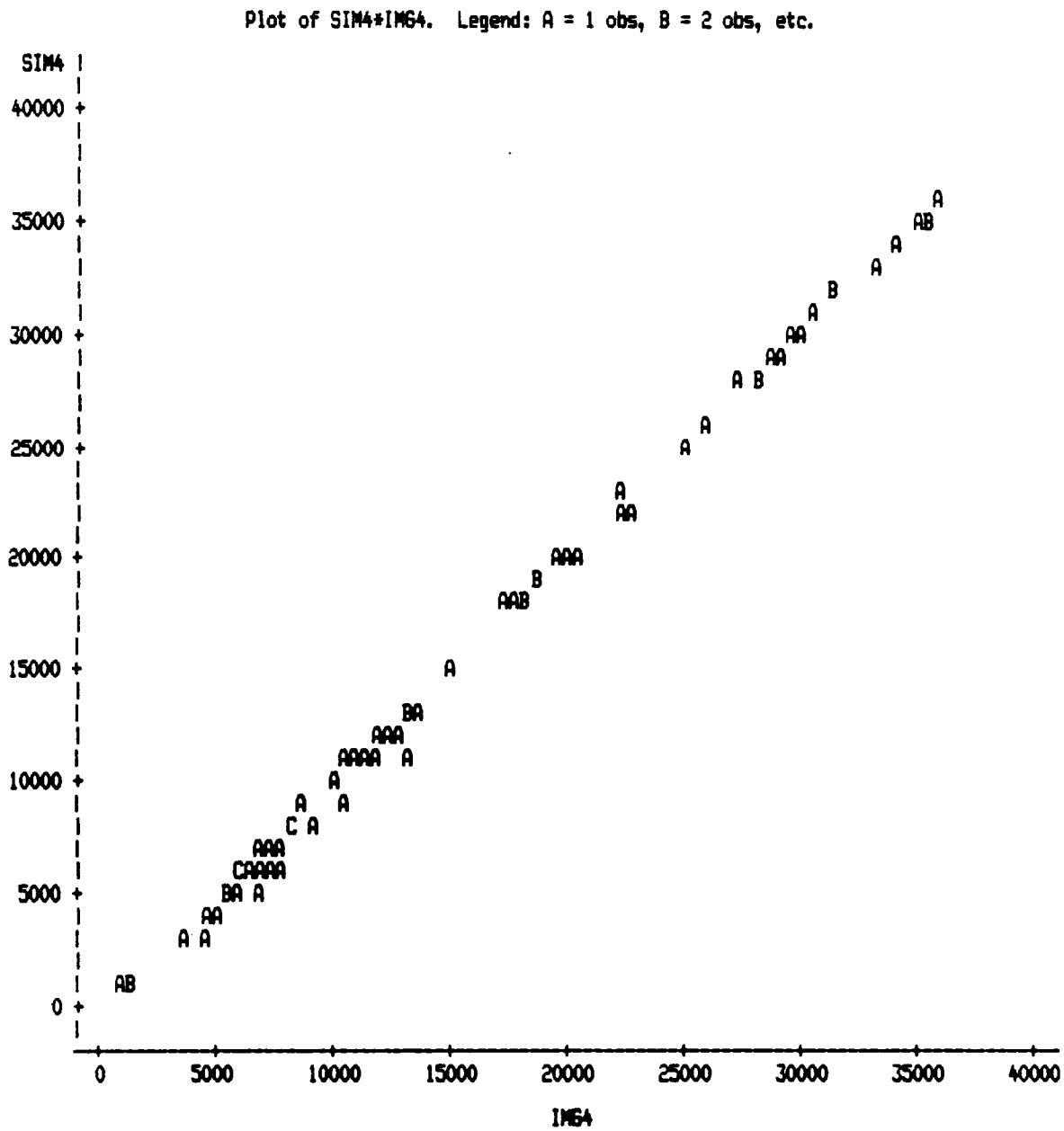

Figure E4-6. TM scenes (SIM4) versus simulations (IMG4) with side adjacency = 4.

Appendix F

Presimulation Predictions from the Knowledge Base

Table F1. Presimulation values of the spatial-pattern indices, predicted from the knowledge base.

Presimulation Predictions from the Knowledge Base

The expert system's estimate of the model parameters W, G, and BC to "best" simulate the disintegration of a specific marsh was derived from separate estimates based on each of the spatial-pattern indices. For instance, the W-estimate is a weighted mean of W's based on matching each of several spatial-pattern indices from the imagery to those in a knowledge base. The knowledge base consists of sets of look-up tables that relate spatial-pattern index values for a given DL to W, G, and BC. The best W-G-BC estimate was determined from the knowledge base in the manner described in Appendix A. Given a W-G-BC estimate, it was possible to work backward through the selection process (relating a given W, G, and BC to spatial-pattern index values) and use the expert system to "predict" the spatial pattern indices for a given DL that would result from a simulation of marsh disintegration using that particular W-G-BC estimate. The presimulation predictions of spatial-pattern indices for the 70 cases of our study are presented in Table F1. The significance of presimulation predictions of the spatial-pattern indices is that they can potentially be used to test and fine tune W-G-BC estimates produced by the expert system. Alternative decision algorithms could be tested for their relative ability to simulate the spatial-pattern indices of a given study site. A comparison of presimulation to simulation values of the spatial pattern indices is presented in Appendix G.

Table F-1. Pre-simulation values of the spatial pattern indices, predicted from the knowledge base: interface length, the side-adjacency statistics (number of water pixels with 0, 1, 2, 3, and 4 sides adjacent to other water pixels), and number of water pixels on the marsh border. Disintegration level (DL, water area as percentage total area) is also shown.

Quad	Quarter	DL	Interface Length	Adj-0	Adj-1	Adj-2	Adj-3	Adj-4	Border Pixels
Late Lafourche, salt									
Leeville	NW	42.94	9,436	19	699	1,903	3,387	9,329	486
	NE	34.93	10,044	21	818	2,036	3,334	6,497	162
	SE	39.91	10,162	10	772	2,083	3,523	8,103	215
	SW	46.74	7,266	451	981	870	723	13,725	473
Mink Bayou	NW	26.59	7,284	25	664	1,496	2,158	5,014	439
	NE	24.54	6,093	251	862	881	696	5,918	431
	SE	29.44	8,971	25	758	1,824	2,860	5,243	134
	SW	29.57	7,993	26	665	1,640	2,544	5,732	287
Caminada Pass	NW	62.09	6,597	46	573	1,347	1,967	18,304	645
	NE	82.87	1,398	71	140	179	318	29,130	703
	SE	99.27	95	9	7	6	12	35,802	750
	SW	58.02	3,734	126	513	561	539	19,125	516
Bay Tambour	NW	51.18	5,780	134	735	980	1,057	15,320	634
	NE	76.55	3,025	92	393	488	472	26,202	566
	SE	88.72	2,020	8	167	377	715	30,720	713
	SW	84.38	3,417	93	364	585	762	28,587	708
Pelican Pass	NW	98.96	336	7	32	56	91	35,535	757
	NE	82.60	2,331	17	224	444	684	28,377	694
	SE	86.68	2,131	53	239	385	395	30,266	611
	SW	97.24	359	4	33	64	107	34,871	764

Table F-1. (cont. 2)

Quad	Quarter	DL	Interface Length	Adj-0	Adj-1	Adj-2	Adj-3	Adj-4	Border Pixels
Early Lafourche, salt									
Grand Bayou du Large	NW	53.83	3,700	136	503	536	546	17,613	506
	NE	67.26	3,720	96	471	641	610	22,425	544
	SE	40.44	7,649	366	971	1,131	956	11,014	464
	SW	83.72	1,645	251	88	82	180	29,643	614
Lake La Graisse	NW	91.13	1,822	6	140	340	683	31,700	721
	NE	99.28	246	4	21	41	73	35,694	759
Central Isles Dernieres	NW	75.77	3,634	81	405	641	803	25,232	764
	NE	90.05	1,458	16	136	278	416	31,631	715
	SE	95.18	722	14	54	125	241	33,910	738
	SW	93.53	711	15	64	122	205	33,304	764
Cocodrie	NW	33.43	9,213	50	868	1,883	2,592	6,458	467
	NE	68.89	7,268	11	428	1,405	3,058	20,049	441
	SE	85.79	3,634	10	275	716	1,288	28,695	634
	SW	54.72	9,752	9	659	1,917	3,831	13,222	527
Dog Lake	NW	62.97	4,440	80	510	822	904	20,357	535
	NE	30.74	8,035	21	710	1,650	2,482	6,018	444
	SE	42.38	8,883	40	800	1,795	2,677	9,831	475
	SW	36.40	8,141	50	756	1,666	2,272	8,357	311

Table F-1. (cont. 3)

Quad	Quarter	DL	Interface Length	Adj-0	Adj-1	Adj-2	Adj-3	Adj-4	Border Pixels
Late Lafourche, brackish									
Lake Bully	NW	33.69	5,920	75	687	1,138	1,267	8,635	611
Camp	NE	47.84	9,490	18	689	1,906	3,467	11,211	338
	SE	22.21	8,629	50	879	1,751	2,212	2,866	423
	SW	50.02	9,251	11	639	1,877	3,509	11,644	754
Golden Meadow	NW	30.91	7,669	56	738	1,561	2,062	6,529	443
Farms	NE	60.69	5,941	26	482	1,226	1,896	18,220	518
	SE	35.56	8,738	16	702	1,755	2,983	7,188	457
	SW	38.95	4,954	47	243	1,085	1,775	11,049	159
Bay L'Ours	SE	81.53	3,333	149	389	477	585	27,750	698
	SW	52.26	2,487	372	133	146	284	17,830	495
Three Bayou	SE	32.93	9,731	48	926	1,958	2,811	5,636	753
Bay	SW	58.71	3,956	114	519	635	641	19,208	519
Golden Meadow	SW	27.66	10,811	49	1,030	2,193	3,021	3,760	137

Table F-1. (cont. 4)

Quad	Quarter	DL	Interface Length	Adj-0	Adj-1	Adj-2	Adj-3	Adj-4	Border Pixels
Early Lafourche, brackish									
Lost Lake	NW	32.65	7,306	231	979	1,213	960	8,193	453
	NE	47.32	9,472	18	692	1,905	3,444	11,043	336
	SE	21.81	8,197	65	850	1,630	2,050	2,855	583
	SW	50.78	10,093	16	706	1,980	3,850	11,606	560
Lake Mechant	NW	64.05	7,113	378	1,011	943	612	20,137	528
	NE	29.91	10,207	48	977	2,060	2,889	4,593	451
	SE	44.91	4,697	58	516	902	1,058	13,533	482
	SW	67.06	3,162	141	426	454	381	22,773	541
Bayou Sauveur	NW	8.72	4,127	30	460	837	921	930	32
	NE	10.90	6,546	108	805	1,257	1,109	680	52
	SE	22.23	6,391	56	680	1,261	1,567	4,198	425
	SW	24.31	6,090	184	852	977	791	5,878	273
Lake Quitman	NE	48.20	8,855	48	739	1,792	2,791	12,025	367
	SE	32.41	7,223	245	987	1,172	884	8,203	453
	SW	31.85	7,783	57	760	1,577	2,074	6,821	446
Dulac	NE	9.63	3,568	14	344	742	967	1,438	40
	SE	66.80							
Montegut	SE	47.48	8,932	14	662	1,800	3,239	11,299	482
	SW	27.16	7,658	16	654	1,543	2,473	5,200	120

Note: No presimulation prediction could be made for Dulac SE, because the model parameters for to simulate this site were determined by extrapolation rather than by interpolation from look-up tables in the knowledge base.

Appendix G

Comparison of Presimulation Predictions to Simulation Values

Table G1. Percentage deviation of simulation values from presimulation-predicted values of the spatial-pattern indices.

Table G2. (A) Mean percentage deviation and (B) mean absolute percentage deviation of simulation from image values and pre-simulation prediction from simulation values of spatial-pattern indices.

Comparison of Presimulation Predictions to Simulation Values

Given the random aspect of the model, we could not expect perfect correspondence of presimulation-predicted and simulation values of the spatial pattern indices. No two simulations were alike, even when the same W-G-BC values were used. Table G1 shows the percentage deviation of simulation values from presimulation predictions (both at the same DL, which was the DL of the study site in the imagery). Average values are given at the bottom of the table. The largest average percentage deviation is in Adj-0, which we know to be the most variable index from one simulation to another.

Average percentage deviations are summarized in Table G2, which also gives average absolute percentage deviations, which provide a slightly different picture. Since deviations can be in either the positive or the negative direction, they tend to cancel each other out in averaging procedures. This is why average percentage absolute deviations are also shown.

In addition to comparisons of simulation to presimulation-predicted values, comparisons of simulation to image values are also given in Table G2. Note that percentage absolute deviations of simulation from image values are notsubstantially higher--and, in fact, are in some cases lower--than deviations of simulation from presimulation-predicted values.

Table G1. Percentage deviation of simulation values from presimulation-predicted values of the spatial-pattern indices.

Quad	Quarter	Interface Length	Percentage Deviation[a] Adj-0	Adj-1	Adj-2	Adj-3	Adj-4	Pixels
Late Lafourche, salt								
Leeville	NW	-3,21	10.53	-4.86	-2.63	-2.72	2.38	-8.85
	NE	-1.09	-19.05	-1.96	0.59	-1.65	0.57	20.37
	SE	-3.45	60.00	-1.55	-6.53	-2.36	2.42	16.74
	SW	7.07	-21.73	19.67	17.93	-0.28	-1.93	5.07
Mink Bayou	NW	-0.59	8.00	-0.90	-2.74	2.78	-0.20	0.00
	NE	4.37	-5.58	4.87	9.99	4.89	-2.37	-1.16
	SE	-3.23	-28.00	-2.77	-4.44	-0.52	2.94	-17.91
	SW	2.13	-30.77	4.96	-0.31	5.27	-2.58	0.70
Caminada Pass	NW	5.94	-28.26	16.40	3.64	3.76	-1.26	5.27
	NE	-5.37	7.04	-6.43	-5.59	-11.95	0.20	0.28
	SE	100.00	33.33	57.14	250.00	341.67	-0.11	-2.27
	SW	5.68	-15.87	4.87	16.40	7.98	-0.62	-2.52
Bay Tambour	NW	1.80	-17.16	1.63	3.37	9.08	-0.77	0.95
	NE	1.06	-10.57	10.18	-2.05	-0.21	-0.04	0.71
	SE	11.63	-12.50	-1.80	19.63	16.22	-0.58	-0.28
	SW	10.45	-24.73	23.08	14.36	4.46	-0.61	0.00
Pelican Pass	NW	58.93	-85.71	6.25	46.43	186.31	-0.50	-1.19
	NE	2.75	-35.29	-8.04	8.56	11.55	-0.33	1.30
	SE	10.61	-15.09	26.36	8.57	4.05	-0.35	1.15
	SW	23.12	75.00	21.21	25.00	25.23	-0.14	0.00
Early Lafourche, salt								
Grand Bayou du Large	NW	2.62	-16.18	1.39	15.30	-0.73	-0.36	0.79
	NE	8.82	-23.96	13.38	9.36	19.02	-0.93	-0.55
	SE	4.30	-18.58	10.92	12.91	-1.99	-1.53	1.51
	SW	2.01	5.98	-5.68	8.54	-12.22	0.01	0.81
Lake La Graisse	NW	11.91	-66.67	5.71	21.47	9.52	-0.43	-0.28
	NE	100.00	-75.00	4.76	39.02	313.70	-0.66	-0.40
Central Isles Dernieres	NW	-2.37	-28.40	-5.68	4.37	3.61	-0.02	0.00
	NE	-9.81	18.75	5.15	-19.42	-13.46	0.29	1.68
	SE	-0.42	-21.43	35.19	-4.00	-12.86	0.07	0.14
	SW	18.43	13.33	15.63	33.61	10.24	-0.20	0.00
Cocodrie	NW	1.76	-20.00	-2.53	3.51	5.75	-2.65	-1.28
	NE	-2.09	-63.64	1.64	-0.57	-4.15	0.72	-1.13
	SE	-10.84	0.00	-16.73	-7.96	-9.55	0.94	-5.84
	SW	-4.85	-22.22	-9.10	-4.96	-1.91	2.03	-6.45
Dog Lake	NW	-0.97	-28.75	-5.88	5.72	5.53	-0.18	-0.56
	NE	1.17	19.05	0.00	0.79	2.42	-1.35	2.03
	SE	6.20	-35.00	-0.25	7.63	13.04	-4.58	-3.37
	SW	5.88	-10.00	6.22	2.76	12.02	-4.39	3.22

Table G1. (cont.)

Quad	Quarter	Interface Length	Percentage Deviation[a] Adj-0	Adj-1	Adj-2	Adj-3	Adj-4	Pixels
Late Lafourche, brackish								
Lake Bully	NW	-1.50	-5.33	-1.31	-1.05	-1.66	0.52	0.98
Camp	NE	-4.12	-50.00	-3.92	-5.56	-1.88	1.73	5.62
	SE	-3.23	-12.00	-8.42	-1.09	0.54	2.97	1.89
	SW	1.59	18.18	5.79	-1.71	2.88	-0.92	0.53
Golden Meadow	NW	4.97	-26.79	3.12	8.33	6.01	-3.80	-1.81
Farms	NE	5.02	-23.08	6.22	2.61	9.28	-1.25	0.19
	SE	-1.96	18.75	-2.71	-0.23	-3.72	1.84	1.09
	SW	-10.58	-93.62	31.28	-21.38	-2.48	2.81	-42.14
Bay L'Ours	SE	-0.75	-28.19	13.88	8.39	-14.02	0.14	-0.57
	SW	-0.21	3.76	3.76	-15.75	-5.28	0.12	0.00
Three Bayou	SE	-4.39	-29.17	-10.26	-3.63	2.70	1.90	0.66
Bay	SW	3.84	-25.44	2.70	17.95	3.59	-0.51	-3.47
Golden Meadow	SW	-5.77	-8.16	-11.75	-5.24	0.27	6.54	-5.84
Early Lafourche, brackish								
Lost Lake	NW	3.62	-13.85	11.13	1.15	5.00	-1.64	0.00
	NE	-0.90	-11.11	-2.89	-2.21	1.97	-0.08	3.27
	SE	0.61	-16.92	-3.41	2.88	4.98	-3.61	0.17
	SW	-8.32	-37.50	-12.18	-6.41	-7.92	4.58	-0.89
Lake Mechant	NW	8.21	8.99	12.46	3.50	-2.94	-0.98	4.92
	NE	-4.02	-18.75	-12.28	-3.01	3.95	1.52	2.88
	SE	3.13	15.52	1.94	4.88	2.93	-0.52	-3.53
	SW	1.93	-4.97	3.29	4.41	3.41	-0.08	-3.14
Bayou Sauveur	NW	-3.15	-20.00	-6.52	-2.03	2.28	3.12	28.13
	NE	-3.51	-36.11	-3.60	-1.03	2.71	5.00	46.15
	SE	5.41	-19.64	-0.29	5.47	16.98	-7.46	-0.71
	SW	3.76	-19.57	5.99	9.21	4.80	-2.52	3.66
Lake Quitman	NE	6.92	-50.00	4.60	4.91	14.94	-4.57	11.17
	SE	0.53	2.86	0.20	-0.43	1.47	-0.22	0.66
	SW	2.81	-36.84	4.87	0.00	10.08	-3.27	0.67
Dulac	NE	-3.45	-28.57	-9.59	-4.58	5.89	1.53	-7.50
	SE							
Montegut	SE	-4.27	35.71	1.21	-7.00	-4.69	2.47	-1.87
	SW	-2.86	-12.50	-11.62	2.20	-2.26	1.98	2.50
Mean		5.07	-15.40	3.39	7.56	14.52	-0.14	0.76

Table G2. (A) Mean percentage deviation and (B) mean absolute percentage deviation of simulation from image values and presimulation predictions from simulation values of spatial-pattern indices.

A. Percentage deviation

Spatial Pattern Index	Mean Simulation from Image	Mean Pre-sim-pred from Simulation	Stand. Dev. Simulation from Image	Stand. Dev. Pre-sim-pred from Simulation
Interface	12.28	18.80	5.07	18.91
Adj-0	105.15	393.28	-15.40	28.62
Adj-1	172.34	191.04	3.39	12.21
Adj-2	-14.28	19.28	7.56	31.80
Adj-3	-3.50	39.44	14.52	59.38
Adj-4	-4.44	8.67	-0.14	2.32
Border water pix	29.10	44.09	0.76	9.62

B. Percentage absolute deviation

Spatial Pattern Index	Mean Simulation from Image	Mean Pre-sim-pred from Simulation	Stand. Dev. Simulation from Image	Stand. Dev. Pre-sim-pred from Simulation
Interface	14.54	8.29	17.08	17.72
Adj-0	189.14	25.68	359.97	19.76
Adj-1	172.34	8.46	191.04	9.38
Adj-2	19.21	11.72	14.30	30.50
Adj-3	32.43	18.10	22.37	58.38
Adj-4	5.59	1.63	7.96	1.64
Border water pix	38.13	4.40	36.44	8.58

Appendix H

Levels of Disintegration by USGS Topographic Map in 1956 and 1978 Data Compiled by Leibowitz (LSU) from Maps by Wicker (1980) with Annual Trend

Table H1. Levels of disintegration in 1956 and 1978 for the areas covered by each U.S. Geological Survey topographic map corresponding to our study sites, and annual trend in DL.

Table H1. Levels of disintegration (DL, water area as percentage total area of site) in 1956 and 1978 for the areas covered by each U.S. Geological Survey topographic map corresponding to our study sites[a], and annual trend in DL.

Quadrangle	Year 1956	1978	Annual Trend
Late Lafourche, salt			
Leeville	20.348	34.866	-0.659
Mink Bayou	16.195	32.606	-0.745
Caminada Pass	74.764	78.267	-0.159
Bay Tambour	68.500	74.506	-0.273
Pelican Pass	88.324	91.086	-0.125
Early Lafourche, salt			
Grand Bayou du Large	62.358	65.693	-0.151
Lake LaGraisse	93.909	96.826	-0.132
Central Isles Dernieres	84.760	87.623	-0.130
Cocodrie	50.914	63.774	-0.584
Dog Lake	38.994	52.395	-0.609
Late Lafourche, brackish			
Lake Bully Camp	4.294	26.711	-1.018
Golden Meadow Farms	16.421	41.627	-1.145
Bay L'Ours	40.193	49.211	-0.409
Three Bayou Bay	24.009	40.360	-0.743
Golden Meadow	7.502	16.180	-0.394
Early Lafourche, brackish			
Lost Lake	29.838	35.709	-0.266
Lake Mechant	31.240	54.635	-1.063
Bayou Sauveur	10.813	25.621	-0.673
Lake Quitman	31.498	44.509	-0.591
Dulac	13.314	32.425	-0.868
Montegut	9.038	33.700	-1.121

Note: Mean annual trend, late Lafourche lobe = -0.567%
Mean annual trend, early Lafourche lobe = -0.563%

[a] Calculated by the authors from original data compiled by Liebowitz (LSU, private communication, 1988) from maps by Wicker (1980).

Appendix I

Shrimp Catch, 1960-1987, in Barataria and Terrebonne-Timbalier Bays

Table I1. Shrimp catch in Barataria Bay and Terrebonne-Timbalier bays, annual rainfall, and number of hours between April 9 and 30 when temperatures were below 20°C, 1960-1987.

Table I1. Shrimp catch (pounds) in Barataria Bay (area = 57,709 acres) and Terrebonne-Timbalier bays (130,101 acres), annual rainfall (inches), and number of hours between April 9 and April 30 when temperatures were below 20°C, by year, from 1960 through 1987.

Year	Catch		Rainfall		Hours
	Barataria	Terr-Timb	Barataria	Terr-Timb	
1960	3,145,172	4,415,118	56.2	46.4	32
1961	1,331,299	2,887,287	73.4	78.6	148
1962	1,407,457	2,507,703	40.4	37.0	37
1963	3,043,799	5,476,282	69.3	51.4	19
1964	1,386,736	2,565,840	72.2	62.3	100
1965	3,625,101	4,283,412	60.6	59.0	0
1966	3,356,306	3,697,933	81.9	72.6	34
1967	4,947,377	6,376,487	65.3	61.7	0
1968	5,538,431	6,759,208	50.8	52.0	0
1969	5,343,343	7,030,628	56.9	58.0	4
1970	6,101,020	6,549,845	55.7	72.1	27
1971	6,243,131	9,276,749	59.4	64.5	11
1972	6,015,595	6,900,478	62.2	70.9	0
1973	3,703,811	5,848,112	77.9	73.4	137
1974	5,159,804	3,935,266	56.2	62.7	18
1975	2,503,492	5,311,733	71.4	72.6	95
1976	7,070,085	8,781,531	47.7	58.4	0
1977	5,480,952	11,011,931	63.9	79.6	9
1978	4,084,009	8,985,448	65.1	61.1	49
1979	3,637,205	6,377,519	72.8	75.3	0
1980	3,340,586	3,638,863	76.8	74.6	92
1981	5,185,351	8,845,254	50.7	54.6	0
1982	5,564,216	8,248,135	67.0	67.7	80
1983	5,488,142	5,937,343	61.8	63.5	205
1984	6,028,856	6,968,363	61.8	64.5	86
1985	3,965,987	4,217,895	68.4	70.1	61
1986	8,532,259	4,736,575	49.4	59.7	7
1987	6,463,704	5,046,182	70.1	65.9	103

Note: Barataria Bay is associated with the late Lafourche lobe, and Terrebonne and Timbalier bays are associated with the early Lafourche lobe. The rainfall station used for the Barataria area was Houma, and the station used for the Timbalier-Terrebonne area was primarily Golden Meadow, supplemented by Galiano and Paraday. Shrimp catch data were compiled from catch-by-area data of the National Marine Fisheries Service, Miami, Florida (G. Davenport, private communication, 1988). Rainfall data were provided by Robert Muller of Louisiana State University (private communication, 1988). Hours of temperatures below 20°C were obtained from Barrett and Gillespie (1975) and B. Barrett of the Louisiana Department of Wildlife and Fisheries (private communication, 1988).